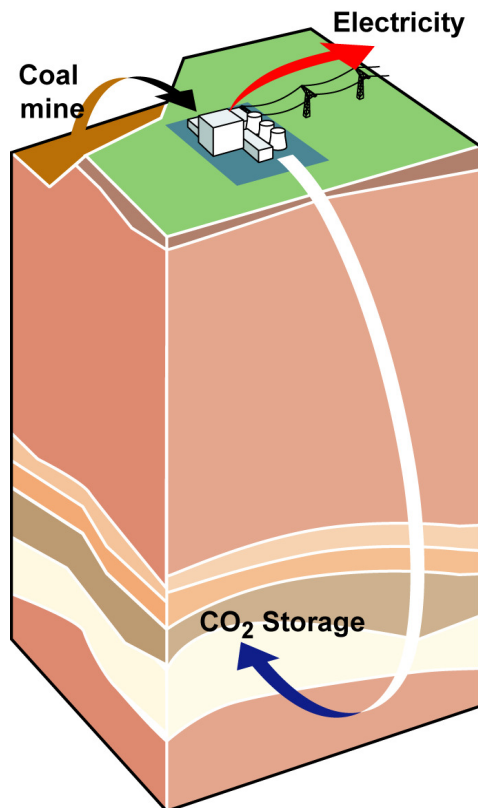2013-11-01

Performance and modelling of the pre-combustion capture pilot plant at the Buggenum IGCC - Public report

A report within the CO$_2$ Free Power Plant Project

Kay Damen, Richard Faber, Radek Gnutek

Vattenfall Research and Development AB

Coal mine

Electricity

CO$_2$ Storage

VATTENFALL

CCS R&D Portfolio

Coal power will continue to be a cornerstone of Europe's energy system in the foreseeable future, due to its economic attractiveness and ability to contribute to secure and stable electricity generation. As such, it will remain part of Vattenfall's generation portfolio.

However, when fossil fuels are combusted in power plants, vehicles, or industrial plants, carbon dioxide (CO_2) is emitted into the atmosphere. The increased levels of carbon dioxide in the atmosphere is the dominating contributor to increased global warming - one of the greatest environmental challenges of our time.

Vattenfall intends to cut its CO_2 exposure from 90 million tonnes in 2010 to 65 million tonnes by 2020. By 2050, the vision is to have a carbon-neutral generation portfolio. Part of the strategy is to develop the Carbon Capture and Storage (CCS) technology to reduce CO_2 emissions into the atmosphere from coal-fired power plants. The idea is to capture CO_2 from a coal-fired power plant, transform it into a liquid, and store it deep underground. The storage repositories will be of the same kind as where oil and gas are extracted - formations of porous rock with a sealing cap on top. The aim is to develop a commercial concept operable by 2025-2030.

Political support, legal framework, and societal acceptance are crucial to make CCS possible, and Vattenfall is collaborating with various stakeholders to develop relationships and requisite conditions. In the long term, new sustainable energy sources will have to be deployed, but the development of emission free fossil fuel utilisation is considered as necessary bridging technology.

The CCS R&D project portfolio is providing options for Vattenfall's fossil based operations in its continental core markets. It has been running since 2001 and involves in addition to Business Unit R&D Projects, also specialists from BU Engineering, BU Production Lignite and a large number of external partners, including several major manufacturers, other power companies, engineering companies and research providers and leading universities in Europe.

The CCS R&D project portfolio consists of three elements:
- Development of concepts and technologies to capture carbon dioxide more efficiently and at less cost
- Investigations of CO_2 transport and geological storage options that are safe, reliable and cost effective
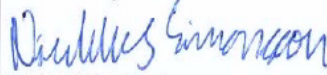- Environmental assessments and acceptance building.

This report is one of several reports produced within the CCS R&D Portfolio. Any questions and inquiries concerning the report should be directed to the authors. Questions and inquiries concerning the Portfolio drivers and roadmap should be directed to R&D Projects/Sustainable Asset Development.

Performance and modelling of the pre-combustion capture pilot plant at the Buggenum IGCC - Public report

Kay Damen, Richard Faber, Radek Gnutek

Vattenfall Research and Development AB

Performance and modelling of the pre-combustion capture pilot plant at the Buggenum IGCC – Public Report

From	Date	Serial No.
Vattenfall Research and Development AB	2013-11-01	U 13:71
Author/s	**Security class**	**Project No.**
Kay Damen Richard Faber Radek Gnutek	Open [S1]	PR.735.10
NDA (Non Disclosure Agreement)	Yes	No X
Customer Vattenfall AB R&D Projects Åse Myringer	**Reviewed by** Nicklas Simonsson
	Issuing authorized by Karin Ifwer
Key Word	**No. of pages**	**Appending pages**
Pre-combustion capture	163	27

Summary

In 2008, Nuon started the so-called CO_2 Catch-up project with the objective to demonstrate pre-combustion CO_2 capture at a pilot plant in Buggenum in order to verify the technology performance and to generate knowledge in the form of validated models and operational experience. It was aimed to apply this knowledge to optimise the design and operation of the full-scale CO_2 capture unit at the Magnum power plant, a multi-fuel Integrated Gasification Combined Cycle (IGCC) planned in Eemshaven, the Netherlands.

The CO_2 Catch-up project consists of 2 parts:
1. Engineering and construction of a pre-combustion capture pilot plant at the Buggenum IGCC (finished in 2011)
2. Operation and execution of the test and R&D programme (2011-2013)

The test programme is the collection of test runs performed at the pilot plant. The results of the test programme are input to the overarching R&D programme aiming to understand and improve the process by means of process modelling and laboratory experiments. The test and R&D programme has been managed by Vattenfall R&D Projects and performed together with Delft University of Technology and Energy research Centre of the Netherlands (ECN) and involves a number of scientists and PhD students. This report summarises the results of the pilot plant operation and test and R&D programme of the CO_2 Catch-up project.

The pilot plant is a simplified, smaller version of the CO_2 capture plant for the Magnum IGCC power plant designed by CB&I Lummus. It was designed to capture 1.4 t /h of CO_2 from 1.2 t/h of syngas (=0.8% of the syngas flow from the Buggenum gasifier). In the pilot plant carbon monoxide (CO) is catalytically converted into carbon dioxide (CO_2) and hydrogen (H_2), the so-called water-gas shift (WGS) reaction, after which CO_2 is separated from H_2 in the absorption-regeneration section. The WGS catalyst applied in the pilot plant is Haldor Topsøe's SK-201-2, a copper promoted iron/chromium based HTS catalyst. The (physical) solvent used to remove CO_2 is Genosorb^R 1753 consisting of dimethyl-ether of poly-ethylene-glycol (DEPEG).

The pilot plant has been operated from January 2011 to March 2013. Total operating hours are 5886 hours and the cumulative CO_2 captured is 4478 ton. The pilot plant has been operated without major problems after some (relatively minor) hardware and control modifications. The sampling conditioning system and analyzers have

been the largest point of concern. From HSE perspective, no incidents occurred (zero lost time incidents, no spills).

The overall mass balance as well as the mass balances for the individual plant sections close very well. For the overall mass balance the relative deviation between input and output is only 0.11%. The measured CO conversion is approximately 93% at reference state (normal operating conditions), which is according expectations. The average CO_2 absorption efficiency is around 86% at the reference state. The results are incomparable as the design was based on a Mellapak 350 Y/750 Y whereas Raschig Super-Ring 0.6 and Raschig Super-Pak 250Y were tested in the pilot plant. As a result, the overall capture efficiency is approximately 80% in reference state.

In the pilot test programme various parametric tests, both steady-state and dynamic, were performed to investigate the performance of the shift and absorption section. The reactor 1 and 2 catalyst activity decreases at a much slower rate than expected by the catalyst vendor. The reactor 3 catalyst has a much lower activity than anticipated. Repeated chemical analysis of reactor 3 catalyst samples hinted towards catalyst damage due to an over reduction as being the probable cause for the observed lower activity. This over reduction might result from steam condensation upstream of the reactor during start-up.
The high and stable activity directly following the rapid initial catalyst deactivation allows reduction of the reactor feed temperatures and lowering of the pilot steam consumption.
Operation at a reduced steam/CO ratio would allow reducing the steam requirement for the WGS section and thus the CO_2 capture penalty, but can lead to carbiding thereby increasing hydrocarbon and especially CH_4 production. Severe carbiding can lead to permanent loss of catalyst activity and/or selectivity and even to physical damage of the catalyst pellets. Compared to reference state operation at steam/CO=3.1 mol/mol (for reactor 2), operation at reduced ratios of 2.6 down to 1.5 indicates no sign of carbiding. It is concluded that the catalyst is stable at the reduced steam/CO ratios tested.
Lowering the reactor 2 steam/CO ratio from reference state conditions to 2.06 mol/mol results in a decrease of the overall conversion by 3.6%-points, while the overall steam/CO ratio decreases by 26%. This means that a small decrease in CO_2 capture ratio saves a significant amount of steam, thereby decreasing the efficiency penalty for CO_2 capture. The exact impact on the efficiency penalty in the full-scale IGCC with CO_2 capture still needs been quantified.

For the absorption section, the parametric tests were performed to evaluate the impact on the CO_2 absorption efficiency, validate the mass transfer coefficients and the thermodynamic model. All trends observed in the parametric tests are in line

with expectations. Results indicate that Raschig Super-Ring 0.6 has a better performance than Raschig Super-Pak 250Y. An analysis of the spent solvent indicates no signs of degradation.

For a better understanding of the CO_2 capture process and explanation of observed performance a series of process models have been developed:
- a heterogeneous adiabatic plug-flow reactor model (Matlab)
- a steady-state model of the syngas conditioning and water-gas shift section (Aspen Plus V7.3)
- a steady-state model of the CO_2 absorption section (Aspen Plus V7.3)
- a dynamic model of the syngas conditioning and water-gas shift section (Dymola/Modelica)
- a dynamic model of the CO_2 absorption section (Dymola/Modelica)

It can be concluded that the validated steady-state and dynamic models are generally capable of predicting the pilot plant performance throughout the entire operational range and can be used for the development of a large-scale model of the capture unit.

In summary, the project objectives to verify the technology performance and to generate knowledge in the form of validated models and operational experience are clearly achieved. However, the knowledge generated in the CO_2 Catch-up project will not be applied directly, as the investment decision for the gasification and CO_2 capture unit in the Magnum project has been postponed beyond 2020. The commercial outlook for IGCC+CCS remains uncertain. The main concern for IGCC plants remain the relatively high costs (both in terms of CAPEX and OPEX). The results of the CO_2 Catch-up project, basically promising an optimised design for the water-gas shift and CO_2 absorption unit with reduced specific energy consumption (and hence OPEX) and possibly CAPEX, are not expected to change much to this problem.

Although direct application in the Magnum plant is not foreseen on the short term, the gasification projects under development in other parts of the world as well as new future projects may benefit from the achievements made in this project. Knowledge dissemination is aimed for by means of (scientific) publications of the researchers involved in the project. Papers in peer-reviewed journals are currently being prepared on the steady-state and dynamic pilot plant modelling work, as well as the results of the WGS reactor modelling and low steam/CO ratio test run. As the suppliers of catalyst, solvent and packing all have been heavily involved in the project to learn on the outcome of the test programme, hopefully the generated insights will be followed up and potentially discussed/offered in any new IGCC + CCS project.

Distribution list

Company	Name	Number of
Vattenfall	Karl Bergman	1 PDF-file
Vattenfall	Göran Lindgren	1 PDF-file
Vattenfall	Åse Myringer	1 PDF-file
Vattenfall	Uwe Burchhardt	1 PDF-file
Vattenfall	Karin Ifwer	1 PDF-file
Vattenfall	Jonas Alin	1 PDF-file
Vattenfall	Matthias Bruhn	1 PDF-file
Vattenfall	Kay Damen	1 PDF-file
Vattenfall	Radek Gnutek	1 PDF-file
Vattenfall	Richard Faber	1 PDF-file
Vattenfall	Sebastian Meinke	1 PDF-file
Vattenfall	Nicklas Simonsson	1 PDF-file
Vattenfall	Jonas Funkquist	1 PDF-file
Vattenfall	Michael Trompelt	1 PDF-file
Vattenfall	Jinying Yan	1 PDF-file
Vattenfall	Clas Ekström	1 PDF-file
Vattenfall	Rainier Giering	1 PDF-file
Vattenfall	Norbert Jentsch	1 PDF-file
Vattenfall	Thomas Porsche	1 PDF-file
Vattenfall	Wolfgang Rolland	1 PDF-file
Vattenfall	Wolfgang Dirschauer	1 PDF-file
Vattenfall	Frans Kornips	1 PDF-file
Vattenfall	Marc Martens	1 PDF-file
Vattenfall	Loek Schoenmakers	1 PDF-file
Vattenfall	Patrick Hendriks	1 PDF-file
Vattenfall	Roel Vranken	1 PDF-file
Vattenfall	Jo Salden	1 PDF-file
Vattenfall	Joost Kaptein	1 PDF-file
Vattenfall	Han Raas	1 PDF-file
Vattenfall	Marco Kanaar	1 PDF-file
Vattenfall	Julia Bell	1 PDF-file
Vattenfall	Roel Kettenis	1 PDF-file
Vattenfall	Boy van Egmond	1 PDF-file
Vattenfall	Maarten Berkhout	1 PDF-file
Vattenfall	Jeffrey Haspels	1 PDF-file

Agentschap NL	Gerdi Breembroek	1 PDF-file
ECN	Eric van Dijk	1 PDF-file
Technische Universiteit Delft	Piero Colonna	1 PDF-file
Technische Universiteit Delft	Carsten Trapp	1 PDF-file
Technische Universiteit Delft	Teus van der Stelt	1 PDF-file
Technische Universiteit Delft	Thijs Vlugt	1 PDF-file
Technische Universiteit Delft	Michiel Makkee	1 PDF-file
Technische Universiteit Delft	Abrar Hakeem	1 PDF-file
RWTH Aachen University	André Bardow	1 PDF-file
Universität Stuttgart	Joachim Groß	1 PDF-file
Universität Stuttgart	Marina Stavrou	1 PDF-file
Institute of Chemical Technology Prague	Lukas Valenz	1 PDF-file
Politecnico di Milano	Carlo de Servi	1 PDF-file
Politecnico di Milano	Fransesco Casella	1 PDF-file
Spie	Perry Brummans	1 PDF-file
Haldor Topsøe	Jan Due Nielsen	1 PDF-file
Haldor Topsøe	Jacob Marcher	1 PDF-file
Raschig	Michael Schultes	1 PDF-file
Raschig	Andreas Danninger	1 PDF-file
Clariant	Kai Schröder	1 PDF-file
Elcogas	Pedro Casero Cabezon	1 PDF-file
Elcogas	Paco Garcia Peña	1 PDF-file
J-Power	Kyohei Nakamura	1 PDF-file
J-Power	Hiroshi Sasatsu	1 PDF-file
J-Power	Kouji Omata	1 PDF-file
J-Power	Masakazu Utano	1 PDF-file
Uhde	Olaf von Morstein	1 PDF-file
CB&I	Michel Hagg	1 PDF-file
CB&I	Michiel van der Griendt	1 PDF-file
CB&I	Jaap van der Wouden	1 PDF-file
CATO-2		1 PDF-file

Table of Contents

Appendices

1 Introduction

1.1 Project rationale and objective

In 2005, Nuon started the development of a multi-fuel Integrated Gasification Combined Cycle (IGCC) power plant, the so-called Magnum project, in Eemshaven, the Netherlands. The application of gasification technology enables pre-combustion carbon dioxide (CO_2) capture in order to store the CO_2 in a geological formation. Hereto, steam is added to convert carbon monoxide (CO) present in the syngas into carbon dioxide and hydrogen (H_2) by means of the water-gas shift (WGS) reaction. Subsequently, CO_2 is separated from H_2 by means of absorption. The original concept for Magnum was to construct the gasification section first, with the option to install the CO_2 capture unit afterwards ("capture ready retrofit").

In 2007, a study was performed by CB&I Lummus, an engineering company managing the EPC of the Magnum IGCC, to select the technology for a CO_2 capture retrofit. The energy consumption of the WGS reaction and CO_2 absorption is significant (see Figure 1-1 for an indication for the Magnum design), comprising of the loss in heating value in the shift reaction, the steam to drive the shift reaction and the power to drive (mainly) pumps and compressors. Therefore, the main task for CB&I Lummus was to minimise the specific energy consumption and costs per tonne avoided CO_2. The result of the technology selection was an open-art design based on existing technologies but with several modifications in the flowsheets typically presented for pre-combustion capture at IGCC's. Note that the optimal capture rate according to CB&I Lummus was 81% ("bulk-removal"), which is below the 85-90% commonly found in literature.

Although CO_2 capture has never been applied in combination with an IGCC unit, many of the elements have been proven in the chemical industry, yet in a slightly different configuration as foreseen in Magnum due to the different purpose of CO_2 capture. Also the syngas composition when gasifying coal (and biomass) in the Magnum plant differs from that when gasifying natural gas or heavy oil residues as performed typically in the chemical industry (for which most experience exists). In addition, the mode of operation in the chemical industry is different than the power sector; in the latter the load of the WGS and CO_2 capture unit should be able to follow the ramping of the power plant. Therefore, it was decided to demonstrate and optimise the concept developed by CB&I Lummus on a small scale first before applying a full-scale commercial CO_2 capture unit at the Magnum plant. This resulted in the so-called CO_2 Catch-up project, encompassing the engineering and construction of a CO_2 capture pilot plant and operation at the site of the IGCC power plant in Buggenum, the Willem Alexander Centrale (WAC).
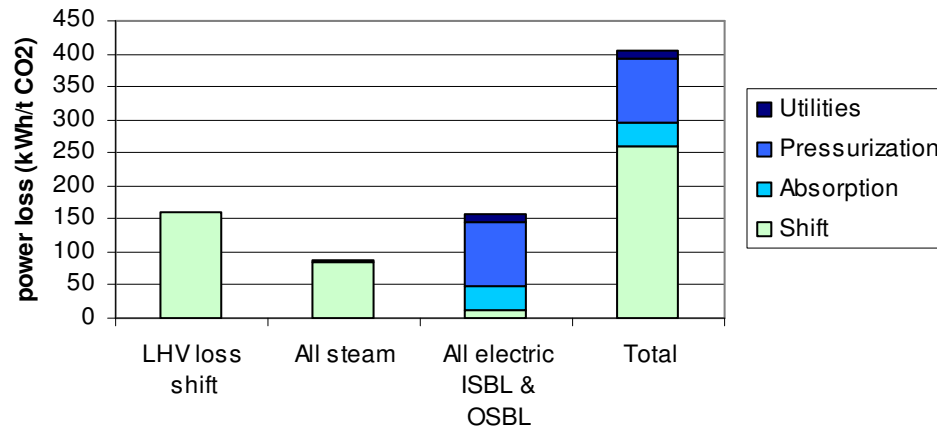
Figure 1-1:   **Specific power loss of CO₂ capture for the Magnum IGCC with 28 bar gasifier pressure (low-pressure case), capture rate of 81% and battery limit CO₂ pressure of 110 bar. For a single train gasifier with the capacity of Buggenum (600 MW$_{th}$), the energy consumption would be 65 MW$_e$. LHV = lower heating value, ISBL/OSBL= inside/outside battery limits**

The objective of the CO₂ Catch-up project is to demonstrate pre-combustion CO₂ capture at the pilot plant in Buggenum in order to verify the technology performance and to generate knowledge in the form of validated models and operational experience that can be applied to optimise the design and operation of the full-scale CO₂ capture unit at the Magnum IGCC.

The CO₂ Catch-up project consists of 2 parts:
3. Engineering and construction of the pilot plant (finished in 2011)
4. Operation and execution of the test and R&D programme (2011-2013)[1]

The test programme is the collection of parametric test runs performed at the pilot plant. The results of the test programme are input to the overarching R&D programme aiming to understand and improve the process by means of process modelling and laboratory experiments. The test and R&D programme has been managed by Vattenfall R&D Projects and performed together with Delft University of Technology and Energy research Centre of the Netherlands (ECN) and involves a number of scientists and PhD students.

---

[1] The PhD projects in the R&D programme last until 2014.

1.2 Overview test and R&D Programme

The test and R&D programme is divided into the following work packages:

1. **Plant operation and optimisation**.
   This work package consists mainly of modelling and simulation activities aimed to:
   a. Verify the overall system performance and operational window
   b. Perform system analysis and optimisation considering heat integration and dynamic performance.

   The obtained process models (steady-state and dynamic) are validated by comparison with data of the pilot plant. The knowledge acquired by means of studies on the pilot plant is used for the optimisation of the CO_2 capture plant in the Magnum IGCC.

2. **Water-gas shift section**.
   This work package involves both experimental and modelling activities. Different catalysts are screened at the ECN laboratories in close cooperation with the catalyst vendors. Hereto, the activity, selectivity and stability of different catalysts and the effect of aging, pressure, sulphur concentration and H_2O:CO ratio are measured in a high-pressure test rig. On that basis, a catalyst was selected for further testing in the pilot test programme. Also kinetic measurements are performed and catalyst physical properties are measured in the lab to generate input for a reactor model, which can be used for reactor design and sizing and process optimisation.

   This work package also includes a PhD project at Delft University of Technology to develop new promising catalysts. This is not further discussed in this report (as it is not directly related to the pilot plant test programme).

3. **CO_2 absorption section**.
   In order to create a better insight in the parameters driving CO_2 absorption and regeneration, first a thermodynamic model for the solvent-water-gas components has been developed. This is the basis for a rate-based steady-state model of the CO_2 absorption and regeneration section used to fit mass transfer coefficients for different packings and compare the performance at on and off design.

   In parallel, a PhD project aiming for simultaneous solvent and process optimisation is executed at Stuttgart/Delft University of Technology. This is not further discussed in this report (as it is not directly related to the pilot plant test programme).

4. **Corrosion**.

   Corrosion rates are monitored using electric resistance probes and wall thickness measurements to get more insight in the corrosiveness of the process media and the solvents used.

This report highlights the results of the test and R&D programme. In chapter 2, first the pilot plant process and design is explained in more detail. Chapter 3 gives an overview of the plants measurements, followed by the operational statistics and lessons learned in chapter 4. The performance of the pilot plant is shown in chapter 5 and the results of the test programme will be discussed in chapter 6. Chapter 7 focuses on process modelling and validation and finally the conclusions are given in chapter 8.

2 Process description and pilot plant design

In this chapter, the design considerations related to the Magnum CO_2 capture plant will be discussed, which will form the basis to understand the pilot plant design (section 2.2) and the R&D questions to be addressed in the Test and R&D Programme.

2.1 Design considerations pre-combustion CO_2 capture

2.1.1 Gasification

The gasifier design is one of the decisive factors for the technology choice of the downstream WGS and CO_2 absorption units. The original Magnum concept (from 2007), from now on referred to as *low-pressure case*, was based on three gasifiers as applied in Buggenum (Shell dry quench gasifier with an operating pressure of 28 bar and a capacity of 2000 t coal/d = 600 MW_{th} = 144,000 Nm^3/hr CO + H_2). The CO_2 capture design from CB&I Lummus is based on these assumptions. In a later stage, both the gasifier capacity and pressure were reconsidered in order to decrease CAPEX and increase efficiency. By increasing the gasifier pressure from 28 bar to 42 bar (*high-pressure case*), the syngas booster compressors, which are required to meet the pressure at the fuel control valve of the gas turbine, can be omitted or minimised, saving costs and increasing the overall plant efficiency. The consequence of the higher gasifier pressure on the WGS section is a somewhat modified heat integration (due to different water dew point). Consequences for the catalyst will be discussed in 6.2.3. The CO_2 absorption section will benefit from higher gasifier pressures due to the higher CO_2 partial pressures as will be further discussed in 6.3.6.

2.1.2 Water-gas shift

In the water-gas shift section the CO contained in the syngas feed is converted into CO_2 by means of slightly exothermal chemical reaction:

$$CO(g) + H_2O(g) \leftrightarrow CO_2(g) + H_2(g), \quad \Delta H°298 = -41.1 \text{ kJ/mol}$$
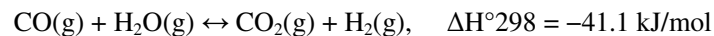
The shift reaction can either take place in the sour syngas before sulphur removal (sour shift) or in the cleaned syngas after sulphur removal (sweet shift). Most IGCC + CCS concepts found in literature are based on sour shift, as the efficiency penalty is slightly lower (IEA GHG, 2003). In addition, the upstream hydrolysis unit can be omitted, since COS is also converted to H_2S in the sour WGS reactor. In the original Magnum concept, a sweet shift concept was foreseen due to its presumed compatibility for easy CO_2 capture retrofit and the ability to bypass the shift and CO_2 absorp-

tion unit (e.g. when CO_2 capture is not economically viable)[2]. Another advantage of a sweet shift is that both desulphurised syngas and H_2 can be delivered over the fence (which was one of the options considered for the Magnum plant). For these reasons, sweet shift catalysts have been considered in the project.

There are two commercially available sweet shift catalysts available: high temperature shift (HTS) and low temperature shift (LTS). HTS consist of copper promoted iron/chromium, typically operated at 350 – 500°C and at sulphur concentrations below 100 ppm. The LTS is more active and operates at lower temperatures, but is very sensitive to sulpur poisoning (requires typically <5 ppb S). When hydrogen production is the objective, generally two reactors in series with intercooling are applied as the shift reaction is equilibrium limited. HTS is used for bulk conversion in reactor 1 and LTS in reactor 2 to minimise CO slip. As the objective in these plants is to maximise the hydrogen yield high OPEX (steam to drive the reaction to the product side) and CAPEX (for extensive gas cleaning in case of coal/oil gasification to protect the LTS catalyst from poisoning) are justified. In the case of IGCC + CO_2 where the driver is cost-efficient CO_2 capture, bulk CO conversion by means of HTS catalyst is considered.

HTS catalysts are commonly applied in hydrogen and ammonia plants, mainly treating syngas from steam methane reforming, but also to shift syngas produced by gasification of heavy oil residues (typically in combination with a Rectisol unit and low-temperature shift catalysts). In those applications, the sulphur level to which the catalyst is exposed is very low (below ppm level) and many of the trace elements are removed in the Rectisol unit or upstream. There are, however, little references where iron/chromium catalysts are exposed to the sulphur levels and trace elements common in a coal gasification plant with a less stringent H_2S removal. This aspect will be studied in more detail in the Test and R&D programme, both by laboratory tests and pilot testing.

As the MP/IP steam needed in the WGS reaction, which is either extracted from the syngas cooler or heat recovery steam generator (HRSG), cannot be expanded to produce electricity, reducing the steam consumption to a minimum is the key to minimise the efficiency penalty of CO_2 capture in IGCC applications. Although adding more steam increases CO conversion, the incremental efficiency penalty does not justify the additional CO_2 captured, so the optimum amount of steam is the minimum steam required by the catalyst. Excess steam (i.e. > stoiciometric ratio) is needed to:

---

[2] In contrast to a sour shift, the syngas flow and composition to the H_2S absorber is unaffected when operating with/without CO_2 capture.

- limit the temperature rise and hotspots (minimising catalyst deactivation)
- prevent the formation of iron carbide (which may cause deactivation, catalyses the Fischer-Tropsch reaction and reduces catalyst strength). Catalyst vendors typically specify a minimum steam:dry gas or steam:CO ratio to prevent carbide formation.

In a conventional scheme with several reactors in series, the temperature rise in the first reactor would determine the steam requirements. Coal syngas from a Shell dry quench gasifier typically contain 60 mol% CO, which results in high reaction rates and temperature rise (in comparison to syngas produced from natural gas and to a lesser extent, heavy oil residues). A H_2O:CO ratio of around 4.3 (on molar basis) would be required to keep the reactor outlet temperature below 500°C (Carbo et al., 2009), which is higher than the minimum to prevent carbide formation. Ideally steam with only part of the syngas is to be fed to the first reactor. As steam and CO are consumed in equal quantities the H_2O:CO ratio increases, thereby allowing part of the syngas feed (containing less steam) to be fed directly to the second reactor. This can be achieved by splitting the syngas flow, a strategy that has been suggested in literature (Carbo et al., 2009) and that has been applied by CB&I Lummus to optimise the flowsheet (see Figure 2-1). As a result, the overall H_2O:CO ratio (and hence overall steam demand) is reduced drastically. Basically, the minimum steam demand is set by the inlet conditions of the second reactor, which equals the minimum to prevent carbide formation.

In order to further reduce the efficiency loss in the water-gas shift reaction, maximum heat integration has been applied by CB&I Lummus (in cooperation with shift catalyst vendors). Instead of using steam from the syngas cooler or the HRSG directly, steam is generated internally, which is the most efficient way to generate the required steam. In this concept, depicted in Figure 2-1, steam is produced by evaporating make-up water and recycled excess water condensed downstream the reactors using the hot syngas outlet from the WGS reactors. This concept makes use of the partial pressure reducing effect of the syngas for generating the steam (similar as in saturator towers). In this way the required steam is generated at a lower temperature than in the HRSG and thus making better use of the heat available in the water-gas shift effluent that is ultimately cooled down to condensate all excess steam.
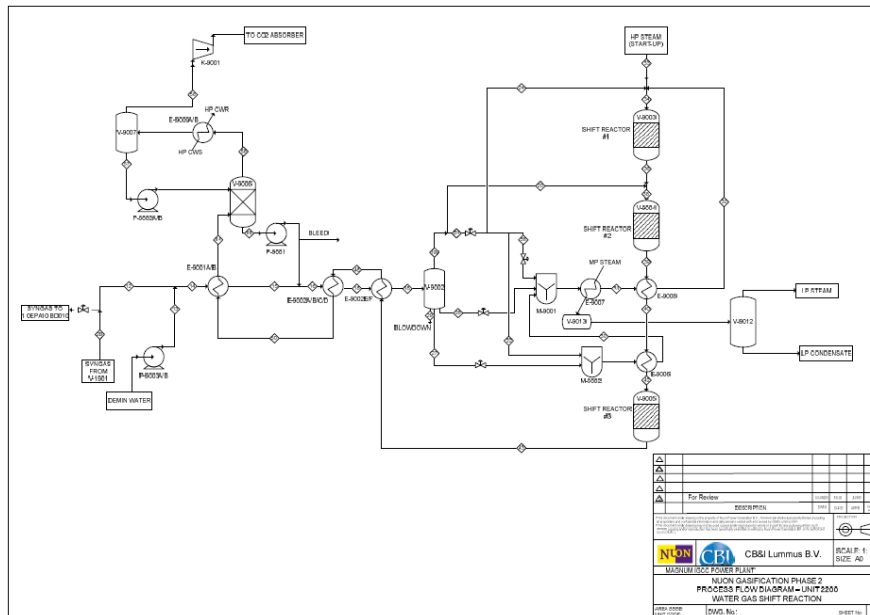
Figure 2-1:   Process flow diagram of the water-gas shift section (high-pressure case)

2.1.3   H₂S and CO₂ absorption

Syngas from the gasification plant is treated in a single integrated $H_2S + CO_2$ removal plant[3] separated by a sweet water-gas shift unit. Commercially available gas treatment technologies can be grouped in chemical and physical solvents (and mixtures thereof). The optimal solvent is determined primarily by the syngas composition and pressure (determining H_2S and CO_2 partial pressure) and the product specifications. In the case of IGCC + CO_2 where the driver is cost-efficient CO_2 capture and not too stringent H_2S removal is required, the Selexol^{TM} process is generally considered the optimal process, although apple-to-apple comparisons between different gas treatment options for IGCC with H_2S and CO_2 removal are scarce. The Selexol process is a proven commercial process licensed by UOP that uses a physical solvent consisting of a mixture of dimethyl ethers of polyethylene glycol (DEPEG) to remove acid gases from synthetic or natural gas streams. It is ideally suited for the selective removal of H_2S, COS and CO_2. Sulphur levels below 1 ppmv can be achieved with variable and optimised CO_2 capture levels. Selexol is a stable and non-corrosive solvent and has a relatively low vapour pressure (i.e. solvent losses are acceptably low).

---

[3] In theory, it is possible to use one solvent to selectively remove H_2S and another solvent for the removal of CO_2, but this is not considered.

One of the key parameters in a typical Selexol flowsheet is the solvent temperature. In some plants, the solvent is chilled as it increases the solvent capacity for acid gas, thereby reducing the solvent flow rates and equipment size. Also the design for integrated H_2S and CO_2 removal for the high-pressure Magnum case proposed by UOP (see Figure 2-2) includes solvent chilling.

CB&I Lummus performed an independent analysis to find the optimal configuration for energy-efficient bulk CO_2 removal (for the low-pressure Magnum case, not considering H_2S removal). It was concluded that the optimal temperature for energy-efficient bulk CO_2 removal is 40°C. A detailed analysis to assess whether the energy use and lifecycle costs when operating at 40°C (larger equipment, large solvent pump duty) are lower in comparison to chilled conditions (smaller solvent flows i.e. smaller equipment and solvent pump duty, additional energy use and costs of chiller) has not been performed though. Also the impact of a higher viscosity at lower temperatures on mass transfer needs to be included in such analysis.

The consequence of a relatively high solvent temperature is a high solvent flow to achieve the required capture efficiency. In the CB&I Lummus design, the solvent flow is around 250 m^3/m^2/h. In order to recover part of the high pump energy, a rich solvent expander is proposed in the CB&I Lummus design, which allows power recovery from the high solvent flows and flashing CO_2 (not standard in UOP design). Another aspect to be considered for such high solvent flows is to select the right packing for optimal mass transfer. The UOP absorber design and most Selexol plants use random packing (such as Raschig Super-Rings), which are typically suitable for high liquid loads. CB&I Lummus considered three beds of structured packing (250 Y and X) in the CO_2 absorber. The main argument for structured packing is the lower HETP versus random packing and also pressure drops are expected to be smaller. However, structured packing has never been tested for DEPEG at these liquid loads at pressurised conditions. The performance of structured packing (versus random packing) needs to be verified by means of experimental data first.
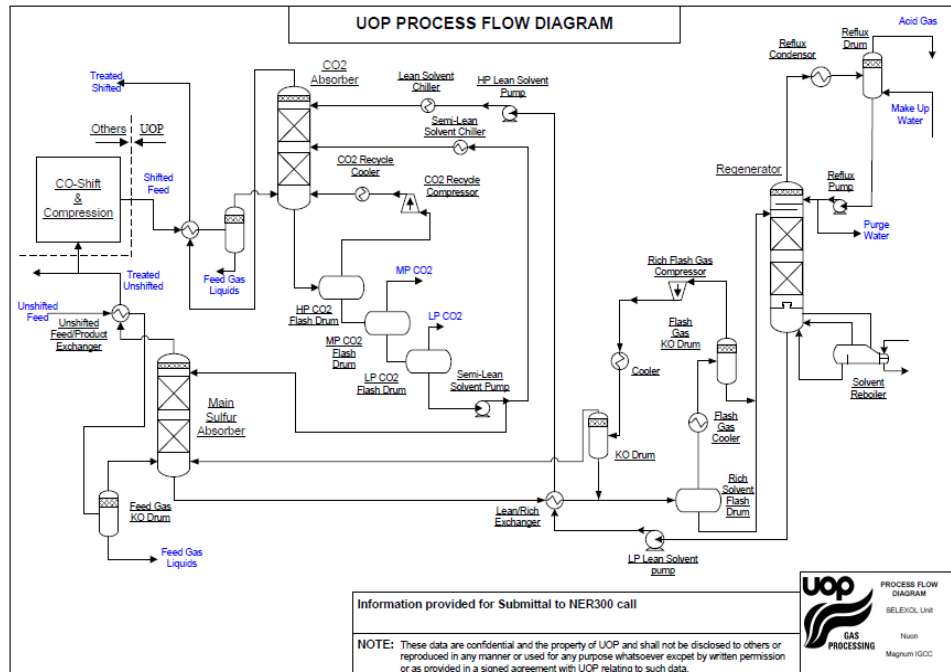
Figure 2-2: **Process flow diagram integrated H$_2$S + CO$_2$ removal (high-pressure case)**

2.2 Design rationale pilot plant

The pilot plant is a simplified, smaller version of the CO$_2$ capture plant for the Magnum IGCC power plant as proposed by CB&I Lummus. It was designed to capture 1.4 t /h of CO$_2$ from 1.2 t/h of syngas (=0.8% of the syngas flow from the Buggenum gasifier). There are also a number of essential differences between the pilot plant and the large-scale capture plant, of which the major are described below:

- Heat integration in the WGS section. In the pilot plant, water is evaporated/condensed by means of electrical heaters and forced-draft air coolers, respectively, instead of shell and tube feed-effluent heat exchangers as foreseen in the Magnum plant. In this way the temperature dependency of two streams (feed-effluent) is avoided and the precise control of the temperature becomes possible. This simplifies the operation, extends the operational flexibility and prevents process fluctuations that could influence the reliability of the test runs in the test programme. However, specific energy consumption figures of the pilot plant are non-representative and incomparable with figures from literature for large-scale plants (and are therefore not discussed). The reason not to use steam instead of water is to demonstrate the principle of internal evaporation. Consequently, the control philosophy and dynamic behaviour are not representative for the large-scale plant.

- No integrated H_2S removal. H_2S is absorbed upstream the pilot plant in the main Sulfinol unit of the Buggenum IGCC. The implications are that the CO_2 absorber has only 1 solvent feed (semi-lean) instead of 2 solvent feeds (lean and semi-lean) as in the integrated $H_2S + CO_2$ removal unit in the large-scale plant. More importantly, the water balance has to be controlled differently. In the integrated $H_2S + CO_2$ removal unit the water content of the solvent is controlled in the reflux section of the regenerator. The solvent water content affects the CO2 loading, as well as physical properties (such as viscosity), which will affect hydrodynamics and mass transfer. Water in the solvent (DEPEG) is also required in order to provide steam to strip the acid gas in the regenerator. Typical water content for DEPEG is 4 wt%. In order to control the water content of the solvent in the pilot plant, a dehydration unit was included in the original design. Potential liquid condensed in the CO_2 compression knockout drums downstream the 1st and 2nd compression stage is routed to the dehydration package (ELJ10 AT040) (see Figure 2-10). Here, entrained solvent is separated from the knockout drum water stream and returned to the 3rd flash vessel. The water removed in the dehydration package is then recycled to the water make-up drum. For several reasons it was decided to exclude this dehydration unit in a later stage (the necessity for this unit was debated as it is not required in the Magnum plant and the design of the dehydration unit was relatively complex). Draining the content of the compression knock-out drums or sending the CO_2 (with water) to the flare and varying the duty of the solvent heater ELH30 AC010 (see Figure 2-9) were considered to be adequate strategies to control the water content.
- Solvent expander. As explained in 2.1.3 a rich solvent expander is proposed in the CB&I Lummus design to recover part of the pump energy. This feature is not present in the pilot plant, as these turbines are commercially available and it was not considered necessary to test it.
- Flash gas recycle compressor. In the integrated $H_2S + CO_2$ removal unit in the large-scale plant a compressor is included to recover the CO and H_2 that are released in the first flash vessel. This is not present in the pilot plant, as measuring the flash gas composition (as function of flow rates and flash pressure) is deemed sufficient. As a consequence the CO_2 product stream in the pilot plant will contain relatively high concentrations of CO and H_2.
- In the Magnum design, a heat exchanger is foreseen which removes low level heat from the overhead vapour of the 3rd Shift Reactor Effluent Rectifier by heating solvent, which provides additional flashing and improves CO_2 recovery. In the pilot plant, an electrical heater is used to study the effect of increased solvent temperatures.
- Packing. Ideally, the absorber is equipped with the same packing (250 Y and X) and distributor as in the large-scale plant. In order to achieve comparable capture efficiencies as in the Magnum design with the same packing, tower

height becomes so high and would require extra support, bracing, and structures which significantly increase the overall cost. Therefore, it was decided to use a finer packing to achieve the same separation efficiency and reduce the tower height. CB&I Lummus suggested using 2 beds with 750 Y and 350 Y, a structured packing with larger specific surface area than the 250 Y/X suggested for Magnum. In further discussions with packing vendors, it became clear that there is no/little experimental data that supports the theoretical performance (hydraulic, efficiency) of structured packing in combination with the high liquid loads of DEPEG at pressurised conditions. Random packing such as Raschig Super-Rings, on the other hand, is generally applied for the Selexol process and can be considered proven packing for this application. Therefore, it was decided to start the test programme with Raschig Super-Rings 0.6 first, after which the packing will be exchanged for Raschig Super-Pak 250 Y.

- Compressor design. In the pilot plant an electric motor-driven 2-stage intercooled reciprocating compressor is used, whereas a multi-stage integrally-geared centrifugal compressor is foreseen for the large-scale application.
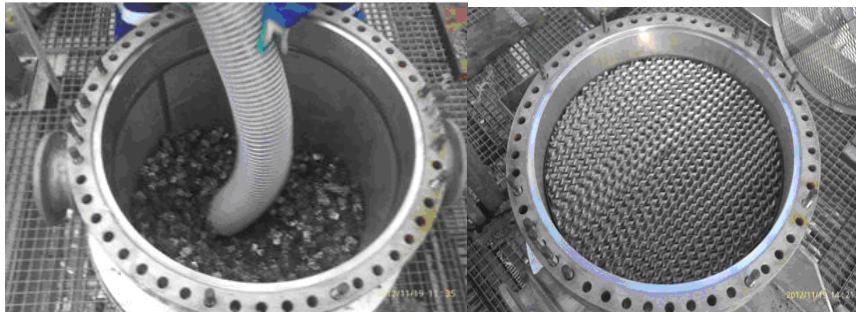

Figure 2-3:   Raschig Super-Rings 0.6 (left) and Raschig Super-Pak 250 Y (right) in the CO$_2$ absorber of the pilot plant

Due to the differences between the pilot plant and full-scale plant, the data from the pilot plant cannot be used *directly* to predict the performance of the full-scale plant. The data from the pilot plant are used to validate models, which will be up-scaled accounting for the differences to simulate the mass and energy balance of the large-scale plant.

2.3   Pilot plant process description

The pilot plant consists of five Sections: Syngas Conditioning and CO shifting, Condensate Recovery, CO$_2$ Absorption, CO$_2$ Compression and Solvent Storage. These Sections are discussed below (for more details see (CB&I Lummus, 2008a)). Figure 2-4 depicts a simplified process flow diagram of the entire process and the pilot plant.
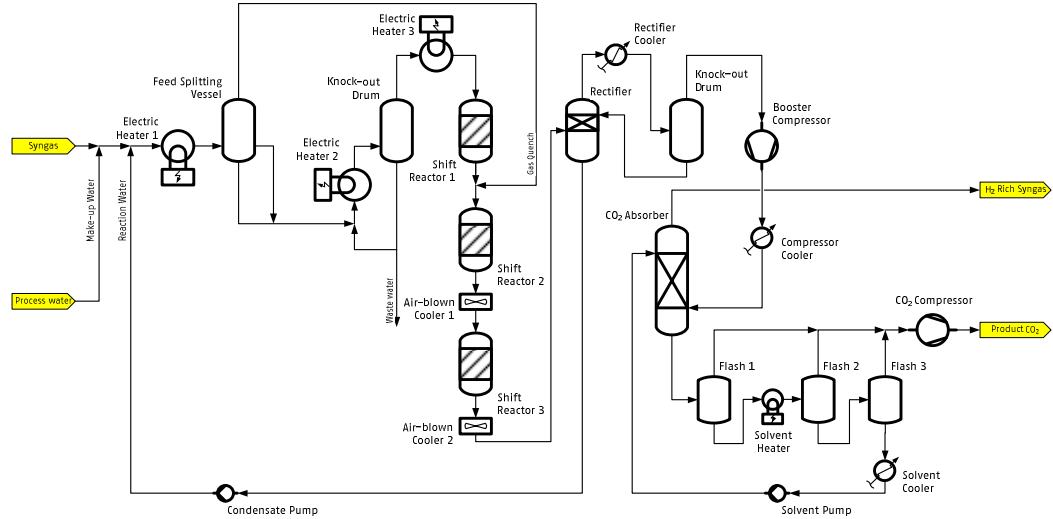
Figure 2-4: Simplified process flow diagram of the CO$_2$ capture pilot plant

Figure 2-5: CO$_2$ capture pilot plant. The tall column in the middle of the picture is the CO$_2$ absorber.

2.3.1 Syngas Conditioning (KKS-code ELF) and CO Shifting Section (KKS-code ELG)

The syngas slipstream is taken from the main syngas line downstream the H$_2$S removal (Sulfinol) unit of the Buggenum plant. Traces of Sulfinol solvent are removed in the Syngas Total Feed Wash Column (ELF10 BD010), an absorber consisting of two beds of structured packing. Demineralized water from the Water Make-Up Pump

(ELG55 AP010) is fed to the top of the column on flow control to wash entrained Sulfinol from the gas feed by absorption. A portion of the water from the column bottoms is recycled by the Wash Column Recirculation Pump (ELF21 AP010) to the top of the second bed, reducing wash water consumption. The remaining waste water discharge stream shall be sent on level control to the existing sour water stripper.
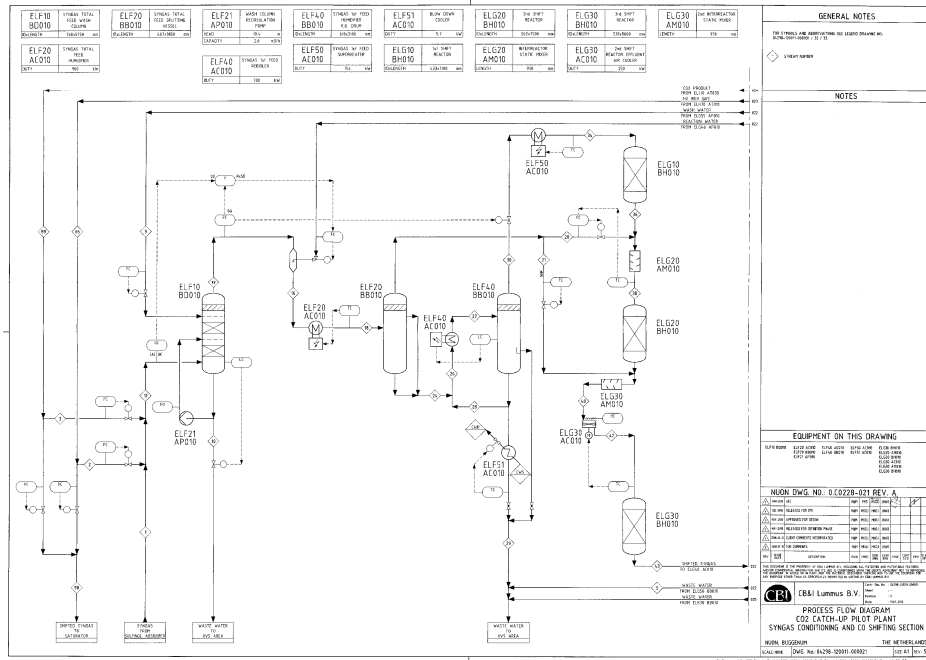

Figure 2-6:   Process flow diagram of the Syngas Conditioning and CO Shifting Section

Washed syngas is mixed with reaction water from the Reaction Hot Water Feed Pump (ELG40 AP010) in the Syngas Total Feed Mixing Eductor (ELF20 AM010). The combined feed is then vaporized and heated to reaction temperature in a series of electrical heaters. The combined effluent from the eductor is first heated on temperature control in the Syngas Total Feed Humidifier (ELF20 AC010) and separated into two vapour streams and liquid bottoms in the Syngas Total Feed Splitting Vessel (ELF20 BB010). The liquid bottoms and the vapour side stream from the vessel are routed to the Syngas 1st Feed Reboiler (ELF40 AC010). The demisted overhead vapour bypasses the first CO shift reactor and quenches the first reactor effluent, and if required, the second reactor effluent as well.

The Syngas 1st Feed Reboiler (ELF40 AC010) operates in thermosiphon fashion with the Syngas 1st Feed Humidifier Knock-Out Drum (ELF40 BB010). The vapour and liquid feeds from the splitting vessel are combined with liquid bottoms from the Feed Humidifier Knock-Out Drum and partially vaporized in the reboiler. The mixed-phase

effluent from the reboiler is separated into a vapour overhead stream and liquid bottoms. A constant flow small waste water blowdown stream is withdrawn from the knockout drum to the Blow Down Cooler (ELF51 AC010), where it is sent to the Sour Slurry Stripper in the WAC. Vapour overhead from the Syngas 1st Feed Humidifier Knock-Out Drum is brought to the desired reaction temperature in the Syngas 1st Feed Superheater (ELF50 AC010) and then fed to the 1st Shift Reactor (ELG10 BH010). Reactor effluent is cooled to the desired reaction temperature by direct quench with vapour on flow control from the Syngas Total Feed Splitting Vessel and then thoroughly mixed in the Interreactor Static Mixer (ELG20 AM010). The quenched feed is then reacted in the 2nd Shift Reactor (ELG20 BH010). The reactor effluent is cooled to the desired reaction temperature in the 2nd Shift Reactor Air Cooler (ELG30 AC010) and then fed to the 3rd Shift Reactor (ELG30 BH010), which is needed to achieve > 90% conversion efficiency. The hot shifted syngas product from the 3rd Shift Reactor is then sent to the Condensate Recovery Section.

Table 2-1:   Shift Reactor Dimensions

Parameter	Reactor 1	Reactor 2	Reactor 3
Diameter (m)	0.432	0.518	0.581
Height (m)	6.19	6.22	6.22
Catalytic Bed (m)	3.50	3.50	3.50
L/d	14.40	11.54	11.52
Catalyst volume (m^3)	0.513	0.740	0.928
Gas hourly space velocity (Nm^3/m^3 h)	3259	4378	3503

The catalyst applied in the pilot plant is Haldor Topsøe's SK-201-2, a copper promoted iron/chromium based HTS catalyst.

2.3.2   Condensate Recovery Section (KKS-code ELG)

Hot shifted syngas from the 3rd Shift Reactor, containing a substantial amount of water vapour, is cooled in the 3rd Shift Reactor Effluent Air Cooler (ELG40 AC010) until most of the water vapour is condensed. The mixed phase effluent is fed to the 3rd Shift Reactor Effluent Rectifier (ELG40 BD010). The vapour phase from the air cooler travels up the randomly packed bed and is counter currently washed with liquid from the Rectifier Cold Effluent Separator (ELG50 BB010) to condense excess water vapour and reduce the recycle of dissolved lights in the reaction water. The rectifier bottoms are recycled on flow control to the CO Shifting Section as reaction water. To maintain adequate level, demineralized water is fed on flow control reset by the rectifier bottoms level.

The overhead vapour from the rectifier is partially condensed in the Rectifier Effluent Condenser (ELG50 AC010) and separated in the Rectifier Cold Effluent Separator (ELG50 BB010). Condensed liquid is refluxed to the rectifier by the Rectifier Cold Reflux Pump (ELG50 AP010). A small blow down of knocked-out condensate is periodically sent to the existing sour slurry stripper to purge the reaction system of contaminants. To periodically analyze the composition of dissolved gases in the condensed liquid, an intermittent stream could be sent to the Water Make-Up Drum on flow control. Shifted syngas vapour from the separator is compressed in the Shifted Syngas Compressor (ELG60 AN010) to overcome the pressure drop of the upstream Syngas Conditioning, CO Shifting and Condensate Recovery Sections, bringing the syngas back to the normal Buggenum operating pressure. The compressed syngas is cooled with cooling water in the Shifted Syngas Compressor Discharge Cooler (ELG60 AC010) and fed to the CO2 Absorber (ELH10 BD010)

The Water Make-Up Drum (ELG55 BD010) is fed with fresh demineralized water on level control. The demineralized water is pumped by the Water Make-Up Pump (ELG55 AP010) and used as wash water in the Syngas Total Feed Wash Column and as supplemental reaction water.
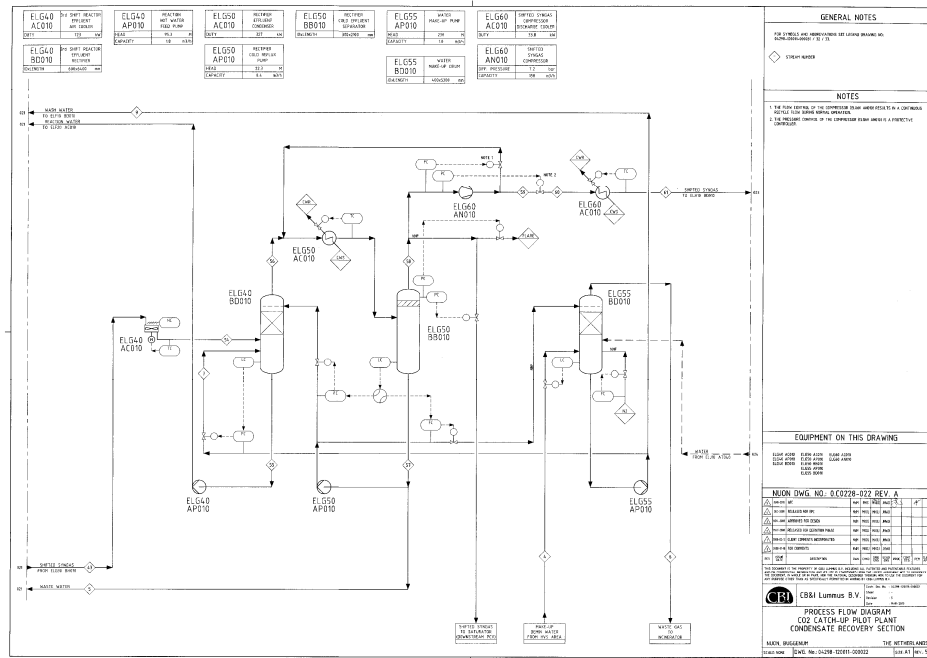

Figure 2-7:   Process flow diagram of the Condensate Recovery Section

2.3.3   CO₂ Absorption Section (KKS-code ELH)

The CO_2 Absorber removes CO_2 from the shifted syngas by absorption using the physical solvent dimethyl-ether of poly-ethylene-glycol (DEPEG). DEPEG is commercially licensed by DOW under the trade name Selexol™ and by Clariant under the trade name Genosorb[R] 1753. In the pilot plant, only the latter solvent has been tested (as the difference between these solvents is marginal).

The shifted syngas is fed at the bottom of the column and counter currently contacts the solvent fed at the top of the column across two beds of packing. The scrubbed overhead vapour exchanges heat with cooling water in the CO_2 Absorber Overhead Cooler (ELH70 AC010) and enters the H_2 Rich Gas Separator (ELH70 AT010) to remove any condensed liquid. The hydrogen rich gas is sent back to the WAC plant. It is also possible to send part of this hydrogen back to the Syngas Conditioning Section to influence the feed composition to the shift reactors.
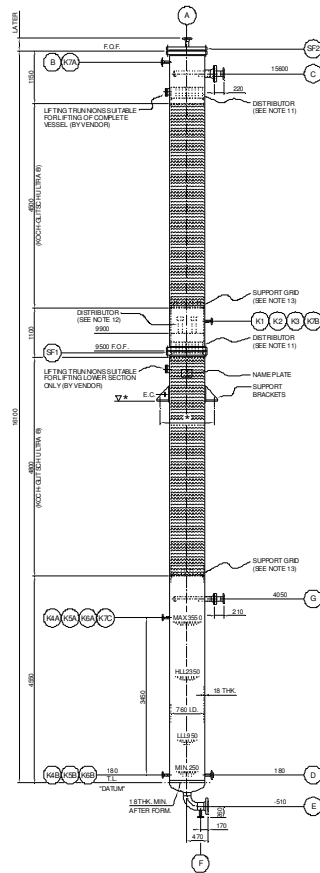

Figure 2-8:   CO₂ Absorber. Height (T-T) is 17 m, diameter is 0.76 m. The two packed beds have a height of 4.5 (top) and 4.8 m (bottom)

CO$_2$ absorbed in the liquid phase is recovered by depressurization of the rich solvent using three flash drums. Rich solvent from the bottom of the CO$_2$ Absorber is flashed and fed to the Solvent 1st Flash Vessel (ELH20 BB010). The first flash drum recovers burnable components (H$_2$ and CO), which is combined with the gas from the 2nd and 3rd Flash Vessels. Liquid from the Solvent 1st Flash Vessel is flashed and can be heated in the Solvent Heater (ELH30 AC010) to increase CO$_2$ recovery and reduce the water content of the solvent. Effluent from the Solvent Heater is fed to the Solvent 2nd Flash Vessel (ELH30 BB010), where more CO$_2$ gas is recovered. To protect against the possibility of solvent foaming and to prevent carryover of small liquid droplets in the exiting vapour phase, demisters have been installed at the vapour outlet of these two vessels. To further protect the downstream CO$_2$ Compression Section from the consequences of foaming in the 1st and 2nd Flash Vessels, the vapour streams from the 1st and 2nd Flash vessels are routed on pressure control to the Solvent 3rd Flash Vessel (ELH40 BB010). The rich solvent liquid stream from the 2nd Flash Vessel is flashed and also fed to the 3rd Flash Vessel. CO$_2$ gas from the Solvent 3rd Flash Vessel is cooled by cooling water in the CO$_2$ Compression 1st Stage Suction Cooler (ELH40 AC010) and fed to the CO$_2$ Compression 1st Stage Suction Knock-Out Vessel (ELH60 AT010). Any liquid that condenses drains back to the 3rd Stage Flash Vessel by gravity. The Solvent Cooler (ELH50 AC010) is used to cool the recovered solvent before it is recirculated to the CO$_2$ Absorber on flow control by the Solvent Circulation Pump (ELH50 AP010). A side stream of solvent is routed to the 1st Flash Vessel through the Solvent Side Stream Filter (ELH50 AT010) and the Solvent Side Stream Adsorption Filter (ELH50 AT020) to remove contaminants.
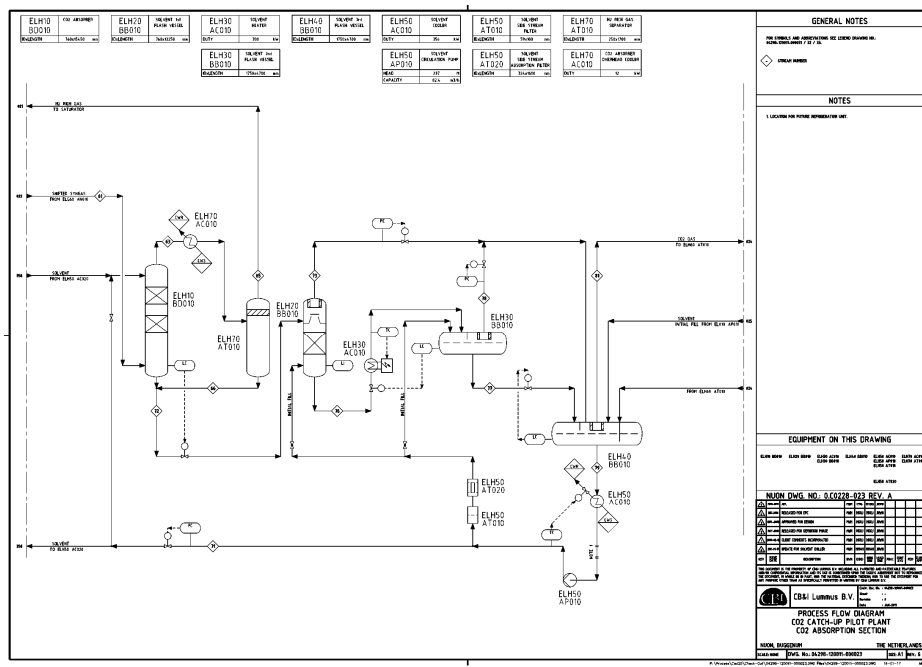

Figure 2-9:   Process flow diagram of the CO$_2$ Absorption Section

2.3.4   CO₂ compression section (KKS-code ELJ)

CO_2 is then compressed in the CO_2 Compressor (ELJ10 AN010). For that purpose an electric motor-driven 2-stage intercooled reciprocating compressor is used. The discharge from the final stage of the compressor is cooled in the CO_2 Compression 2nd Stage Discharge Cooler (ELJ10 AC020) and then fed to the CO_2 Compression 2nd Stage Discharge Knock-Out Vessel (ELJ10 AT020) to remove condensed liquid. Potential liquid condensed in the CO_2 Compression 1st Stage Discharge Knock-Out Vessel (ELJ10 AT010) and CO_2 Compression 2nd Stage Discharge Knock-Out Vessel (ELJ10 AT020) are recycled to the Solvent 3rd Flash Vessel (ELH40 BB010). The resulting CO_2 product is mixed together with the H_2-rich gas from the top of the absorber and fed back to the main syngas line of the Buggenum plant. There is also a possibility to recycle the CO_2 and H_2-rich gas in order to study the effect of different syngas compositions or to send the products to the flare.
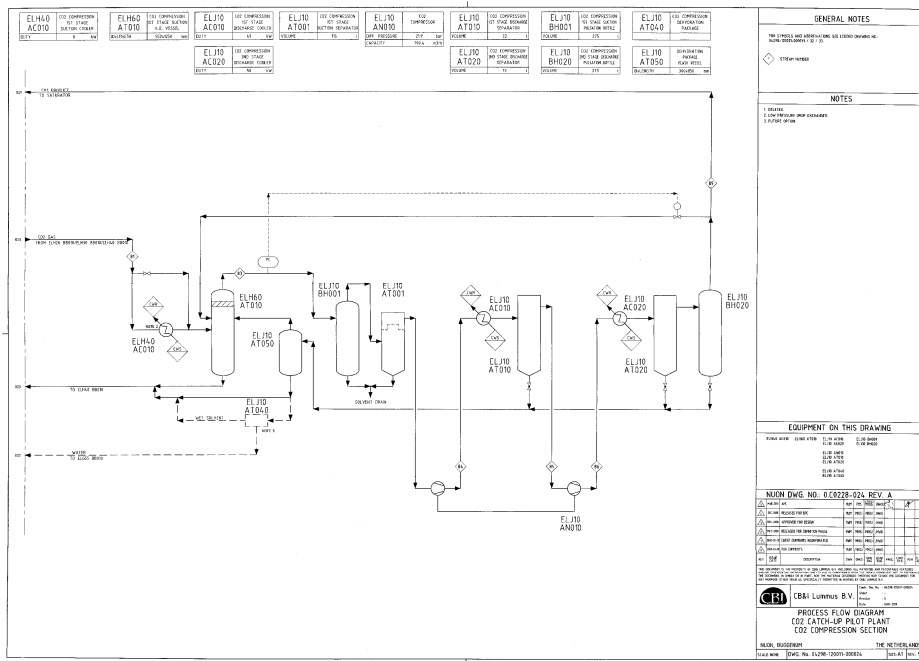
Figure 2-10:   Process flow diagram of the CO₂ Compression Section

Figure 2-11:   CO$_2$ Compressor

2.3.5   Solvent storage section (KKS-code ELK)

The Fresh Solvent Storage Tank (ELK10 BB010) will hold all the fresh DEPEG solvent, which is supplied to the unit by tanker truck. Fresh solvent is supplied to the system by the Fresh Solvent Make-Up Pump (ELK10 AP010) upstream of the Solvent Side Stream Filter, but only during the initial filling stage and to make up losses during normal operation. The CO$_2$ Spent Solvent Drain Vessel (ELK20 BB010) is used as the DEPEG closed drain system and to store the entire solvent inventory of the CO$_2$ Absorption Section. CO$_2$ Spent Solvent Pump (ELK20 AP010) is a sump pump within the drain vessel used to deinventory the system to a tanker truck, if necessary. The CO$_2$ Catch-Up Area Waste Water Pump (GUE10 AP010) is a sump pump used to transfer any waste water spilled in the diked storage area for treatment.

Figure 2-12:   Process flow diagram of the Solvent Storage Section

3 Pilot plant measurements

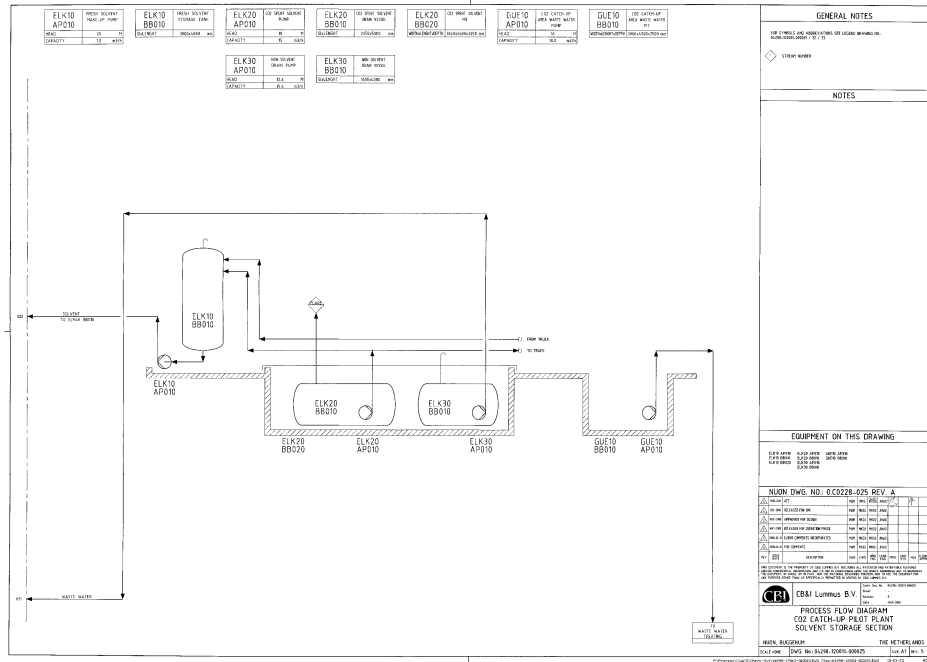## 3.1 Data storage and extraction

Actual and historical measurement data (pressure, temperature, flows, concentrations etc) were stored in ABB's Power Generation Information Manager (PGIM), which is also used for the Buggenum IGCC plant. The data can be presented with the PGIM software itself or can be extracted to Excel for further data analysis.

3.2 Online measurements

In addition to the pressure, temperature, flow and level measurements needed to control the process, the pilot plant is equipped with measurements to get better insights in the process and to validate the models.

Shift reactor temperature profile
The three shift reactors are equipped with multiple thermocouples that allow measuring the axial and radial temperature profiles. The axial temperature profile gives a good indication whether and at which coordinate equilibrium is reached and how it moves in time and upon changes in process conditions. Radial temperature profiles are used to calculate heat losses. Figure 3-1 depicts the three shift reactors and the location of the catalyst bed and thermocouples.
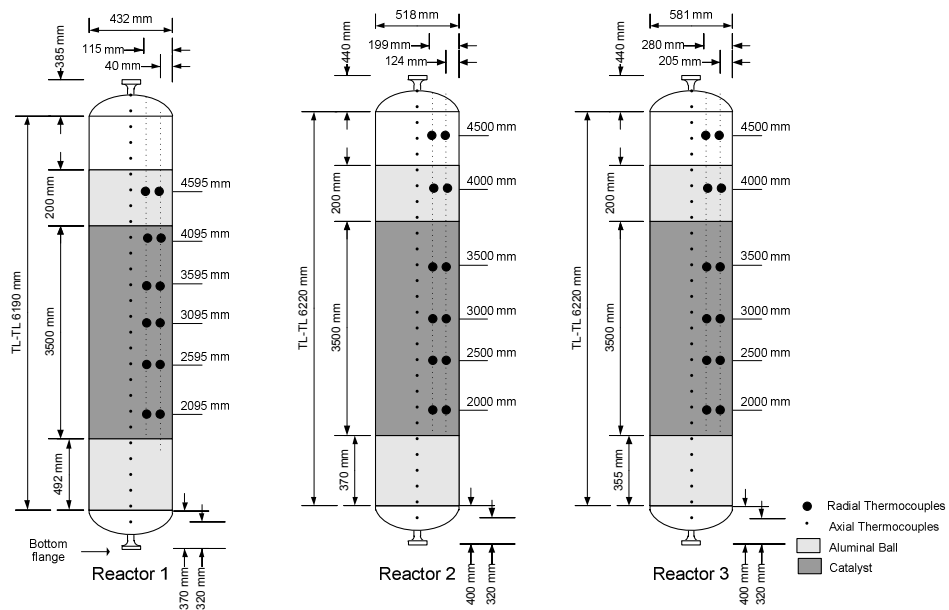

Figure 3-1:   Position of axial and radial thermocouples in Shift Reactors

Gas composition

Two process gas chromatographs (type PCG Maxum II from Siemens) are used to measure the gas composition. The syngas analyzer (ELF50 CQ201) is a 10-stream analyzer (2 parallel blocks of 5 streams) measuring CO, CO_2, H_2, H_2O, N_2 and CH_4 (see Table 3-1). In auto-sequence, it takes 15 minutes for the analyzer to complete the entire cycle of 5x2 streams. It is also possible to put a pair of streams in repeat mode, which enables a more frequent (3 min) measurement of the composition.

Table 3-1:   Syngas analyzer streams (R = Shift Reactor)

Left	Right
A (syngas inlet)	H (syngas in between packed beds absorber)
C (outlet R1)	B (inlet R1)
E (outlet R2)	D (inlet R2)
G (outlet R3)	F (inlet R3)
J (inlet shifted syngas compressor)	I (outlet absorber)

The CO_2 analyzer (ELH20 CQ204) measures the CO, CO_2, H_2, H_2O, N_2, CH_4, H_2S and COS concentration from the flash vessel gas outlets (1, 2, 3) and the compressed CO_2 stream. In auto-sequence, it takes 12 minutes for the analyzer to complete the entire cycle of 4 streams. It is also possible to put a stream in repeat mode, which enables a more frequent (3 min) measurement of the composition.

Both analyzers were regularly validated and (if needed) calibrated with a calibration gas (see Table 3-2). Water was initially calibrated by means of a nitrogen flow saturated in an ice bath. Later, a response factor ratio between CO_2 and H_2O (using thermal conductivity factors for both gasses) was used to calculate the H_2O concentration from the response factor of CO_2.

Table 3-2:   Calibration gas composition

Component (mol/mol)	ELF50 CQ201	ELF50 CQ201
CO	0.1	0.0081
H_2	0.6502	0.082
CO_2	0.199	0.904
H_2O	0.004	0.004
N_2	0.05	0.0081
Ar	0	0
H_2S	0	0.000042
COS	0	0.0000157
CH_4	0.00082	0

Solvent composition

The solvent analyzer (ELH10 CQ202) measures the CO_2 and H_2O concentration from the lean (absorber inlet), semi-lean (in between the packed beds) and rich (absorber outlet) solvent in parallel (3 minutes cycle time).

The analyzer is calibrated using a DEPEG-H_2O blend, of which the composition was measured offline using the Karl-Fischer method. Since the CO_2 will flash from the solvent upon a reduction in pressure, it is impossible to calibrate the analyzer with a calibration blend of DEPEG and CO_2. Therefore, a response factor ratio between CO_2 and H_2O (using thermal conductivity factors for both gasses) derived from an experiment performed by Siemens has been implemented to calculate the CO_2 concentration.

Water pH and conductivity

In order to monitor the quality of the reaction water (outlet ELG40 BD010), rectifier reflux (outlet ELG50 BB010) and waste water (outlet ELF40 BB010), the electric conductivity is measured. The pH, an indicator for the presence of organic (by-) products, is measured in the reaction water (outlet ELG40 BD010), rectifier reflux (outlet ELG50 BB010) and waste water (outlet ELF10 BD010).

3.3   Offline measurements

In order to verify online measurements and get more insight in the chemistry of process gas, water and solvent, a number of several manual sample points are present. The table below gives an overview of manual sampling options.

Figure 3-2:   Example manual sample

Table 3-3:   **Manual sampling options**

KKS code	Medium	Purpose
ELF20 CQ201	Washed syngas	Measure Sulfinol concentration
ELF21 CQ201	Wash water	
ELF51 CQ202	Waste water	Analysis of organic by-products
ELG40 CQ204	Reaction water	
ELG50 CQ203	Reflux water	
ELG57 CQ201	Waste gas	
ELH20 CQ202	Rich solvent	Analysis of degradation products/impurities
ELH20 CQ203	Semi-lean solvent	Measure CO_2 and H_2O concentration
ELH40 CQ201	Semi-lean solvent	
ELH50 CQ201	Lean solvent	
ELH80 CQ201	H2 rich gas	Measure solvent concentration (entrainment)
ELJ10 CQ202	Water	
ELJ10 CQ203	Water + Solvent	
ELJ20 CQ201	CO_2	
ELK10 CQ201	Fresh solvent	Analysis of degradation products/ impurities
ELK20 CQ201	Spent solvent	Measure water concentration

In case the activity, selectivity or stability of the catalyst shows unexpected behaviour, a sample can be taken from a single pellet string reactor (SPSR), two of which are installed in parallel to the 1st Shift Reactor. This allows easy access to the catalyst that has been exposed to the syngas. Additionally, different catalysts can be tested at the same time.

Figure 3-3:   Parallel shift reactors

3.3.1 Water analysis

In addition to online analysis of the syngas CH_4 content, which is an indicator of (changes in) catalyst selectivity, the water streams in the shift section can be sampled for offline analysis of organic by-products like oxygenates (methanol, ethanol, formic acid, acetic acid) and higher hydrocarbons (ethylene, ethane, propylene, propane). Methanol will be present up to a few ppm (dry syngas basis) after the first reactor, and up to 20-30 ppm after the second/third reactor and will dissolve in condensate. Typically, 5% of methanol is converted into ethanol. Formic acid is typically a few ppm in dry syngas and acetic acid is generally not found in HTS (personal communication Haldor Topsøe). Fischer-Tropsch reaction is catalysed by Fe_5C_2 (which can be formed when operating the catalyst at too low steam/CO ratio). Also Ni from the gasifier may deposit on catalyst and cause methanation. C1 (already present in syngas up to 100 ppm) and C2 (probably below detection limit) will stay in the syngas, C3 and C4 will dissolve in the condensate when formed.

Intertek Polychemlab measured the organic by-products (specifically the oxygenates) in 2 batches of water samples. Ethanol and methanol were measured with GC-FID and formic acid and acetic acid are measured with HPLC. The results are given in the table below.

Table 3-4:   Water analysis for oxygenates in [mg/kg]

Sample	CH_3OH	C_2H_5OH	$CHOOH$	C_2H_3OOH
Reference	<5	<5	<0.1	<0.1
Reaction water ELG40 CQ204 (12-04-2012)	6	<5	4.4	1.7
Reflux water ELG50 CQ203 (12-04-2012)	260	55	4.5	224
Reaction water ELG40 CQ204 (25-04-2012)	12	<5	2.9	1.0
Reflux water ELG50 CQ203 (25-04-2012)	474	30	0.3	0.8

Generally, the repeatability is poor (which may be explained by the way the samples are taken). During the test programme a method was developed using CH_4 concentra-

tions measured by the GC as indicator for carbide formation/Fischer-Tropsch reaction and the offline water measurements were stopped.

The Sulfolane concentration of the waste water from the Syngas Total Feed Wash Column (sampling point ELF21CQ201) was measured at 37 mg/l (18 and 19 December 2012).

3.3.2 Solvent CO_2 concentration (loading)

During the test programme, several samples were taken from the solvent in order to measure the CO_2 concentration in the DEPEG (so-called loading), as the online measurement was either not available or unreliable (in case of semi-lean and rich loading, where flashing in the sampling system prevented reliable measurements) or to verify the online measurement (in case of the lean loading, which was derived via the H_2O:CO_2 response factor ratio).

Two attempts were made to set up a methodology to measure the lean loading. In the method developed by Intertek Polychemlab, first a helium[4] flow was submitted to the bottom of the cylinder containing the DEPEG-CO_2-H_2O mixture. The stripped CO_2 was led into three sequential bottles with potassium hydroxide. After the last bottle a bottle with calcium chloride was placed. If any CO_2 that was not trapped by the three KOH bottles white deposits from the $CaCO_3$ formed would become visible. The potassium hydroxide solutions were analyzed with help of a total carbon analyzer to calculate the CO_2 concentration. Unfortunately, the measured concentrations were significantly lower than the expected equilibrium concentrations, so it was decide to stop the experiments.

ECN developed a two-step approach:
1. Perform saturation/stripping experiments in order to determine the maximum amount of CO_2 (g/ml) that is dissolved in lean DEPEG (i.e. temperature and pressure in the 3rd Flash Vessel). Stripping is performed by nitrogen.
2. Recover CO_2 by means of Total Inorganic Carbon analysis. Initially attempts were made to trap the CO_2 released from the DEPEG in the desorption step into a washing bottle filled with 200ml 0.1 M NaOH. It appeared that the trapping liquid did not capture all CO_2 and a significant amount bypassed the liquid resulting in a poor recovery. Therefore the trapping of the CO_2 released from the DEPEG was performed on an "Ascarite" solid absorber column, that is NaOH absorbed on a solid material. It was verified that the CO_2 slip using this column was negligible

---

[4] Nitrogen was tested as well, but performance was not satisfactory

With this approach, the theoretical loading (equilibrium data) of CO_2 in DEPEG is experimentally confirmed. The capture of CO_2 desorbed from the DEPEG on an Ascarite column, followed by TIC analyses resulted in a $100 \pm 2\%$ recovery of CO_2.

A next step would be to verify the approach using pressurized samples as taken in the pilot plant. The main concern during pressure release is to prevent solvent carry-over to the Ascarite column. Due to time constraints, this exact experimental lay-out, however, has not been tested at ECN. It also needs to be verified whether the method is suitable to measure rich loading.

4 Pilot plant operation

After introducing the mode of operation in 4.1, an overview of plant statistics will be presented in 4.2 together with a time line of events happening along the plant operation. An overview of plant modifications in terms of hardware, control approach and instrumentation is presented in 4.3. The results of plant inspections and corrosion measurements after plant shutdown is discussed in 4.4 followed by the lessons learned in the area of health, safety and environment (HSE).

4.1   Mode of operation

The plant was operated from the local control room by dedicated operating crew, originally consisting of 5 operators and 1 O&M coordinator. In the first period the plant was operated 24/7 and continuously supervised. As the plant was generally fully automated, the operating crew was relieved from implementing simple control and sequential actions and focus on more demanding fine-tuning of the plant parameters as well as on executing test runs. After the initial functional testing period it was confirmed that the plant operates stable and does not require continuous control actions from the operators for maintaining stable operation. The testing process requires however crew-member presence in order to monitor the quality of experiments. Especially important were transition moments from one set-point to another requiring an educated judgement on whether a steady state was reached. The time to reach a new steady-state after some parameter change could take a few hours, which allowed for setting the experiment as the last action before the night shift and collect results in the morning. In addition, the syngas composition could change during the test runs due to change in load and fuel (coal type, biomass co-firing).

After the initial period it was decided to change the operating regime to fully automatic with manned supervision during the work-days only. Some small adjustments to the supervisory control systems were implemented for shortening start-up times and to prevent excessive thermal stress on the catalyst in case of an automatic trip. The changes resulted in reducing the operating team to 2 operators and 1 O&M coordinator. During night shifts and weekends the plant was handed over to the WAC shift for emergency supervision only. Additionally a remote control access was realised to allow the O&M coordinator to act upon undesired operational incidents happening in those periods.

Some external factors also had impact on the operation of the plant. In the beginning of 2011 it was decided to shut down the Willem-Alexander IGCC Power Plant for summer months as a reaction to the changing market conditions. During May through

August the plant was undergoing scheduled maintenance. Due to the unavailability of syngas, the pilot plant operation was also suspended.

4.2 Operational statistics

Table 4-1 and Figure 4-1 give an overview of the plant operational statistics.

Table 4-1:   Operational statistics

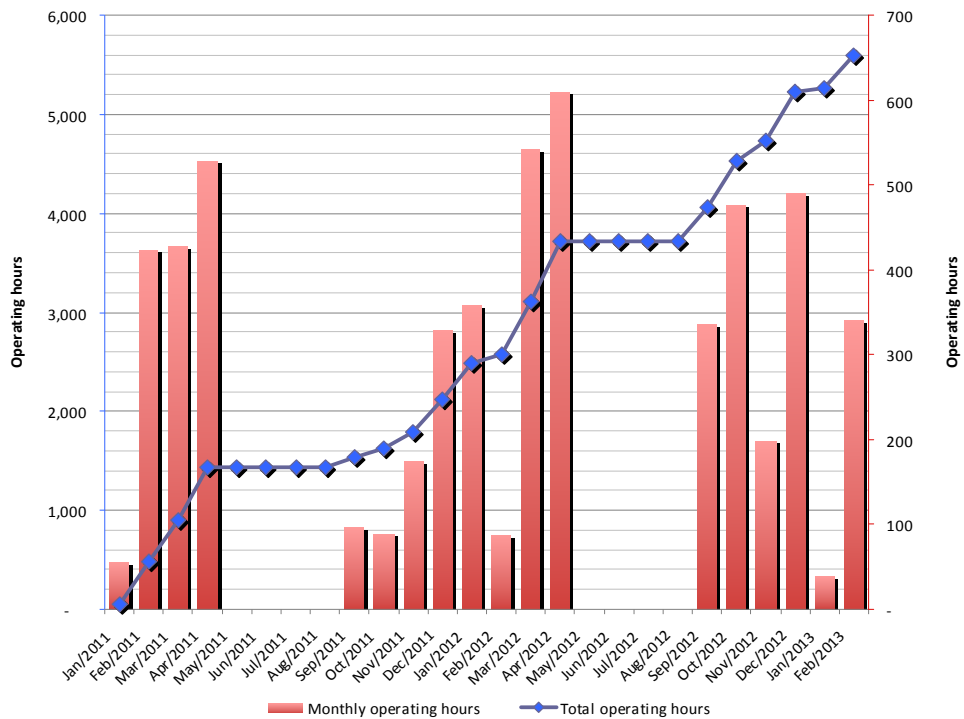| Total operating time:	5886	Hours
Total Syngas consumption:	6235	Ton
Total CO_2 production:	4478	Ton
Total electricity consumption:	9184	MWh
Number of starts:	39	
Number of trips/shut downs:	16	
Number of test runs:	61	
Number of Lost Time Incidents in the lifetime of the project:	0	

Figure 4-1:   Pilot plant operating hours

The first CO_2 molecules were captured on 28 January 2011. The following months brought increasing trend of operating hours leading to stable operation in April 2011. During this period the main issues with plant stability were resolved and the problems with the sampling and analyser system were investigated. During the maintanance shut down in May-August 2011 a number of improvements and corrections were implemented (see Figure 4-2). The main focus was on installing additional instrumentation identified as desirable by the R&D team but omitted during the initial design. After resuming the operation in September 2011 a new test campaign was initiated. Although the analyzers were available, there were still problems which will be discussed later. One of the causes identified was related to the sample supply line tracing. New sampling tubes were ordered and installed later in this operating period. In May 2012 the plant was again taken out of operation due to the planned maintanance stop of the WAC plant during the same period. The time was used to implement some more hardware changes and adjustments to the DCS control loops. The plant was started for the last test campaing in September 2012 and operation stopped March 20 2013.
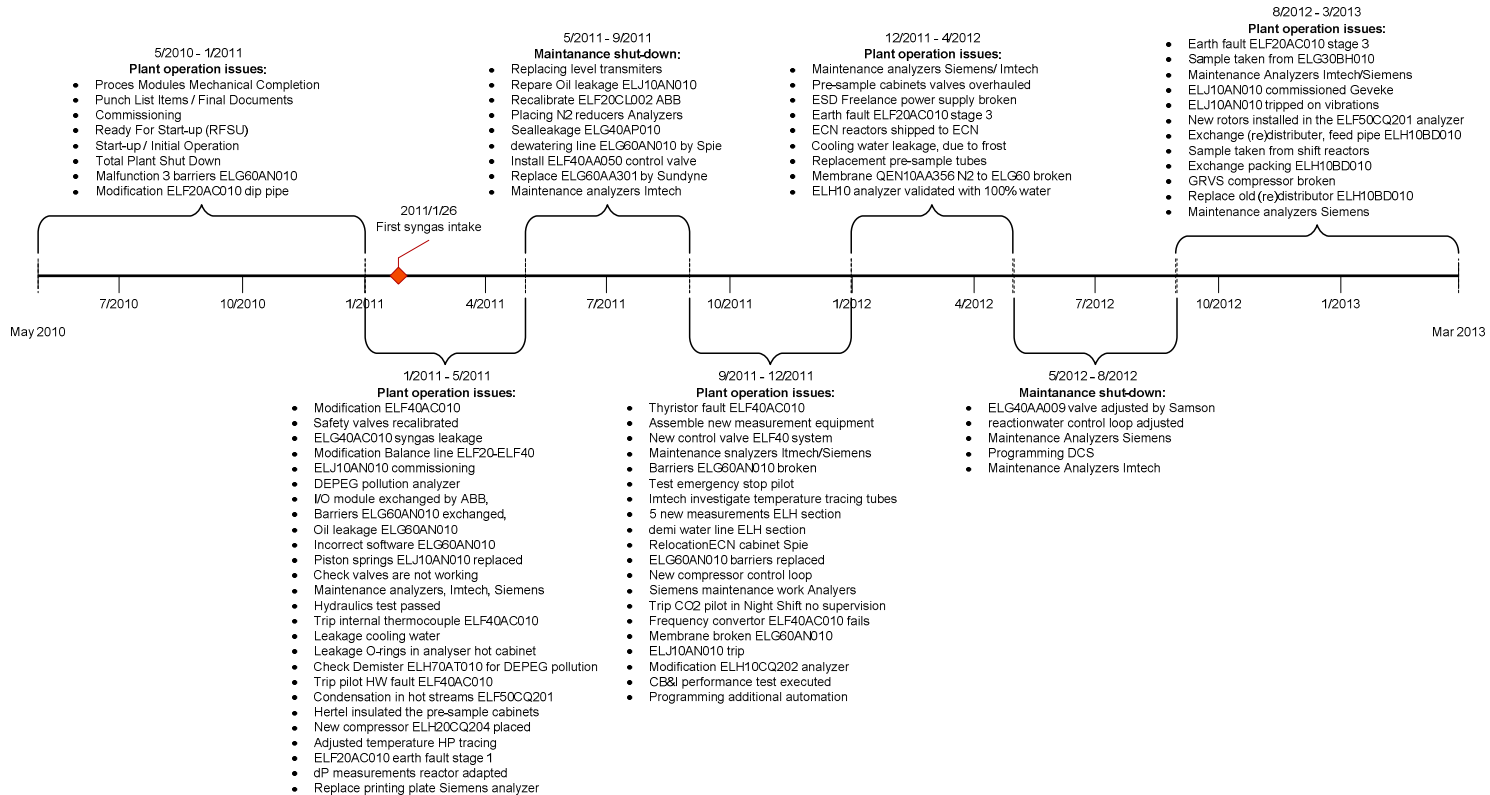
Figure 4-2:   Timeline

4.3   Plant design and operational issues

4.3.1   Hardware

4.3.1.1   Syngas conditioning section (KKS section code: ELF)

The main troubles in operating the ELF section were encountered in between two vessels: ELF20 BB010 and ELF40 BB010. The initial set-up proved to be unstable in operation due to variations in liquid levels and various equipment design errors discussed below.

Equipment name:	Syngas total feed humidifier
KKS code:	ELF20 AC010
Problem:	Outlet temperature of the syngas-water mixture is insufficient
	Plant trips due to electrical rod overheating.
Solution:	Install a dip pipe for creating a water level and immersing electrical rods in the liquid.
	Disconnect a part of electrical rods.

Initially the heater ELF20 AC010 was designed to heat a mixture of syngas and a fine mist of liquid water in order to evaporate the droplets. However the liquid water injection valve ELG40 AA050 did not function properly resulting in uneven vapour/liquid flow. The reason was that the required discharge pressure of ELG40 AP010 was not reached due to pump inefficiency. Additionally the orientation of the baffles in the heater was mistakenly implemented (horizontal plane instead of vertical). As a result liquid water was flowing through the supply line to the heater accumulating in the bottom and draining through the outlet nozzle. When trying to vaporize the water by increasing the duty, the additional generated heat is evenly distributed over the cross-sectional area of the electric heater and not properly transferred to the liquid water. Consequently the generated heat will heat-up the (upper) thermocouples of the electric heater to temperatures above the trip setting of 350 ˚C. Basically, the heating rods were designed for a mixture of syngas and water with a heat capacity higher than that of syngas alone.

In consultation with the equipment supplier a solution was decided to change the principle of operation to directly evaporating water by creating a liquid level and immersing the electrical heating rods. Installing a dip pipe (see Figure 4-3) at the outlet nozzle created a water level in the shell of the heater. A part of the heater's electric rods were immersed in the liquid and provided sufficient quantity of energy to evaporate. The remaining rods in the gas path were disconnected to avoid overheating.
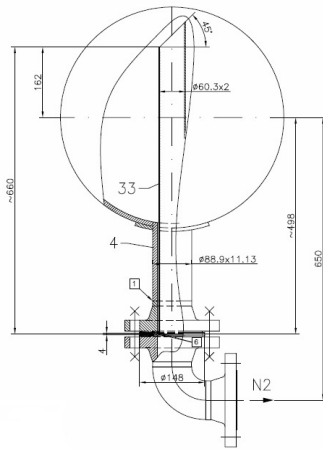
Figure 4-3:   Dip pipe installed at the syngas total feed humidifier

The problems are due to the fact that the water pump, injection valve and evaporator were not engineered as a single package by a specialist vendor. For the full-scale plant, it is therefore recommended to engineer the entire package including control (like for desuperheaters). An alternative approach would be to implement the current solution from the pilot plant (evaporate the water), however the design of the gas-gas heat exchangers as applied in the full-scale plant will be more complex for 2-phase flows. A third option would be to abandon the approach of internal evaporation and inject steam directly. In this way, the costs of the heat exchangers are avoided (capital expenditures) at the expense of energy requirements (operational expenditures). So for the full-scale plant it is recommended to study this in more detail.

Equipment name:	Syngas 1st Feed Reboiler
KKS code:	ELF40AC010
Problem:	The circulation function is disturbed by unexpected flow effects
Solution:	Modify the supply line

The functioning of the reboiler was tested with nitrogen only and worked properly. During initial operation with nitrogen and water the plant tripped due to electrical rods overheating although the desired temperature was still not reached. It was observed that there was not enough liquid in the reboiler. After investigation it was noticed that the syngas supply line from ELF20 BB010 was connected to the effluent line at the bottom of the ELF40 BB010 vessel (see Figure 4-4a). Instead of flowing to the ELF40 AC010, the syngas was flowing to ELF40 BB010 (lower pressure drop), causing the liquid circulation (thermo-siphon function) to be disturbed and even reversed. In effect there was no sufficient supply of the liquid to the reboiler. The problem was resolved by connecting the supply line ELF40 BR010 to the drain nozzle of ELF40 AC010.
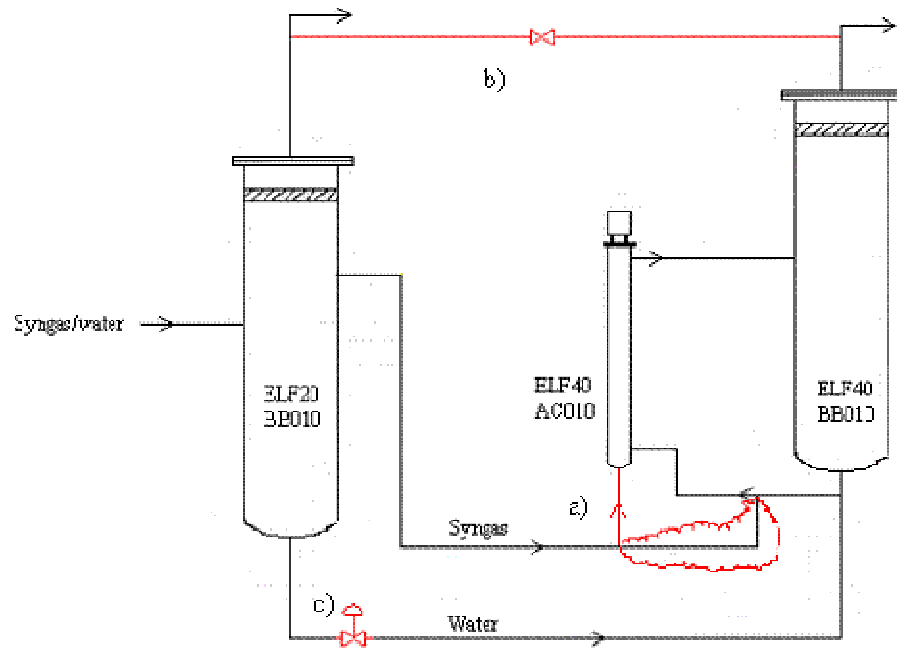
Figure 4-4:   Modifications of the ELF20-ELF40 system: a) modified supply line to the Syngas 1st Feed Reboiler (ELF40AC010); b) So-called "balance line"; c) Check valve ELF21 AA015

Equipment name:	Balance line
KKS code:	Line between ELF20 BB010 and ELF40 BB010
Problem:	Pre-heating catalyst with dry nitrogen not possible
Solution:	Install additional balance line

During the start-up process the catalyst beds are preheated with pure nitrogen. However since it passes two vessels ELF20 BB010 and ELF40 BB010 upstream, the nitrogen becomes saturated with water, which subsequently condenses at the catalyst beds in the CO shift reactors. The proposed solution is to reroute the nitrogen stream to bypass the vessels and avoid saturating with water. A so-called "balancing line" was installed (see Figure 4-4b).

Equipment name:	Check valve
KKS code:	ELF21 AA015
Problem:	Minimum flow through the valve is not reached
Solution:	Remove the valve

During initial plant operation it was found out that the check valve ELF21 AA015 (see Figure 4-4c) causes significant pressure drop and results in not reaching minimum flow required. Therefore it was decided to remove the valve from the system. This is a typical problem related to the scale of the pilot plant, where proportions between the required flow and flow resistance through due to small diameters are different that those in a full-scale plant.

After implementing the above plant modifications the stability of the system improved significantly, which can be seen in Figure 4-5.
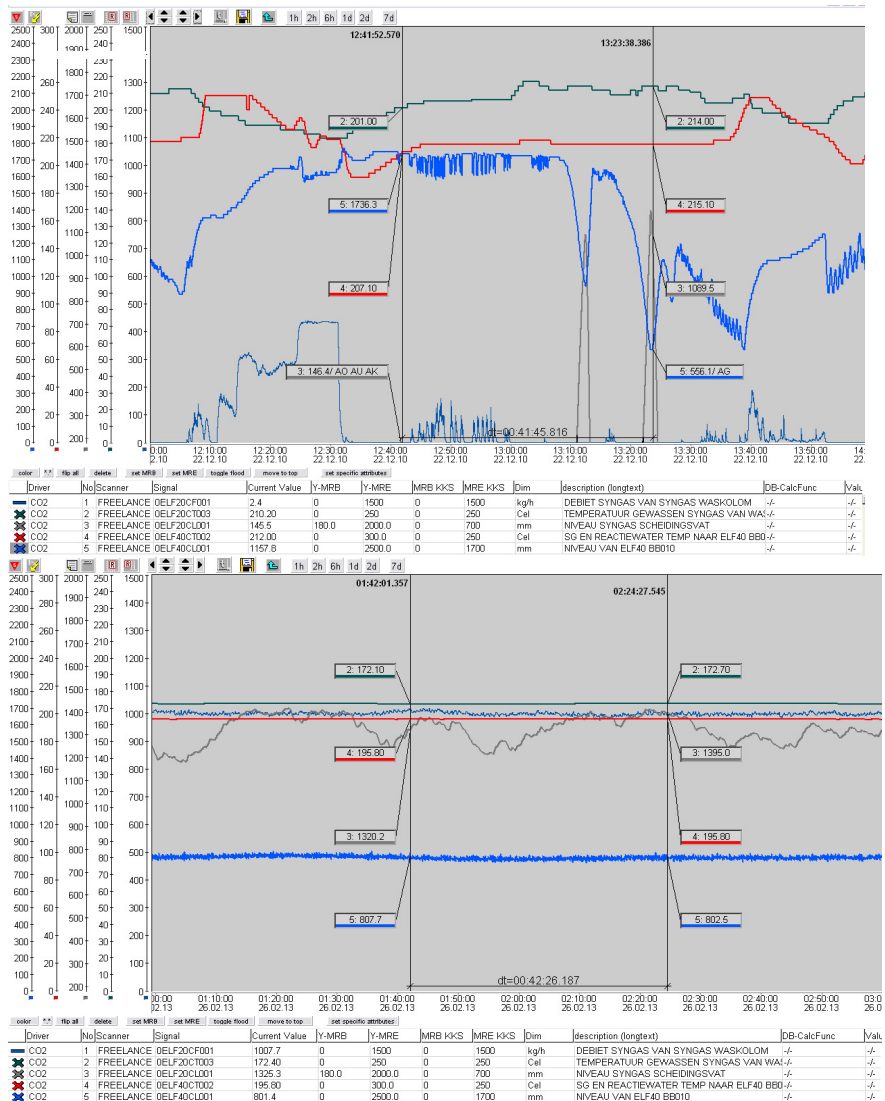

Figure 4-5:   **Parameter stability before (above) and after (below) implementing plant modifications in the ELF20-ELF40 system**

4.3.1.2   CO shifting and condensate recovery section (KKS section code: ELG)

Equipment name:	Parallel reactors
KKS code:	ELG11/12 BH010
Problem:	No reaction taking place
Solution:	Reduce heat losses

In order to allow for easy access to the catalyst samples without opening the main reactors, two small single-pellet-wide tubes loaded with various catalysts were installed in parallel to first reactor. Initial operation indicated however that the CO shift reaction was never started in those parallel reactors. The reason was found in the large heat loss along the gas supply line. The heated cabinet containing the parallel reactors was located far away from the main reactors causing a long supply line, which was not sufficiently traced. The diameter of the line was very small and there-fore causing difficulties to apply electrical wiring around it. As a solution the cabinet was relocated to reduce the supply line and the diameter of the line was also increased. Finally the electrical tracing applied was maintaining the desired inlet temperature.

Equipment name:	3rd Shift Reactor
KKS code:	ELG30 BH010
Problem:	Inlet temperature not reached during start-up
Solution:	Insulate the cooler ELG30 AC010

During the initial start-up of the CO shift section, which occurred in the winter period the inlet temperature of the 3rd reactor was not reached and subsequently the CO shift reaction was not started. The cause was the heat loss in air cooler upstream the reactor (ELG30 AC010), where even with fully closed louvers some heat losses occurred. The problem was solved with additional insulation applied around the cooler. The problem could have been easily avoided by installing a bypass line around the cooler.

4.3.1.3   CO$_2$ absorption section (KKS section code: ELH)

Equipment name:	Absorption section
KKS code:	ELH
Problem:	Control of water content in the solvent
Solution:	Direct Water injection

In order to control the water content of the solvent, a dehydration unit was included in the original design. Potential liquid condensed in the CO$_2$ compression knockout

drums downstream the 1st and 2nd compression stage is routed to the dehydration package. Here, entrained solvent is separated from the knockout drum water stream and returned to the 3rd flash vessel. The water removed in the dehydration package is then recycled to the water make-up drum. For several reasons it was decided to exclude this dehydration unit in a later stage (the necessity for this unit was debated as it is not required in the Magnum plant and the design of the dehydration unit was not that straight-forward). Draining the content of the compression knock-out drums or sending the CO_2 (with water) to the flare and varying the duty of the solvent heater ELH30AC010 were considered to be adequate strategies to control the water content.

In the first test campaign, 3 modes of operation were tested:
- heater ELH30 AC010 in operation and sending the CO_2 (with water) to the flare, resulting in an equilibrium water content of 0.65 wt%.
- heater ELH30 AC010 out of operation and sending the CO_2 (with water) to the flare, resulting in an equilibrium water content of 0.90 wt%.
- heater ELH30 AC010 out of operation and recycling the contents of ELJ10 AT050 back to ELH40 BB010, which resulted in water contents above 7 wt% and still equilibrium was not achieved, resulting in excessive pressure drops in the absorber.

Hence 2 stable points were achieved with water contents that are low in comparison to the typical values applied in the Selexol process of around 4-5 wt%. In order to increase the plant flexibility it was decided to implement a water connection to the lean solvent line allowing for adding a controllable amount of water to the system.

4.3.1.4 CO_2 compression section (KKS section code: ELJ)

Equipment name:	CO_2 compressor
KKS code:	ELJ10 AC010
Problem:	Deposits at the compressor parts downstream the intercooler
Solution:	unknown

In December 2011, during maintenance activities it was found that traces of some unidentified substance (possibly DEPEG) deposited on CO_2 compressor pistons in the second stage downstream of the intercooler. Attempts by the equipment supplier to identify and explain the cause of the problem were not successful. If the traces are indeed DEPEG the question remains why no traces were found in the first compression stage. This issue needs to be investigated in more detail for the design of the full-scale plant.
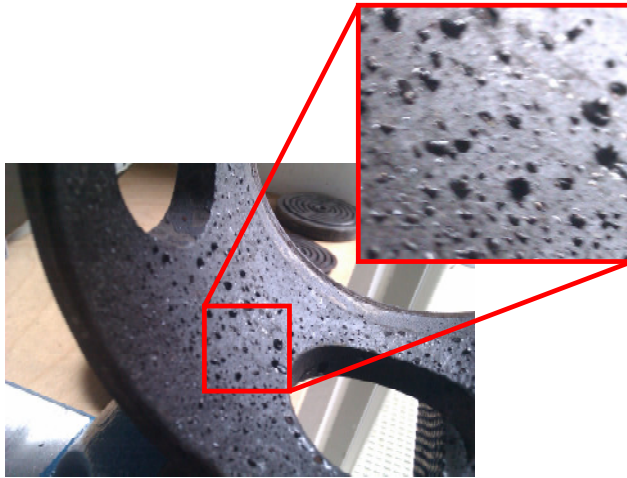
Figure 4-6:   **Deposition on the compressor components**

4.3.2   *Control system*

4.3.2.1   Syngas conditioning section

System name:	ELF20-ELF40 system
Problem:	Unstable behaviour
Solution:	Adjusted control loop, valve replacement

As mentioned before the ELF20-ELF40 system was unstable during the initial start-up of the plant. Proposed solution led to a number of hardware modifications as already described. There was also a need for control system adjustments. It was found that the reaction water injection valve (ELG40 AA050) was highly non-linear causing difficulties in precise control leading to fluctuations in the water flow, which affected the parameters in the shift section downstream. The valve was replaced for a more suitable one and the control loop was reprogrammed. Also the reboiler control needed to be reprogrammed.

The relevant control loops of the ELF and ELG section are the following:
- The ELF20 AC010 heater duty is determined by the ELF30 CT002 temperature measurement. This control loop directly determines the steam content of the quench to reactor 2.
- The water feed flow ELG40 CF001 is determined by the levels within the ELF20 BB010.
- The level of the ELF40 BB010 is controlled by the valve ELF40 AA050.
- The syngas flow ELF20 CF001 results from the reactor 1 feed flow (valve position ELF50 AA050, flow measured by ELF50 CF001) and the reactor 2

quench flow (valve position ELF31 AA050, flow measured by ELF31 CF001).

- The quench flow ELF31 CF001 is determined by the quenched syngas temperature ELG20 CT003.
- The ELF40 AC010 heater duty is determined by comparing the measured reactor 1 feed flow ELF50 CF001 with its calculated value. The calculation of this value is schematically represented in Figure 4-7. The calculated ELF50 CF001 SP is the difference between the feed flows of syngas and water on the one hand and the quench flow, water drain and reactor 2 bypass flow on the other hand. All flows are measured, except for the water feed flow, which is calculated based on the syngas feed flow ELF20 CF001 and the ratio setpoint. The ratio setpoint is the mass ratio of water over syngas entering ELF20BB010. Within this control structure, correction parameters can be set for fine-tuning of the heater duty.
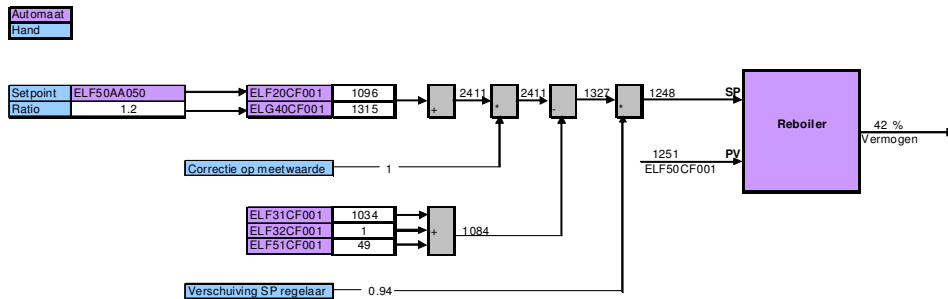
Figure 4-7:   Control structure of ELF40 AC010
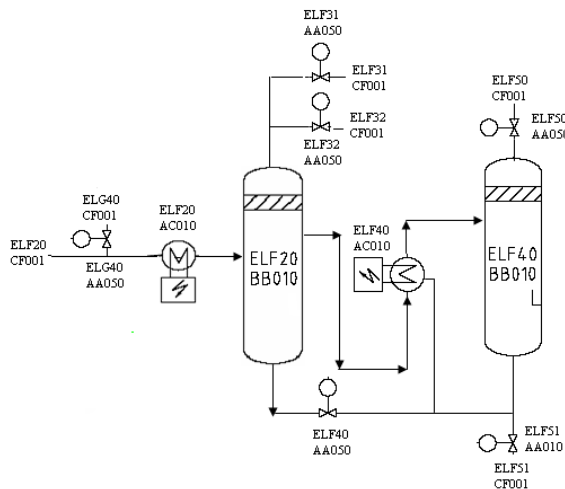
Figure 4-8:   ELF20-ELF40 system

The above-mentioned changes resulted in the improved stability as seen in the trends in Figure 4-9.
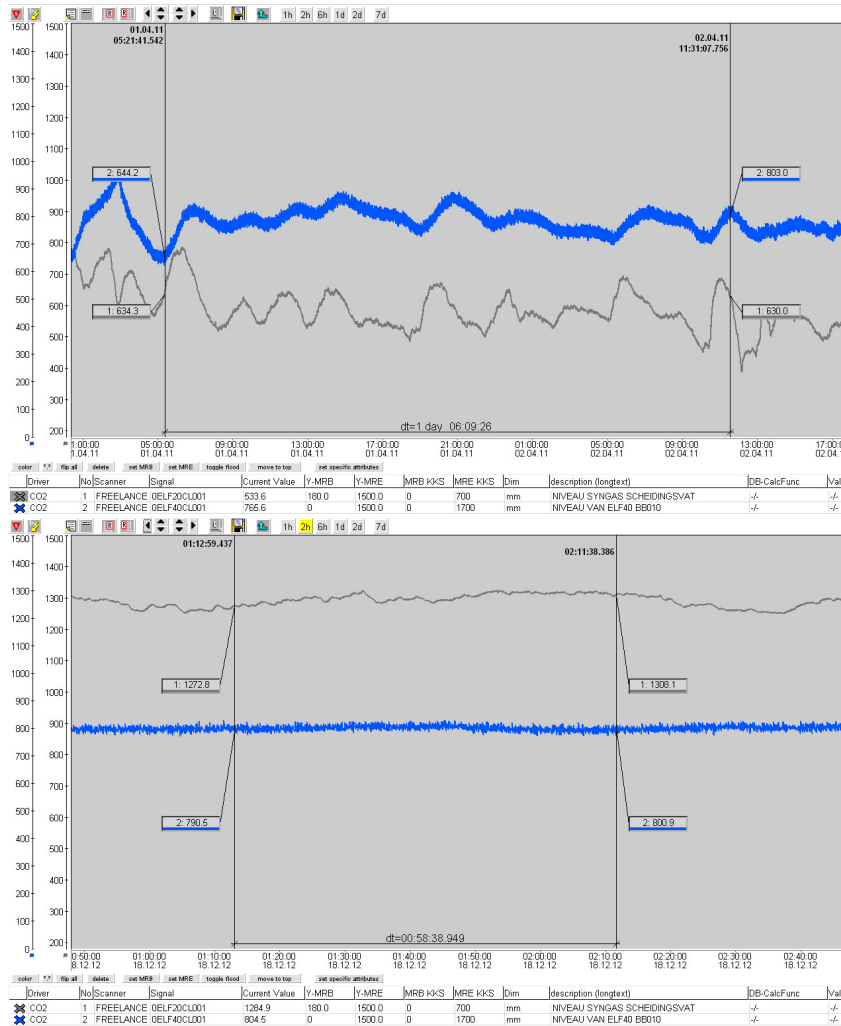
Figure 4-9:   Improvement in level stability of ELF20-ELF40 system; the initial state with visible instabilities in the signal trends (above) and the state after the modifications, showing clear improvements in signal stability (below).

System name:	ELF section
Problem:	Temperature excursions in 1st reactor upon trip
Solution:	Ensure that syngas is shut-off when reboiler (or water supply) trips.

A trip of the pilot occurred on March 3, 2011, resulting in a temperature excursion of reactor 1 to values well above 600°C, while operation of reactor 2 and reactor 3 was

not compromised. This occurred at a time on stream of about 450 hr. The resulting bed temperatures in time and the evolution of the axial temperature profiles in time are represented in Figure 4-10 and Figure 4-11, respectively. The trip consisted in a failure of the ELF40 heater, while the syngas feed flow was not stopped directly. This caused the steam content of the reactor 1 feed to temporarily drop, causing a large increase in the adiabatic temperature rise within the reactor.

Figure 4-10:   The reactor 1 bed temperatures in time during the trip

Figure 4-11:   The reactor 1 axial temperature profiles for different times during the trip

In Figure 4-11 it is observed that the high temperature is already reached for the front part of the bed. As this temperature increase travels through the reactor it broadens and probably the p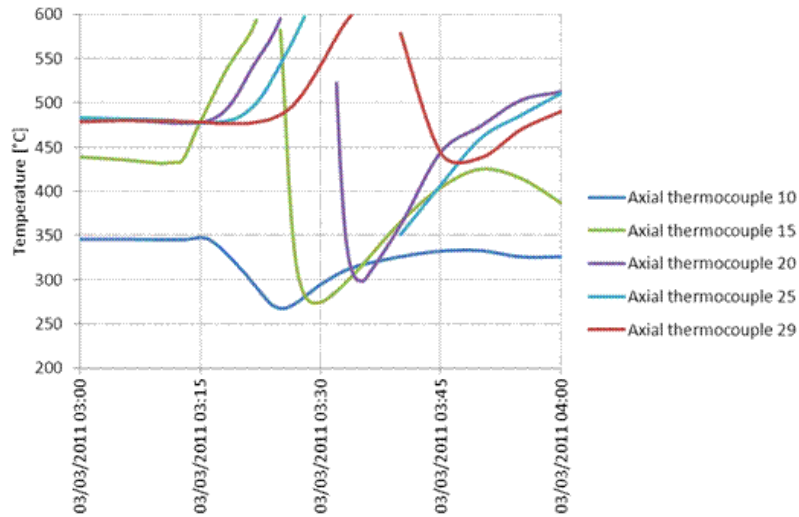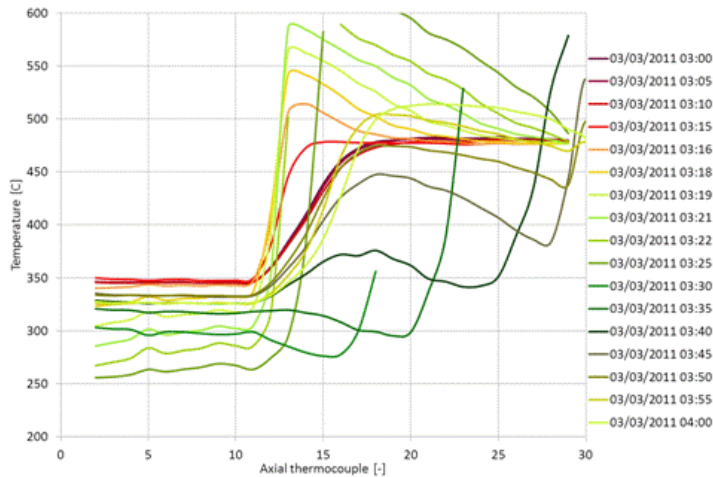eak temperature decreases going through the bed. For the front part of the bed, therefore the peak temperature was highest but travelled fastest (catalyst was exposed to >600°C for a few minutes), while the downstream part experienced the lowest peak temperature but for a longer period (catalyst was exposed to >600°C for 15 minutes).

To avoid such temperature excursions, it is essential to ensure that when the water supply is stopped (e.g. by tripping the reboiler) the syngas flow is shut-off immediately. Fortunately, it can be concluded from the relative activity calculations that the reactor 1 catalyst activity did not suffer noticeably from the observed large temperature excursion. Possibly, the exposure time was sufficiently short not to have caused excessive sintering or reduction of the catalyst.

4.3.2.2   CO shifting and condensate recovery section

System name:	Syngas compressor
Problem:	DEPEG found upstream of the absorber, no stable control of the absorber pressure
Solution:	Adjust control loop of ELG60AN010

By inspection of the mechanical filter upstream of the CO_2 absorber it was found that some DEPEG was carried over with the H_2 rich gas and trapped in the filter. Problem investigation indicated that during the plant start-up, when there was no sufficient pressure in the absorber, the syngas compressor discharge valve was opening too quickly. The large quantity of syngas rapidly entering the absorber was blowing the solvent away.

A solution included an adjusted start-up procedure in which the discharge valve of the compressor ELG60 AN010 is initially shut-off and the anti-surge recycle valve is fully opened in order to circulate the gas and ramp the compressor up. After reaching the operating point the discharge valve is being slowly opened introducing the shifted syngas to the absorber.
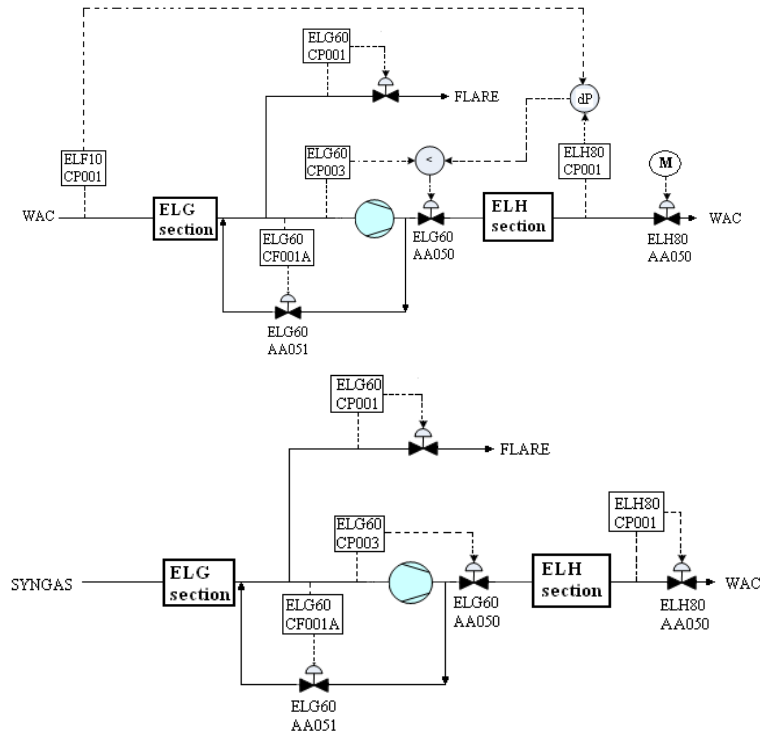
Figure 4-12:   Syngas compressor ELG60 AN010 control loop; initial set-up (above) and the state after the modifications (below)

The overall control loop of the ELG60 AN010 compressor was complex and difficult to manage (see Figure 4-12). It included a case selector for the discharge valve control. On one side the compressor discharge was controlled based on the suction pressure but additionally based on the pressure difference between discharge and suction sides. Besides the regular control loop an anti-surge loop is installed acting on the recycle valve ELG60 AA051 based on flow measurement ELG60 CF001A located on the suction line. It was decided to simplify the initial control approach. Therefore the compressor discharge valves became directly controlled based on the suction pressure.

Additionally the valve ELH80 AA050 setting the flow to the CO_2 absorber was controlled manually. Due to long reaction time adjusting the flow was very laborious and time consuming. The research objectives required the shifted syngas flow to be controlled in a stable manner. Therefore, the valve ELH80 AA050 was automated allowing for fine adjustments of the flow in a stable manner.

4.3.2.3 CO$_2$ absorption section

System name:	Solvent loop
Problem:	Difficulties with the plant start-up
Solution:	Pressurize ELH20 and ELH30 vessels with syngas

During the plant start-up not enough CO$_2$ is absorbed and flashed to create the pressure in the flash vessels required to enable solvent circulation. Initially this problem was solved by pressurizing the first and the second flash vessels with nitrogen using flexible hoses. Later the absorption system was pressurised directly by opening the syngas supply valve enabling solvent circulation.

System name:	Solvent loop
Problem:	Instable behaviour of ELH20 BB010
Solution:	Level control of ELH30 BB010

In the original design the level of the second (ELH30 BB010) and the third flash vessels were controlled and the level of the first flash vessel (ELH20 BB010) was resulting. Consequently the level in ELH20 BB010 (and also the pressure) was fluctuating strongly. The control approach was converted such that the ELH20 BB010 level is controlled instead of the ELH30 level. ELH20 BB010 is a vertical vessel with the level changing more with a comparable volume of liquid. As a consequence even the smaller variation, previously fitting in the dead band of controller tolerance, is acted upon by the control system and the respective valve openings are adjusted accordingly leading to less hectic operation.

4.3.3 Instrumentation

During the test programme, it was found out that several measurements (see below) could only be monitored locally and not very precise (not available through the PGIM system), which complicated the (analysis) of the experimental data. This was changed in the first plant shutdown:

- pressure transmitters in the Syngas Conditioning Section:
    - ELF40 CP001 – Feed Splitting Vessel pressure ELF20 BB010
    - ELF40 CP002 – Humidifier KO Drum pressure ELF40 BB010
    - ELF50 CP001 – Inlet pressure parallel reactors (equal to ELG10 BH010 inlet pressure).
- Pressure transmitters in the CO Shift Section: ELG40 CP003, ELG60 CF006, ELG60 CP007.
- Pressure transmitters in the Condensate Recovery Section: ELG40 CP003, ELG60 CF006, ELG60 CP007.

- Pressure transmitters in the CO_2 Absorption section: ELH10 CP003, ELH40 CP001.
- Internal thermocouples in electric heaters: ELF20/40/50 AC010.

Some measurements were added on request of the research team to enable more precise measurements/analysis among which:
- Mass flow meter on the syngas inlet to the absorber (stream ELG60 BR030)
- Pressure measurement ELH10 CP003 in the CO_2 absorber shifted syngas supply line

It is recommended to assess the system degrees of freedom in order to define sufficient number of instrumentation, as well as the required accuracy of the instrumentation, based on the requirements of the system models (both steady-state and dynamic).

4.3.4   Analyzers

Throughout the test programme, the analyzer and sampling conditioning system was a permanent point of concern. A general lesson learned is that a clear verification and calibration protocol needs to be developed in order to define the frequency of inspection, procedure and at what deviation the analyzer specialists need to re-calibrate the analyzer. Below, a summary of problems specific for each analyzer is given.

ELF50 CQ201 (Gas chromatograph for syngas streams)
After commissioning, it appeared that the water concentration in the streams with high water content showed a large variation (more than could be explained by process pressure and temperature fluctuations) and in some streams the water concentration was also much lower in comparison to the heat and mass balance (resulting in too high concentrations of CO, CO_2 and H_2). Investigation into the sampling conditioning section made clear that the specified temperatures were not achieved. First, the bottlenecks were identified and resolved by changing pressure and temperature (tracing & insulation). At some moment, it was clear that the specified temperatures in the low-pressure tubes could not be reached and these were replaced. Although the water concentration appeared more stable, a detailed analysis explained below indicates condensation, although reduced, still occurs. Although the specified temperatures were reached, cold spots are very difficult to avoid affecting the quality of the measurements. Therefore, in any future application it is recommended to remove the water, analyse the dry gas and calculate the wet gas composition from the mass balance.

In Figure 4-13 the concentration difference between inlet and outlet based on *measured* wet compositions are compared to *calculated* wet compositions derived from dry gas measurement.   For the WGS reaction, the following reaction stoichiometry holds:

$$- \Delta F_{CO} = - \Delta F_{H_2O} = \Delta F_{CO_2} = - \Delta F_{H_2}$$

$$- \Delta x_{CO,wet} = - \Delta x_{H_2O,wet} = \Delta x_{CO_2,wet} = - \Delta x_{H_2,wet}$$

It is observed that the directly measured wet composition gives a significant spread in the concentration difference for both reactors, while the values based on the dry gas components are much more in agreement. Therefore, the dry gas measurements are used for analysis of the WGS performance.

Figure 4-13:   **Reactor 1 ΔCO, ΔH_2O, $-\Delta CO_2$ and $-\Delta H_2$ for directly measured values (top) and the calculated values based on the measured dry gas components (bottom)**

Apart form the sampling conditioning, several issues occurred with the analyzers themselves. In the beginning of the test programme, a significant variation existed among the sum of all components among the 10 streams (some added up close to 100% and some below 90%). Also reactor 2 outlet was not always identical to reactor 3 inlet (should give the same values as it is the same gas), and certain peaks (CO, H_2O, CH_4) suddenly disappeared (measurement in PGIM indicated zero). Afters several service visits by Siemens, during which regular maintenance was performed, leaking injection valves were replaced and the analyzer was re-calibrated, results improved (which is confirmed by the high accuracy of the molar balances). Nevertheless, some streams still did not add up to 99-100%, which according to Siemens may be caused by the difference between process gas and calibration concentrations (see Figure 4-14). For the analysis of the CO_2 absorber, it is essential to prevent contamination of the column by entrained DEPEG in the gas samples.
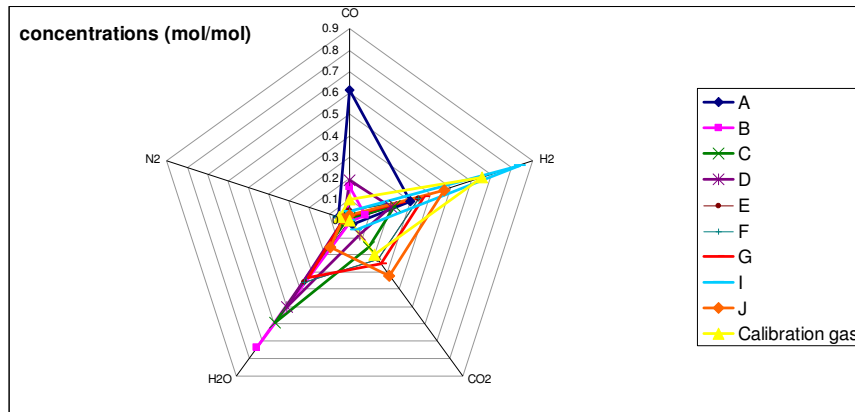
Figure 4-14:   **Process gas concentrations versus calibration gas for ELF50 CQ201 analyzer.**

ELF10 CQ202 (Gas chromatograph for solvent streams)
Unfortunately, the GC was unable to measure the CO_2 and H_2O concentration in the semi-lean (in between the packed beds) and rich (absorber outlet) solvent. The flow through the analyzer was unstable, which is most likely due to flashing of the CO_2 upon a pressure reduction in the analyzer system. Although the specified temperatures for the coolers were reached, this problem could not be avoided. Also reallocation of the sample shutoff valves did not solve the problem. It was decided to accept this flaw, as the rich solvent measurements were not essential for the model validation.

ELF20 CQ204 (Gas chromatograph for CO_2 streams)
Relatively few problems occurred with this GC analysing only 4 streams with comparable concentrations. Small interruptions in the H_2S/COS detector occurred, which were resolved quickly.

4.4 Corrosion

Monitoring of corrosion rates will give more insight in the corrosiveness of the process media and the solvents used. Generally a complete picture with respect to the corrosiveness of a system is obtained by combining the results of (CB&I Lummus, 2008b):

- Corrosion probes. The pilot plant is equipped with 7 probes, mainly in the absorption section. The probe itself is made of stainless steel. The measuring element on top of the probe is made of carbon steel material. In the probe a reference element is installed. By measuring the difference in electrical resistance between the two elements the corrosion rate can be determined.

- Direct (wall thickness) measurements (ultrasonic testing). This is applied at several locations (piping and reactors) in July 2010, November 2011, September 2012 and March 2013.
- Analysis of produced fluids
- Analysis of the operating conditions

One of the main corrosion mechanisms that could occur in the pilot plant is wet CO_2 corrosion. In an aqueous phase containing CO_2, the CO_2 will react with unalloyed and low-alloyed steels releasing hydrogen in the process. If the environment contains no free water, then there is no risk of CO_2 corrosion. In gas piping, there may be a risk of condensation of water if the temperature of the line drops below the water dew point. Therefore, most piping is insulated and/or traced. Furthermore, it should be sloped and without pockets to minimize corrosion. Most equipment, piping and tubing susceptible to wet CO_2 corrosion are made of stainless steel (SS304(L) or SS316(L)), which are completely resistant against CO_2 corrosion.

4.4.1   Syngas conditioning section

A probe is installed at the overhead of ELF10 BD010 (Syngas total feed wash column), the results of which are given in Figure 4-15. In the operating time (6000 hours) the total material loss is 0.128 mm (of which approximately 50 µm is lost during downtime), which is below the expected 0.85 mm/yr as specified in the material selection report (CB&I Lummus, 2008b). There is no sound explanation for this since the operators preserved the line with nitrogen. In addition, ultrasonic measurements were performed at the point where CO_2 was injected and some potential cold-spots. No CO_2 corrosion has been detected around the injection point. Little corrosion (approximately 0.2 mm) has been detected on possible cold spot points/drains.
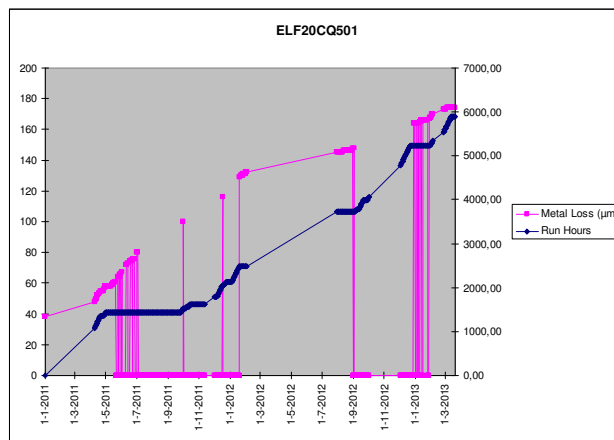
Figure 4-15:   Results corrosion probes overhead of ELF10 BD010 (Syngas total feed wash column)

4.4.2   WGS section

The material of construction for the reactors is 2.25Cr-1Mo (ASTM A335 GR P22), as this material is resistant to high temperature hydrogen attack[5]. In several locations the wall thickness was measured on the 27th of March 2013. For the 1st shift reactor (ELG10 BH010), a difference in wall thickness of 2.5 mm in a horizontal cross section was noticed on locations North and South in the lower part of the reactor. This measurement was only done once, so a trend can not be observed. The original wall thickness was 38.1 mm. A minimum wall thickness was measured in the lower part of the reactor of 36.8 mm. A maximum wall thickness of 39.4 mm was measured in the top section of the reactor. The deviation in wall thickness is within the tolerance of the pipe, however this deviation is quite unusual. A second wall thickness measurement was done to exclude a measurement error. The same values for the wall thickness were found. To exclude corrosion as a failure mode an endoscopic inspection was performed at the location were also the difference in wall thickness was measured. This inspection did not show any sign of corrosion (see Figure 4-16). The conclusion is that the difference in wall thickness can be explained by the tolerances that apply for fabrication of this pipe. For the 2nd shift reactor (ELG20 BH010) a similar deviation in wall thickness was found and the same hypothesis applies as for the 1st shift reactor.

weld pipe/ pipe-cap   pipe at elevation +4500

---

[5] In the material selection report, 1Cr-½Mo or 1¼Cr-½Mo is recommended (or 2¼Cr-1Mo if more economic) for H_2 partial pressures up to 11 bar and operating temperatures up to 520°C.

inlet flange   outlet flange
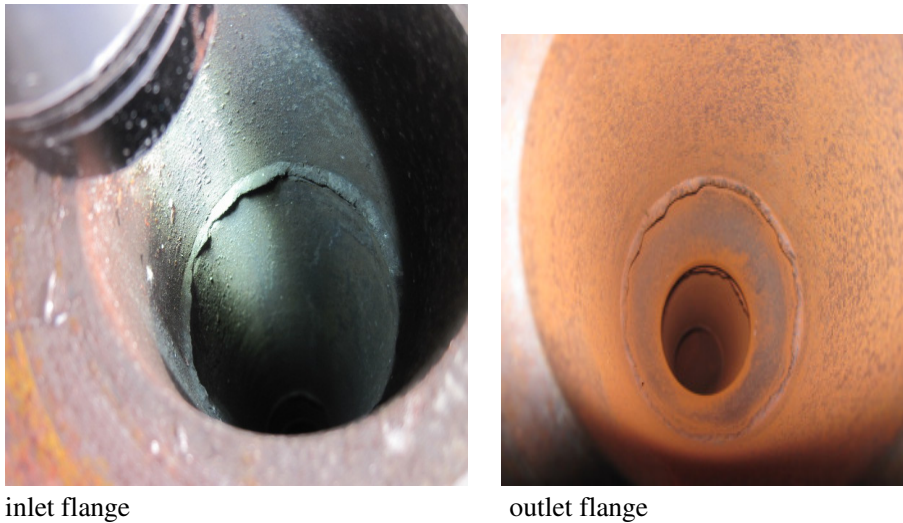
Figure 4-16:   Endoscopic inspection 1st shift reactor (ELG10 BD010)

4.4.3 CO_2 absorption section

DEPEG will protect the surface of piping and equipment and wet CO_2 corrosion will be strongly reduced. Therefore carbon steel with 3 mm corrosion allowance is selected for wet DEPEG piping and equipment. If not a continuous DEPEG film is formed (e.g. for equipment top sections and top outlet piping or flashing conditions), stainless steel is applied. Probes are installed at the overhead of ELH10 BD010 (absorber) and ELH70 AT010 (H_2 rich gas separator), bottom outlet of ELH10 BD010, ELH70 AT010 and ELH20 BB010 (1st Flash Vessel). The results indicate that corrosion rates at the bottom outlets are 2-5 μm in 6000 hours operation. As can be seen from Figure 4-17, the overhead of ELH10 BD010 and ELH70 AT010 shows somewhat higher corrosion rates (23-37 μm in 6000 hours operation), the majority of which occurred during the 2012 downtime (as the top absorber could not be preserved with nitrogen). Note that this is below the expected corrosion rate of 2.3 mm/yr as specified in the material selection report (CB&I Lummus, 2008b). The ultrasonic measurements of carbon steel piping in the absorption section indicate no corrosion, with the exception of ELH30 BR010 (measuring point is just downstream the probe located in the outlet of ELH20 BB010 (1st Flash Vessel). The measurement shows a reduction of 0.4 mm has taken place (but the probe did not show any sign of material loss). The reduction in wall thickness might be explained by the fact that this measuring point was not fully covered with DEPEG.
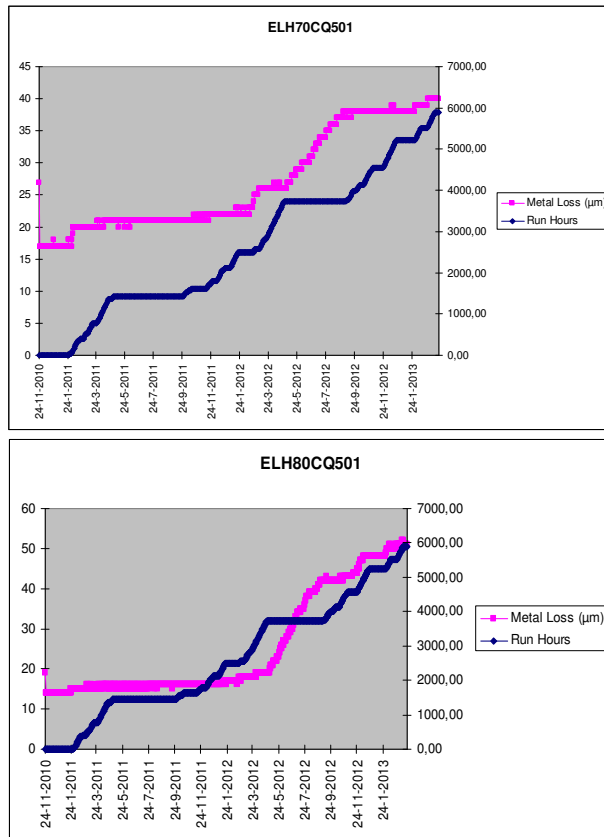
Figure 4-17:   **Results corrosion probes overhead of ELH10 BD010 (CO_2 absorber) and ELH70 AT010 (H_2 rich gas separator)**

In conclusion, the corrosion rate for carbon steel parts in the CO_2 absorption section of the pilot plant is very low as long as the wall is covered with DEPEG. Carbon steel with 3 mm corrosion allowance can be selected. Care should be taken for a good conservation during shutdown.

4.5   Health, safety and environment (HSE)

In this section, some specific HSE risks and events related to the chemical components used in the process will be highlighted. For the general HSE approach during the pilot plant engineering and design, the reader is referred to the HSE philosophy for the CO_2 Catch-up pilot plant (CB&I Lummus, 2008c).

Throughout the plant no large volumes of flammable gas are present. Therefore the fire hazards within this plant are low. However, to detect CO (toxic and flammable), CO_2 (asphyxiation) and H_2 (flammable) in an early state of release, detectors will be installed at locations the specific gas is the major component.

The solvent used to capture CO_2, Genosorb 1753 (or DEPEG) is a low-viscous, colourless to yellowish liquid. It has a flash point of 137°C. As the solvent is used at 40°C, the fire risk is low. Genosorb 1753 has a high boiling point/low vapour pressure and therefore solvent losses to the environment via the treated gas are minimal. No spills occurred during operation.

The catalyst applied in the WGS section is a copper promoted iron/chromium catalyst. After the final plant shut down, the catalyst needs to be oxidized in a controlled manner to avoid that the catalyst will heat up during unloading (as the oxidation is an exothermic process). During oxidation, some amount of the Cr(III) present in the catalyst will be transferred into Cr(VI), which is recognized as a human carcinogen. This means that workers should wear proper protection gear in order to avoid getting in contact with the catalyst pellets and to inhale catalyst dust.

The normal procedure prescribed by Haldor Topsøe is to purge the catalyst with steam until the temperature is 200-250°C, after which the airflow is gradually increased and controlled such that the catalyst temperature does not exceed 300°C. For operational reasons and the fact that catalyst sampling was planned (which could contain traces of carbides that may be removed by steam), it was decided to perform the oxidation in nitrogen. When adding air, the observed exotherm in reactor 1 and 2 was much higher than the recommended temperature rise of 50°C. With exception of the top later, the catalyst at the centre of the bed has been exposed to temperatures (peaks) between 600 and 800°C. These high temperatures are caused by the fact that nitrogen was used instead of steam (the heat capacity of nitrogen is lower than steam) and that the air-flow (which could not be measured) was too high.

5 Mass balances and pilot plant perform-ance

5.1 Reference state

This section presents the mass balances of the plant at reference state. These conditions are close the original design point; small deviations are explained by plant operation considerations. For the mass balance the period 04.04.2012 15:00 – 22:00 has been selected. In Figure 5-1 the boundary conditions at the inlet of the pilot plant are shown (flow rate and composition). It can be seen that stationary operating conditions have been reached for the entire time period. Only the CO_2 and CH_4 concentrations show a slight drift which has been considered insignificant for the overall mass balance evaluation during this period. The CO concentration and the syngas flow rate show very low fluctuations in the range of only 2% during the entire period. The levels within the pilot plant vessels show only little fluctuations below 5%. Therefore, stationary operating conditions can be assumed.
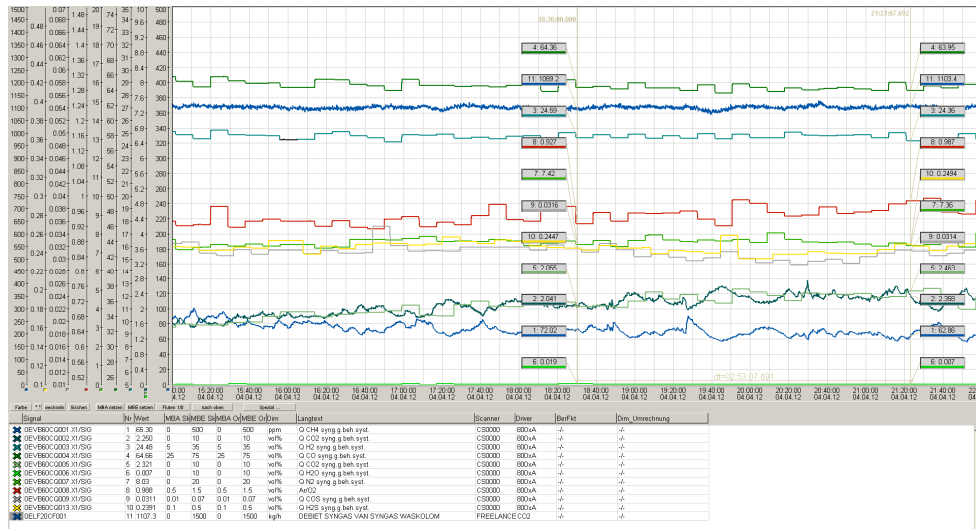
Figure 5-1: **Syngas flow and composition during observed time period (04-04-2012 15:00-22:00)**

5.2 Scope and methodology

In addition to the overall mass balance, mass balances of the syngas conditioning, WGS shift and condensate recovery and CO_2 absorption section have been performed. These mass balances per section are needed for the validation of the respective

models. The purpose was to check the quality of the raw measurement data from the plant and to see if it can be used for model validation. A deviation in the mass balances at steady-state conditions would indicate the presence of measurement errors. A simplified process flow-sheet including the different balance regions is shown in Figure 5-2.
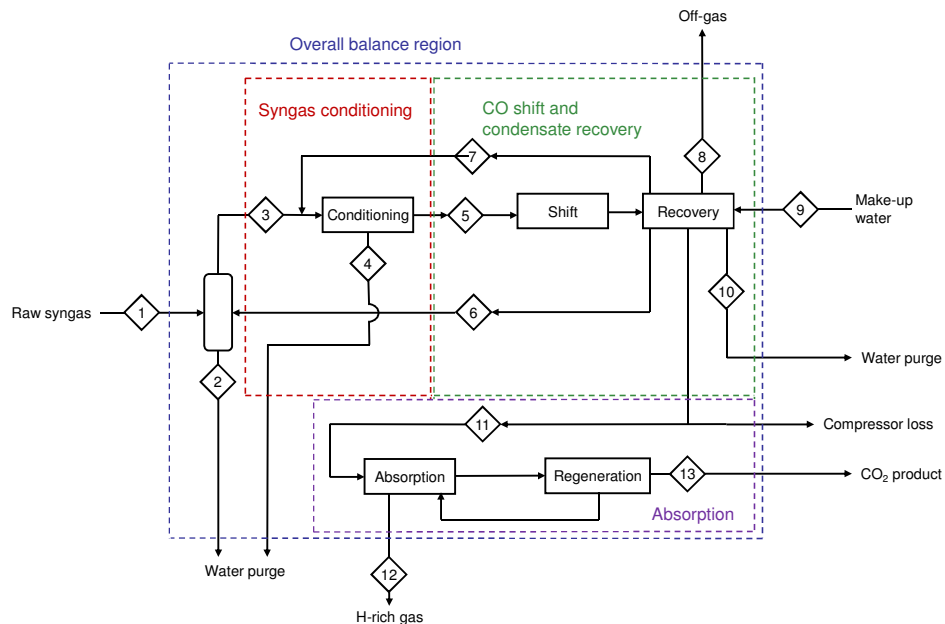
Figure 5-2:   Simplified process flow sheet with balance regions

In a first step, the mass balances have been evaluated using the raw measurement data which still contains random and probably systematic measurement errors. The balances on the raw measurement data have been performed using the mass flow and concentration measurements from the PGIM system for selected time periods. In most cases, the mass flow measurements in PGIM are given in kg/h while they are actually measured in m³/h. The kg/h value is then calculated using a fixed density (conversion factors are given in (Kaptein, 2011)). In order to use realistic mass flow measurement data, the actual density calculated from measured concentrations has to be used to back-calculate the mass flow from volume flow measurements. For the raw concentration data, which are given in vol% or ppm, the summation correlation is not fulfilled in most cases. Therefore the concentration measurement data has been normalized to fulfil the summation correlation for the calculation of density data.

After the evaluation of the mass balances based on raw measurement data, a data reconciliation approach has been applied in order to identify measurement errors and improve the quality of the measurement data. The procedure aims at closing the mass

and component balances around a selected balance region. For the concentration measurements, elementary molar balances have been set up additionally as boundary conditions as the process involves chemical reactions changing the composition of the in- and outgoing streams. With the data reconciliation procedure, the raw measurement data are adjusted in order to fulfil the specified equation system (balance equations). A detailed description of the data reconciliation procedure is given in (Faber, 2012b). It has to be mentioned that the data reconciliation procedure used in this investigation does not contain any physical or thermodynamic correlations of the variables except mass and elementary balances around the balance region and summation equation for the individual concentration measurements. Therefore the result of this data reconciliation may not provide physically meaningful results (e.g. water concentration still may be larger than saturation concentration at given pressure and temperature). The purpose of the applied procedure was to test if a simple data reconciliation procedure could improve the accuracy and reliability of the raw measurement data without having to use the full process model. Therefore the limitations of this approach have to be taken into account when analysing the results. A rigorous data reconciliation procedure using the entire process model has been applied in the model validation procedure (see 7.3.1.2).

5.3   Mass balances

First the overall mass balance of the entire pilot plant has been evaluated (see Figure 5-2 blue balance region). The in-going streams are the raw syngas (stream 1) and the make-up water (stream 9). The out-going streams are the H_2-rich gas after the absorber (stream 12), the CO_2 product (stream 13), water purge at various locations (streams 2, 4 and 10) and a small off-gas from the recovery section (stream 8).

Additionally, the mass balances have been evaluated for different sub-sections of the plant. In the syngas conditioning section (red balance region), the ingoing streams are the raw syngas after the washing column (stream 3) and the recycled reaction water from the recovery section (stream 7). The outgoing streams are the syngas bypass to 2nd and 3rd reactor as well as the syngas to the 1st shift reactor (combined in stream 5) and the wastewater (stream 4).

In the CO shift and condensate recovery section (green balance region), the in-going streams are the syngas to the shift reactors (stream 5) and the make-up water (stream 9). The out-going streams are the shifted syngas to the CO_2 absorption unit (stream 11) which is not density-corrected as this measurement is a coriolis mass flow measurement, the reaction water (stream 7), the wastewater (stream 10) and the washing water (stream 6).

In the absorption section (purple balance region), the only in-going stream is the shifted syngas (stream 11). The out-going streams are the H_2-rich gas (stream 12) and the CO_2 product (stream 13).

Additionally, for all balance regions the changes in hold-up measurements during the entire time period have been accounted for. It should be noted that the flow sheet given in Figure 5-2 is very simplified and does not represent all process streams involved. Some streams have been merged and internal process streams are omitted. For a description of the entire process flow sheet see 2.3.

Table 5-1:   **Results mass balances for different balance regions**

Balance region	Mass flow in [kg/h]	Mass flow out [kg/h]	Relative difference [%]
Overall	**1722.67**	**1724.64**	**0.11**
Syngas conditioning	**2192.95**	**2238.03**	**2.06**
Dry (non-normalized)	1113.61	1037.38	6.85
Wet (non-normalized)	1079.33	1200.40	11.22
Dry (normalized)	1103.92	1117.51	1.2
Wet (normalized)	1087.36	1120.10	3.0
CO shift and condensate recovery	**2812.23**	**2701.28**	**3.95**
CO$_2$ Absorption	**1595.78**	**1660.07**	**4.03**
Water balance	5.53	18.56	235

From Table 5-1 it can be seen that the overall mass balance as well as the mass balances for the individual plant sections close very well. For the overall mass balance the relative deviation between input and output is only 0.11%, which is significantly below the measurement accuracy of the individual measurement devices. Also for the sub-sections the mass balances close well.

During the pilot plant test program, it has been observed that the water concentration measurements were error-prone and therefore the mass balance has been investigated for the dry syngas and the water separately for some balance regions. In Table 5-1 the results of this investigation is shown for the syngas conditioning section and the CO$_2$ absorption section. In the syngas conditioning section, the raw dry mass balance is clearly more accurate than the wet balance. The deviations can already be significantly reduced when using normalized concentration data that fulfils the summation equation.

The large deviation in the water balance for the absorption section (235%) can be explained by the fact that the water mass flows in this section are very small and therefore measurement errors for the water concentration has a large effect on relative errors. Especially the water concentration measurement of the CO$_2$ product stream after the 3rd flash vessel (stream 13) seems to be too high. However, as the absolute water concentration in this stream is very low (~3%) and this value has no significant impact on the overall process efficiency and the model validation this was considered not to be a major issue.

5.4   Pilot plant performance

The main performance parameters of the plant are the efficiencies for converting CO into CO_2 in the shift section and the CO_2 absorption efficiency in the absorption section as these determine the overall carbon capture efficiency of the plant.

Different approaches can be used to calculate the CO conversion efficiency. Some of these approaches are model-based (e.g. adiabatic temperature rise) and some of them can be applied to the raw measurement data. However, because the wet gas analysis of the syngas composition in the shift section was not reliable as explained in 4.3.4, the dry gas analysis is used to calculate the CO conversion efficiency according the equation below.

$$\frac{x_{CO,dry}^{in} - x_{CO,dry}^{out}}{x_{CO,dry}^{in} \cdot \left(1 + x_{CO,dry}^{out}\right)} \qquad \textbf{5-1}$$

The CO_2 absorption efficiency can be calculated in two ways:

- Using the CO_2 molar flow of the shifted syngas (input) and the CO_2 product (output):

$$1 - \frac{\left(\dot{m}_{CO_2,in} - \dot{m}_{CO_2,out}\right)}{\dot{m}_{CO_2,in}} \qquad \textbf{5-2}$$

- Using the CO_2 molar flow of the shifted syngas (input) and the H_2-rich gas (output):

$$\frac{\left(\dot{m}_{CO_2,in} - \dot{m}_{CO_2,out}\right)}{\dot{m}_{CO_2,in}} \qquad \textbf{5-3}$$

The overall plant carbon capture efficiency can be calculated based on the CO and CO_2 molar flows of the raw syngas (input) and the CO_2 product (output):

$$1 - \frac{\left(\left(\dot{m}_{CO_2,in} + \dot{m}_{CO,in}\right) - \left(\dot{m}_{CO_2,out} + \dot{m}_{CO,out}\right)\right)}{\left(\dot{m}_{CO_2,in} + \dot{m}_{CO,in}\right)} \qquad \textbf{5-4}$$

5.4.1 CO conversion efficiency

In Table 5-2 the performance of the WGS section according to the CB&I and Haldor Topsøe calculations are compared to the actual pilot plant operation in reference state. Besides the CO conversions per reactor (Xco), the progressive conversions per reactor ($\sum$ Xco, Ri) and the cumulative progressive conversions ($\sum$ Xco) are calculated. The progressive conversion is related to the total amount of CO fed to the pilot. The progressive conversion per reactor is the contribution in absolute terms of the specific reactor to the cumulative progressive conversion.

In the Haldor Topsøe calculations, all reactors are assumed to reach thermodynamic equilibrium, while the CB&I calculations assume a 20°C approach to equilibrium (ATE) for each reactor. Both calculations reach a 92-93% overall conversion for the entire WGS section. Similar overall CO conversions are measured in the pilot, i.e. 92.7% and 92.6% for the two reference state operational points. However, the test runs indicate that the reactor 3 catalyst activity is insufficient (see 6.2.3), so a lower C conversion would be expected. Comparing the pilot operation with the simulations leads to the conclusion that in the pilot operation the better than expected overall performance is due to a higher split flow of the syngas going towards reactor 1. In addition, the steam content of the pilot is slightly larger. The insufficient reactor 3 activity is thus compensated mainly by the improved reactor 1 operation (van Dijk, 2012c).

Table 5-2:   CO conversion efficiency

			Reactor 1		Reactor 2		Reactor 3	
			in	out	in	out	in	out
CB&I	T	°C	340	488	340	486	340	366
	ATE	°C		20		20		20
	H_2	%wet	7.76	22.51	20.03	34.23	34.23	36.78
	N_2	%wet	1.48	1.48	2.42	2.42	2.42	2.42
	CO	%wet	16.02	1.27	18.81	4.61	4.61	2.06
	CO_2	%wet	0.63	15.38	8.38	22.58	22.58	25.13
	Ar	%wet	0.29	0.29	0.47	0.47	0.47	0.47
	H_2O	%wet	73.83	59.08	49.88	35.68	35.68	33.13
	S/CO=	mol.mol-	4.61		2.65		16.07	
	Flow=	kmol.h-1	68.53		137.43		137.43	
	Xco	%		**92.1%**		**75.5%**		**55.3%**
	$\sum$ Xco, Ri	%		**28.1%**		**54.3%**		**9.7%**
	$\sum$ Xco	%		**28.1%**		**82.4%**		**92.1%**

Haldor	T	°C	340	488	340	490	340	365
Topsøe	ATE	°C		0		0		0
	H_2	%wet	7.74	22.64	20.09	34.65	34.65	37.01
	N_2	%wet	1.48	1.48	2.42	2.42	2.42	2.42
	CO	%wet	15.99	1.09	18.76	4.19	4.19	1.83
	CO_2	%wet	0.62	15.52	8.44	23.00	23.00	25.36
	Ar	%wet	0.29	0.29	0.47	0.47	0.47	0.47
	H_2O	%wet	73.88	58.98	49.82	35.26	35.26	32.90
	S/CO=	mol.mol-	4.62		2.66		8.42	
	Flow=	kmol.h-1	61.90		124.33		124.33	
	Xco	**%**		**93.2%**		**77.7%**		**56.3%**
	∑ Xco, Ri	**%**		**28.3%**		**55.7%**		**9.0%**
	∑ Xco	**%**		**28.3%**		**84.0%**		**93.0%**
Buggenum	T	°C	334	486	338	470	336	346
Ref point	ATE	°C						
10	H_2	%wet	7.81	23.11	20.45	33.54	33.54	34.80
	N_2	%wet	1.87	1.87	2.82	2.82	2.82	2.82
	CO	%wet	16.42	1.12	16.20	3.11	3.11	1.84
	CO_2	%wet	0.70	16.00	9.70	22.78	22.78	24.05
	Ar	%wet	0.25	0.25	0.38	0.38	0.38	0.38
	H_2O	%wet	72.94	57.64	50.46	37.37	37.37	36.10
	S/CO=	mol.mol-	4.44		3.12		12.03	
	Flow=	kmol.h-1	59.24		104.76		104.76	
	Xco	**%**		**93.2%**		**80.8%**		**40.7%**
	∑ Xco, Ri	**%**		**34.9%**		**52.7%**		**5.1%**
	∑ Xco	**%**		**34.9%**		**87.6%**		**92.7%**
Buggenum	T	°C	334	484	340	467	334	345
Ref point	ATE	°C						
11	H_2	%wet	7.86	23.10	20.43	33.29	33.29	34.50
	N_2	%wet	1.90	1.90	2.85	2.85	2.85	2.85
	CO	%wet	16.35	1.11	15.82	2.96	2.96	1.75
	CO_2	%wet	0.78	16.02	9.83	22.68	22.68	23.89
	Ar	%wet	0.22	0.22	0.33	0.33	0.33	0.33
	H_2O	%wet	72.89	57.65	50.74	37.89	37.89	36.68
	S/CO=	mol.mol-	4.46		3.21		12.78	
	Flow=	kmol.h-1	61.31		108.39		108.39	
	Xco	**%**		**93.2%**		**81.3%**		**40.8%**
	∑ Xco, Ri	**%**		**35.2%**		**52.4%**		**4.9%**
	∑ Xco	**%**		**35.2%**		**87.6%**		**92.6%**

5.4.2   CO$_2$ absorption efficiency

Table 5-3 shows the CO$_2$ absorption efficiency during reference state calculated using raw measurement data. Using the reconciled values for the flow rates and CO$_2$ concentrations the CO$_2$ absorption efficiencies are 88.91 and 86.45% based on the CO$_2$ stream and H$_2$-rich stream, respectively. It was concluded that the CO$_2$ measurement in the H$_2$-rich stream is generally more reliable as it is measured with the same analyser as the shifted syngas and therefore more consistent data can be expected.

Table 5-3:   CO$_2$ absorption efficiency

	Shifted syngas (in)	CO$_2$ product (out)	H$_2$-rich gas (out)
Flow rate [kg/h]	1595.78	1200.1	455.11
CO$_2$ concentration [vol% wet]	0.3604	0.8927	0.0795
CO$_2$ flow [kmol/h]	29.35	26.52	4.10
CO$_2$ absorption efficiency [%]		90.35	86.05

According the heat and mass balances from CB&I Lummus the CO$_2$ absorption efficiency is 90.8%. However, the results are incomparable as the design from CB&I Lummus was based on a Mellapak 350 Y structured packing at the bottom and a Mellapak 750 Y packing at the top.

5.4.3   Carbon capture efficiency

Table 5-4 shows the carbon capture efficiency during reference state calculated using raw measurement data. There is almost no difference when calculating the overall capture efficiency using reconciled values (77.84%). As a check, the carbon capture efficiency can be estimated by the product of the CO conversion efficiency (93%) and the CO$_2$ absorption efficiency (86%), which renders a carbon capture efficiency of 80%. This method overestimates the overall carbon capture efficiency (generally less than 1% absolute), because the CO$_2$ that is already present in the raw syngas and also the CO slip with the CO$_2$ product and H$_2$-rich stream are not considered.

Table 5-4:   Carbon capture efficiency

Stream	Syngas from WAC (in)	CO$_2$ product (out)
Flow rate [kg/h]	1102.34	1200.07
CO concentration [vol% wet]	0.6552	0
CO$_2$ concentration [vol% wet]	0.014	0.8927
carbon / CO$_2$ flow [kmol/h]	33.95	26.52
Carbon capture efficiency [%]		78.12

6 Pilot plant test programme

The test programme is subdivided into test campaigns covering a period in which a number of test runs are performed.

- TC-I: trial period to understand the operating window and limits of the pilot plant, define reference state. No composition measurements were available as the analyzer commissioning and calibration was not yet finished (Jan 2011 – April 2011)
- TC-II: execution of main parametric tests of shift section and absorption section with random packing in absorber (September 2011 – April 2012, September 2012 - November 2012)
- TC-III: repetition of several parametric tests with structured packing in absorber (November 2012 – February 2013)

Appendix A.1 gives an overview of all relevant test runs performed, the results of which are discussed in the remaining part of this chapter. The results of the dynamic test runs TR-020 to TR-030, TR-033 and TR-034 are not discussed here as most of these test runs describe transients for the validation of sub-component. The results of the most relevant dynamic test runs are discussed in section 7.

6.1 Syngas conditioning and water-gas shift section

6.1.1 Test run TR-CII-001: Shift reactors inlet temperatures

The purpose of this test run is to investigate the stationary operation of the pilot plant for different values of the inlet temperature for all three reactors (ELG10 BH010, ELG20 BH010, ELG30 BH010). The variation of the reactor inlet temperature whilst keeping the other feed variables constant will influence the CO conversion. A lower inlet temperature will yield a higher CO conversion whereby also the adiabatic temperature rise will be higher. By lowering the reactor inlet temperature the reaction front and hence the location where equilibrium is reached within the reactor will move towards the end of the catalytic bed. Depending on the catalyst activity a lower inlet temperature limit exists at which a further temperature decrease would result in not reaching equilibrium within the reactor. The influence of the reactor inlet temperature on the CO conversion is summarized in Table 6-1.

Table 6-1: CO conversion of the individual reactors and of the entire shifting section for the different set points

|	Unit	Reference state	SP3-1	SP4	SP5	SP6	SP7
Inlet temperature	°C						
Reactor 1		335.2	325.6	320.6	315.8	344.8	354.9
Reactor 2		334.3	334.4	334.4	334.4	343.8	353.8
Reactor 3		333.9	333.5	333.5	332.2	343.6	354.5
Outlet temperature	°C						
Reactor 1		493.5	488.3	486.5	482.6	506.8	517.8
Reactor 2		464.3	466.8	467.1	464.2	474.2	480.9
Reactor 3		347.2	344.8	345.4	343.0	358.9	372.3
Adiabatic temperature rise	K						
Reactor 1		158.3	162.7	165.8	166.8	162.0	162.9
Reactor 2		129.9	132.4	132.7	129.8	130.4	127.1
Reactor 3		155.2	152.8	153.4	151.0	166.9	180.3
CO conversion	%						
Reactor 1		91.9	92.10	92.13	92.42	90.92	90.57
Reactor 2		80.3	79.98	79.61	80.12	78.80	78.44
Reactor 3		45.6	37.32	38.92	36.03	47.84	50.90
Overall		93.1	92.08	92.08	92.10	93.03	93.40
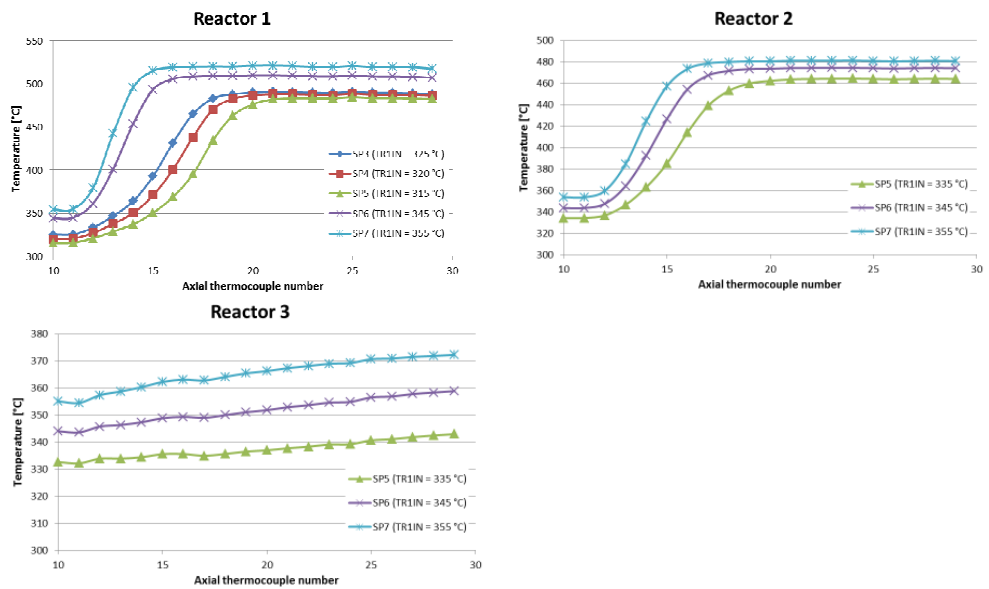
Figure 6-1: Axial temperature profiles for reactor 1, 2 and 3 for different set points for TR-CII-001

The decrease of the inlet temperature of reactor 1 results in a clear movement of the reaction front towards the end of the catalyst bed. For SP7 (R1 inlet 355°C) equilibrium is already reached within the first third of the catalyst bed while for operation SP5 (R1 inlet 315°C) it is achieved in the last third. The CO conversion of reactor 1 increases from 90.6% (SP7) to 92.4% (SP5). The effect on the overall conversion efficiency cannot be judged with this test run as the conversion efficiency of each reactor varies significantly.

Also for reactor 2 a decrease in CO conversion is observed when increasing the inlet temperature. For reactor 3 this effect is reversed. The activity of the reactor 3 catalyst is lower than expected (which will be further discussed in TR-CII-016) and equilibrium is not reached within the bed for SP 5. Therefore, increasing reactor 3 inlet temperature will boost the reaction rate and equilibrium is almost reached at the end of the bed (SP 7).

An optimal operation of the shift reactors in terms of high CO conversion and low heating requirement could be achieved by adapting the reactor inlet temperatures such that equilibrium is just reached within the last third of the catalyst bed. Therefore, the reactor inlet temperature of reactor 1 should be lowered to 315 °C (possibly even 5-10 K lower). For reactor 2 the reaction front at reference condition is well within the catalyst bed and hence the inlet temperature of reactor 2 might also be decreased.

6.1.2   Test run TR-CII-002: Syngas composition

The purpose of this test run is to investigate the stationary operation of the pilot plant for different syngas compositions. The syngas composition is, for example, influenced by the gasifier fuel (coal or/and biomass, type of coal/biomass) and gasifier load. In Table 6-2 the wet inlet composition into the first reactor is shown for the individual set points. SP3 represents normal operation i.e. full-load at 100% coal. SP 1 and 2 represent normal variations in gasifier operation. SP4 represents gasifier part load and co-gasification of high biomass contents, which results in a higher CO_2 content.

Table 6-2:   Syngas inlet composition and CO conversion of executed set points of TR-CII-002 for reactor 1

TR-CII-002	SP4	SP3	SP1	SP2/A
CO [mol %]	16.54	16.73	17.53	16.91
CO_2 [mol %]	1.96	1.37	0.97	0.61
H_2 [mol %]	9.58	9.21	7.94	9.72
H_2O mol %]	69.44	69.64	70.24	70.42
N_2 [mol %]	2.21	2.74	2.94	2.08

The impact of syngas composition on the CO conversion and the adiabatic temperature rise is presented in Table 6-3. The influence of the variation in the syngas composition is best evaluated considering the performance of reactor 1. Although an increase in reaction products concentration should result in a decrease of the CO conversion (and vice versa), this is not always observed. Generally, for the expected range in syngas composition the influence on the CO conversion is minor.

Table 6-3:   **CO conversion of the individual reactors and of the entire shifting section for the different syngas compositions**

	Unit	SP4	SP3	SP1	SP2/A
Inlet temperature	°C				
Reactor 1		335.4	335.5	335.7	335.1
Reactor 2		334.5	334.2	334.6	334.2
Reactor 3		333.7	333.7	333.8	333.7
Outlet temperature	°C				
Reactor 1		486.4	488.8	495.6	489.5
Reactor 2		454.3	457.9	468.2	461.5
Reactor 3		342.3	343.0	344.8	344.4
Adiabatic T rise	K				
Reactor 1		151.0	153.4	159.9	154.4
Reactor 2		119.8	123.7	133.6	127.3
Reactor 3		150.3	151.0	152.8	152.4
CO conversion	%				
Reactor 1		91.72	91.90	91.84	92.03
Reactor 2		81.03	80.79	80.34	80.80
Reactor 3		35.48	36.69	38.36	37.63
Overall		92.36	92.36	92.20	92.45

6.1.3   *Test run TR-CII-003: Syngas mass flow*

The purpose of this test run is to investigate the stationary operation of the pilot plant for part load and high load operation whereby the focus will be on the hydrodynamic conditions due to load change. For the comparison of measured and expected pressure losses, suitable pressure drop correlations should be developed (also needed for dynamic test runs). In addition, the minimum and maximum capacity of the plant is determined during this test run.

In the pilot plant pressure measurements are not available at the inlet and outlet of each component but rather at some locations within the process where measurements are in particular required for performance evaluation. Therefore, pressure losses over

component groups including piping have been determined in the shifting section. Table 6-4 indicates which components are influencing the respective measured pressure loss and which flow regime is present. The calculated pressure drops, based on the individual plant pressure measurements are summarized in Table 6-5. A set point with reference state syngas mass flow (TR-CII-001/SP3-1) has been added as comparison.

Table 6-4:   **Pressure drops determined for the evaluation of TR-CII-003 and the components which contribute to the individual pressure losses.**

Pressure drop	Included components			Flow regime
dP ELF20	ELF10 BD010	ELF20 AC010	ELF20 BB010	2ph flow
dP ELF40	ELF40 AC010	ELF40 BB010		2ph flow
dP ELF50	ELF50 AC010			1ph flow
dP ELG10	ELG10 BH010			1ph flow
dP ELG20	ELG20 BH010			1ph flow
dP ELG30	ELG30 BH010			1ph flow
dP ELG40	ELG40 AC010	ELG40 BD010		2ph flow
dP ELG50	ELG50 AC010	ELG50 BB010		2ph flow

Table 6-5:   **Calculated pressure losses of TR-CII-003**

	TR-CII-001 /SP3-1	SP2	SP4	SP3/A	SP2/A	SP4/A
Syngas mass flow [kg/h]	1100	850	1240	1000	850	1240
dP ELF20 [bar]	0.111	0.102	0.123	0.219	0.168	0.310
dP ELF40 [bar]	0.375	0.403	0.403	0.219	0.206	0.230
dP ELF50 [bar]	1.364	2.243	1.034	1.906	2.463	0.822
dP ELG40 [bar]	0.783	0.719	0.714	0.568	0.419	0.882
dP ELG50 [bar]	0.278	-0.025	0.161	0.141	0.114	0.190

The syngas inlet pressure is usually around 21 bar. The back pressure of the shifting section is controlled via the valve ELG61 AA050 and is kept constant at approximately 16.5 bar. With these rather fixed pressure settings and the opening limitations of the syngas control valve (ELF50 AA050) the range of possible syngas mass flows is determined (850 – 1240 kg/h).

In Figure 6-2a-d, the dependency of the pressure drops of the individual plant sections on the syngas mass flow is shown.

The reactor pressure losses (Figure 6-2a) can be clearly correlated to the mass flow. With increasing flow the pressure drop increases almost in a linear manner. A simple pressure drop correlation for turbulent and incompressible flow can be used to first fit the friction coefficient based on the measured data and then to predict the pressure changes for different operations.
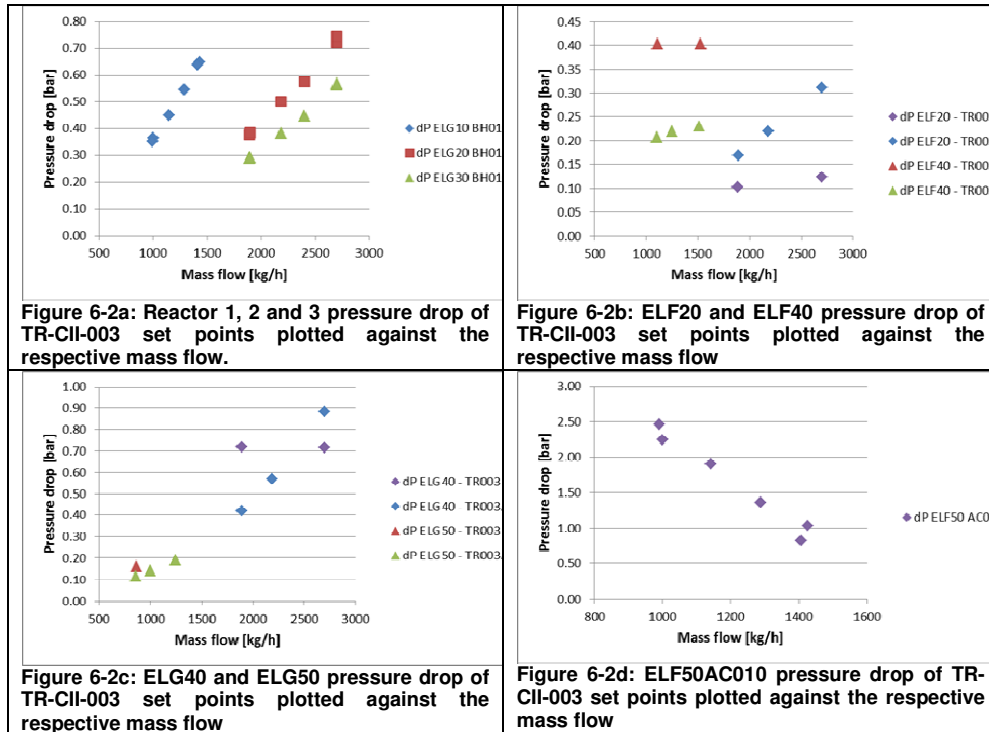

Figure 6-2a: Reactor 1, 2 and 3 pressure drop of TR-CII-003 set points plotted against the respective mass flow.

Figure 6-2b: ELF20 and ELF40 pressure drop of TR-CII-003 set points plotted against the respective mass flow

Figure 6-2c: ELG40 and ELG50 pressure drop of TR-CII-003 set points plotted against the respective mass flow

Figure 6-2d: ELF50AC010 pressure drop of TR-CII-003 set points plotted against the respective mass flow

Figure 6-2:   Influence of syngas mass flow on pressure drops during TR-CII-003

For the pressure loss over the ELF20 and ELF40 section the relation to the mass flow is more difficult to interpret (Figure 6-2b). It seems that the pressure losses are different for the two separately executed test runs TR-CII-003 and TR-CII-003A (the latter is a repetition). Evaluating the test runs independently a linear trend between pressure loss and mass flow can be observed. A common analysis results in an unclear correlation. In both component groups vapour-liquid flows of unknown regime (well mixed, presence of droplets, phase separation) are present and possibly other factors like liquid levels have influence on the pressure drop of these sections. Therefore, it can be concluded that due to the 2-phase flows present in the ELF20 and ELF40 section no simple pressure drop correlation can be developed. In order to predict the performance of the shifting section highly accurate pressure prediction are not required and therefore the assumption of constant pressure drop over ELF20 and ELF40 will serve the modelling purpose.

For the pressure loss over ELG40 BD010 and ELG50 BB010 a similar unclear correlation is observed (Figure 6-2c). It is suggested to assume an average constant pressure drop for both components.

For the superheater ELF50 AC010 the pressure loss shows a clear correlation to the respective mass flow (Figure 6-2d). With increasing mass flow the pressure drop decreases in a rather linear manner. Typically a reversed correlation would be expected. The specific design of this component might give the explanation for the observed pressure correlation.

6.1.4   Test run TR-CII-004: Steam to carbon ratio

The purpose of this test run is to investigate the stationary operation of the pilot plant for different values of the H_2O/CO ratio for the reactors. Operation at low H_2O/CO ratio, which implies that less steam is required to be conditioned and recycled in the shifting section, is energetically more efficient and thereby decreases the energy penalty of CO_2 capture. However, operation at lower H_2O/CO ratios would lead to higher reactor outlet temperatures which will result in catalyst sintering and deactivation. The operation at lower H_2O/CO ratio also comes at a cost of decreased CO conversion which leads to a reduction in CO_2 capture rate. In addition, such operation can also lead to iron carbide formation within the catalyst, which is investigated in more detail in TR-CII-017.

The influence of the H_2O/CO ratio on the CO conversion efficiency and the adiabatic temperature rise is summarized in Table 6-6. SP3/A represents reference state.

Table 6-6:   **Performance data of individual reactors and entire shifting section for the different steam/CO ratios.**

		TR-CII-004A		
	Unit	**SP2/A**	**SP3/A**	**SP1/A**
Inlet temperature	°C			
Reactor 1		335.9	335.7	335.3
Reactor 2		334.8	334.7	334.4
Reactor 3		334.2	333.9	333.8
Outlet temperature	°C			
Reactor 1		483.8	496.3	507.7
Reactor 2		467.2	471.0	472.8
Reactor 3		344.4	346.2	348.8
Adiabatic T rise	K			
Reactor 1		147.8	160.6	172.4
Reactor 2		132.3	136.2	138.4
Reactor 3		152.4	154.2	156.8

CO conversion	%			
Reactor 1		93.43	91.76	89.70
Reactor 2		82.05	79.75	77.51
Reactor 3		39.69	40.01	41.44
Overall		93.02	92.16	91.49
Steam/CO ratio	mol/mol			
Reactor 1		4.57	4.00	3.51
Reactor 2		3.33	3.01	2.75
Reactor 3		13.98	10.90	8.79
Steam/syngas ratio overall	kg/kg	1.31	1.22	1.13
Steam/syngas ratio overall	mol/mol	1.55	1.43	1.33

The increase of the overall H_2O/CO ratio to 1.31 kg/kg (SP2/A) leads to an increase of overall efficiency by 0.86% points. This comes at a cost of 6% higher steam content in the system. The decrease of the overall H_2O/CO ratio to 1.13 kg/kg (SP1/A) leads to a drop in CO conversion efficiency of 0.7% points at a reduction of the steam content by 8%. For this set point the adiabatic temperature rise increased especially for reactor 1 where the outlet temperature is approaching its safety limit (material design temperature is 550°C, but normal operation temperatures are kept below 520°C). In order to further reduce the overall steam requirements reactor 1 H_2O/CO ratio has been kept constant and then the reduction only affects reactor 2 and 3, which outlet temperatures are still far from their limitations.

It can be observed that with decreasing H_2O/CO ratio of reactor 3 its conversion efficiency increases (contrary to observation for reactor 1 and 2). This is explained by the fact that equilibrium is not reached in reactor 3 at normal operation and hence the increase in CO content (less CO is shifted in the upstream reactor 1 and 2) boosts the reaction rate. Therefore, the overall CO conversion reduction for the lowest steam/syngas ratio might be even lower assuming a normal reactor 3 catalyst activity (equilibrium reached within the bed).

6.1.5   TR-CII-005: Part load operation

The purpose of this test was to evaluate the pilot plant performance under part-load conditions (gasifier as well as the CO_2 capture unit) i.e. reduced flow and changing composition. However, the period of steady-state operation during gasifier part load operation during the night was too short to obtain sufficient measurement. Only one hour of stable part-load operation could be established, which is not sufficient (steady-state operation should last at least 2 to 3 hours). Considering the success of the other

steady-state test runs (TR-CII-002 and 003) the model validation can be performed without a specific data set for gasifier part load operation and a repetition of this test run was not considered necessary.

6.2   Shift reactor tests

6.2.1   Test run report TR-CII-006: Verify axial and radial reactor temperatures with nitrogen

In order to verify the temperature measurements of the WGS reactors and whether heat losses occur, the axial and radial temperature profile are investigated using nitrogen. Since nitrogen is an inert, a flat axial temperature profile is expected. This verification has been done before the pilot plant is operated on syngas for the second test campaign. A detailed description and evaluation of the test run can be found in (Kaptein, 2012).

From the results of the test run it was observed, that for reactor ELG10 BD010, the standard deviation of the average axial catalytic bed temperatures lies between 0.3 and 0.6°C. For reactor ELG20 BD010, the standard deviation of the average axial catalytic bed temperatures lies between 0.4 and 0.6°C. For reactor ELG30 BD010, the standard deviation of the average axial catalytic bed temperatures lies between 0.5 and 0.7°C, which was considered acceptable.

6.2.2   Test run TR-CII-007: 3rd Shift reactor inlet temperature

The purpose of this test run is to study the dynamic behaviour of the 3rd WGS reactor during a rapid variation in the inlet temperature. The 3rd WGS reactor was chosen because a perturbation will not affect the operation of the 1st and 2nd WGS reactors.
Upon a fast change of the reactor inlet temperature, the thermal buffering of the catalyst will result in a small inverse response of the outlet temperature: upon a sudden decrease of inlet temperature, the outlet temperature will first increase slightly before decreasing towards its new steady state value. Similarly, the increase in inlet temperature will result in an initial small drop in outlet temperature before it starts to increase. An explanation of this effect is described in (van Dijk and Boon, 2011). The expected response is shown in Figure 6-3. The magnitude of the change depends on the speed of the perturbation at the inlet, the kinetics, the thermodynamic equilibrium and the thermal inertia of the reactor.
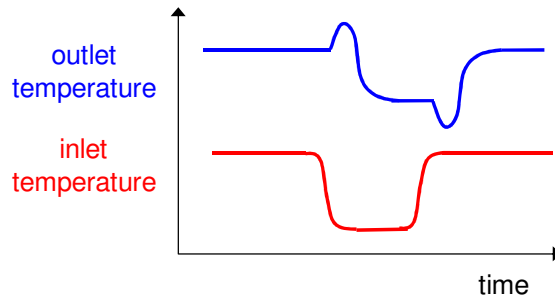
Figure 6-3:   **Expected response of the reactor outlet temperature when per-forming a step down and a step up in the reactor inlet temperature**

Reference state operation at reactor 3 inlet temperature of 340°C indicated that the activity of the catalyst bed is less than expected, meaning that the axial temperature profile stretched throughout the entire length of the reactor without reaching its equilibrium. In order to do a meaningful transient experiment, the reaction front had to be positioned within the catalyst bed. Therefore, the reaction rate was boosted by:

   i)   increasing the feed CO content via bypassing part of the 2nd reactor feed to the 3rd reactor (ELF32 CF001)
   ii)   increasing the 3rd reactor inlet temperature by operating the air cooler ELG30 AC010 with zero fan speed and closed louvers.

Accordingly, the bed inlet temperature rose by 15K from 335°C to 350°C, while the reactor feed CO content increased from about 3.0% to 6.6%. Both effects caused the reaction front to be positioned within the 3rd reactor catalyst bed, as seen in Figure 6-4.
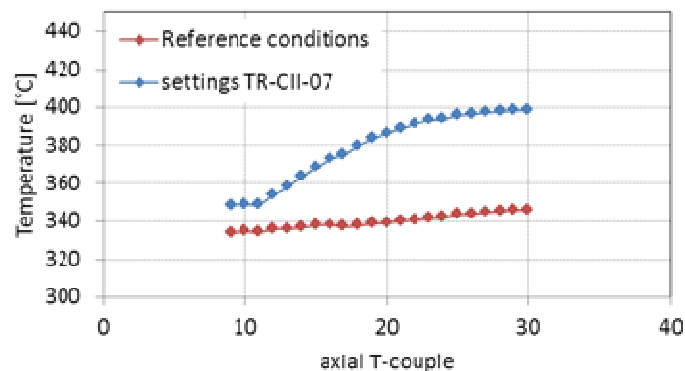
Figure 6-4:   **3rd reactor axial temperature profiles for operation in the reference state and during the increased activity of test run TR-CII-007**

Starting at steady-state operation, the experiment then consisted of rapidly decreasing the reactor inlet temperature by means of manually opening the louvers of the air cooler ELG30 AC010 while maintaining a zero fan speed. After again reaching steady state, the reverse experiment is performed by manually closing the louvers of the air cooler ELG30 AC010 in order to provoke a rapid increase of the inlet temperature. A detailed description and evaluation of the test run can be found in (van Dijk, 2012d). The PGIM plot of the measured temperatures and the outlet composition is given in Figure 6-5 for the period of the transient experiment covering the sudden reactor inlet temperature drop at 8:00 h and the sudden increase in temperature at 12:00 h. When opening the louvers, the reactor inlet temperature drops by 50°C with an initial ramp of 1.7K/min and an overall ramp of 0.9K/min. After opening the louvers, the inlet temperature starts to fluctuate more than operation with closed louvers due to the natural draft created by the opened louvers. The inlet temperature eventually drops to <300°C, extinguishing the WGS reaction and resulting in a flat axial temperature profile throughout the reactor. This is the starting situation for the 2nd transient where the inlet temperature is increased by manually closing the louvers at 12:00 h. The resulting transient describes the start-up of the reactor without any inverse transient responses. The initial steady state operation is again reached.
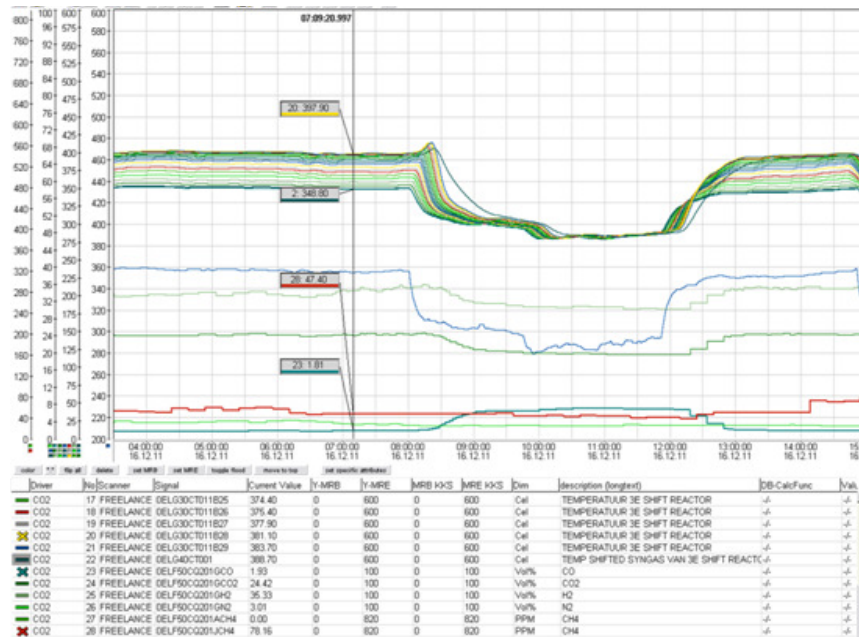

Figure 6-5: PGIM plot of the measured temperatures and outlet composition of the 3rd reactor during the transient operation. Upper band of lines represent the axial reactor temperatures. The blue line below is the feed gas temperature and the other lines represent the syngas composition of the reactor outlet (stream G).

The maximum temperature of the inverse temperature response is observed at about 12 minutes after the inlet perturbation is halfway through. This timescale corresponds well with the thermal time constant of the reactor, which is estimated at 16 minutes. Simulations indicate that for such a transient experiment, the top of the inverse response is observed at about 4/5th of the thermal time constant, depending on the ramp-rate and shape of the perturbation. In other words, on first glance, the transient response has the expected timescale.

6.2.3   Test run TR-CII-016: Catalyst stability and selectivity

In contrast to the other test runs concerning the WGS section, the catalyst stability has to be evaluated over the entire operating period of the reactors. The axial temperature profiles of the reactors, together with the in- and outlet conditions on throughput and composition, provide information on the catalyst activity at a certain moment in time.

At normal operating conditions, the decrease of the FeCr catalyst pellet activity in time is mainly due to two parallel effects, both related to sintering:
1. decrease of the active surface area
2. change of the physical properties of the catalyst determining the inter-pellet transport properties.

The sintering rate increases with increasing temperature and steam content of the feed. Additionally, catalyst activity can change due to poisoning and carbiding, both affecting the number of active sites. Poisoning is case specific and depends on the syngas impurities while carbiding is a more general phenomenon and mainly depends on syngas composition with respect to the steam and CO contents.

At normal operating conditions, the activity for a fresh catalyst decreases by 50% during the first 1000 h operation, after which the decrease in activity is slower. Normal catalyst lifetime is in the order of 3 years. It is expected that operation for 3000-5000 h gives sufficient information on catalyst stability to estimate catalyst requirements for 3 years operation.

Considering the 3 reactors in the pilot plant, reactor 1 has the harshest operation conditions (high outlet temperature and high steam content of the feed of typically 72%) and its rate of deactivation is therefore expected to be highest. Reactor 2 has only slightly milder operating conditions and its catalyst bed is also expected to display a significant deactivation rate. Reactor 3 on the other hand has mild operating conditions compared to the two upstream reactors and catalyst deactivation rate is expected to be lowest for this reactor.

By operating the pilot plant at reference conditions regularly in time, comparing the axial temperature profiles would directly reveal catalyst deactivation. Attempt to do this graphical comparison appeared not fruitful since identical operational conditions concerning throughput, WAC syngas composition, saturator settings and reactor inlet temperature were rarely met. Therefore, the catalyst activity must result from modelling. For this purpose, the catalyst vendor Haldor Topsøe has been involved to support the evaluation of the data acquired from the pilot plant with their in-house models in addition to the model developed by Delft University of Technology and ECN within the project (Hernadez, 2011 and van Dijk, 2012a). The reactor model developed within the project is based on intrinsic kinetics combined with a pellet diffusion model and heat and mass transfer from the bulk gas phase to the pellet surface. The proprietary kinetic model applied by Haldor Topsøe uses lumped pellet kinetics, linking the catalyst pellet activity directly with bulk gas-phase composition, temperature and pressure.

It is assumed that during pellet deactivation, the intrinsic rate of the active site does not change, merely the number of active sites and the accessibility of these sites. The effect of deactivation on the intrinsic reaction rate is described by a time dependant activity factor, which is assumed to have an exponential decay in time.
A dead zone was assumed with respect to the height of the fresh catalyst bed to account for pellet settling and shrinkage, in which the catalyst activity within the models was set to zero. Besides the catalyst activity, the length of this dead zone was estimated for every selected steady state over the entire operation time of the pilot plant, including test campaigns I and II. A detailed description of the data acquisition procedures for both test campaigns is presented in (van Dijk, 2012c).

From the simulations performed by Haldor Topsøe and ECN (which are not presented in this report due to confidentiality), the main observations from the analysis are:

- The behaviour of the catalyst in reactor 1 and reactor 2 is much better than expected. Haldor Topsøe indicates that operation of this catalyst in plants using similar high CO syngas and associated high operating temperature (at a European refinery and at a refinery in Brazil) displays more sintering of the catalyst and thus a stronger decrease of catalyst activity than observed in Buggenum.
- The decrease in reactor 1 activity is much less than expected and the catalyst appears to perform rather stable.
- The reactor 2 catalyst does not appear to deactivate at all and its operation is rather stable in time.
- The reactor 3 catalyst behaves much worse than anticipated. The operating conditions for this reactor are mildest (lowest temperature, lowest steam content, highest steam/CO ratio). Earlier simulations of reactor 3 with settings

that boosted the reaction (higher inlet CO content and temperature compared to reference operation, see 6.2.2), also indicated a lower catalyst activity. The present simulations illustrate that the reactor 3 catalyst does not perform as it should, but are considered much less accurate compared to reactor 1 and reactor 2 simulations due to the flat temperature profile within the reactor (reactor 3 does not reach the thermodynamic equilibrium at reference operation).

On September 13, 2012, catalyst samples were taken from reactor 3 in the pilot. This sample was analysed by Haldor Topsøe on elemental composition, phase composition (XRD) and activity tests. The major findings are summarized below:

- The elemental composition analysis did not reveal the presence of any unusual components, indicating that catalyst poisoning cannot explain the lower activity. The components that have increased contents compared to conventional operation in natural gas originating syngas: Al and S. The Al most likely results from the alumina balls that are on top of the bed, while sulphur is present because the syngas in the pilot plant contains in the order of 10-20 ppm H_2S+COS.
- The X-ray diffraction analysis revealed the presence of a small amount of metallic iron, which is unusual for a catalyst at normal operation.

Haldor Topsøe obtained similar conclusions analysing reactor 3 samples taken after shutdown of the pilot early 2013. No unusual components were identified with chemical analysis, but small amounts of metallic iron were identified by XRD. Although the activity appeared to have increased somewhat, it is still far below the expected activity for normal operation. Metallic-Fe cannot be transformed into the active magnetite phase at normal operating conditions. At the Haldor Topsøe laboratories, a controlled reoxidation followed by activation via reduction did not result in recuperation of the activity: the measured activity did not change and metallic Iron was still identified by subsequent XRD.

Due to catalyst deactivation, the feed temperature is low for a fresh catalyst and increases in time, leading to better than design operation at first and ending with operation at design near the end of catalyst lifetime. Since catalyst deactivation appears mainly triggered by high pressure, high temperature steam, the deactivation rate at a lowered feed temperature for a fresh catalyst is likely to be lower. Moreover, lower initial feed temperatures also allow for lower feed steam contents. This especially concerns reactor 1 operation, since its large surplus of steam (steam/CO=4.1 for reference state operation) serves to control the adiabatic temperature rise. Operation at a lower steam content is again likely to decrease the reactor 1 deactivation rate.

It should be noted that the Buggenum pilot is operated at roughly 20 bar, while the full-scale capture plant is envisioned to be operated at circa 40 bar. The higher steam pressure will enhance catalyst deactivation by thermal sintering, especially for reactor 1. This effect, however, cannot be taken into account quantitatively, but it must be noted that this increases the uncertainty of the predictions. Note that an increased pressure does not result in a significant increase in net reaction rate. The net reaction rate is a trade-off between intrinsic reaction rate and pellet diffusion. Since the reaction is mainly operated in the diffusion controlled regime, the increased intrinsic reaction rate is damped by the decreased diffusion rate within the pellet. Accordingly, the effect of increased pressure is progressively dampened at higher pressures. This is illustrated in Figure 6-6, where the axial temperature profiles at different operating pressure are simulated for reactor 1 reference state operation, together with the position of the reaction front within the bed (at $\beta=0.9$) at increasing pressure. The effect of a potential increased catalyst deactivation rate at higher pressure "overrules" the increased catalyst activity; meaning that a higher operating pressure is likely to lead to an increased deactivation rate.
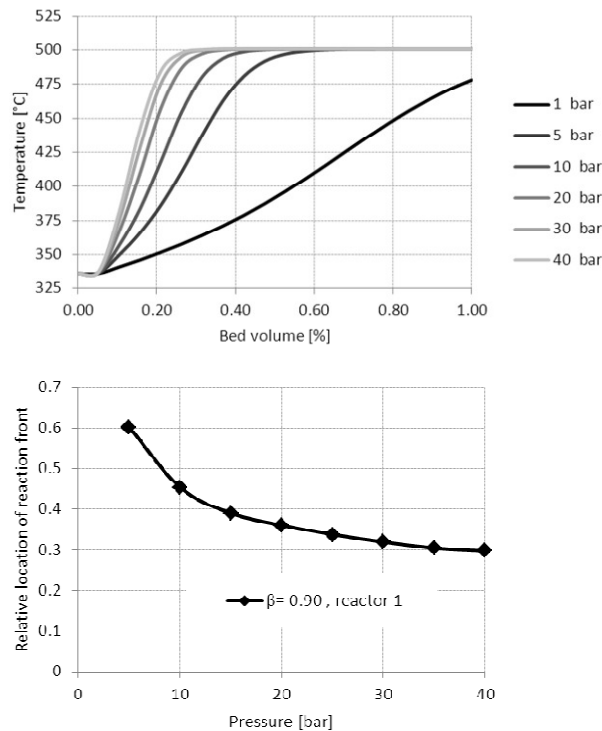

Figure 6-6:   Simulated axial temperature profiles for reactor 1 reference conditions (relative activity factor=0.67) at increasing reactor pressure (top) and the resulting position of the reaction front (at $\beta=0.9$) within the bed as a function of operating pressure (bottom)
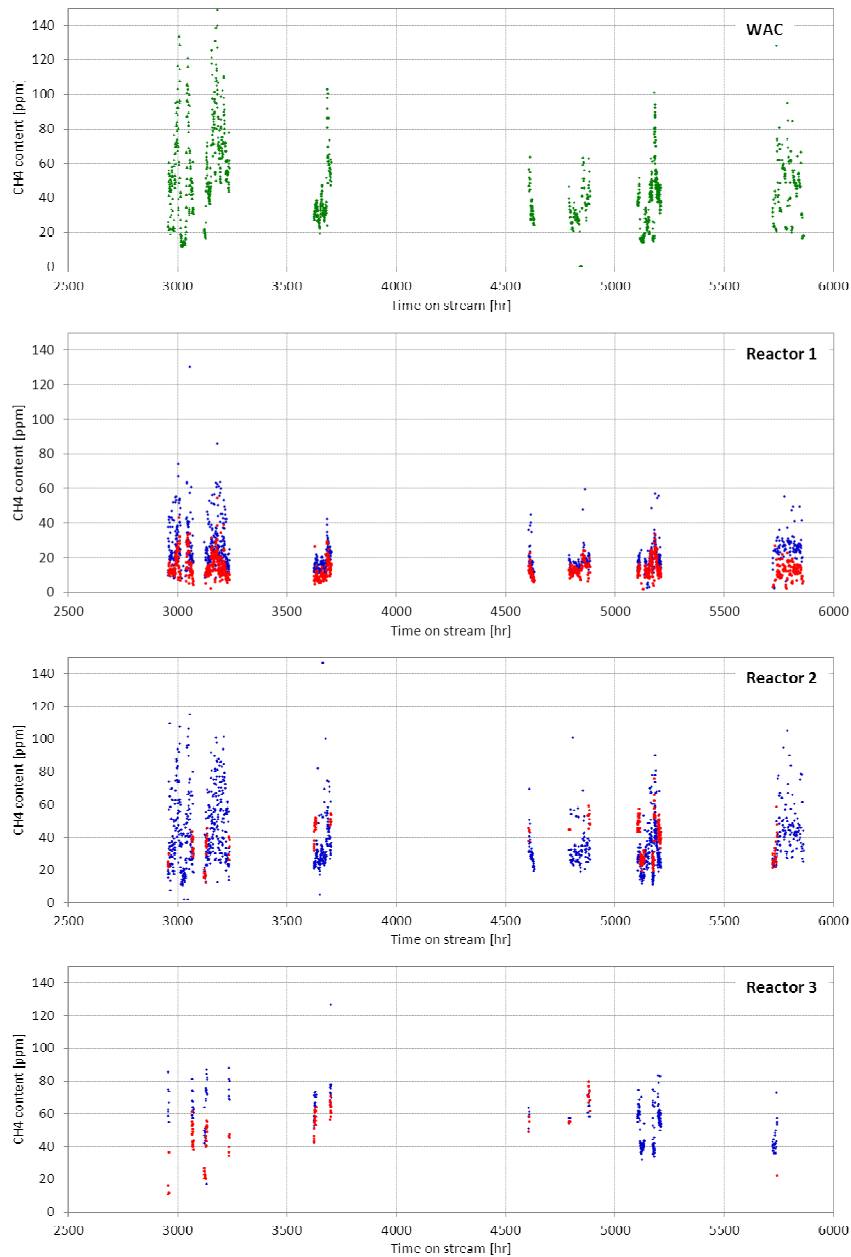
Figure 6-7:   **Methane content of the feed and effluent for reactors 1, 2 and 3 as a function of time. Blue markers: feed, Red markers: effluent**

Catalyst selectivity

CH_4 is an important by-product for any WGS catalyst. For FeCr-based catalysts, the catalyst CH_4 production is an indication of the catalyst selectivity. The CH_4 content for a selected number of steady state operational points is shown in Figure 6-7. Note

the relatively large spread in CH_4 measurement is directly related to the spread of the CH_4 content of the syngas entering the pilot plant, represented by the top graph (analyser EVB60 CQ001). The CH_4 content of the reactors is significantly lower than the WAC CH_4 content due to dilution with steam. During the entire operating period, the CH_4 content of the syngas is low at <50 ppm. The CH_4 production by the catalyst does not increase in time, except maybe for reactor 3, where the CH_4 content of the effluent appears to increase from 40 ppm to 60 ppm.

6.2.4   Test run TR-CII-017: Catalyst coking

The purpose of this test run is to study the effect of reduced steam content on the catalyst resistance to iron carbide formation. Operation at a reduced steam/CO ratio would allow reducing the steam requirement for the WGS section and thus the CO_2 capture penalty, but can lead to reduction of the magnetite phase, Fe_3O_4, to FeC, which is active in hydrocarbon formation, noticeably CH_4. This so-called carbiding of the catalyst is reversible if the extent of carbide formation is not too severe. Severe carbiding can lead to permanent loss of catalyst activity and/or selectivity and even to physical damage of the catalyst pellets.

Carbiding of the catalyst is a function of operational conditions and, more importantly, of the catalyst age. The tendency for carbide formation increases at catalyst age, increasing total pressure, reduced steam content and increased CO content of the feed. Since the main hydrocarbon formed is CH_4, this indicator can be monitored to investigate the catalyst tendency for carbiding. Setting a decreased steam/CO feed ratio leads to an increase of the CH_4 content at the reactor outlet. Progressive carbiding of the catalyst is represented by a continuously increasing CH_4 content once the steam/CO ratio is set. Excessive carbiding results in a sudden increase of the CH_4 formation rate. As the CH_4 content of the syngas varies with the gasifier load, either the difference between reactor inlet and outlet concentration or an indexed concentration should be used as indicator (van Dijk, 2012b).

The majority of the industrial experience with HTS is for CO conversion in NG-derived syngas for e.g. H_2 and ammonia production. The syngas coming from a steam reformer has a feed CO content in the order of 12-18%dry, much lower than coal gasification syngas which is >45%dry and typically 60%dry in case of the Shell dry gasifyer such as applied in Buggenum. Natural gas derived syngas generally has a high CH_4 content (%-level), making on-line monitoring to spot catalyst carbiding pointless. Coal derived syngas, on the other hand, has a low CH_4 content and on-line monitoring to detect the onset of catalyst carbiding becomes feasible. To our knowledge, this strategy has not been pursued before because of the lay-out of the WGS section in gasification applications: reactors in series. Because of the high CO content of the gasification syngas, the 1st reactor then required large amounts of steam to limit the

reactor outlet temperature. The downstream reactors automatically have a high surplus of steam to drive the CO conversion reaction. In other words, all reactors are operated far from the carbiding limit of the catalyst and there is no need to monitor the CH_4 make by the catalyst. The Buggenum and Magnum layout of the WGS section is in that respect rather special, since the reactor 2 steam feed content is not entirely dictated by the reactor 1 steam requirements. Reactor 1 will still be operated with steam feed contents that are dictated by the maximum allowable outlet temperature, but reactor 2 allows operation close to the carbiding limit of the catalyst.

During the test run a series of set points with low steam/CO ratios has been performed, which are tabulated in Table 6-7 (van Dijk, 2012b).

Table 6-7:   Executed set points of TR-0017

|	Date and dura-tion		Reactor 2 S/CO		Overall S/syngas	ELF20 temperature	ELF40 temperature
		Hr	mol/mol	kg/kg	kg/kg	°C	°C
					ELG40CX001	ELF30CT002	ELF40CT002
Ref.	22-04-12	6	$3.09_{\pm0.03}$	$1.99_{\pm0.02}$	1.23	$172.4_{\pm0.3}$	$195.0_{\pm0.1}$
SP 1	26-03-12	101	$2.58_{\pm0.17}$	$1.66_{\pm0.11}$	1.04	$163.2_{\pm0.2}$	$195.2_{\pm0.4}$
SP 2	02-04-12	94	$2.23_{\pm0.08}$	$1.44_{\pm0.05}$	0.98	$160.8_{\pm0.4}$	$195.0_{\pm0.5}$
SP 5	23-04-13	59	$2.06_{\pm0.06}$	$1.32_{\pm0.03}$	0.89	$151.7_{\pm0.4}$	$194.8_{\pm0.3}$
	26-11-12	12	$2.06_{\pm0.02}$	$1.32_{\pm0.01}$	0.92	$151.6_{\pm0.2}$	$195.4_{\pm0.1}$
SP 6	26-11-12	11	$1.71_{\pm0.03}$	$1.10_{\pm0.02}$	0.79	$140.4_{\pm0.2}$	$195.2_{\pm0.1}$
	04-12-12	76	$1.75_{\pm0.02}$	$1.13_{\pm0.02}$	0.80	$140.5_{\pm0.1}$	$194.1_{\pm0.2}$
	18-12-12	21	$1.75_{\pm0.03}$	$1.12_{\pm0.02}$	0.79	$138.5_{\pm0.3}$	$194.4_{\pm0.4}$
SP 7	19-12-12	10	$1.62_{\pm0.01}$	$1.04_{\pm0.01}$	0.77	$136.5_{\pm0.2}$	$194.0_{\pm0.2}$
	20-12-12	10	$1.58_{\pm0.03}$	$1.01_{\pm0.02}$	0.76	$132.7_{\pm0.3}$	$193.9_{\pm0.6}$
SP 8	07-03-13	117	$1.45_{\pm0.03}$	$0.93_{\pm0.02}$	0.74	$126.5_{\pm0.2}$	$195.1_{\pm0.4}$
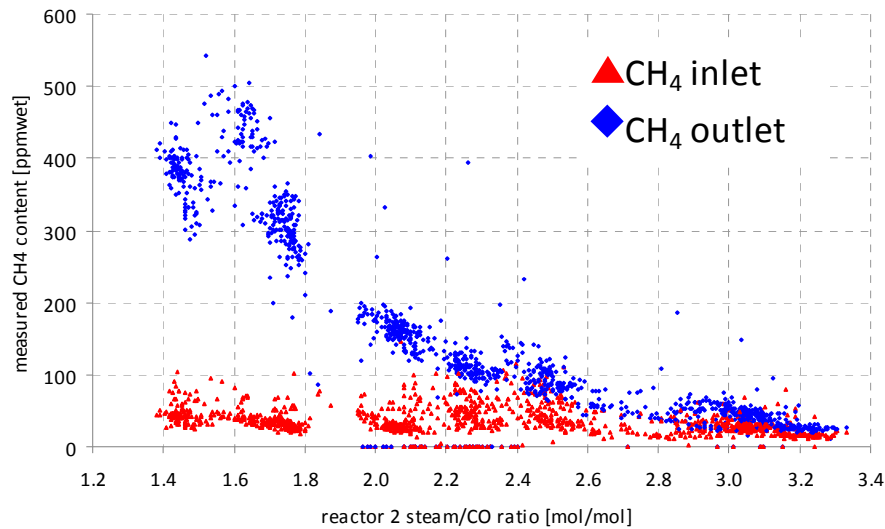
Figure 6-8:   **Measured CH$_4$ contents of the reactor 2 inlet and outlet during TR-CII-017**

In Figure 6-8 the 2nd reactor CH$_4$ content of the feed and effluent are plotted as a function of the feed molar steam/CO ratio. Operation at all set points ranging from steam/CO=2.5 to 1.45 indicates that the catalyst does have an increased CH$_4$ production activity at reduced steam/CO ratio, but that this productivity does not increase in time for the duration of the tests. Even at 116 h operation at steam/CO=1.45, the CH$_4$ content of the outlet syngas is constant, although the absolute amount of CH$_4$ in the reactor 2 outlet is lower than expected, which is probably due to an offset of the analyser. This would signify that the catalyst in its current state is resistive towards reduced steam content of the feed and that progressive carbiding of the catalyst does not occur. Haldor Topsøe stated that carbiding of a fresh catalyst at a steam/CO ratio in the range of 1.8-2.0 could take up to 1 week of operation. For a catalyst that has experienced carbiding and for a catalyst in end-of-life state, carbiding occurs much faster. The TR-CII-017 set points have been executed on a catalyst that has already experienced its initial fast deactivation and was operated for 3000 h. The most demanding SP 8 operation at a steam/CO ratio of 1.45 was performed for a 116 h period on a catalyst that has been operated already for 5750 h. Hence the catalyst is more resistant for progressive carbiding than what was indicated by the vendor.

A second indication that excessive carbiding did not occur during testing is that decrease of the catalyst activity factor in time does not correlate to the TR-017 operation. The overall drop in catalyst activity does not appear to correlate with the lowered steam/CO ratio operation: the demanding operation corresponding to SP 6 and SP 7 does not appear to appear to lead to a reduced catalyst activity. The same conclusion was drawn when comparing the axial temperature profiles before and after

the execution of each set point, see Figure 6-9. When returning to reference conditions, catalyst activity and CH_4 make was similar to operation prior to the lower steam/CO excursion.

A third indication that excessive carbiding did not occur during testing is the absence of C_2 and C_3 hydrocarbons in the reactor 2 effluent during SP 8 operation. In the absence of excessive carbiding, the production of C_2 and C_3 hydrocarbons by the catalyst is very low and these hydrocarbons are virtually absent in gasification syngas. An increase in these hydrocarbons might be a more sensitive indicator for catalyst carbiding. During the catalyst screening at the ECN laboratories (van Dijk et al., 2011) it was observed that no C_1-C_3 hydrocarbons were produced at similar conditions. At 350°C, an aged catalyst (24 hr at 500°C and 2 activity plots till 500°C) was exposure to lower steam contents of 1.4, 1.0, 0.6 and 0.4 in 8 hr runs respectively. The pellets did not produce any C_2-C_3 hydrocarbons at steam/CO=1.4 and 1.0. Only at steam/CO=0.6 and 0.4, the catalyst produced 75 ppm and 250 ppm C_2H_6 and 75 ppm and 125 ppm C_2H_4, respectively.

A fourth indication that excessive carbiding did not occur during testing is that the strength of the catalyst pellets from the top of the reactor 2 bed was not compromised. After the test campaign, the catalyst was unloaded and pellet strength was analysed by Haldor Topsøe. The reactor 2 pellets displayed a normal strength, indicating that pellet weakening by excessive carbiding did not occur.
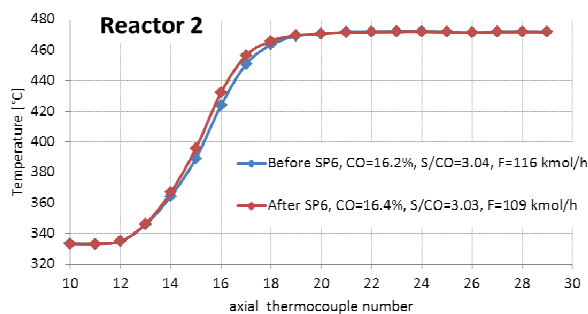

Figure 6-9:   **Axial temperature profiles for reactor 2 during reference conditions before and after SP 6 operation**

To illustrate the effect of lowering the steam/CO ratio on the overall CO conversion, the SP 5 performance of the WGS section is plotted in a CO vs. temperature plot in Figure 6-10. Since reactor 1 operation is not changed, its performance is represented by a single line. For the SP 5 operation, the steam content of the reactor 2 feed is lowered, resulting in a higher equilibrium CO content (dashed red line) compared to reference state operation (solid red line). The reactor 2 feed CO content increases due to the lower steam content of the quench, causing an increase in the adiabatic tempera-

ture rise. Similar changes for reactor 3 are observed. Reactor 3 still does not reach equilibrium but displays a larger temperature rise compared to operation at the reference conditions.
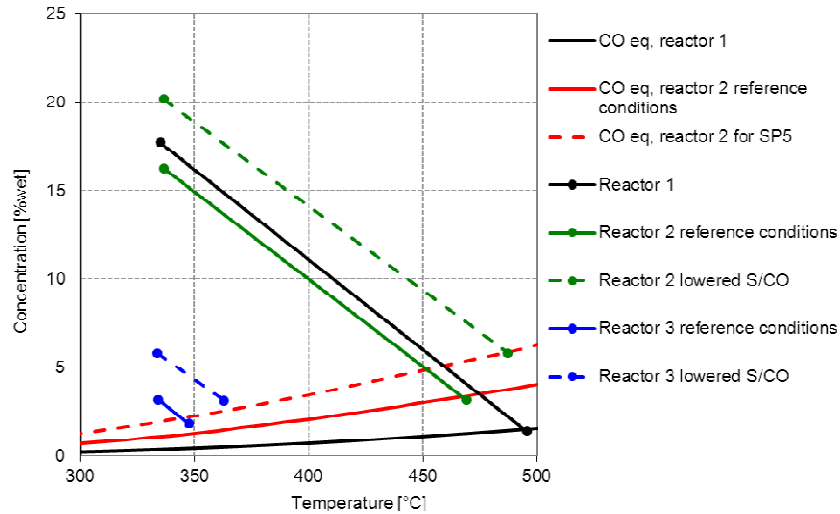

Figure 6-10: **Measured CO content as a function of temperature for the reference state compared to SP 5 operation together with the equilibrium CO lines for the different reactors and operating conditions.**

The WGS section performance for SP 5 and 8, representing a modest and extreme scenario, compared to reference state is listed in Table 6-8. For SP 5 operation, a decrease in total steam consumption by 26% is realised in SP 5 operation at the expense of only a small drop in CO conversion by 3.6%-points. This means that a small decrease in CO_2 capture ratio saves a significant amount of steam, thereby decreasing the efficiency penalty for CO_2 capture. For SP 8 operation, the steam feed decreases by 35% resulting in a 9.2%-points drop in CO conversion. Here it has to be taken into account that SP 8 has been performed with an increased feed temperature for reactor 3 in order to reach equilibrium. Therefore, the absolute values cannot be compared directly.

Table 6-8: Measured feed flows, overall CO conversion and overall steam/CO ratio for SP 5 and SP 8 operation

		SP 5 operation		SP 8 operation	
		Reference state	R2 S/CO=2.06	Reference state	R2 S/CO=1.45
Syngas feed	kmol/h	50.1	50.3	48.6	46.0
Reaction water feed	kmol/h	70.8	52.9	71.3	44.1
CO content syngas	%dry	59.8	60.5	61.9	63.4
Overall steam/syngas	kg/kg	1.20	0.89	1.23	0.80
Overall steam/CO	mol/mol	2.36	1.74	2.37	1.51
Overall X_{CO}	%	92.9	89.3	93.8	84.6

Lowering the steam/CO feed ratio also causes the reaction rate to increase because of the higher reaction order for CO than for H_2O (van Dijk and Booneveld, 2011). This is also observed experimentally in Figure 6-11 where the axial temperature profile for the reference operation is compared to the profile during SP 6 operation. Note that the during SP 6 operation, the total reactor 2 feed flow decreased from 114 to 95 kmol/h. The axial temperature profile during SP 6 operation is much steeper than during reference operation, evidencing a much higher reaction rate compared to reference state operation. This implicates that at lowered steam/CO ratio, the inlet temperature can be lowered and/or the catalyst volume can be smaller.
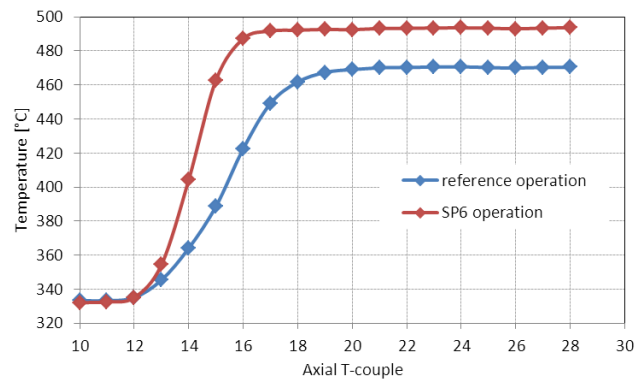
Figure 6-11: Axial temperature profile during reference state operation and SP 6 operation

Quantification and optimisation of the efficiency penalty by decreasing the steam content should be based on a system evaluation. This system evaluation should consider lowered steam contents of both the reactor 1 as the reactor 2 feeds. Reactor 1 steam content is determined by the allowable adiabatic temperature rise. Reactor 2 steam content is determined by the minimum required to prevent progressive catalyst

carbiding, and thus to ensure catalyst lifetime. Steam savings for both reactor 1 and reactor 2 are possible. For reactor 1, the high catalyst activity allows to decrease the feed temperature and thus the steam content without compromising the maximum reactor outlet temperature. For reactor 2, the measurements in this report indicate that catalyst resistance against progressive carbiding is good at lowered steam contents and decreasing the steam content of the quench is feasible. Similar to reactor 1, reactor 2 temperature can also be lowered.

For start-of-life conditions, the catalyst is active and resistant against excessive carbiding. This would allow operation at significantly reduced steam content for both reactor 1 and reactor 2 operation, in combination with as low as possible inlet temperatures for all three reactors. For reactor 1, the steam/CO ratio is always sufficiently high to prevent excessive carbiding, even for a catalyst at end-of-life activity. Since catalyst deactivation by thermal sintering increases with increasing steam content of the feed, lowering reactor 1 steam content might improve catalyst lifetime, provided that the reactor outlet temperature does not increase by simultaneously decreasing the inlet temperature. The rate of catalyst deactivation for reactor 1 was indeed found to be higher as for the reactor 2 catalyst. For end-of-life conditions, the required steam content for reactor 2 might have to be increased to prevent progressive carbiding.

For the Magnum design the design pressure is 35 bar instead of 20 bar for the Buggenum pilot operation. Besides the effect of an increasing pressure on activity and stability (see 6.2.3), the catalyst tendency for carbiding increases at increasing pressure. Haldor Topsøe calculations indicate that a pressure increase from 20 to 40 bar would lead to an increase of the steam/CO ratio of approximately 8% relative.

Although the tests presented in this report show promising resistance towards progressive carbiding, catalyst lifetime over several thousands of hours for this significantly dryer operation remains uncertain. Therefore, on-line monitoring of the CH_4 content is crucial: at the moment an exponential increase of the CH_4 content is observed, the steam content should be increased to stabilize the CH_4 content. As the CH_4 content of the entering syngas has the same order of magnitude than the CH_4 production by the catalyst at reduced steam/CO ratio operation, an accurate indirect measurement of catalyst carbiding is possible in entrained flow IGCC systems. Using this characteristic, the steam content of the quench flow can be controlled by means of the measured CH_4 content in the reactor 2 effluent over the catalyst lifetime.

A strategy to learn about the operating limits at this dryer operation could be the following. For the 1st batch of catalyst, the catalyst is operated at a decreased steam content, while continuously monitoring catalyst carbiding via the CH_4 content. When carbiding occurs, the steam content should be increased such that the hydrocarbon production is stable again. This is done throughout the remaining catalyst lifetime. For

the 2nd batch, operation starts at the lowered steam content, but the steam content is increased some time before carbiding was observed for the 1st time for the 1st batch. This operation is then maintained until the CH_4 content indicates carbiding, necessitating increasing the steam content again. For the 3rd batch, operation starts at the lowered steam content and the steam is increased at the pre-set time in a similar way as for the 2nd batch. A second increase in steam content is then executed some time before carbiding was observed for the 1st time in the 2nd batch. This operation is then maintained until the CH_4 content indicates carbiding, necessitating increasing the steam content again.

Applying this procedure allows building up a strategy for the required steam content throughout the catalyst lifetime, such that the catalyst is always operated outside the carbiding regime. The steam consumption is thus optimizing throughout the catalyst lifetime. The downside of this strategy, especially for the first few batches, is that the catalyst is operated close to the carbiding regime for significant periods of time. It can thus occur that the catalyst is exposed to excessive carbiding, limiting the catalyst lifetime for that batch. Moreover, it could lead to unplanned downtime of the plant if the catalyst is too badly damaged. This strategy should therefore be subject to an economic evaluation (steam savings versus catalyst costs and downtime).

6.3   CO$_2$ Absorption section

6.3.1   Test run TR-CII-009: Water mass flow absorption section

In order to investigate the influence of the water content in DEPEG on the absorption performance and the hydrodynamic conditions of the absorption plant, the water content in the solvent has been varied by changing the make-up water flow rate. Three different set points have been established with water flow rates of 0.5 kg/h, 1.5 kg/h and 4.0 kg/h. A detailed description and evaluation of TR-009 can be found in (Valenz, 2012a).

The overall process is adapting very slowly and after changing the water flow rate it takes up to 14 days to reach new steady state conditions due to the large DEPEG hold-up in the entire system (20 tons). The slow adaption of the process to the new conditions can be seen for set point 2 in Figure 6-12.
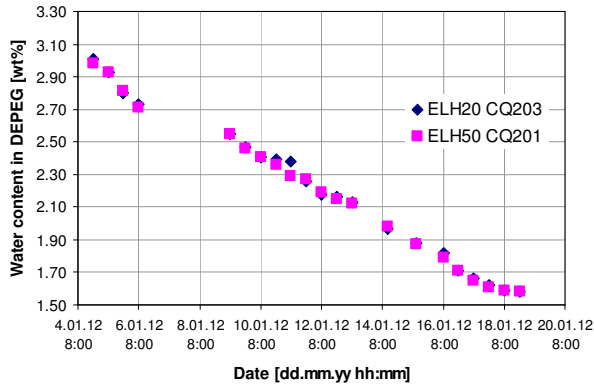
Figure 6-12:   Water content dependency on time during the 2nd set point.

One important purpose of this test run is to validate is the binary interaction coefficient between water – DEPEG in the PC-SAFT equation of state (see 7.3.2 for PC-SAFT equation of state). For model validation it is important that the concentration differs significantly between the set points. As shown in Figure 6-13, the water content changed by a factor four during the performed set point, which should be sufficient to allow for successful model validation.
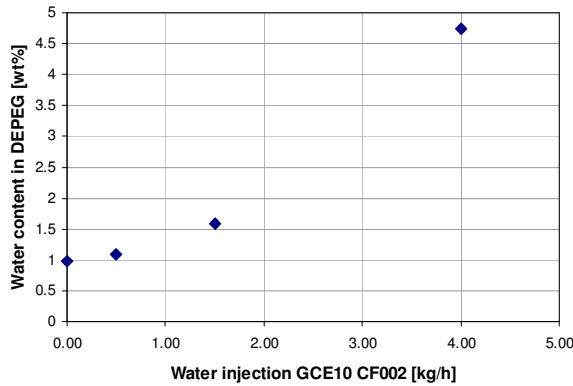
Figure 6-13:   Dependency of water content in DEPEG on the water mass flow rate

In Figure 6-14, the dependency of the CO_2 absorption efficiency on the water content is shown. The CO_2 absorption efficiency is slightly decreasing with the increase of the water content as expected. It can be concluded that as long as the water content is about 1 ± 0.5 wt%, steady-state can be assumed and the influence on the process variables is negligible. Therefore all further test runs can be performed for a single water content in DEPEG (1 ± 0.5 wt%).
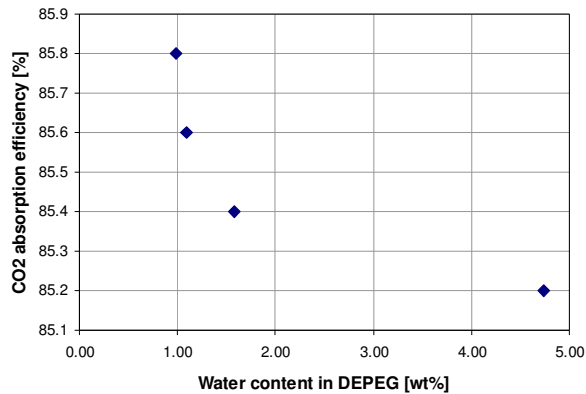
Figure 6-14:   Dependency of CO$_2$ absorption efficiency on the water content in DEPEG

6.3.2   Test run TR-CII-010: Solvent heater power input

The purpose of this test run was to validate the temperature dependency of the binary interaction coefficient between water – DEPEG. Therefore the solvent heater power input has been changed in order to vary the temperature of the solvent from the 1st flash vessel (ELH30 CT001). This leads to new equilibrium conditions with a changed water content in DEPEG. As in TR-CII-009 this is a very slow process that takes a long time before the new steady-state set point is established. Only one set point could be performed as described in (Valenz, 2012b) where the temperature of ELH30 CT001 was set to 48°C at a water flow rate of 4 kg/h.

In Figure 6-15, the water content in DEPEG is shown during the executed set point for TR-010. The water content decreased from 4.70 wt% (stable water content of set point 3 of TR-CII-009) to 2.14 wt% (steady state value) within 16 days. The difference is more than a factor 2, which should be sufficient to allow for successful model validation.

Figure 6-15: **Water content in DEPEG dependency on time for a change in the ELH30 CT001 temperature to 48°C**

It is interesting to point out that the CO_2 absorption efficiency for the performed set point (86.6%) is higher than the one in the reference state (85.8%) even though higher water content should cause lower CO_2 absorption efficiency. It is caused by the higher temperature of the DEPEG in 2nd and 3rd flash vessel and therefore more CO_2 is desorbed and lean solvent contains significantly less CO_2 than in the reference state.

6.3.3   Test runs TR-CII-011 and TR-CIII-011: Solvent mass flow

This test run was performed in order to investigate the influence of the solvent flow rate on the absorber performance. The results will be used together with the data from TR-012 (see 6.3.4) to validate the mass transfer coefficients in the absorber model (see 7.3.2.4 for results). TR-CII-011 has been performed for the random packing Raschig Super-Ring 0.6 and TR-CIII-011 for the structured packing Raschig Super-Pak 250Y. In the first series of tests during TR-CIII-011, the plant had been re-configured for the high solvent flow rate test (see 6.3.8) and equipped with a different distributor for high solvent flow rates. Therefore the results from this test TR-CIII-011a were not fully comparable with the tests performed in TR-CII-011 and the test has been repeated as TR-CIII-011b with the distributor for reference conditions as used in TR-CII-011. In addition, the reference conditions for the syngas flow rate have changed during TR-CIII (1400 kg/h instead of 1600 kg/h). Therefore, one set point has been performed additionally at 1570 kg/h shifted syngas flow rate and 10 kg/s solvent flow rate.

The tests and the results are described in detail in (Valenz, 2012c; Valenz, 2013a and Valenz, 2013b). A summary of the performed test runs and the most important settings for the individual set points is shown in Table 6-9. For TR-CII-011 (SP4) and TR-CIII-011a (SP5) the reference conditions are also given (taken from previous test runs).

Table 6-9:　　　**Performed test runs and set points for solvent flow rate tests**

Test run	Set point	Solvent flow rate [kg/s]	Shifted syngas flow rate [kg/h]	Distributor type[6]
TR-CII-011	1	13	1612	A
	2	11	1677	A
	3	10	1590	A
	4[7]	15	1603	A
TR-CIII-011a	1	13	1409	B
	2	11	1400	B
	3	10	1405	B
	4	10	1571	B
	5[8]	15	1394	B
TR-CIII-011b	1	13	1406	A
	2	11	1393	A
	3	10	1420	A
	4	11	1576	A
	5	13	1534	A
	6	15	1406	A

The most important variables to validate the mass transfer coefficient in the liquid phase are the CO_2 concentrations in between the packed bed and in the H_2 Rich gas. In Figure 6-16 the measured CO_2 concentrations in-between the packed beds and at the outlet of the absorber are shown for TR-CII-011 (SP1 – SP4) and TR-CIII-011a (SP1 –SP3 and SP5). As shown in Figure 6-16, the CO_2 concentrations changed by a factor 2 or more during the performed set points, which should be sufficient to allow for successful model validation.

The CO_2 absorption efficiency as a function of the solvent mass flow rate is shown in Figure 6-17. The CO_2 absorption efficiency is decreasing with the decrease of the solvent mass flow rate which is according expectations. Note that the absolute values shown in Figure 6-16 and Figure 6-17 cannot be compared directly due to the different distributor and changed shifted syngas flow rates.

---

[6] For definition see 6.3.8
[7] Reference state for TCII performed in previous test run
[8] Reference state for TCIII performed in previous test run
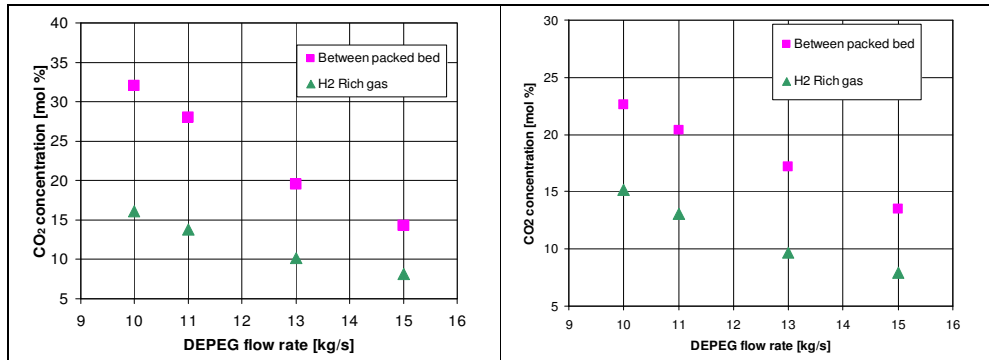
Figure 6-16: **Dependency of CO$_2$ concentration in between packed beds and in the H$_2$ rich gas stream on the solvent mass flow rate for TR-CII-011 (left) and TR-CIII-011a (right)**
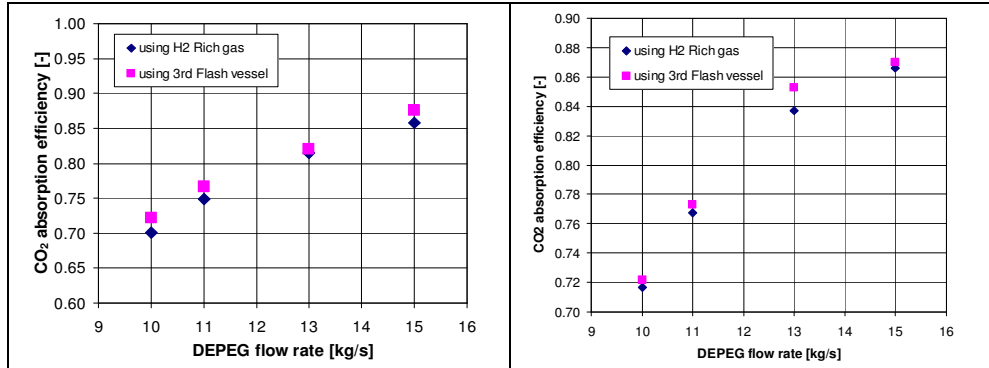
Figure 6-17: **Dependency of CO$_2$ absorption efficiency on the solvent mass flow rate for TR-CII-011 (left) and TR-CIII-011a/b (right)**

A comparison of the set point that has been performed at the same shifted syngas flow rate for TR-CII-011 (SP3) and TR-CIII-011a (SP4) at 10 kg/s showed that the calculated absorption efficiency for the Raschig Super-Ring 0.6 at 70.1% was higher than the absorption efficiency for the Raschig Super-Pak 250Y packing at 67.8%. However these tests still include the influence of the different distributor that influences the flow pattern within the column and therefore it is difficult to directly compare these values.

To allow for a better comparison of the two types of packing, TR-CIII-011b has been performed with the distributor type A. Three set points have been performed at the new reference conditions (1400 kg/h shifted syngas flow rate). Two additional set points (SP4 and SP5 see Table 6-9) have been performed at the "old" reference conditions to provide data that could be compared with the results from TR-CII-011.

Due to the simultaneously running test run in the WGS section the absorber inlet concentrations of CO was about three times higher compared to the reference conditions for the entire TR-CIII-011b (consequently the absorber inlet concentrations of CO_2 and H_2 were lower). CO concentration was about 6 % instead of 2% and CO_2 and H_2 concentrations were about 2 % absolute lower in comparison with reference state measured at 23-11-2012. In addition, the pressure in the 3rd flash vessel was higher than in previous reference conditions (1.35 bar instead of 1.20 bar).

In order to be able to at least quantitatively compare TR-CIII-011b (SP4 and SP5) with the results from TR-CII-011 (SP1 and SP2) the influence of the mentioned differences (higher CO inlet concentrations and higher pressure 3rd flash vessel), TR-CIII-011b is compared with the results from TR-CIII-011a. The main differences in the boundary conditions are:

- The liquid distributor (Type A for TR-CIII-011b and Type B for TR-CIII-011a). If any influence is to be expected, then the Type A distributor used in TR-CIII-011b should allow for a better performance as it suitable for the tested solvent flow rates.
- Higher pressure in 3rd flash vessel during TR-CIII-011b. This causes higher CO_2 concentration in the lean solvent and consequently the decrease of the driving force for mass transfer which should decrease the absorption efficiency.
- Lower concentration of CO_2 at the inlet into the absorber. This also decreases the driving force for mass transfer and reduces the absorption efficiency.

As seen in Figure 6-18, the absorption efficiency for TR-CIII-011b (repetition) is lower than in TR-CIII-011a for 13 and 15 kg/s solvent flow rate. In this operating region, only the influence of the increased pressure in the 3rd flash vessel and the increased CO_2 concentration in the shifted syngas can be seen as both distributors are designed to operate in that region although minor differences still could occur. For lower solvent flow rates the influence of the distributor type B, which is not designed for these low flow rates, increases with decreasing flow rate. In conclusion for solvent flow rates higher than 13 kg/s the data are not (or negligibly) influenced by the used internals. At lower flow rates the effect of the liquid distribution is significant and therefore for the model validation the data of TR-CIII-011b should be used.
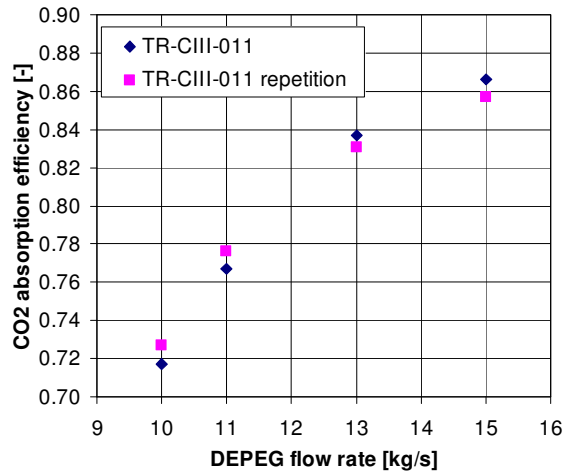
Figure 6-18: **Dependency of CO$_2$ absorption efficiency (calculating using H$_2$ rich gas stream) on the solvent mass flow rate for TR-CIII-011a and TR-CIII-011b (repetition)**

6.3.4 Test runs TR-CII-012 and TR-CIII-012: Shifted syngas flow rate

This test run was performed in order to investigate the influence of the shifted syngas flow rate on the absorber performance. The results will be used together with the data from TR-011 (see 6.3.3) to validate the mass transfer coefficients in the absorber model (see 7.3.2.4 for results). TR-012 has been performed for the random packing (TR-CII-012) as well as for the structured packing (TR-CIII-012). The tested set points are shown in Table 6-10. A detailed description and evaluation of the test runs can be found in (Valenz, 2012d and Valenz, 2013c).

Table 6-10: **Performed test runs and set points for shifted syngas flow rate tests**

Test run	Set point	Shifted syngas flow rate [kg/h]	Solvent flow rate [kg/s]	Distributor type[9]
TR-CII-012	1	1376	15	A
	2	786	15	A
	3	1754	15	A
TR-CIII-012	1	1573	15	B
	2	1246	15	B
	3	819	15	B

---

[9] For definition see 6.3.8

The dependency of the concentration profile on the shifted syngas mass flow rate is shown in Figure 6-19 for both packings. It can be seen that the concentrations in-between the packed beds changes around 2 times and at the absorber outlet around 50% for both test runs, which should be sufficient to allow for successful model validation.
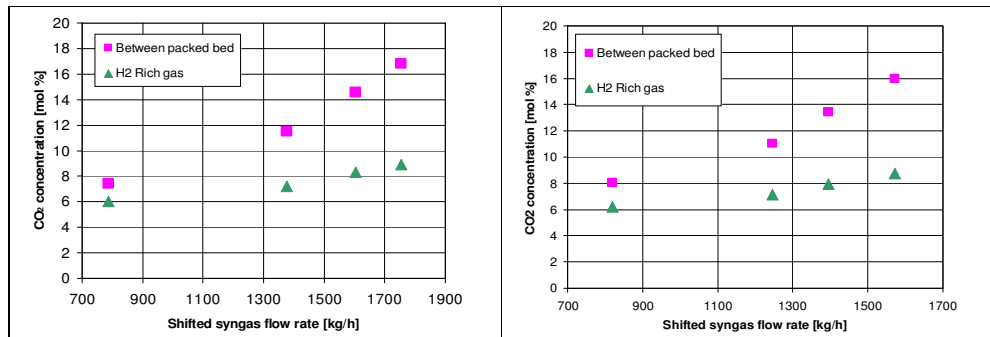
Figure 6-19:   **Dependency of CO$_2$ concentration in between packed beds and in the H$_2$ rich gas stream on the shifted syngas mass flow rate for TR-CII-012 (left) and TR-CIII-012 (right)**

A comparison of the absorption efficiency can be seen in Figure 6-20. From this evaluation it seems that, against expectations, the random packing has better absorption efficiency than the structured packing. The packing performance and comparison is discussed in more detail in 7.3.2.4.
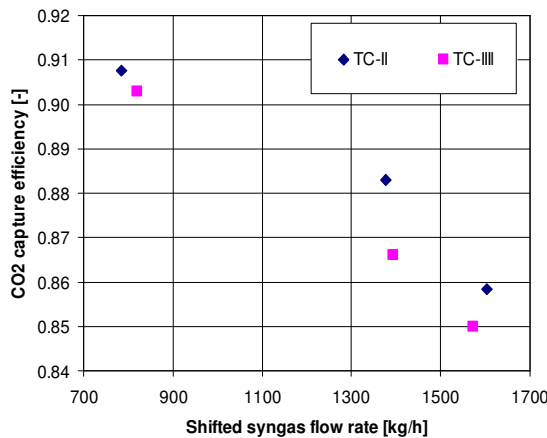
Figure 6-20:   **CO$_2$ absorption efficiency at different shifted syngas flow rates for TR-CII-012 and TR-CIII-012**

6.3.5   Test runs TR-CII-013 and TR-CIII-013: Solvent temperature

In this test run series, the influence of the solvent temperature (ELH50 CT003) on the absorption efficiency was investigated for both types of packings. The lean solvent temperature was varied and in TR-CII-013, the temperature of the shifted syngas (ELG60 CT003) was changed accordingly. For both test runs, the solvent temperature ELH30 CT001 (temperature between 1st and 2nd flash vessel controlled by the heater ELH30 AC010) was also changed in order to maintain the water content in the solvent on the level up to 1.5 wt%. The tested temperatures for the individual set points are shown in Table 6-11. A detailed description of the test runs and the evaluation can be found in (Valenz, 2013d and Valenz, 2013e).

Table 6-11:   Setting of solvent and shifted syngas temperature

Test run	Set point	ELH50 CT003 [°C]	ELG60 CT003 [°C]	ELH30 CT001 [°C]	Water content [vol%]
TR-CII-013	1	35	35	40	1.1
	2	30	30	40	1.2
	3	25	25	35	1.5
	4^{10}	40	40	43	-
TR-CIII-013	1	30	30	34	1.1
	2	25	30	38	1.3
	3	17.5	30	22.5	1.5
	4^{11}	40	40	44	1.0

In Figure 6-21, the CO_2 absorption efficiency is shown for the different solvent temperatures. The CO_2 absorption efficiency is increasing with decreasing solvent and shifted syngas temperature as expected. For TR-CII-013, the change between reference state and set point 1 is not significant which is caused by a different temperature in the 3rd flash vessel (44°C reference state and 40°C SP1). Higher temperature causes leaner solvent and therefore better CO_2 absorption efficiency which compensates for the effect of the lower lean solvent and shifted syngas temperature. A similar situation is applicable for the 2nd and 3rd set point where the temperature in the 3rd flash vessel was 40°C and 35°C, respectively. The effect of lean solvent and shifted syngas temperature can best be evaluated by comparing SP 1 and SP 2, where the 3rd flash vessel temperature is equal. For TR-CIII-013, the change between set point 2 and set point 3 does not follow the expectation (it behaves reverse) which is again caused by a different temperature in the 3rd flash vessel (38°C SP2 and 22.5°C SP3).

---

[10] Reference state for TC-II from previous test run (TR-CII-09)
[11] Reference state for TC-III from previous test run (TR-CIII-011)
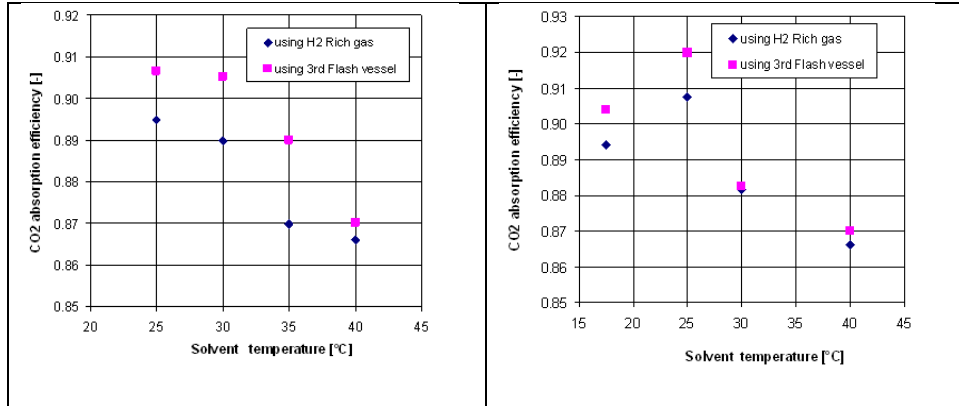
Figure 6-21:   CO$_2$ absorption efficiency at different solvent temperatures for TR-CII-013 (left) and TR-CIII-013 (right)

6.3.6   Test runs TR-CII-014 and TR-CIII-014: Absorber pressure

The purpose of this test run was to investigate the influence of the absorber pressure on the CO$_2$ absorption efficiency. Two additional absorber pressures at 21 bar(a) and 23 bar(a) have been tested in addition to the reference pressure of 22 bar(a) for the random packing (TR-CII-014) and the structured packing (TR-CIII-014). However the tests have been performed at different shifted syngas flow rates (1600 kg/h for TR-CII-014 and 1400 kg/h for TR-CII-014) due to the changed reference conditions for the different packings and therefore a direct comparison is not possible. As can be seen from the figures below for both packings the absorption efficiency increases with increasing absorber pressure, which was to be expected due to the higher partial pressure in the gas phase.
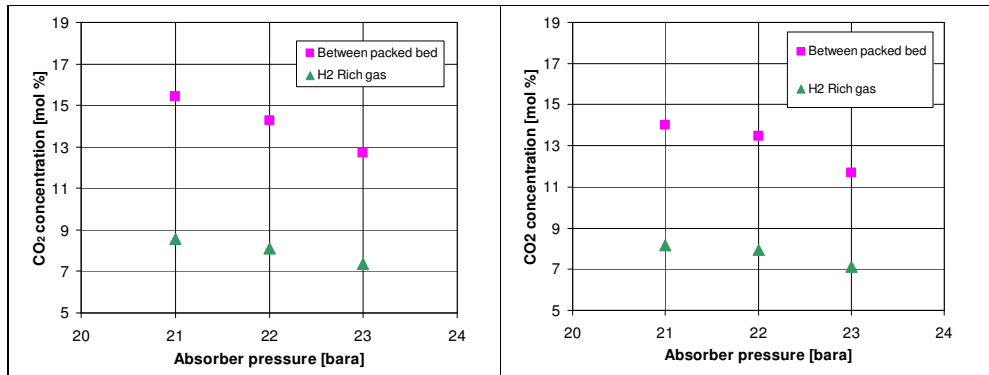
Figure 6-22:   Dependency of CO$_2$ concentration in between packed beds and in the H$_2$ rich gas stream on the absorber pressure for TR-CII-014 (left) and TR-CIII-014 (right)
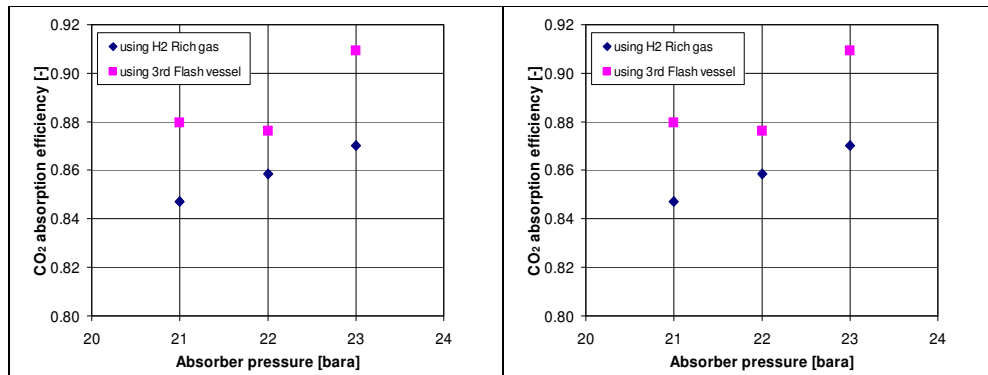
Figure 6-23:   CO$_2$ absorption efficiency at different absorber pressures for TR-CII-014 (left) and TR-CIII-014 (right)

6.3.7   Test run TR-CII-015: 1st flash vessel pressure

The purpose of this test run was to investigate the influence of the pressure in the 1st flash vessel on the phase equilibrium and the gas-phase concentrations. More specifically, the binary interaction coefficients between gases (CO$_2$, H$_2$, CO and N$_2$) and DEPEG in PC-SAFT equation of state will be qualitatively validated based on real operational data. Two additional pressures at 6.5 bar(a) and 8.5 bar(a) have been tested in addition to the reference pressure of 7.5 bar(a). A detailed description and evaluation of the test run can be found in (Valenz, 2012f).

In Figure 6-24, the influence of the pressure in the 1st flash vessel on the main components CO$_2$ and H$_2$ in the gas phase is shown. It can be seen that the CO$_2$ concentration is reduced significantly with increasing flash pressure, as less CO$_2$ is evaporated from the DEPEG solution. As a result, the H$_2$ concentration increases, as at all of these pressure levels, almost all H$_2$ is released from the liquid phase. The CO$_2$ concentration changed by 16% and the H$_2$ concentration changed by 33%, which should be sufficient to allow for successful model validation.

The mass flow for CO and H$_2$ increases only by 20% and 15% when reducing the flash pressure by 2 bar indicating that also at higher pressure levels the bulk of these components is released and a reduction of the pressure does not influence the release of these components very much. On the other hand the CO$_2$ mass flow doubles when reducing the pressure from 8.5 bara to 6.5 bara.

The pressure in the 1st flash vessel does not influence the overall CO$_2$ absorption efficiency of the plant as this is determined by the pressure in the 3rd flash vessel. Indeed the calculated absorption efficiencies are very similar for all three set points (85.7% (reference state), 86.1% (set point 1) and 86.2% (set point 2)).
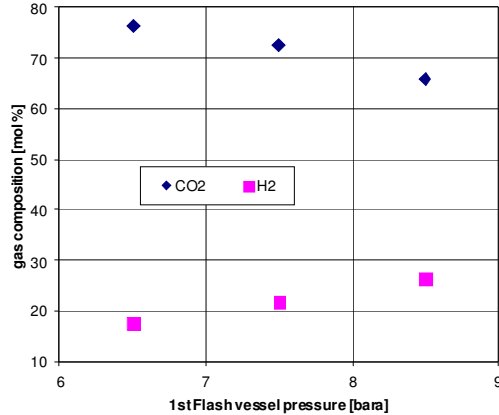
Figure 6-24: **Dependency of CO$_2$ and H$_2$ concentration in outlet stream from 1st flash vessel on the 1st flash vessel pressure**

Table 6-12: **Component mass flows from 1st flash vessel for different pressures**

Set point	CO [kg/h]	CO$_2$ [kg/h]	H$_2$ [kg/h]
1 (8.5 bara)	3.23	189.87	2.60
2 (reference 7.5 bara)	4.04	130.45	2.37
3 (6.5 bara)	4.85	259.63	2.73

6.3.8   Test run TR-CIII-031: High solvent flow rate

As explained in 2.1.3 the utilisation of structured packings in the CO$_2$ absorber is foreseen in the large-scale application with high L/G operating conditions and especially high liquid flow rates to enhance the capacity for capturing CO$_2$. These operating conditions where the packed absorption column is operated at such specific L/G values (high liquid flow rate and low gas flow rate) has never been tested before from a hydraulic and separation efficiency point of view. To test the column hydraulics and the separation efficiency under these conditions, the high solvent flow rate test run TR-CIII-031 will be performed. The main purpose of this test run is:

- Test high L/G operating conditions with solvent flow rate up to max. 108 m³/h corresponding to 240 m³/m^2/h (the solvent flow rate foreseen in the CB&I Lummus design of the CO$_2$ absorber for Magnum).
- Test hydraulic limits of the absorber column.
- Test separation efficiency at high solvent flow rates (probably re-estimate C$_L$ and Cv values).
- Comparison of different packings (structured and random).

Within TR-CIII-031, a series of pre-test have been executed in order to identify the hydraulic limitations of the pilot plant when it comes to high solvent flow rates and define the optimal settings for the high solvent flow rate test which will be used to identify the separation efficiency of the absorption unit at high solvent flow rates with two different types of packings.

The tested packings/distributors are:

- Packing type A: Raschig Super Rings 0.6 (random packing)
- Packing type B: Raschig Super Pack 250Y (structured packing)
- Distributor type A (for low solvent flow rates 32-59 m³/h
- Distributor type B (for high solvent flow rates 54-113 m³/h)

The test runs planned during TR-31 are shown in Table 6-13 and the pressure settings applied during the individual test runs are shown in Table 6-14[12]. Unfortunately test runs 3 and 4 could not be executed (which also makes test run 2 obsolete) due to time restrictions and therefore only the plant limitations and pressure drop correlation could be evaluated for the random packing. Therefore the focus in this report will be on the comparison of the hydrodynamic conditions for the two tested packings and on the evaluation of the separation efficiency of the structured packing for high solvent flow rates. A detailed description and evaluation can be found in (Faber, 2012c).

Table 6-13:   Test runs performed during TR-031

Test runs	Purpose	Date	
		Start	End
1	Check relation between the solvent flow rate and pressure drop Type A packing and Type A distributor	06-9-2012 13:30	06-9-2012 15:00
2	Identify limitations for solvent flow rate with Type A packing and Type A distributor	14-9-2012 09:00	14-9-2012 13:20
3	Identify limitations for solvent flow rate with Type A packing and Type B distributor	-	-
4	Identify absorption efficiency at high solvent flow rates with Type A packing and Type B distributor	-	-

---

[12] Pressure settings had to be adjusted for the high solvent flow rates to avoid certain operational bottlenecks (pump capacities, valve capacities) that prevented higher liquid flow rates

5	Identify limitations for solvent flow rate with Type B packing and Type B distributor	29-11-2012 08:20	29-11-2012 15:30
6	Identify absorption efficiency at high solvent flow rates with Type B packing and Type B distributor	30-11-2012 10:00	04-12-2012 08:00

Table 6-14: **Parameter setting for the individual test runs within TR-031**

Parameter	Unit	TR 1	TR 2	TR 5	TR 6
Shifted syngas flow rate	kg/h	1425	1425	1400.01	1403.25
Absorber pressure	bara	20.2	21.4 – 22.4	19.2 – 22	20.21
Achieved/tested liquid flow rate	[kg/s]	17 – 25.5	17 – 25.5	16 – 30	15 – 30
Pressure 1st flash vessel	bara	6.50	6.5 – 7.5	5.5 – 7.6	5.50
Pressure 2nd flash vessel	bara	2.90	2.90	2.90	2.90
Pressure 3rd flash vessel	bara	1.76	1.2 – 1.7	1.2 – 1.7	1.71
Packing type		Type A	Type A	Type B	Type B
Distributor type		Type A	Type A	Type B	Type B

6.3.8.1   Column hydraulics at high solvent flow rates

Pressure drop – Flow rate correlation for random packing Type A
In the first test run, the relation between the solvent flow rate and the measured pressure drop in the two packing sections of the column was investigated in order to check if a clear and expected relation can be identified that can be used to assess the hydrodynamic conditions within the column. This is especially important for high solvent flow rates in order to avoid going into the flooding region of the column. Therefore, over a wide range of liquid flow rates and at constant gas flow rate, the pressure drop has been measured.

In Figure 6-25 the measured correlation between the solvent flow rate and the pressure drop over the upper (ELH10 CP001) and lower (ELH10 CP002) packing sections are shown. It would be expected that the lower packing section shows a higher pressure drop, as the height of the packing sections is the same and the lower pressure drop measurement even includes the chimney tray for liquid collection. Additionally the gas flow rate in the lower section is considerably higher than in the upper section and therefore also a higher pressure drop would be expected for this section. Nevertheless, it can be seen that the upper section shows a higher pressure drop. The higher pressure drop in the upper section could be explained by column internals (feed pipe, distribu-

tor) that influence the pressure drop in the void column section. Both pressure drops show an exponential correlation to the solvent flow rate where the pressure drop in the lower section increases faster than in the upper section. At around 19.5 kg/s a step-wise increase in the pressure drop of the upper section can be seen. This might indicate a flooding of the liquid distributor.

At around 23.5 kg/s both pressure drops show almost the same value. Above 23.5 kg/s, the pressure drop in the upper section starts to increase much faster, whereas the increase in the lower pressure drop reduces to almost the same slope as the upper section showed below 23.5 kg/s. Just below 23.5 kg/s a strong increase in the lower pressure drop can be identified. One explanation for that behaviour could be that at 23.5 kg/s the lower section floods and some of the liquid solvent is entrained into the upper section where it increases the pressure drop.

Generally it can be concluded that a clear and expected relation between the solvent flow rate pressure drop could be identified and that a flooding of the column can be identified based on the measured pressure drop.
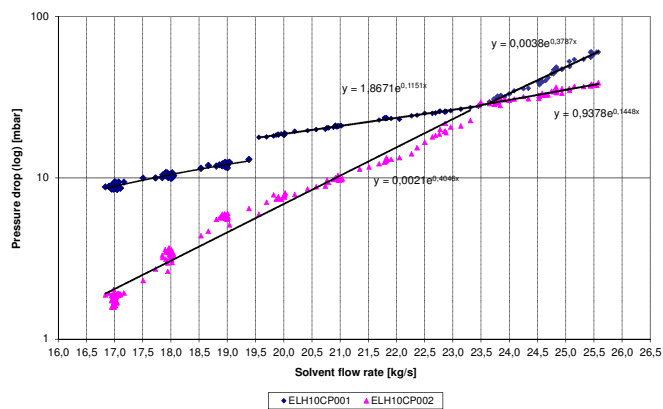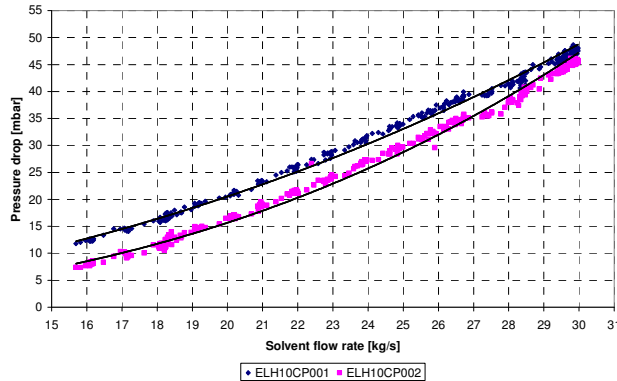

Figure 6-25:   Correlation between pressure drop over packing sections and solvent flow rate for test run TR-31_1 (packing/distributor type A)

Pressure drop – Flow rate correlation for structured packing Type B

Test run 5 was used to investigate the hydraulic limitations of the plant with the structured packing and the new distributor and to check for possible bottlenecks. Thereby, the pressures in the absorption column and the 1st and 3rd flash vessel have been varied. In Table 6-14 the range of the tested pressures in the individual flash tanks and the absorption column are shown. The highest solvent flow rate that could be reached was 30 kg/s at the following pressure settings:

ELH10CP001: 20.2 Bara
ELH20CP001: 5.6 Bara
ELH30CP001: 2.9 Bara
ELH40CP001: 1.7 Bara

In addition the correlation between solvent flow rate and pressure drop was again investigated for the packing type B with the distributors type B. In Figure 6-26, the correlation between the solvent flow rate and the pressure drop measured during test run 5 is shown. It can be seen that the pressure drops show a much smoother behaviour compared to the previous test with the distributor/packing type A configuration. No sign of flooding of the packing or the distributor can be identified. In addition, the absolute values of the pressure drops are considerably lower than before. Also the slope of the pressure drop curve is considerably lower than during the experiments with the distributor/packing type A configuration. An almost linear correlation can be seen, indicating, that the plant is operating still away from the loading region. The slight reduction in the absolute values around 27 kg/s can be explained by a reduction of the absorber pressure around this region.

Figure 6-26:   **Correlation between pressure drop over packing sections and solvent flow rate for test run TR-31_5 (packing/distributor type B)**

6.3.8.2 CO_2 absorption efficiency at high solvent flow rates

In test run 6, the absorption efficiency of the absorption column with the structured packing at high liquid loads was determined using the settings identified in test run 5. Therefore, longer steady-state operation periods are necessary in order to allow the plant to establish also steady-state conditions for the concentrations. The parameters established are shown in Table 6-14. In addition 2 set points have been performed at reference conditions for a solvent flow rate of 15 kg/s and 19 kg/s to allow for a direct comparison of the adjusted plant conditions with reference state conditions.

The most important variables to validate the mass transfer coefficient in the gas phase are the CO_2 concentrations in between the packed bed and in the H_2 Rich gas. In Figure 6-27, the correlation between solvent flow rate and CO_2 concentration at the absorber outlet and in-between the packed beds is shown. It can be seen that, as

expected, the concentration is reduced with increasing solvent flow rate. Towards higher solvent flow rates, the slope levels out, indicating that the process gets becomes limited by mass transfer and no more CO_2 can be absorbed at these conditions.
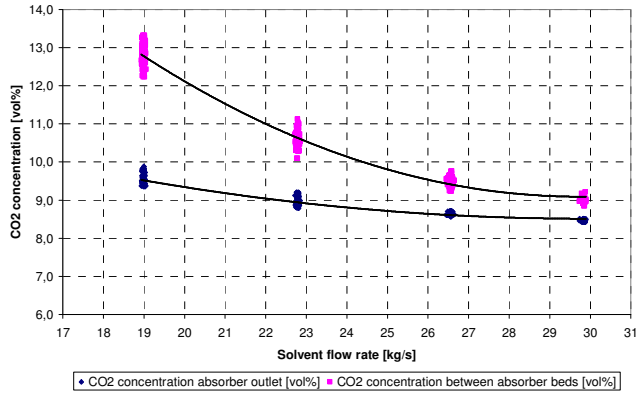

Figure 6-27: Correlation between CO_2 concentration in the absorber and solvent flow rate based on results from TR-31_6.

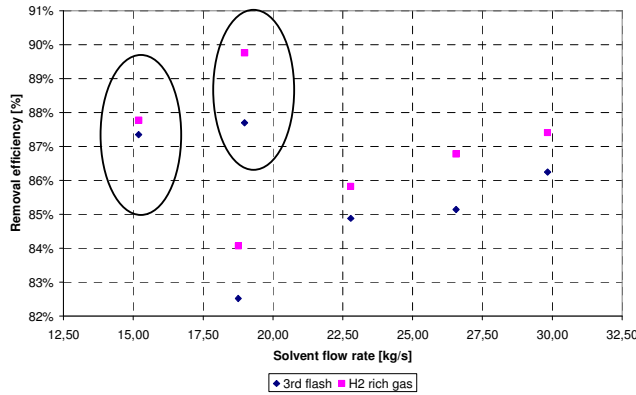In Figure 6-28, the absorption efficiency is shown for the different set points.

Figure 6-28: Correlation between CO_2 absorption efficiency and solvent flow rate based on the results from TR-31_6

The reason for the higher absorption efficiency for set points 5 (right circle) and 6 (left circle) is the higher pressure in the absorber and the lower pressure in the 3rd flash vessel at reference conditions compared with the settings for SP1-SP4.

6.3.9   Solvent composition

After the test programme was finished, a sample of fresh solvent (which has not been exposed to process gas) and spent solvent (exposed to process gas for > 5000 hours) was taken for analysis by Clariant. In comparison to the fresh sample the spent sample has:

- A slightly lowered pH-value and increased acid value (due to the small amount of CO_2 and increased formic acid)

- A higher water content (which also causes the higher viscosity)

- A slight shift in homologues

In summary, the spent solvent is still in good conditions, which is confirmed by the fact that the solvent performance (as indicated by the capture efficiency) was not deteriorating in time and the solvent physical appearance did not change in time.

7 Process modelling

This section describes the models developed for the pilot plant. The models cover all pilot plant sections. Depending on the required level of detail (e.g. overall plant performance evaluation or detailed plant component analysis) and the purpose of the models (steady-state or dynamic process evaluation), various software tools have been used in this project (Aspen Plus®, Matlab, Dymola/Modelica). The model development approach has been defined in the modelling master plan (Kaptein, 2010 and Faber, 2012a) in order to ensure that the developed models serve the purpose of the project and that a consistent modelling approach and thermodynamic data is taken by the individual research groups that have been involved in the model development. Following the outline in the modelling master plan, the individual steps that have to be taken during model development have been defined (Trapp, 2011).

After a description of the modelling objectives in section 7.1, the individual models and their validation are described, as well as an outlook for up-scaling.

7.1 Modelling objectives

For a better understanding of the CO_2 capture process and explanation of observed behaviour during plant operation a series of process models have been developed within the Catch-up project. By validating the pilot plant models against real operational data, more reliable and accurate models applicable to the large-scale capture plant can be obtained. For this purpose, the pilot plant models are to be extended and extrapolated to the full-scale operational range based on theoretical scale-up rules and physical insights. The developed process models serve multiple objectives:

- Verify overall pilot plant performance

- Evaluate the performance of a specific technology component (e.g. assess catalyst activity, mass transfer coefficients in the absorber, etc.)

- Identify measurement errors in the data obtained from the pilot plant

- Simulate different operation scenarios in order to perform energy optimisation with respect to input process variables.

- Evaluate the dynamic response of the system in order to improve the controllability and modifying/improving the control system.

- Develop methods for (automated) process and control optimisation

Note that the development of a full-scale capture plant model and energy optimisation is ongoing work and is therefore not described in this report.

7.2 WGS reactor model

A reactor model has been developed in Matlab with the objective to predict the temperature profile of the WGS (Hernandez, 2011). The reactor is modelled as a heterogeneous adiabatic plug-flow WGS reactor, meaning:

  i)   Heterogeneous: Transports of heat and mass to and within the catalyst pellets are taken into account.
  ii)   Adiabatic: Heat loss of the reactor is neglected. No radial temperature profile exists.
  iii)   Plug-flow: No axial dispersion of heat or mass is considered.

The physical parameters required for the pore-diffusion model, being the average pore diameter, the porosity and the tortuosity, were quantified by separate measurements on pellets of a spend catalyst.
The model uses intrinsic reaction kinetics in the form of a power-law rate equation. The parameters of this rate equation, being the catalyst activity factor, the apparent activation energy and the reaction orders for the reactants and the products, were quantified by regression analysis of experimental measurements (van Dijk and Booneveld, 2011).

A data set of 20 settings for reactor 1 and reactor 2 has been selected for the regression, representing variations in inlet temperature, throughput and syngas composition. The entire set spans a period of 1869 h operation. Model validation resulted in parameter estimates for the catalyst activity factor and length of dead zone for reactor 1 and reactor 2. For each reactor, single estimations of these parameters allowed to accurately describe the whole data set. This means that:

  i)   All trends with temperature, throughput and syngas composition are predicted.
  ii)   The activity over the 1869 h period is constant, meaning that catalyst deactivation over this operational time is insignificant.
  iii)   The length of the dead zone over the 1869 h period is constant, meaning that following initial settling and shrinkage, further settling, shrinkage and possibly also fouling are insignificant.

The model can be used to simulate the reactor performance. Up scaling to model the reactor behaviour for the Magnum layout only requires adaptation of the dimensions of the reactor. No other model parameters need adjustment.

7.3   Steady-state models of the pilot plant

The steady-state models serves as a tool for validation of the on-design plant performance which then can be verified by comparison with the design calculations performed by CB&I Lummus and on-design operational data obtained from the pilot plant. The developed steady-state models have been validated against experimental data sets obtained from the pilot plant during the 2nd and 3rd test campaign. Extensive, rigorous data reconciliation and parameter estimation techniques have been used in order to improve the quality of the data and the accuracy of the process models.

Furthermore, the steady-state models have been developed to predict the performance of the plant and its subcomponents for off-design operation. This will allow to analyse the influence of process parameters, like $H_2O:CO$ ratio, shift temperature, flash pressure, solvent circulation rate on the plant performance. Off-design performance predictions can further be used to judge if a given operation is safe and no process or material limitations are violated. Finally, the steady-state pilot plant model serves as a reference tool for a) the development of the full-scale CO_2 capture model and b) for the initialization and validation of the dynamic capture models.

The pilot plant model has been divided into two sections: a) the syngas conditioning, WGS and condensate recovery section (referred to as WGS section) and b) the absorption section. In the overall system model the individual models of the two sections have been combined making use of the Aspen Plus hierarchy blocks that provide hierarchical structures to complex simulations (Aspen Plus Help). This way the models of the syngas conditioning and WGS section and absorption and regeneration section remain as individual models which can easily be exchanged or updated.

7.3.1   Steady-state model of the WGS section

A simulation model for the syngas conditioning, WGS and condensate recovery section has been set up in Aspen Plus V7.3. The flow sheet of the model is shown in Figure 7-1. A detailed description of the steady-state model including boundary conditions for modelling and design data can be found in (Trapp, 2013a).
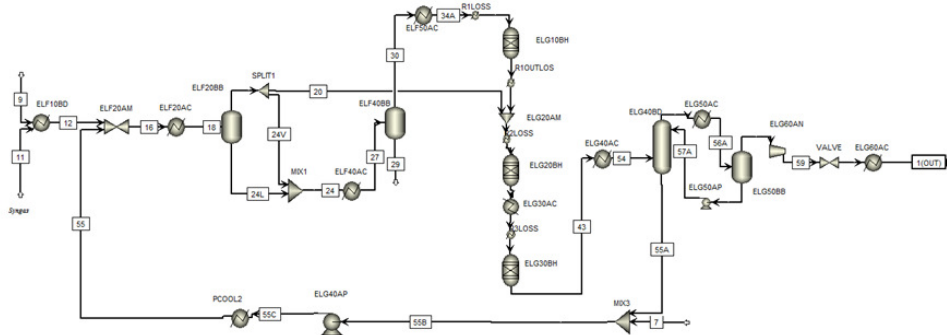
Figure 7-1:   Flow sheet of the WGS section in the Aspen Plus model.

For validation of the syngas conditioning and WGS section, the data derived in the following tests have been used:

1)   TR-001: reactor inlet temperature variations
2)   TR-002 and TR002A: syngas inlet composition variations
3)   TR-003: syngas mass flow variations
4)   TR-004A and TR-017: H$_2$O/CO variations

From the above mentioned test runs 20 individual data sets were selected for model validation based on criteria discussed in the section data analysis.

7.3.1.1   Data analysis and handling

From the raw experimental data of the test runs first the periods of steady-state operation were determined via visual inspection of the main process variables. A minimum period length of 3 hours was considered to ensure a sufficient number of recorded data points, which applies especially for the discrete composition measurements (normal GC analysis mode 1 measurement every 15 minutes at each location). Outliers in composition measurements were removed from the steady-state period on a heuristic basis. For further data analysis the mean and the relative standard deviation of all variables were determined for each identified steady-state period and compared to other data sets.

Coriolis and vortex flow meters are used for mass flow measurements in the pilot plant. The Coriolis meters measure mass flow rates which are directly recorded in PGIM. The vortex meters measure volumetric flow rates which are converted into mass flow rates using stream dependent density conversion factors and then recorded in PGIM. The data analysis is based on mass flow rates and therefore Coriolis measurements can be used straightforward whereas recorded vortex measurements need to be corrected according to the actual density which changes during operation based

variations in pressure, temperature and composition of the measured stream. The density calculations were performed with the PC-SAFT library available in FluidProp. In order to prepare the raw measurement data from the plant to be used as a basis for model validation the procedure described in A.2 has been applied.

7.3.1.2   Data reconciliation and parameter estimation

Despite the pre-treatment of the raw measurement data that has been applied (see A.2), the measurement data still contains random errors, outliers or constant offsets that could not be identified by visual inspection of the data. As these data are used to tune the models with parameter estimation techniques in order to obtain more reliable parameter estimates, these measurement errors have to be identified and corrected as good as possible. Therefore a simultaneous data reconciliation and parameter estimation strategy is used which results in an identification (and correction) of measurement errors and reliable parameter estimates.

Commonly, multiple sets of independent data, whereby all measurements change with each data set, are used in order to obtain reliable parameter estimates (for present case: multiple data sets from independent test runs). In case the model parameters do not change throughout the measurements sets, representing an operational period whereby the process performance is not influenced by fouling, degradation or deactivation, and assuming all measurements are subject to errors, the individual data sets are coupled through the parameter estimates. This simultaneous data reconciliation and parameters estimation (DRPE) problem is described as an errors-in-variables measured problem (EVM). The formulation of the EVM problem is shown in A.3.

The formulation of the objective function is crucial for the results of the data reconciliation and strongly depends on the distribution of the measurement errors. If a normal Gaussian distribution exists, a standard Weighted-Least-Squares (WLS) formulation gives unbiased results. However in the presence of non-Gaussian distribution and in the presence of larger measurement outliers, a robust formulation of the objective function should be used in order to limit the influence of the outliers on the results of the data reconciliation. For the data reconciliation presented in this report the contaminated Normal estimator was used (see equation A-2).

The process model contains 3 main parameters, the approach to equilibrium of the water-gas shift reactors, 30 independent variables (input variables), which are determining the state of the process, and a large number of dependent variables (out-put variables) whereby 32 of them are used to determine the performance of the system.

In order to assess the possibilities to reduce the complexity of the optimization problem, a sensitivity analysis was conducted in order to identify both the set of independ-

ent variables, which cause significant uncertainty in the system performance, and variables which have minor or no effect on the outcome.

As a result, 20 independent variables were identified whose uncertainty have minor impact on the performance and as a consequence the optimization problem can be reduced. For these variables the measured values are taken directly as input which is equivalent to the assumption that these variables are error-free.

Further, a preliminary analysis was performed in order investigate if the reactor model parameters are time- dependent and therefore different for each data set. The estimates for reactor 1 and reactor 2 parameter were constant with a value of 0 Kelvin through-out all data sets. This observation has been confirmed during the detailed reactor model validation (van Dijk 2012a). Therefore, both parameters are removed from the optimization problem and assumed constant with a value of 0 Kelvin. During the test period equilibrium in reactor 3 was not always reached and the performance varied during the test period. Therefore reactor 3 model parameters differ for each data set.

To summarize, the number of independent variables can be reduced from 30 to 10 variables, reactor 1 and 2 model parameters can be considered constant with a value of 0 Kelvin for the considered measurement period and reactor 3 model parameter is data set dependent.

Therefore, the optimization problem is successfully reduced to a DRPE, which can be performed for each data set individually, as no common parameters couple the individual data sets. The objective function is formulated in terms of the contaminated Normal distribution and was implemented in Matlab. The non-linear equality and inequality process constraints are represented by the process model, which is linked via a COM interface to the programming environment. The DIRECT algorithm has been used for solving the non-linear optimization problem. A detailed description of this procedure is described in (Trapp, 2013a).

7.3.1.3   Results of model validation

Mass flows

To improve the accuracy of the process model and the quality of the raw measurement data, the data reconciliation and parameter estimation procedure (DRPE) has been applied to the data gathered during the individual test runs for the shift section using the process model. The results of the simultaneous DRPE in terms of the standardized residuals, which are defined as deviations between measured and reconciled values (residuals) divided by the corresponding standard deviations of the main mass flows within the shifting section, are depicted in Figure 7-2 and Figure 7-3. Relatively large errors are observed mainly in the syngas and in the quench mass flow measurements. From Figure 7-3, which displays the absolute residuals of the mass flows, it can be concluded that the measured syngas values are systematically too high by approximately 35 kg/h. For the majority of the measured values of the quench flow and the reactor 1 inlet flow the deviations are very small. Values for the make-up water and

shifted syngas (SYNOUT_M) are measured slightly too high and the reaction water mass flow is systematically too low by approximately 25 kg/h. In general, except for a few outliers, mainly present in the quench flow, the mass flow residuals are randomly distributed.

Considering the possibility that the indicated errors are not the result of measurement errors but of inaccuracies related to the process model, in particular to the thermo-dynamic model used for the prediction of the thermophysical properties, the average accuracy of the model predictions (calculated dependent variables) with respect to the raw measurements is summarized in Table 7-1. The accuracy for all mass flows in the shifting section is below 3.2%, which can be considered as a good agreement between the raw measurements and the model predictions.

To summarize, considering the systematic errors in the syngas and reaction water mass flow measurements, it can be concluded that these measurement instruments are not calibrated correctly.
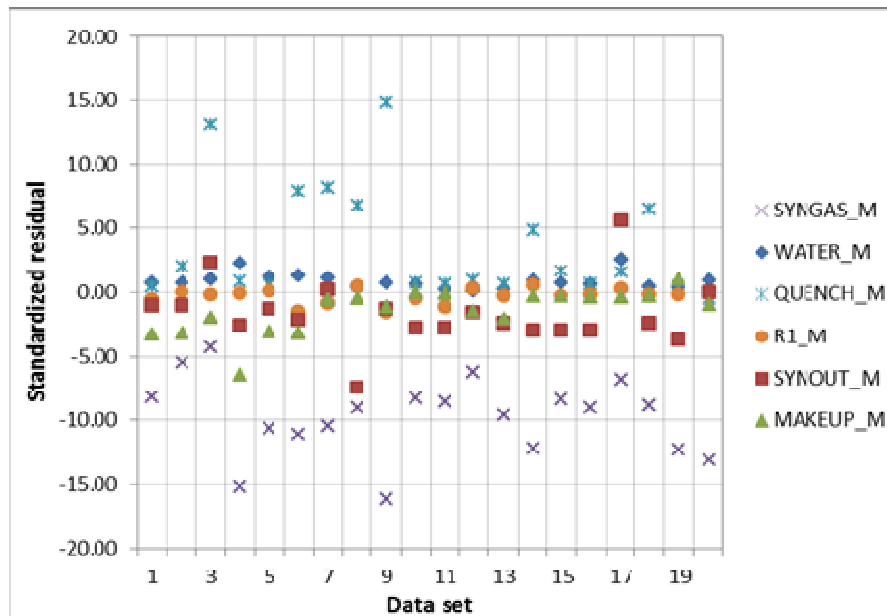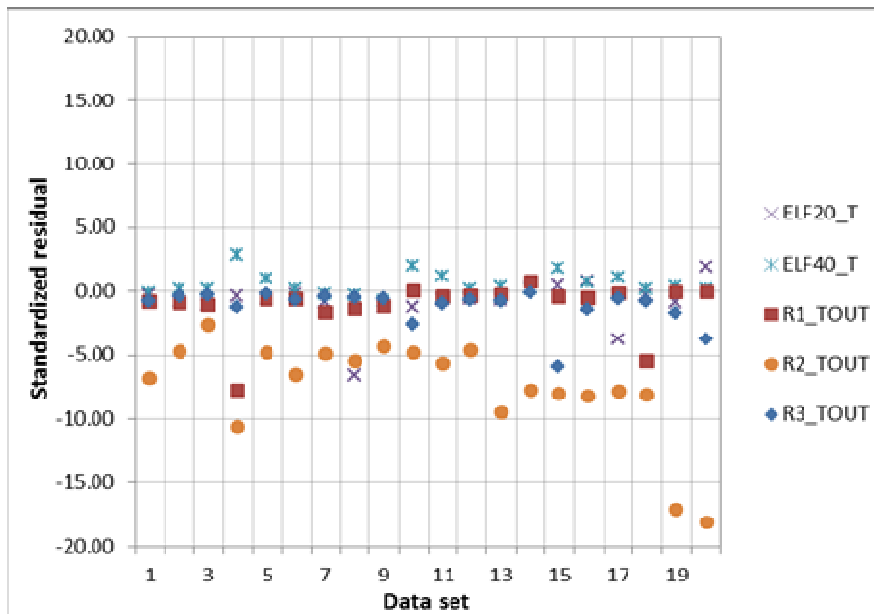

Figure 7-2:   **Standardized residuals of mass flow measurements within the shifting section for 20 data sets as a result of simultaneous DRPE using the contaminated Normal estimator.**
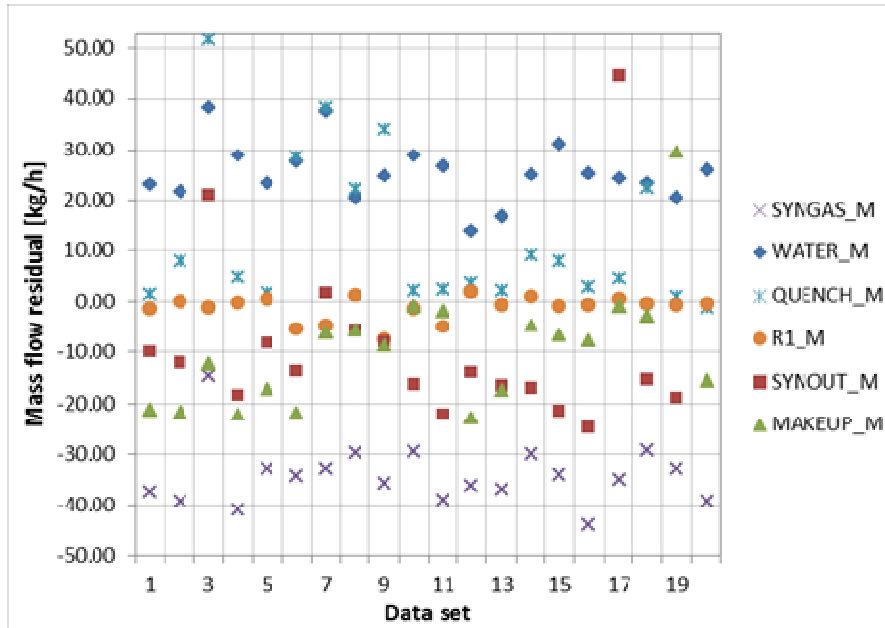
Figure 7-3:   **Residuals of all measured mass flows within the shifting section for 20 data sets as a result of simultaneous DRPE using the contaminated Normal estimator.**

**Table 7-1:**   **Average accuracy of model predictions with respect to raw measurements**

Mass flow measurement	Average accuracy [%]
Reaction water	1.92
Syngas	3.11
Quench	1.19
Reactor 1 inlet	0.09
Shifted syngas	0.58
Make-up water	1.63

Temperatures

The standardized and absolute residuals of the temperature measurements are depicted in Figure 7-4 and Figure 7-5. For reactor 1 outlet temperature, the model predicts on average 0.6 K lower temperatures than the measurements. These results can in general terms be considered as a good agreement between the recorded measurements and the process simulation results. The WGS reactor model validation indicated a systematic over prediction by 4.1±0.7 K of reactor 1 outlet temperature for the case that heat losses are not considered, hence the actual temperature would be a few degrees lower

(van Dijk 2012a). The system model documented here includes heat losses of 2000 W for each reactor and therefore both estimates are in the same order of magnitude.

Reactor 2 outlet temperature is systematically underestimated by the process model in the range of 2 to 5.5 K and therefore detected as a gross error (deviations larger than 3.34 σ). In the WGS reactor model validation report an under prediction by 1.0±0.9 K is documented (van Dijk 2012a), which will be slightly lower as reactor heat losses were not considered. In conclusion, both analyses give comparable results for the adiabatic temperature rise of reactor 2.

Figure 7-4:   **Standardized residual in temperature measurements within the shifting section for 20 data sets as a result of simultaneous DRPE using the contaminated Normal estimator.**
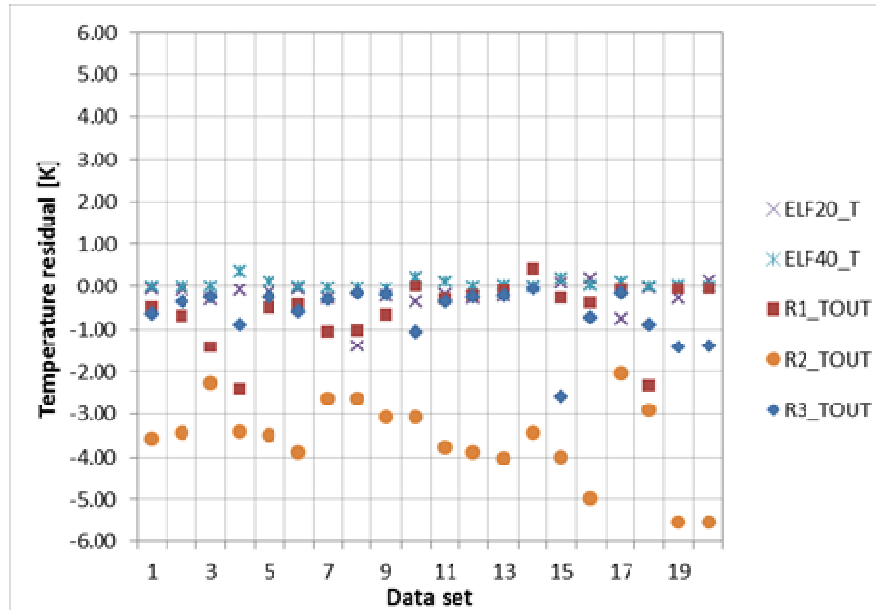
Figure 7-5:   **Residuals of measured temperatures within the shifting section for 20 data sets as a result of simultaneous DRPE using the contaminated Normal estimator.**

Concentrations

The standardized residuals of the composition measurements at the inlet and outlet of the reactors are represented in Figure 7-6 to Figure 7-11 and of the syngas inlet in Figure 7-12. In general, it can be observed that the majority of the residuals range between ±2σ. Larger errors and outliers are mainly observed in measurements of reactor outlet compositions (Figure 7-7, Figure 7-9 and Figure 7-11). For reactor 2 larger deviations might also be related to the observed mismatch in adiabatic temperature rise. The highest systematic bias in terms of standardized residual is observed in the CO measurements of reactor 1 outlet which corresponds to an average absolute residual of 0.21%-points. Reactor performance simulations carried out by Haldor Topsøe indicate a similar absolute systematic error in the dry CO exit concentration for reactor 1 by 0.4%-points (van Dijk, 2012b].
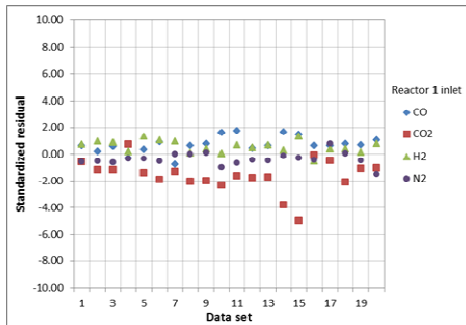
Figure 7-6: Standardized residual in *reactor 1 inlet* composition measurements for 20 data sets as a result of simultaneous DRPE using the contaminated Normal estimator.
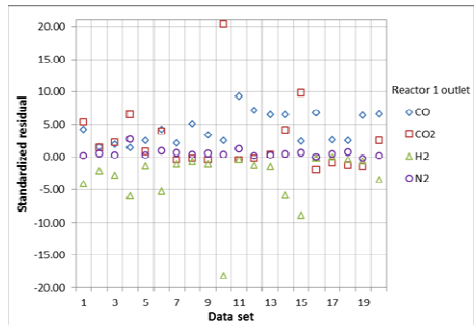
Figure 7-7: Standardized residual in *reactor 1 outlet* composition measurements for 20 data sets as a result of simultaneous DRPE using the contaminated Normal estimator.
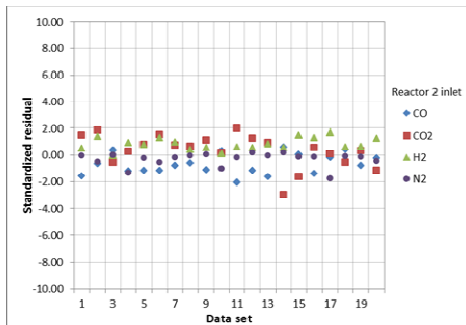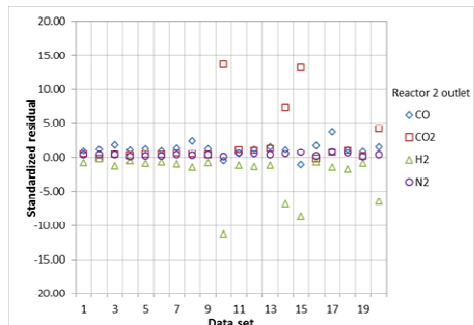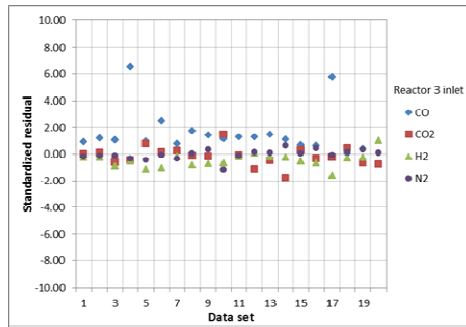

Figure 7-8: Standardized residual in *reactor 2 inlet* composition measurements for 20 data sets as a result of simultaneous DRPE using the contaminated Normal estimator.
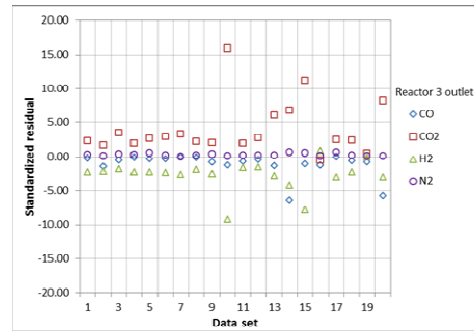

Figure 7-9: Standardized residual in *reactor 2 outlet* composition measurements for 20 data sets as a result of simultaneous DRPE using the contaminated Normal estimator.
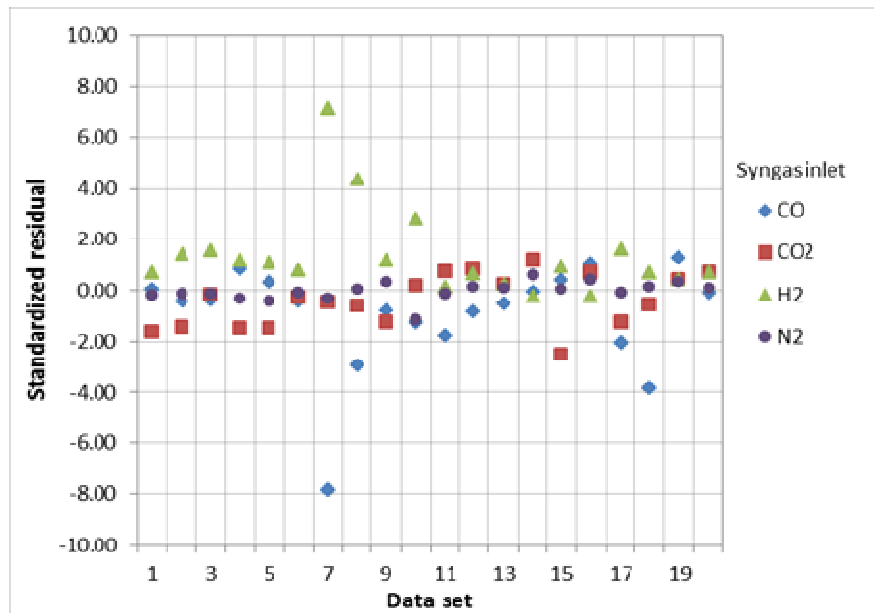
Figure 7-10: Standardized residual in *reactor 3 inlet* composition measurements for 20 data sets as a result of simultaneous DRPE using the contaminated Normal estimator.

Figure 7-11: Standardized residual in *reactor 3 outlet* composition measurements for 20 data sets as a result of simultaneous DRPE using the contaminated Normal estimator.

Figure 7-12:   Standardized residual in syngas inlet composition measurements for 20 data sets as a result of simultaneous DRPE using the contaminated Normal estimator.

In conclusion, the model predictions for mass flows, temperatures and compositions show good agreement with the measured values and 90% of the reconciled estimates (independent and dependent variable values) are within a deviations of ±3.34σ (gross error cut point). Hence the steady-state model can be used for accurate performance

predictions throughout the entire operational range. In addition, the model can also be used for the development of models of the large-scale capture unit. In this case, some of the components that are specific to the pilot plant must be replaced with those that would be utilized in an actual CO_2 capture plant (for example electrical heaters and coolers). In the shifting section no parameters need to be adjusted.

7.3.2 Steady-state model of the absorption section

A simulation model for the absorption and regeneration section has been set up in Aspen Plus V7.3. A flow sheet of the model is shown in Figure 7-13. The following components have been considered in the model: pseudo pure fluid DEPEG[13], CO, CO_2, H_2, N_2 and H_2O. The perturbed chain statistical associating fluid theory (PC-SAFT) equation-of-state is used for the calculation of thermodynamic properties, because of its success in predicting VLE of complex fluids and especially fluid mixtures for a broad range of conditions. Equations of state based on molecular models, like PC-SAFT, have several advantages. Due to its physically-sound framework, a SAFT-based EoS is robust, consistent and extrapolative (Gross and Sadowski, 2001). The values of the parameters for the PC-SAFT equation of state were fitted on the experimental data provided by the vendor of the solvent Genosorb 1753 and are reported in (de Servi, 2013a).

The pilot plant model setup and the description of all used parameters and model settings are described in detail in (Valenz, 2013g]. The most crucial part of the process model is the absorber model with the description of the mass transfer between the gas-phase and the liquid-phase. Both equilibrium and rate-based approaches to describe the mass transfer have been investigated.

In the equilibrium model, equilibrium is assumed between the components in the two phases for each theoretical stage. To account for any limitation to this assumption, Murphree efficiencies can be used for individual components.

The rate-based approach provides the possibility to account for phenomena limiting the mass transfer on both sides of the interfacial area and is more suitable for systems where the mass transfer is limited due to the mass transfer resistance towards the interfacial area. On the other side it is usually computationally more demanding as it requires the calculation of certain component and transport properties (like densities, diffusion coefficients, viscosities, surface tension etc.) and also a high number of discretisation points along the column axis. In this study the Billet-Schultes mass transfer model has been used with 60 discretisation points along the column height.

---

[13] Genosorb 1753 is a blend composed of polyethylene glycol dimethylethers (different homologues). Therefore the solvent is modelled as a pseudo pure substance with an equivalent molecular weight of 302 kg/kmol.
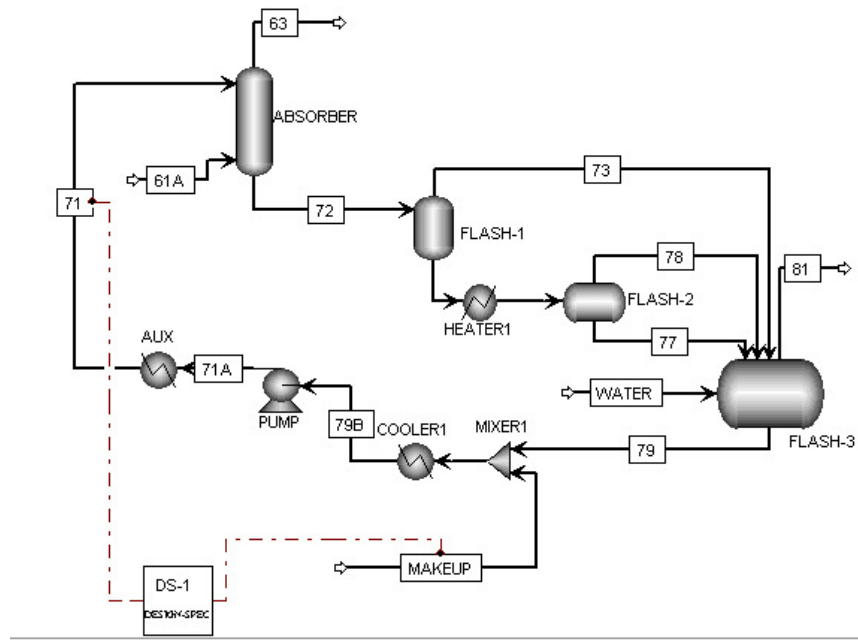
Figure 7-13: **Flow sheet diagram for the absorption and regeneration section in the Aspen Plus model**

7.3.2.1 Test runs used for model validation

To validate the process model of the absorption and regeneration section, the results from the following test runs have been used:

Test run 9 – change of the water content in the solvent
– The purpose is to validate the thermodynamic model with regard to the VLE of water – DEPEG

Test run 10 – change of the solvent temperature between 1st and 2nd flash vessel
– The purpose is to validate the temperature dependency of the thermodynamic model with regard to the VLE of water – DEPEG

Test run 11 – change of the solvent mass flow rate
– The purpose is to validate together with data from Test run 12 the mass transfer coefficients

Test run 12 – change of the shifted syngas mass flow rate
– The purpose is to validate together with data from Test run 11 the mass transfer coefficients

Test run 13 – change of the solvent and shifted syngas temperature
             – The purpose is to validate the model at different temperatures. The operating absorption data will be used for qualitative validation of the absorption model. As Selexol plants are typically operated at lower temperature than 40°C, it is required to know the accuracy of predictability of the model at lower operating temperatures. The operating flash data will be used for qualitative validation of the temperature dependency of the binary interaction coefficients between gases (CO_2, H_2, CO and N_2) – DEPEG and water – DEPEG in PCP-SAFT equation of state.

Test run 14 – change of the absorber pressure
             – The purpose is to validate the influence of VLE on the absorption mass transfer rate

Test run 15 – change of the 1st flash vessel pressure
             – The purpose is to validate the model accuracy of 1st flash vessel variation

Test run 31 – high solvent flow rate
             – The purpose is to validate mass transfer dependency on the high solvent flow

7.3.2.2 Data handling and processing

From the graphs of the process variables the period of steady state was visually determined and the outliers were excluded. Then the following steps, in order to determine the mass balance and CO_2 absorption efficiency, were performed with the data.

1) The values of each variable were averaged over the steady state period.
2) Calculation of the relative standard deviation for each process variable.
3) The composition of each stream (molar concentrations in percentage) was normalized to 100%.
4) Calculation of the average molar weight.
5) True mass flow rate was calculated from the measured one.
6) Calculation of the overall and component mass balance deviation.
7) The CO_2 absorption efficiency was evaluated.

Ad 2): The relative standard deviation (RSD) was calculated according to the following equation:

$$RSD = \sqrt{\frac{1}{N}\sum_{i=1}^{N}\left(\frac{x_i - \bar{x}}{\bar{x}}\right)^2} \qquad \textbf{7-1}$$

Where N is number of values at steady state period, x_i is measured value and $\bar{x}$ is mean value of measured values.

Ad 6): The overall and component balance deviation was calculated as a difference between the inlet (61 – shifted syngas) and the outlet (63 – H_2-rich gas; 81 – CO_2 product) streams.

$$balance \quad deviation = \dot{m}_{61} - \dot{m}_{63} - \dot{m}_{81} \qquad \textbf{7-2}$$

$$component \quad balance \quad deviation = \dot{n}_{61}x_{i,61} - \dot{n}_{63}x_{i,63} - \dot{n}_{81}x_{i,81} \qquad \textbf{7-3}$$

Where $\dot{m}$ is mass flow rate, $\dot{n}$ is molar flow rate and x_i is the molar fraction of the component i (CO, CO_2, H_2, H_2O, N_2).

7.3.2.3   Parameter estimation method

Similar to the procedure used for the model validation in the syngas conditioning and shifting section (see 7.3.1.2) model parameters have been adjusted using the developed process model together with the measurement data from the selected test runs. However, no data reconciliation has been applied for the absorption model due to the fact that less process streams are involved and that no chemical reactions occur which enabled the utilization of component balances to check overall mass balances.

Parameters

For the description of the absorption process using the rate based approach it is crucial to correctly predict the absorption transfer rate. The absorption mass transfer rate is calculated as the product of the volumetric mass transfer coefficient (k_La, k_Va), concentration driving force and column cross section. The column cross section is given. The concentration driving force is the difference between the phase concentration and the concentration at the interface. The liquid and gas concentrations at the interface are in equilibrium and they are calculated from pressure and temperature at the interface. The bulk concentration in the lean solvent is calculated on the basis of the temperature and pressure in the third flash vessel. The volumetric mass transfer coefficient depends on the liquid and gas flow rate, physical properties of the phases and type of packing. In Aspen Plus such dependency is described by the mass transfer correlations. The Billet and Schultes correlation was selected as it is the only one which contains the adjustable parameters which can be optimized. Another advantage is that it is

the same mass transfer correlation for both studied types of packing. However, the correlation was developed and parameters C_L and C_V were validated based on the distillation and absorption experiments under different hydraulic conditions than those in the CO_2 capture pilot plant. The ratio u_L/u_G is very high in Buggenum pilot plant (around 0.2) in comparison with common values for distillation/absorption (0.01, see (Rejl et al. 2010)), which may cause a significant deviation in optimized parameters.

The simplified correlation is given in the equation below:

$$k_L a = C_L \cdot u_L^\alpha \cdot u_L^\gamma \cdot A_L(phys.properties)$$
$$k_V a = C_V \cdot u_V^\beta \cdot u_L^\gamma \cdot A_V(phys.properties)$$

7-4

C_L and C_V are the liquid respectively vapour mass transfer coefficient parameters, which are characteristic for the shape and structure of the selected packing. These are also the parameters that have been used for model fitting. u_L^α and u_V^β describe the dependency of the liquid and vapour mass transfer coefficients (k_L and k_V) on the liquid (u_L) and vapour (u_V) flow rate. The term u_L^γ originates from the dependency of interfacial mass transfer area (a) on the liquid flow rate. The influence of u_L on k_V and of u_V on k_L is considered negligible. A_L and A_V summarize the dependency of $k_L a$ and $k_V a$ on the physical properties. The Billet and Schultes correlation is described in (Billet and Schultes, 1993).

Objective function

Two different objective functions for the parameters determination both in a standard least squares formulation have been used in the parameter estimation procedure. The objective function f_1 is the sum of the squared absolute deviation between experimental and calculated molar fractions in between the packed beds (stream H) and in H_2 Rich gas stream (stream I – outlet from the absorber) for seven sets of data. This objective function was used in order to correctly describe the concentration profile along the column. As it is shown in the results (see 7.3.2.4) the objective function f_1 is not describing very well the CO_2 absorption efficiency. Therefore the objective function f_2 was used which contains only the sum of the squared absolute deviation between experimental and calculated molar fractions in H_2 Rich gas stream (stream I – outlet from the absorber) for seven sets of data.

$$f_1 = \sum_{m=1}^{7} \left[\left(x_{co_2,I,\exp,m} - x_{co_2,I,calc,m} \right)^2 + \left(x_{co_2,H,\exp,m} - x_{co_2,H,calc,m} \right)^2 \right]$$

7-5

$$f_2 = \sum_{m=1}^{7} \left[\left(x_{co_2,I,\exp,m} - x_{co_2,I,calc,m} \right)^2 \right]$$

7-6

Optimization structure

The reference state data, three set points data of test run 11 and test run 12 were used for the optimization of packing characteristic constants C_L and C_V. As the optimization tools in Aspen Plus are limited the optimization was performed using mathematical software Matlab. A code was developed which fed the Aspen Plus model with the experimental data and first estimation of C_L and C_V parameters. Then the simulation was started. The output variables are the CO_2 concentrations in between the packed bed and in the outlet of absorber. Those concentrations were compared with the experimental one and the objective function was calculated. Then the C_L and C_V parameters were changed and the simulation was repeated until the minimum of the objective function was found.

7.3.2.4   Packing evaluation

The results of the optimisation of the model parameters C_L and C_V for the two packings used in the pilot plant – random packing Raschig Super-Ring 0.6 (RSR) and structured packing Raschig Super-Pak 250 (RSP) – are shown and a sensitivity analysis of the parameters on the experimental data is performed from which conclusions about the measurement quality can be deducted. For both packing two optimization runs were performed, using the objective functions f_1 and f_2. By using objective function f_1 all the outlet concentrations were underestimated by the model and consequently the CO_2 absorption efficiency was overestimated in all optimized cases. This is not a satisfactory basis for up-scaling studies based on the process model and therefore the optimization was performed with the objective function f_2. The results from the optimization with the objective function f_2 show a significantly better fit for the outlet concentrations and CO_2 absorption efficiency.

The default values in Aspen Plus are $C_L = 1.38$ and $C_V = 0.40$ for RSR and $C_L = 1.35$ and $C_V = 0.44$ for RSP. Those values are similar to the values for other packings published in Billet and Schultes (1999) and similar to the values used in Winsorp, the proprietary model used by Raschig GmbH (for RSR). The packing parameters (C_L and C_V) are usually obtained from the absorption experiments using air and water as a carrier and under different hydraulic conditions (significantly lower ratio between liquid and gas velocities) in comparison with the hydraulic conditions in the pilot plant. Those values substantially over predict the mass transfer rate in the CO_2 Catch-up pilot plant as it is shown in Figure 7-14 for the reference state and RSR (see discussion on packing comparison on page 126 and 127). The green points show the measurements at the inlet and outlet gas streams from the absorber and the concentration between the packed beds. Pink dots correspond to the profile calculated with original C_L and C_V values and blue points show the concentration profile using optimized C_L and C_V values.
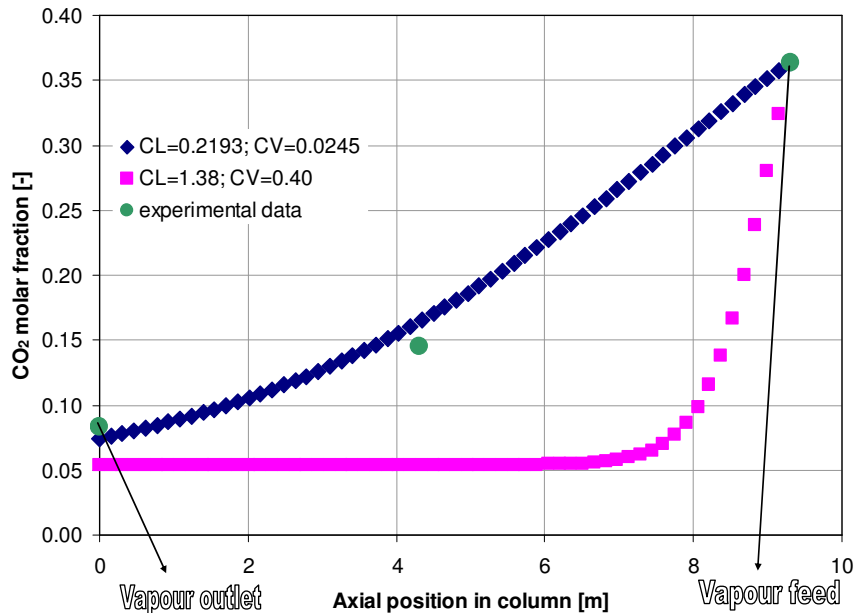
Figure 7-14: **CO$_2$ concentration profile along the column for original and optimized values of C$_L$ and C$_V$ for the reference state for RSR.**

Raschig Super Ring 0.6

The optimized values of the parameters by using objective function f$_1$ are C$_L$ = 0.2193 and C$_V$ = 0.0245. The quality of the fit was evaluated from the comparison of the experimental and calculated CO$_2$ concentrations (see Figure 7-15) and the value of the objective function. The minimum value of the objective function is 0.00511 which correspond to value of mean standard deviation of 0.0191. It says the outlet and middle bed molar fractions are on average fitted with an accuracy of 1.9% absolute. The standard deviation calculated only from the outlet concentrations (stream I) is 0.0151. From Figure 7-15 it can be observed that the concentrations between the packed beds are over predicted (except set points 2 and 3 of TR-CII-011) and the outlet concentrations are under predicted by the model. It shows a good optimization result because some concentrations are over and other ones are under predicted. This means that the Aspen Plus model over predicts the CO$_2$ absorption efficiency as can be seen in Figure 7-16 (see also discussion on packing comparison on page 126 and 127). The CO$_2$ absorption efficiency is predicted with mean standard deviation of 0.026.
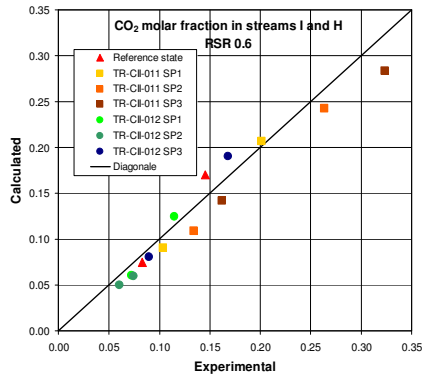
Figure 7-15: Comparison of the experimental and calculated CO$_2$ concentration in the absorber outlet (stream I) and between the packed beds (stream H) for RSR by using objective function f1. The higher concentration for the particular set point corresponds to the stream H.
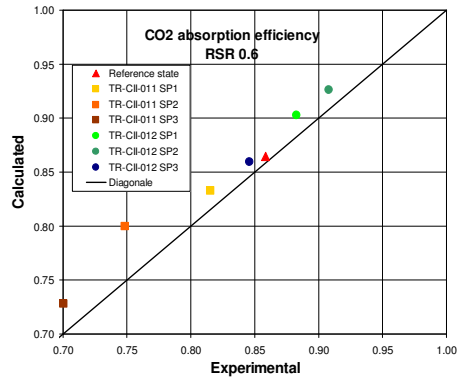
Figure 7-16: Comparison of the experimental and calculated CO$_2$ absorption efficiency in the absorber by using objective function f1

Raschig Super-Pak 250

The optimized parameters by using objective function f_1 are $C_L = 0.161$ and $C_V = 0.103$. The minimum value of the objective function is 0.00578 which correspond to value of mean standard deviation of 0.0203. The outlet and middle bed molar fractions are on average fitted with an accuracy of 2.0% absolute which is almost the same standard deviation as for RSR. The standard deviation calculated only from the outlet concentrations (stream I) is 0.0242. From Figure 7-17 it can be observed that the concentrations between the packed beds are over predicted and the outlet concentrations are under predicted by the model even more significantly than for RSR. It shows a good optimization result because some concentrations are over and other ones are under predicted. This means that the Aspen Plus model over predicts the CO$_2$ absorption efficiency as can be seen in Figure 7-18 (see also discussion on packing comparison on page 126 and 127). The CO$_2$ absorption efficiency is predicted with mean standard deviation of 0.044 which is almost two times worse than in case of RSR.
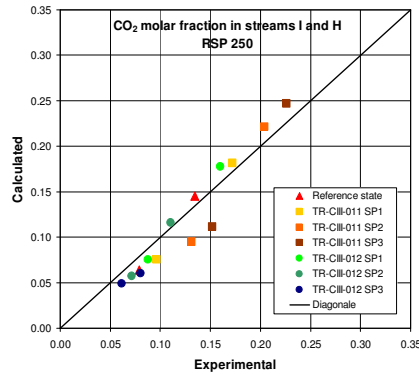
Figure 7-17: Comparison of the experimental and calculated CO_2 concentration in the absorber outlet (stream I) and between the packed beds (stream H) for RSP by using objective function f1. The higher concentration for the particular set point corresponds to the stream H.
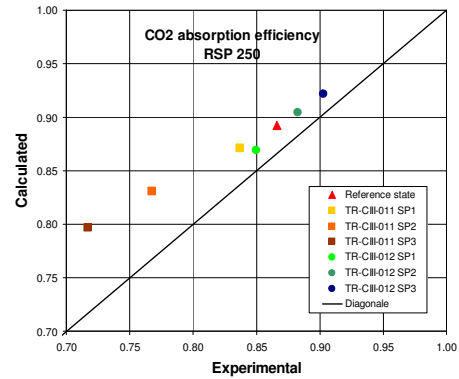
Figure 7-18: Comparison of the experimental and calculated CO_2 absorption efficiency in the absorber by using objective function f1.

The optimized values of the parameters by using objective function f2 are $C_L = 0.1179$ and $C_V = 0.06242$. The minimum value of the objective function is 0.00052 which correspond to value of mean standard deviation of 0.0086. The outlet molar fractions are on average fitted with an accuracy of 0.86% absolute which is comparable to the standard deviation of RSR. The standard deviation calculated from the outlet and middle bed concentrations is 0.0317. This means that the outlet concentrations are almost three times better fitted than in case of utilizing the objective function f_1. On the other hand the middle bed concentrations are predicted significantly worse and therefore the concentration profile along the column is not described as good as in the case of utilizing the objective function f_1. Same as for RSR, both the outlet concentrations (see Figure 7-19) and CO_2 absorption efficiency (see Figure 7-20) are equally distributed around the diagonal (see Figure 7-19) The CO_2 absorption efficiency is predicted with same mean standard deviation of 0.016 as in case of RSR and it is almost three times better fit than in case of utilizing the objective function f_1. For the further evaluation parameters $C_L = 0.1179$ and $C_V = 0.06242$ will be used.
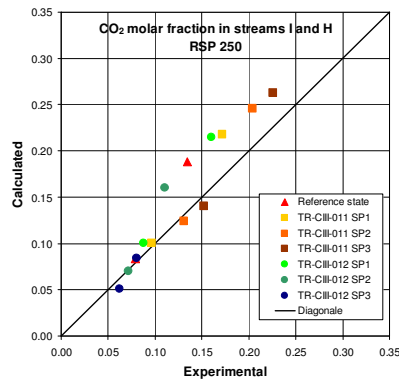
Figure 7-19: Comparison of the experimental and calculated CO$_2$ concentration in the absorber outlet (stream I) and between the packed beds (stream H) for RSP by using objective function f2. The higher concentration for the particular set point corresponds to the stream H.
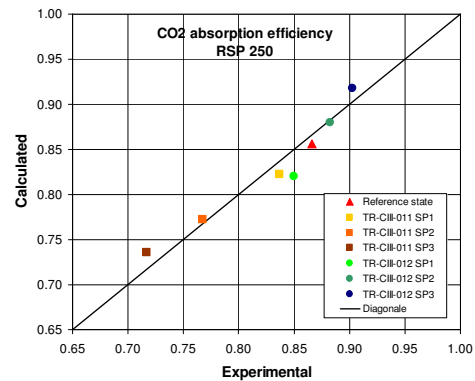
Figure 7-20: Comparison of the experimental and calculated CO$_2$ absorption efficiency

Sensitivity analysis

A sensitivity analysis of C_L and C_V parameters to the experimental concentrations was performed on the RSP packing using the objective function f$_2$. All seven experimental CO$_2$ concentrations at the outlet of the absorber were decreased by 1% and 10% relative. The change of 10% relative is up two times higher than the repeatability of the measurement declared by the vendor of the gas analysers (0.5 mol% absolute). The obtained values of the parameters are $C_L = 0.1185$ and $C_V = 0.07975$ for 1% relative change and $C_L = 0.1323$ and $C_V = 0.08231$ for 10% relative change. The original ones are $C_L = 0.1179$ and $C_V = 0.06242$. The relative change of the parameter C_L is 0.5% respectively 10.5% and the relative change of the parameter C_V is 21% respectively 24%. Significantly higher change in C_V parameter is caused by the distribution of the resistance against the mass transfer. The resistance is mainly concentrated into the liquid phase and it reaches around 90% under the hydraulic conditions at the bottom of the column and around 70% under the hydraulic conditions at the top of the column. Thus, large changes of the gas mass transfer coefficients, represented by the parameter C_V, have only a small effect on the outlet concentrations. In contrast, The C_L value seems to be as accurate as the accuracy of the measurement. The strongly nonlinear behaviour in C_L and C_V parameters changes (approximately the same change in C_V parameter for the 10 times different change in CO$_2$ concentration) is caused by the fact that the 10% relative change in the CO$_2$ concentrations change the distribution of the

resistance against the mass transfer. Hence the accuracy of the concentration measurements is sufficient in order to get reliable C_L value. The C_V value is much more sensitive and not so reliable but it is determined by the system behaviour and it cannot be changed. Further investigation showed that the data can be well described by a single fitting parameter C_L which is then determined statistically more reliable.

Packing comparison

The optimization results show that the parameter C_L is about 25% higher for Raschig Super-Ring 0.6 than for Raschig Super-Pak 250. As the resistance against the mass transfer is concentrated in the liquid phase, Raschig Super-Ring 0.6 seems to be a more suitable packing for the physical absorption of CO_2 for the specific hydraulic conditions tested in the pilot plant.

Using rate-based modelling with Billet and Schultes correlations, the measured concentrations could not be reproduced with standard mass transfer parameters C_L and C_V. Equilibrium was already reached half-way along the column. In order to reproduce the measured outlet concentration and also the concentration measured in-between the packed bed, C_L and C_V had to be reduced by a factor of approximately 10.

To check whether there is an error in the Aspen calculations, a comparing simulation has been made with Winsorp, using the same boundary conditions and equilibrium data. From this comparison it can be concluded that the implementation of the mass transfer correlations in Aspen is correct. Almost the same k_L and k_V values and effective mass transfer area have been calculated in Winsorp and Aspen.

From these investigations several questions arise:
1. Is the pilot plant under-performing and if yes what is the cause of the reduced performance?
2. Are the hydrodynamic conditions in the plant (very low gas flow rate and very high liquid flow rate) outside the region where usual mass transfer correlations can be applied?

In discussion with Raschig, several potential causes for underperformance were highlighted. One possibility can be the occurrence of foaming in the absorber, which could be result in higher pressure drops and fluctuations in the pressure drop. The measured values of dynamic pressure drop were indeed fluctuating (between 2.0 and 2.5 mbar/m in both sections) and are up to 20 times higher than the once provided by vendor. On the other hand, no liquid was detected in the overhead lines (although foam may have the chance to "settle down" in the void at the top of the absorber). Unfortunately, no anti-foam was tested during pilot plant operation. Therefore, a test was performed in the laboratory by injecting nitrogen from the bottom into a frit filled with the used

solvent (bubbling app. 1 l/min N_2 through a 40 mm frit) in order to verify the occurrence foaming. Foaming was seen which could explain the pressure drop characteristics though it is hard to categorize it as heavy, normal or slight foaming. After adding a little anti-foam, the foaming vanished (comparable to reference bubbling nitrogen through methanol).

A second possibility can be gas back-mixing as the gas velocity is very low and liquid can entrain the gas. To judge on the back-mixing Raschig uses the "Phasenverhältnis" factor (ratio of effective velocities u_L/u_V) which should not exceed 5 (general rule of thumb applied by Raschig). In the pilot plant, this factor is 2.2 for the bottom hydraulic conditions and 3.2 for the top hydraulic conditions. This is a general rule of thumb though so back-mixing cannot be ruled out.

For the design of the large-scale plant it may be recommended to apply a higher gas velocity to avoid the risk of back-mixing and add some anti-foam to ensure that the mass transfer is optimal. Because the structured packing is more sensitive to foaming, the expected performance increase by adding anti-foam is higher for the structured packing. The mass transfer performance should improve similarly for both packings by increasing the gas velocity because the back-mixing is packing independent. Assuming approximately two times higher gas velocity for the large-scale plant design versus the pilot plant, the hydraulic limit (loading point) of the random packing Raschig Super-Ring 0.6 is reached. Hence it is recommended to use structured packing Raschig Super-Pak 250 for the large-scale plant.

7.3.2.5   Verification of validated model

The verification of the model is based on the remaining test run data and their comparison with calculated ones using the validated model. For the calculations the optimized packing characteristic parameters C_L and C_V obtained by utilizing the objective function f_2 were used.

Solvent temperature

The CO_2 absorption efficiency using optimized model parameters is slightly under predicted for both packings (see Figure 7-21 and Figure 7-22). The maximum difference between experimental and calculated CO_2 absorption efficiency is 1.9% absolute and the other ones are below 1.6% absolute which is also in the range of the accuracy of the validated model. The trend that with a decreasing temperature (solvent and shifted syngas) the CO_2 absorption efficiency is increasing is fitted perfectly and the difference between experimental and calculated data is almost constant. The results also indicate that not only temperature dependence of the physical properties and their influence on the mass transfer but also the VLE between CO_2 – DEPEG is described correctly at least relatively.
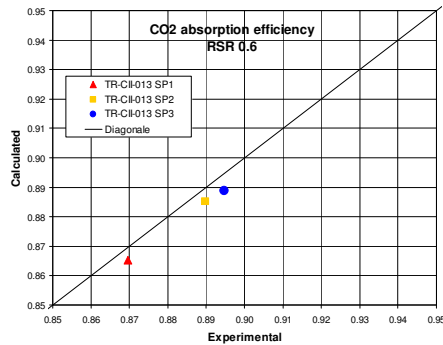
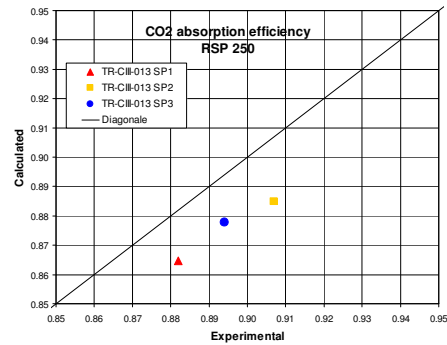**Figure 7-21: Comparison of the experimental and calculated CO$_2$ absorption efficiency in the absorber for RSR.**

Figure 7-22: Comparison of the experimental and calculated CO$_2$ absorption efficiency in the absorber for RSP.

Absorber pressure

The optimized CO$_2$ absorption efficiency is slightly under predicted in the reference state for both packings (see Figure 7-23 and Figure 7-24). The maximum difference between experimental and calculated CO$_2$ absorption efficiency is 2.4% absolute for set point 1 of TR-CIII-014. The rest of the differences is in the range of the accuracy of the validated model at reference conditions. The trend that with an increasing pressure the CO$_2$ absorption efficiency is increasing can be reproduced accurately but the difference between experimental and calculated data is not constant (as the diagonal is significantly closer to the points at higher absorber pressure). It leads to the conclusion that at higher absorption pressure the model will slightly over predict the CO$_2$ absorption efficiency but the trend will be correctly described.

The reason why the model over predicts the CO$_2$ absorption efficiency at higher pressure (relative to low pressures) may be the quality of the fit of the gas – liquid equilibrium data (de Servi, 2013a). The PC-SAFT EoS predicts higher equilibrium concentration of CO$_2$ in the liquid phase at higher pressures in comparison with the experimental data which means that more CO$_2$ can be absorbed. This deviation in the equilibrium model is most likely the cause for the observed deviation in the absorber model for pressure changes. For the high pressure operation in the full scale plant, it is recommended to refit the experimental equilibrium Px-data of the binary mixture DEPEG - CO$_2$ in the relevant pressure range in order to predict the CO$_2$ absorption efficiency with the same accuracy as for the change of other process variables.
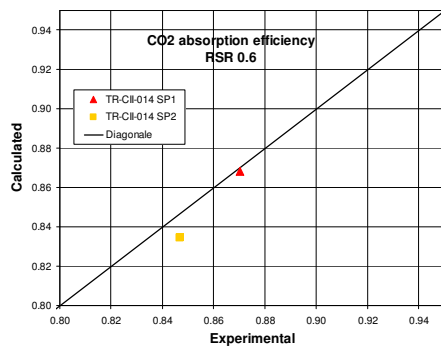
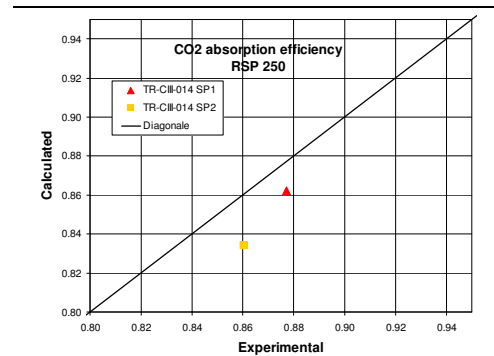**Figure 7-23: Comparison of the experimental and calculated CO$_2$ absorption efficiency in the absorber for RSR.**

Figure 7-24: Comparison of the experimental and calculated CO$_2$ absorption efficiency in the absorber for RSP.

Water content

The water content in the lean solvent is strongly under predicted (see Figure 7-25). Fortunately, as was shown experimentally in TR-009 the water in the system has a negligible effect on the mass transfer in the absorber.
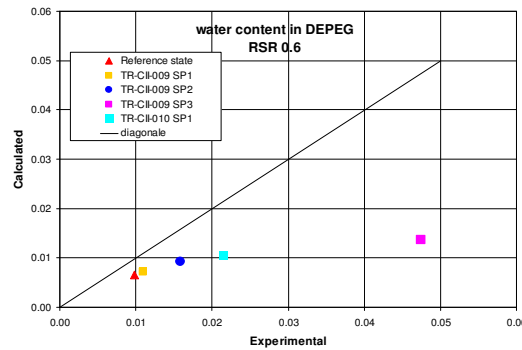
Figure 7-25:   Comparison of the experimental and calculated water content in DEPEG for RSR.

Pressure 1st flash vessel

Figure 7-26 shows that the relative difference between experimental and calculated gas flow from 1st flash vessel stays constant at different pressures. The trend that with an increasing pressure the gas flow from the 1st flash vessel is decreasing is fitted perfectly. The absolute difference between experimental and calculated data is most probably caused by the error in CO$_2$ absorption efficiency which is due to the accuracy

of the optimization. The total mass of the other gases (except CO_2) is only 2.7 % of the total mass of the outlet gas stream from the 1st flash vessel.

The concentrations at the outlet of the 1st flash vessel are very sensitive on the composition of the rich solvent (stream 72). The underestimation of the CO_2 absorption efficiency implies that the actual rich loading (which is not measured) is higher than the simulated values. In order to evaluate the accuracy of the flash vessel calculations and the VLE data between DEPEG - H_2 and DEPEG - CO the rich solvent composition should be identical to the actual value. For this purpose the following simulation was performed: The absorber was excluded from the model flowsheet. Stream 72 was created by mixing the liquid outlet stream from 3rd flash vessel together with experimentally determined absorbed amount of all components (this is referred to as experimental value). The results of the outlet gas flow rates are shown in Figure 7-27. The trend is again fitted perfectly. The difference between experimental and calculated data is almost constant which means that the VLE dependency on the pressure is correctly implemented in the model.

The comparison of the calculated and experimental H_2 molar fraction in the gas outlet from 1st flash vessel for RSR is shown in Figure 7-28. The trend that with an increasing pressure the H_2 concentration is increasing is fitted perfectly. The difference between experimental and calculated data is almost constant which means that the VLE dependency between DEPEG - H_2 on the pressure is correctly implemented in the Aspen Plus model. The absolute difference is around 4 mol% which is significant. However, the hydrogen mass flow is negligible in comparison to the overall flow from the flash vessel. Hence the experimental data are not sufficiently accurate in order to evaluate PC-SAFT EoS quality of DEPEG - H_2.

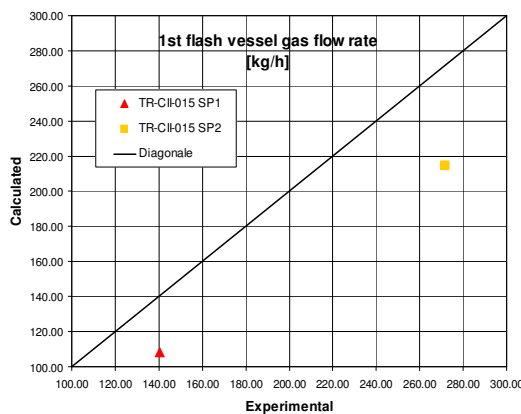**Figure 7-26:**   **Comparison of the experimental and calculated gas flow rate from 1st flash vessel for RSR.**

Figure 7-27: Comparison of the experimental and calculated gas flow [kg/h] from 1st flash vessel for RSR.

Figure 7-28: Comparison of the experimental and calculated H_2 concentration [mol/mol] in the gas outlet from 1st flash vessel for RSR.
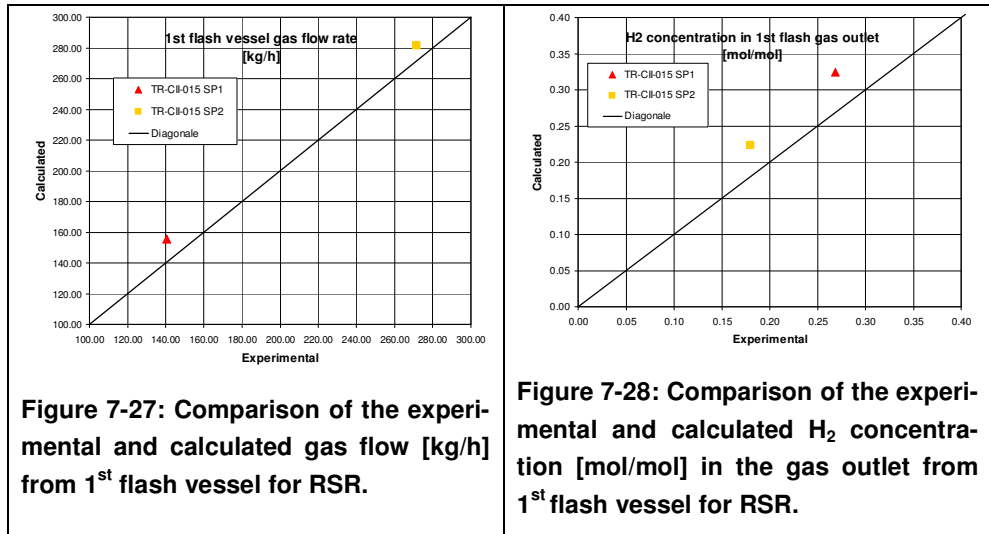
High solvent mass flows

The CO_2 absorption efficiency using optimized model parameters is slightly over predicted (see Figure 7-29). The maximum difference between experimental and calculated CO_2 absorption efficiency is 0.72% absolute which is more than two times better than the accuracy of the validated model (±1.6% absolute). The trend that with an increasing solvent flow rate the CO_2 absorption efficiency is increasing is fitted perfectly. The difference between experimental and calculated data is almost constant which means that the mass transfer dependency on the high solvent flow rate is described correctly in the model.

Figure 7-29:   Comparison of the experimental and calculated CO_2 absorption efficiency in the absorber for RSP 250.

7.3.2.6   Model limitations

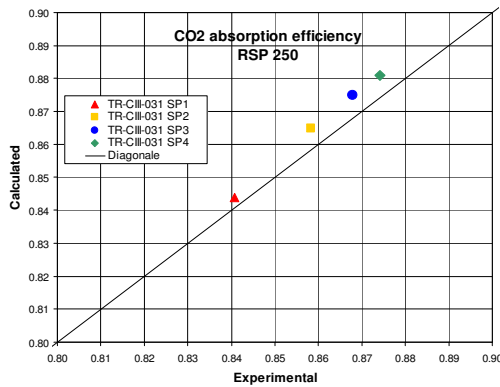The validated model can be used for both packings with the same accuracy in all tested cases (CO_2 absorption efficiency ±1.6% absolute). The trends in CO_2 absorption efficiencies with the change of the process variables (mass flows, concentrations, temperatures, pressures) are always predicted correctly. The model can be used in the range of conditions applied in the pilot plant where it mostly underestimates the CO_2 absorption efficiency which results in a safe prediction.

The model is validated for the liquid load in the unusually broad range from 80 m³/h to 225 m³/h which covers common absorption operation conditions. On the other hand the validated gas velocity range is quite narrow (from 0.025 m/s to 0.06 m/s) but still applicable for high pressure operation conditions for which the low gas velocities are typical. The validated solvent temperature range (from 17.5°C to 45°C) is quite broad and there is no reason to be concerned about the extrapolation to chilled operation (5°C to 10°C) as in the UOP design. The results show overestimation of the CO_2 absorption efficiency for high pressures. Once the PC-SAFT parameters of the binary mixture DEPEG - CO_2 will be refitted for higher pressure, the model will accurately predict the performance at operating pressure beyond the tested range of 21-23 bar (for the full-scale plant the pressure is approximately 35 bar). The equation of state (PC-SAFT fitted on Clariant VLE data) is not capable to accurately predict the water content in DEPEG. This is not problematic for the modelling of the CO_2 absorption process, but may be a problem to accurately calculate the stripper performance in the integrated H_2S and CO_2 removal unit.

7.4   Dynamic models of the pilot plant

In order to study the transient performance of the pre-combustion CO_2 capture unit during load variations dynamic models of the entire system and models of the sub-systems have been developed. The models are developed following a state-of-the-art, object-oriented, lumped-parameter modelling approach, using the open-source Modelica language (Fritzson, 2003), implemented in a commercial software tool (Dymola). One of the advantages of the Modelica language is the availability of various open-source and commercial libraries covering different engineering fields, such as electrical, mechanical or thermal. Whenever possible, models have been reused from available Modelica libraries. Basic components, such as valves, pumps, heat exchange and flow models, are taken from the ThermoPower library (Casella and Leva, 2006). This library contains reusable components for the modelling of thermo-hydraulic processes and power plants using medium models from the Modelica.Media library. The fluids available in the Modelica.Media library are water described with the IAPWS-IF97 steam tables and multi-component gases described with the ideal gas model and NASA coefficients. Therefore, ThermoPower components are used when-ever the fluid is water or behaves as ideal gas. The thermophysical properties of the

highly non-ideal mixtures involved in the capture process are calculated with the PC-SAFT Equation of State. This EoS has been implemented, together with fast and robust algorithms, into an in-house property package called FluidProp (Colonna et al., 2004) which is interfaced with the dynamic modelling tool.

The models are developed following a modular way in order to master system complexity. Therefore, the overall system is decomposed into suitable sub-system models which are connected through interfaces. The sub-system model are formed of basic modules, which either describe simple process units (e.g., a pump or a valve), or defined physical processes (e.g., accumulation of mass, energy and momentum) (Casella and Colonna, 2012). The requirements that have been defined in order to ensure that the developed dynamic models are suitable for the objectives of this project are defined in (Faber, 2012a). A detailed description of the dynamic modelling approach can be found in (Trapp, 2013b).

7.4.1   Dynamic model of the WGS section

In this section the development of the dynamic component models and the system models covering the conditioning, WGS and condensate recovery process are described. The purpose of the models is to study the transient performance during load variations and to design control strategies aiming at the improvement of the dynamic operation. Therefore, the modelling is focused on the accurate description of the relevant thermo-physical phenomena which have a significant contribution to the transient behaviour. The main phenomena are storage of mass and energy, heat transfer and the water-gas shift reaction. A detailed description of the developed models, including the balancing equations and the mathematical implementation of the equation system can be found in (Trapp, 2013b).

Various transient test runs have been performed during pilot plant operation in order to obtain data that can be used to validate the dynamic behavior described by the dynamic plant component models. The validation of the individual plant component models for the syngas conditioning, WGS reactor and recovery section is described in (Trapp, 2013b). In this section, the results of the validation of the entire system model are shown (for flow sheet see Figure A 1).

7.4.1.1   Model validation

For the validation of the conditioning, shifting and recovery section of the CO_2 capture unit a realistic load change experiment was performed. The plant was ramped from part-load to full-load in closed-loop operation, which corresponds to a change in syngas mass flow rate from 850 kg/h to 1100 kg/h. This experimental test aims at the validation of the entire process and control system performance. Further, the load change abilities of the pre-combustion capture process are evaluated.

It is expected that the syngas mass flow controller will slowly increase the syngas flow from part-load to full-load while the other flows adapt smoothly. Disturbances are expected in some of the temperatures along the process due to the load changes and the inertia of thermal storage. The comparison of the measurements and simulation results for the main flow rates and temperatures are visualized in Figure 7-30 and Figure 7-31.

The first analysis of the measurements revealed that the values of the syngas control valve opening were completely biased. At 850 kg/h the opening was measured with almost 0 % which increased to 25 % at 1100 kg/h. This cannot be reproduced with normal valve model. As a consequence of the biased measurements the control action is different, which explains the large overshoot in the simulation results of reactor 1 mass flow which is the corresponding flow to the syngas control valve (see Figure 7-30 (a)). However, satisfactory agreement is achieved between the measurements and the model predictions for the reactor 1, quench and syngas mass flow. Regarding the water mass flow, the trend is reproduced correctly. However, the initial flow decrease and the slope of the increase are not predicted accurately. For reasons of computational efficiency this water flow is not modelled as a recycle but with a sink of constant back pressure which causes these differences. The variations in the make-up water flow in the recovery section are directly related to the water flow. Model predictions show good agreement with the experiments. However, the measurements depict a rather poor signal-to-noise ratio. The shifted syngas mass flow is visualized in Figure 7-30 (f). The initial increase is predicted somewhat faster by the model with is related to the overshoot in reactor 1 flow. At 1400 kg/h the measurements remain constant which is most probably caused by an opening of the flare valve upstream the mass flow measurement point. The quench and superheater inlet temperature as well as the reactor outlet temperatures show satisfactory agreement between the measurements and model predictions in terms of trend, settling time and steady-state values. The maximum overshoot of reactor 1 outlet temperature is under predicted by roughly 5 K, whereas the model over predicts the overshoot of reactor 2 and 3 outlet temperature slightly by approximately 1 K.

To summarize, the steady-state values of the main process variables are reproduced at part-load and full-load with an error of maximum 3%. The steady-state data reconciliation indicates systematic biases in the water and syngas mass flow measurements (see 7.3.1.2). Hence, these flow measurements have been corrected for the dynamic analysis. With respect to the dynamic performance the comparison can be evaluated based on the main transient parameters such as time and value of maximum overshoot, settling time, frequency and damping of oscillations. For the presented transient these parameters are predicted with less than 10 % error. These results can be considered as satisfactory and subsequently the dynamic model serves as a reliable basis for the development of a large-scale process model and the analysis of control strategies. However it has to be mentioned that up-scaling investigations based on the current

dynamic model is very questionable due to the fact that certain process parameters have been tuned specifically to the pilot plant process and a re-tuning or more rigorous thermodynamic description would be necessary.

Considering the load change performance of the pilot plant it is apparent that a settling time of 9 hours is unacceptable for flexible and fast load variations. Considering also the damping performance of some controllers observed during the shifting test run, it is obvious that the dynamic performance of the system can be improved by better tuning of the control parameters. The dynamic models are a helpful tool for control parameter tuning and identification of other operational issues such as biased sensors. However, even with tuned parameters it is unlikely that the current control system is able to facilitate fast load changes, thus the development and test of a new control strategy is of paramount importance.

Figure 7-30: Comparison of measurements and simulation results for change from part-load to full load operation. a) Reactor 1 mass flow rate. b) Quench mass flow rate. c) Syngas mass flow rate. d) Water mass flow rate. e) Make-up water mass flow rate. f) Shifted syngas mass flow rate.
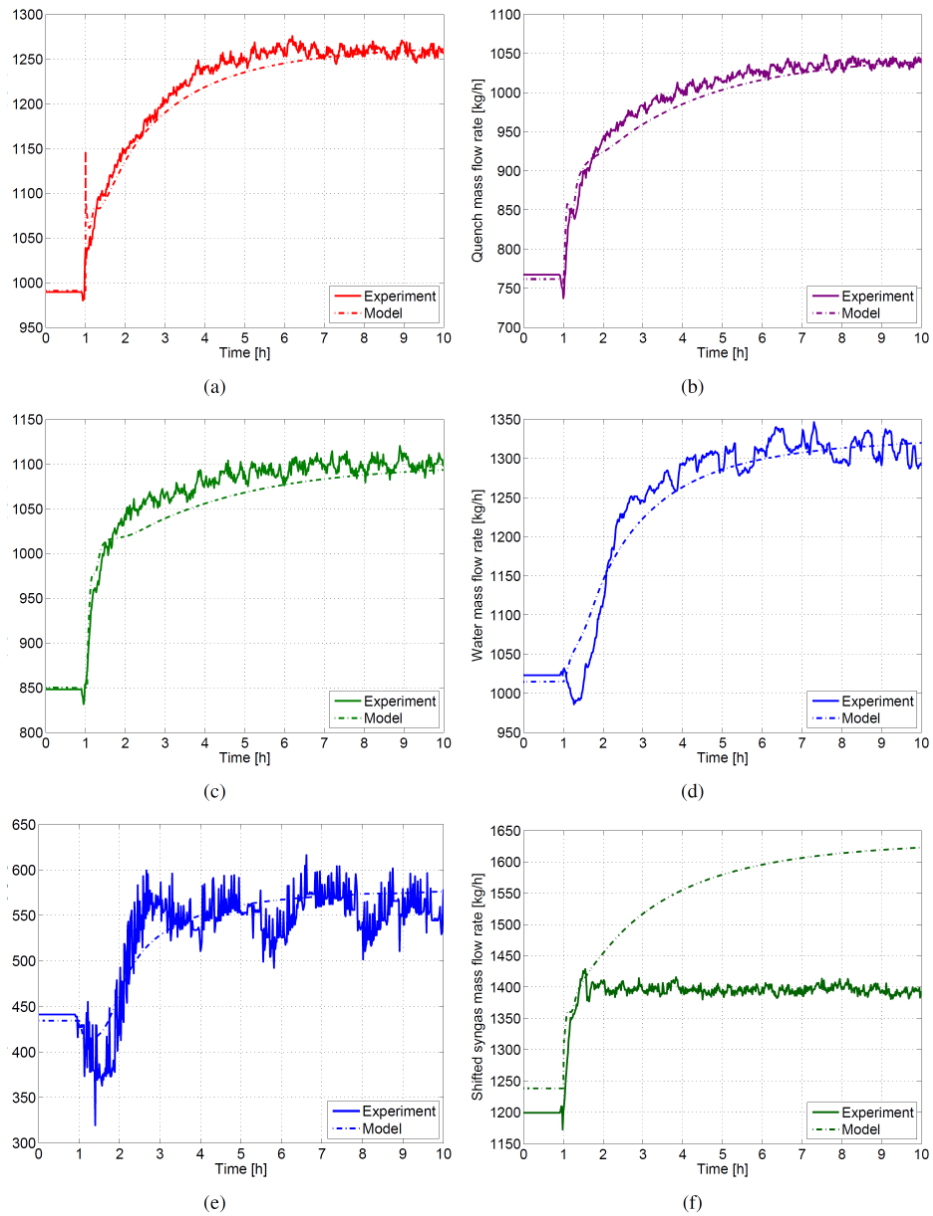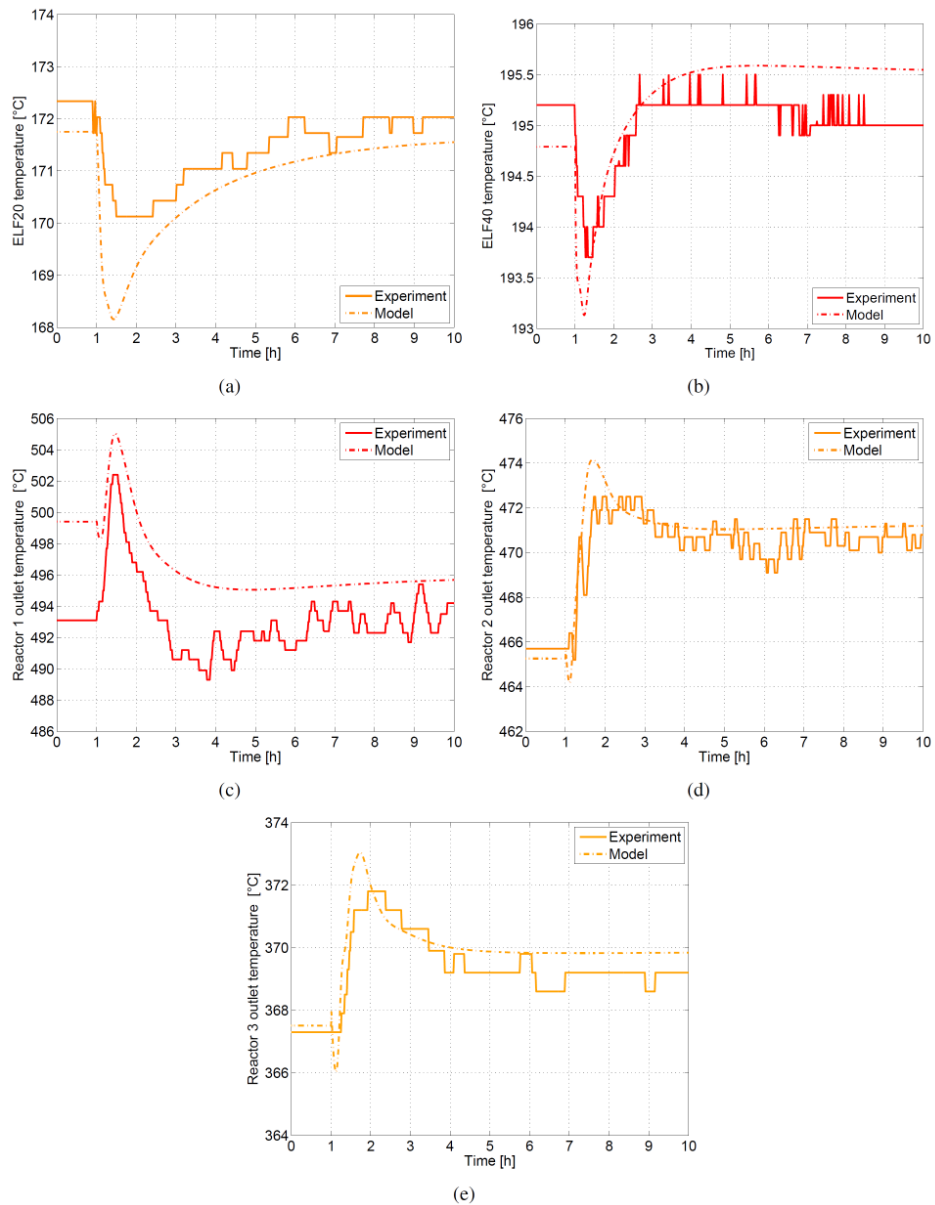
Figure 7-31: Comparison of measurements and simulation results for change from part-load to full-load operation. a) Quench temperature (ELF20 BB010). b) Superheater inlet temperature (ELF40 BB010). c) Reactor 1 outlet temperature. d) Reactor 2 outlet temperature. e) Reactor 3 outlet temperature.

7.4.2 *Dynamic model of the absorption section*

The model comprises the absorber column and sump, a syngas, lean solvent and rich solvent flow source, a pressure drop representing frictional losses of the H_2 rich gas in the overhead cooler, a gas tank representing storage of mass in the overhead cooler, the H_2 rich gas control valve including the PI absorber pressure controller, a quadratic pressure drop representing the frictional losses in the piping guiding the H_2 rich gas to the flare and a pressure sink representing the flare. The flowsheet diagram of the system model used for the validation is depicted in Figure A 2. Due to the complexity of the process model for the absorption column (mass transfer between gas phase and liquid phase, multiple recycle streams due to counter current flow operation) special attention has been paid to the development of the dynamic model for this component.

In dynamic models, the number of state variables is significantly higher than in steady-state models due to time discretization of the system and the addition of mass and energy hold-up terms. This implies a higher complexity of the equations set to be solved. Therefore it is often required to reduce the degree of detail of dynamic models in comparison with the steady-state representation. For this reason, the absorber packed column has been described by a simple equilibrium model. From a comparison between the rigorous rate-based model and the simplified equilibrium approach it can be inferred that the equilibrium model has an adequate accuracy for the aims of dynamic simulation (de Servi and Trapp, 2013b and Valenz, 2013g).

The absorption column is composed of a series of equivalent trays (storage modules) and valves or liquid heads (resistive modules) (see Figure 7-32). In the equivalent trays, pressure, temperature and composition of liquid and vapour phase are determined by solving the mass and energy balance of the system and assuming equilibrium between the two phases. In the resistive modules liquid and vapour mass flow rate are determined. For description of the pressure drop and the liquid hold-up inside the column, the Billet and Schultes correlations have been used. To ensure a consistent modelling approach, the thermophysical properties have been calculated with the PC-SAFT EoS which has been implemented through the external FluidProp library as in the steady-state models. A detailed description of the dynamic absorber model, including a description of the mathematical modelling approach and of the model parameters can be found in (de Servi and Trapp, 2013b).

The initialization is a crucial step of dynamic simulation, because the solution of ODE/DAE sets depends on the initial conditions. A rigorous initialisation routine has been implemented that allows for robust initialisation of the absorption column model. The rough outline of the initialisation approach is described in A.6.
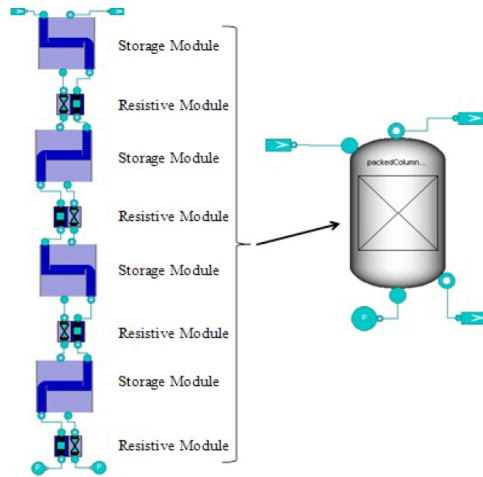
Figure 7-32:   Structure of the dynamic absorption column model

7.4.2.1   Model validation

For validation of the absorber model with Raschig Super-Pak 250 two test runs were performed (TR-CIII-029 and TR-CIII-030). During the first set of tests, TR-029, the solvent mass flow was changed stepwise while keeping the syngas mass flow, the absorption pressure and temperature constant. In the second tests, TR-030, the syngas mass flow rate was perturbed stepwise while maintaining unchanged the values of the other input variables.

The holdup in the liquid and vapour phase of the absorber column is the main process variable which determines the dynamic system response. The hydrodynamic coefficient of the holdup correlation is tuned in order to achieve good agreement between model predictions and measurements. The process variables used for this quantitative model validation are volumetric flow rate, temperature, CO_2 and H_2 concentration of the H_2 rich gas, absorber pressure and column pressure drop. The absorber pressure and H_2 rich gas flow rate are the most important variables for the parameter tuning process. The best agreement between measurements and model predictions for TR-CIII-029 and TR-CIII-030 is achieved with a value of 1 for the hydraulic coefficient (default value provided by Raschig for Super-Pak 250 is 0.65) Below the results of the test runs versus the modelled values are presented.

Test run TR-CIII-029: Dynamic solvent mass flow

During this experiment, manual step changes, upward and downward, were applied directly to the solvent mass flow control valve (ELH50 AA051) without the solvent flow controller in operation. The change in solvent mass flow rate which is in reality a fast ramp is depicted in Figure 7-33(a). The syngas mass flow rate is shown in Figure

7-33 (b). The opening of the valve controlling the syngas mass flow is maintained during the test in order to keep the syngas flow constant. However, as the absorber column pressure changes, which represents the back pressure to the syngas control valve, the syngas mass flow varies (therefore dynamic boundary condition is applied). The experimental data and simulation results for the transient of the pressure at the absorber top are compared in Figure 7-33 (c). The dynamic trend of the absorber pressure with its fluctuations is predicted correctly by the model. However, the model over predicts especially the initial increase in pressure by 0.3 bar. Further deviations are smaller than 0.1 bar. These deviations are related to the absorber pressure control. Considering the comparison of measurements and model predictions for the valve opening of the H_2 rich gas flow valve (ELH80 AA050), similar differences are observed (see Figure 7-33 (d)). The model over predicts the initial valve opening when the implemented pressure controller uses the same gain and integration time as the controller in the pilot plant. However, the back pressure of the valve which is represented by a constant flare pressure and a quadratic pressure drop is most likely not reproduce correctly causing the deviation in valve opening and subsequently absorber pressure. Limited data was available to accurately model the back pressure.

The comparison of the measurements and model predictions for the pressure drop over first and second packing are visualized in Figure 7-33 (e) and Figure 7-33 (f). For the first packing the absolute values and the trend are not predicted correctly by the model. The predicted transient of the pressure drop only depends on the solvent and syngas volumetric flow rate and the densities of the vapour and liquid (see Billet and Schultes pressure drop correlation (Valenz, 2013g)) while the pressure loss induced by the liquid distributor situated above the packing is not modelled. This might be the main reason why the measurements and simulation results differ.

For the second packing the absolute values are not predicted accurately. However, the dynamic trend is reproduced correctly by the model. Similar to the first packing, differences are related to the pressure drop of the redistributor situated above the second bed which is not included in the model.

Due to numerical instabilities of the simulation at low dynamic pressure drops, the friction coefficient has been adjusted such that the overall column pressure drop is approximately 20 mbar which promotes robust simulations. The pressure drop does not affect the dynamic performance of the absorber column in terms of heat and mass transfer and hence adjustment of the pressure drop for numerical reasons is justified.

Figure 7-34(a) depicts the comparison of the experimental data and the model predictions for the H_2 rich volumetric flow rate. The trend of the transient is predicted correctly by the model. With the increase in solvent flow rate the CO_2 capture is enhanced leading to a lower H_2 rich gas flow. The model under predicts the initial steady-state value. However, this under prediction was also observed during analysis of the experimental results with steady-state simulation tools. Measurements and simulation results for the H_2 and CO_2 content in the H_2 rich gas flow are depicted in

Figure 7-34 (b) and Figure 7-34 (c). Similar to the H_2 rich gas flow the absolute values for off-design operation (solvent mass flow rate 10 kg/s) cannot be matched. The dynamic trend is predicted satisfactory by the model. However, a time delay of approximately 6 to 9 minutes is observed. Note that the composition is not measured in a continuous manner and measurements are only available every 3 minutes. However, the observed time delay cannot be fully explained by this. Further investigations are required.

Finally, the measurements and model results for the response in gas temperature between the packings is compared in Figure 7-34 (d). A temporary increase in gas temperature is observed, which is caused by the fluctuations in the lean solvent temperature which is therefore applied as a dynamic boundary condition. The model predictions show satisfactory agreement with the measurements.
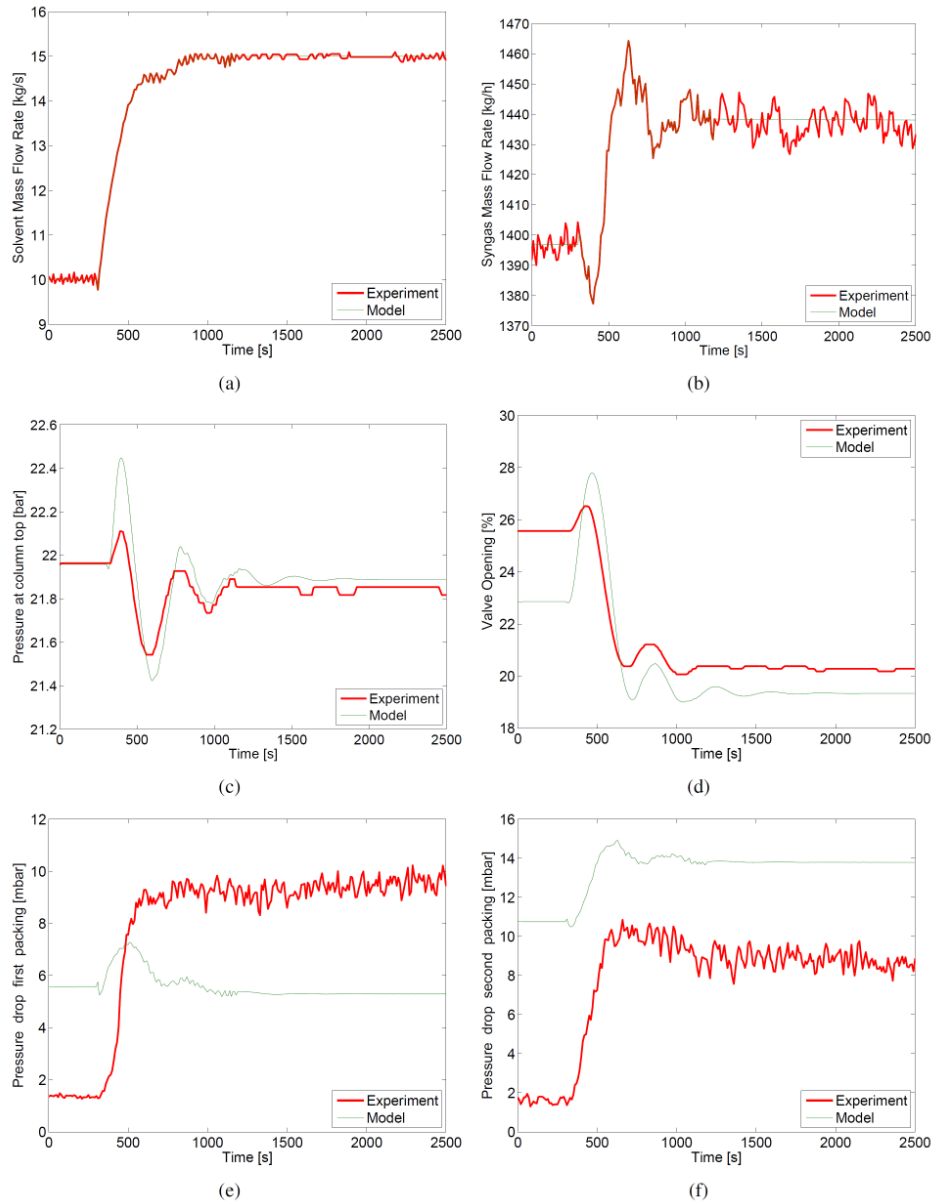
Figure 7-33: Comparison of measurements and simulation results for TR-CIII-029. a) Solvent mass flow rate (model input). b) Syngas mass flow rate (model input). c) Pressure at column top. d) Valve opening H2 rich gas valve. e) Pressure drop first packing. f) Pressure drop second packing.

Figure 7-34: **Comparison of measurements and simulation results for TR-CIII-029. a) H$_2$ rich gas volumetric flow rate. b) H$_2$ content in H$_2$ rich gas flow. c) CO$_2$ content in H$_2$ rich gas flow. d) Gas temperature between packings.**

Test run TR-CIII-030: Dynamic solvent mass flow rate

During this test run manual step changes, upward and downward, were applied to the back pressure control valve (ELG60 AA050) of the syngas compressor without the pressure control in operation. The perturbations in valve opening correspond to a change in syngas mass flow rate of 600 kg/h starting with a step decrease from 1400 kg/h and returning to the initial value with a step increase.

The change in syngas mass flow rate is depicted in Figure 7-35(b). The set point of the lean solvent mass flow controller is kept constant during the transient in order to maintain the flow rate. However, as the absorber column pressure changes, which supplies the back pressure to the solvent control valve, the flow controller needs to adjust and hence the solvent mass flow rate fluctuates slightly (see Figure 7-35 (a)). Therefore, the solvent flow rate is applied as dynamic boundary condition.

The measurements and simulations results for the pressure transient at the column top are compared in Figure 7-35 (c). A satisfactory agreement is achieve for the dynamic

trend as well as the absolute values with deviations during the transient smaller than 0.1 bar. The agreement is related to good predictions of the absorber pressure control. Exemplary measurements and model predictions of the valve opening of the H_2 rich gas flow valve, which is adjusted by the pressure control in order to maintain the absorption pressure, is depicted in Figure 7-35 (d). In comparison to TR-CIII-029 the model predictions for the pressure control and valve back pressure conditions are significantly better. This is probably explained by the fact that the perturbation of the syngas mass flow rate for this experiment is a ramp with a duration of approximately 600 seconds, whereas the ramp duration of solvent mass flow test TR-CIII-029 is roughly 300 seconds.

The comparison of the experimental data and model predictions for the pressure drop over the first and second packing are depicted in Figure 7-35 (e) and Figure 7-35 (f). For both packing sections the dynamic trend, a decrease in pressure drop caused by a decrease in vapour flow, is predicted correctly. The change in vapour flow has two reasons: first the decrease in entering syngas mass flow and second the decrease in H_2 rich product as a result of enhanced CO_2 removal. However, the absolute values for the initial and final steady-state are not predicted correctly. As explained previously, the pressure drop of the liquid distributors above the first and second bed are not modelled and therefore measured losses cannot be compared with model predictions, which only represent the dynamic pressure drop.

The measurements and simulation results for the H_2 rich volumetric flow rate are compared in Figure 7-36(a). The trend as well as the absolute values is predicted accurately by the model.

Figure 7-36 (b) and Figure 7-36 (c) depict the comparison of the experimental data and model predictions for the H_2 and CO_2 content in the H_2 rich gas flow. The dynamic trend as well as the steady-state values is predicted correctly. With an increase in syngas mass flow at constant solvent flow rate, the CO_2 absorption efficiency increases which leads to a lower CO_2 content and higher H_2 content in the H_2 rich product flow. Similar to test run TR-CIII-029 a time delay of approximately 9 minutes is observed, which is slightly higher than expected.

Finally, the measurements and model predictions for the transient of the gas temperature between the packing sections is compared in Figure 7-36 (d). Again, the model predictions show satisfactory agreement with the experimental data.
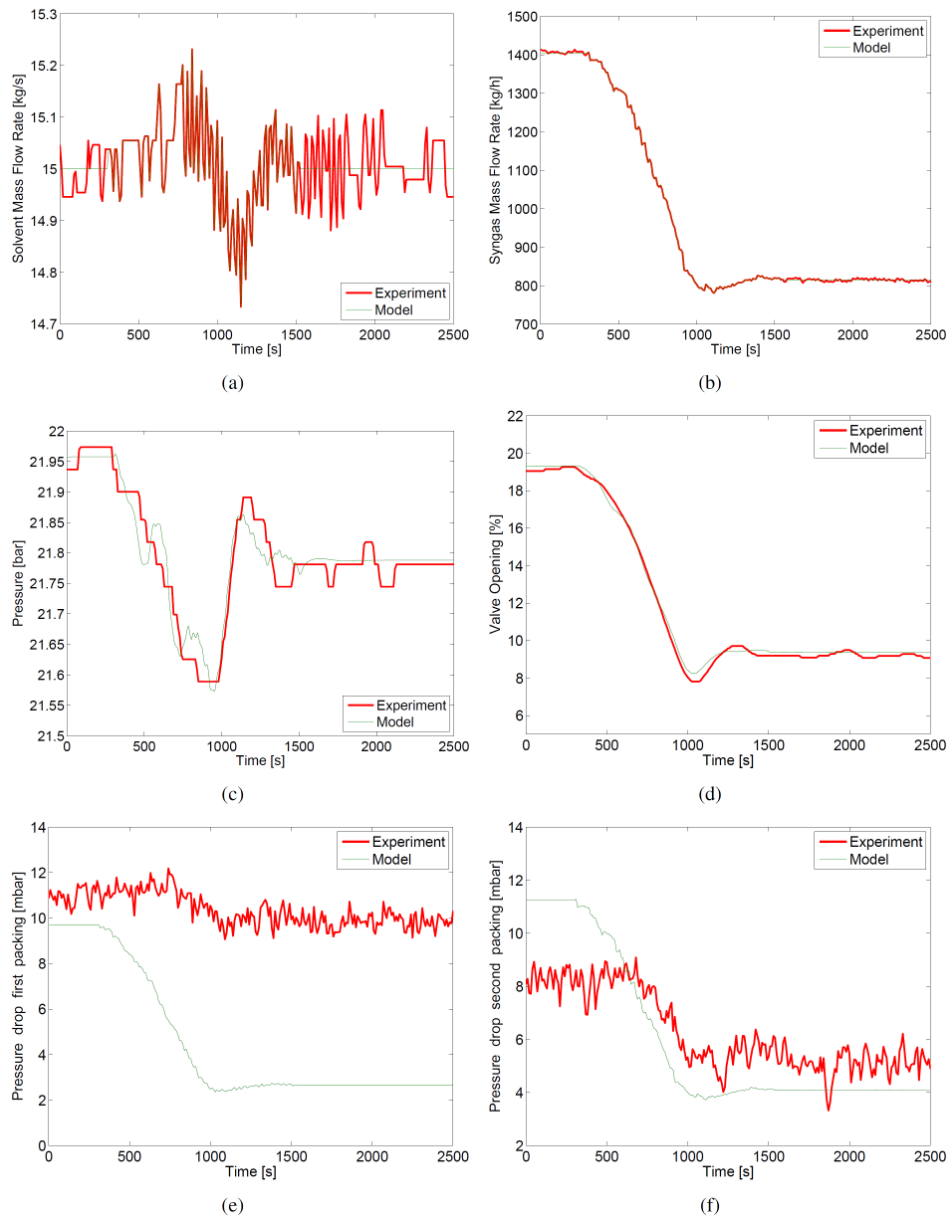
Figure 7-35: Comparison of measurements and simulation results for TR-CIII-030. a) Solvent mass flow rate (model input). b) Syngas mass flow rate (model input). c) Pressure at column top. d) Valve opening H2 rich gas valve. e) Pressure drop first packing. f) Pressure drop second packing.
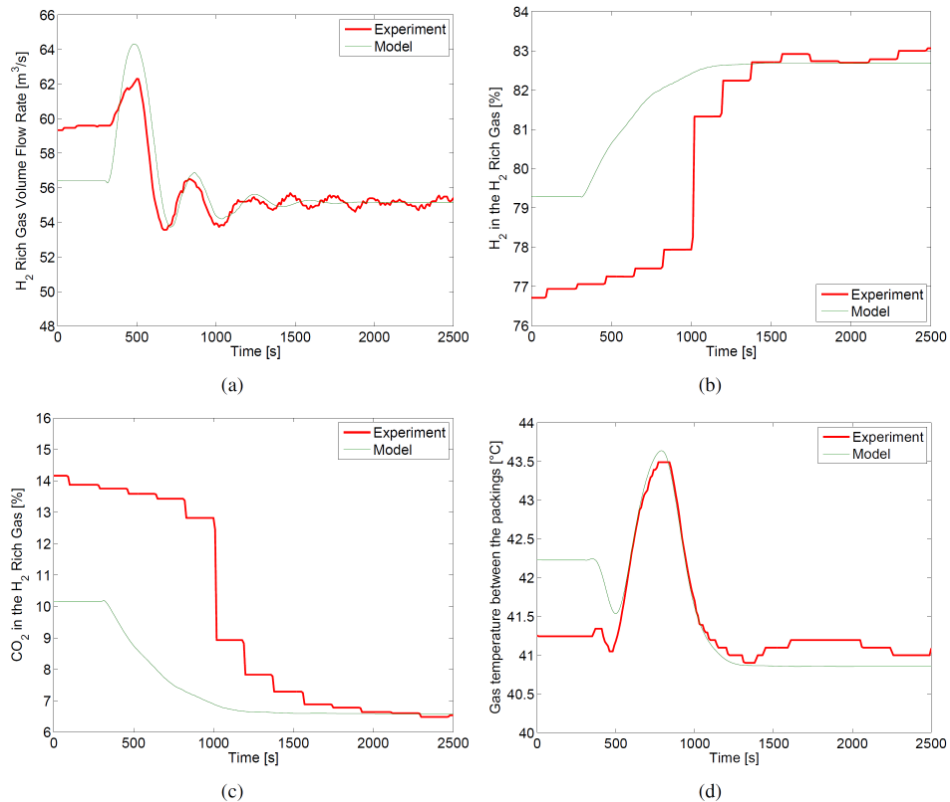
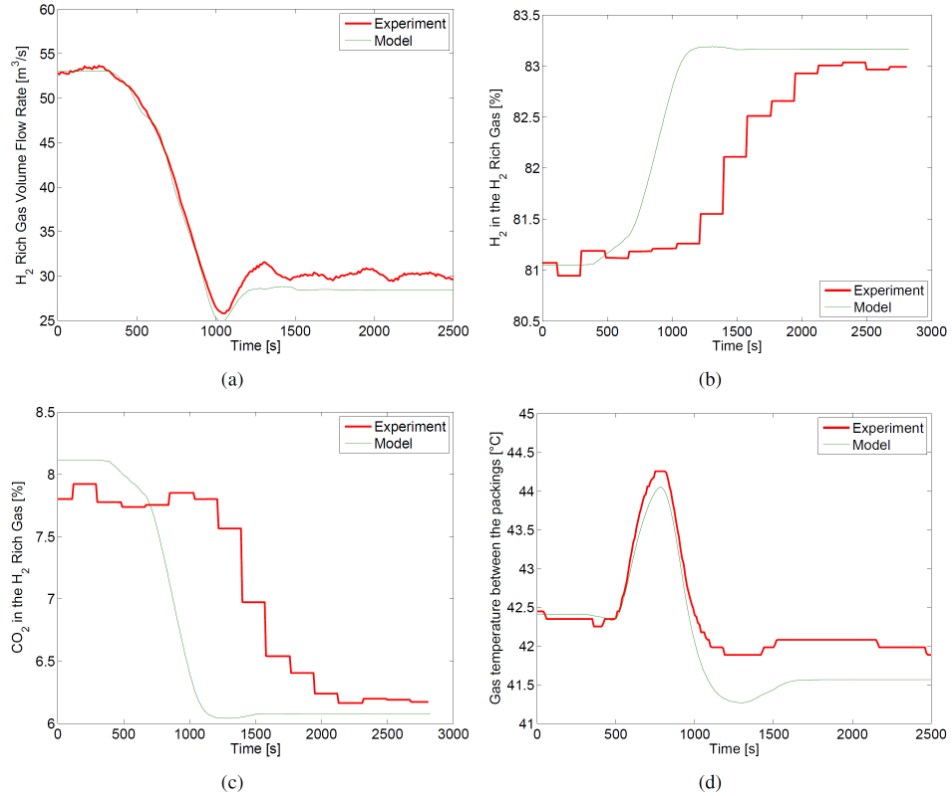**Figure 7-36:** Comparison of measurements and simulation results for TR-CIII-030. a) H_2 rich gas volumetric flow rate. b) H_2 content in H_2 rich gas flow. c) CO_2 content in H_2 rich gas flow. d) Gas temperature between packings.

8 Conclusion

In 2008, Nuon started the so-called CO_2 Catch-up project with the objective to demonstrate pre-combustion CO_2 capture at a pilot plant in Buggenum in order to verify the technology performance and to generate knowledge in the form of validated models and operational experience. It was aimed to apply this knowledge to optimise the design and operation of the full-scale CO_2 capture unit at the Magnum power plant, a multi-fuel Integrated Gasification Combined Cycle (IGCC) planned in Eemshaven, the Netherlands.

The CO_2 Catch-up project consists of 2 parts:
5. Engineering and construction of a pre-combustion capture pilot plant at the Buggenum IGCC (finished in 2011)
6. Operation and execution of the test and R&D programme (2011-2013)

The test programme is the collection of test runs performed at the pilot plant. The results of the test programme are input to the overarching R&D programme aiming to understand and improve the process by means of process modelling and laboratory experiments. The test and R&D programme has been managed by Vattenfall R&D Projects and performed together with Delft University of Technology and Energy research Centre of the Netherlands (ECN) and involves a number of scientists and PhD students. This report summarises the results of the pilot plant operation and test and R&D programme of the CO_2 Catch-up project.

Pilot plant design
The pilot plant is a simplified, smaller version of the CO_2 capture plant for the Magnum IGCC power plant designed by CB&I Lummus. It was designed to capture 1.4 t /h of CO_2 from 1.2 t/h of syngas (=0.8% of the syngas flow from the Buggenum gasifier). In the pilot plant steam carbon monoxide (CO) is catalytically converted into carbon dioxide (CO_2) and hydrogen (H_2), the so-called water-gas shift (WGS) reaction, after which CO_2 is separated from H_2 in the absorption-regeneration section. The WGS catalyst applied in the pilot plant is Haldor Topsøe's SK-201-2, a copper promoted iron/chromium based HTS catalyst. The (physical) solvent used to remove CO_2 is dimethyl-ether of poly-ethylene-glycol (DEPEG). DEPEG is commercially licensed by DOW under the trade name Selexol™ and by Clariant under the trade name Genosorb[R] 1753. In the pilot plant, only the latter solvent has been tested (as the difference between these solvents is marginal).

There are a number of essential differences between the pilot plant and the (future) large-scale capture plant. The most important difference is the heat integration in the

WGS section. In the pilot plant, water is evaporated/condensed by means of electrical heaters and forced-draft air coolers, respectively, instead of shell and tube feed-effluent heat exchangers as foreseen in the Magnum plant. In this way the temperature dependency of two streams (feed-effluent) is avoided and the precise control of the temperature becomes possible. This simplifies the operation, extends the operational flexibility and prevents process fluctuations that could influence the reliability of the test runs in the test programme. As a consequence specific energy consumption figures of the pilot plant are non-representative and incomparable with figures from literature for large-scale plants (and are therefore not discussed).

Pilot plant operation
The pilot plant has been operated from January 2011 to March 2013, with two major (initially unforeseen) interruptions during summer in which the IGCC was shut down for several months. Total operating hours are 5886 hours and the cumulative CO_2 captured is 4478 ton. After an initial period with 24/7 manned operation, it was decided to change the operating regime to fully automatic with manned supervision during the work-days only.

The pilot plant has been operated without major problems after some (relatively minor) hardware and control modifications, most of them being specific for the pilot plant design. The sampling conditioning system and analyzers have been the largest point of concern. Condensation in the sampling lines caused inaccurate composition measurements in the shift section. Fortunately, the dry gas composition measurements were reliable and these were used to evaluate the WGS performance. It also took some time to produce reliable results from the analyzers.

Some of the specified functionalities (measurement of wide range of water/steam content, analysis of rich solvent with high CO_2 loading and hence risk of flashing) proved to be too complex and not strictly necessary. These issues were unknown or underestimated by the supplier responsible for sampling conditioning and analyzer systems. A more detailed discussion between researchers and analyzer specialists at the start of the project may have avoided some of the problems. On the other hand, the test programme was not sufficiently mature yet in the engineering phase, which made it difficult to specify the exact requirements of the instrumentation in terms of functionality and accuracy.

Corrosion and material issues
In the pilot plant, corrosion probes were installed and wall thickness measurements were performed at several locations before, during and after operation. One of the main corrosion mechanisms that could occur is wet CO_2 corrosion. Most equipment, piping and tubing susceptible to wet CO_2 corrosion are made of stainless steel (SS304(L) or SS316(L)), which are completely resistant against CO_2 corrosion. DEPEG will protect the surface of piping and equipment and wet CO_2 corrosion will be strongly reduced. Therefore carbon steel with 3 mm corrosion allowance is selected

for wet DEPEG piping and equipment. If not a continuous DEPEG film is formed (e.g. for equipment top sections and top outlet piping or flashing conditions), stainless steel is applied. Generally it was observed that corrosion rates (for carbon steel as indicated by the corrosion probes) were below the expected values.

Traces of some unidentified substance (possibly DEPEG) deposited on CO_2 compressor pistons in the second stage downstream of the intercooler were found during maintenance activities. Attempts by the equipment supplier to identify and explain the cause of the problem were not successful. This issue needs to be investigated in more detail for the design of the full-scale plant.

HSE
During pilot plant operation, no incidents occurred (zero lost time incidents). The HSE risks identified relate mainly to the chemicals present in the plant. Throughout the plant no large volumes of flammable gas/liquid are present. Therefore the fire hazards within the pilot plant are low. To detect CO (toxic and flamable), CO_2 (asphyxiation) and H_2 (flammable) in an early state of release, detectors were installed at locations where the specific gas is the major component.
The solvent used to capture CO_2, Genosorb 1753 (or DEPEG) is a low-viscous, colourless to yellowish liquid. Genosorb 1753 has a high boiling point/low vapour pressure and therefore solvent losses to the environment via the treated gas are minimal. No spills occurred during operation.
The catalyst applied in the WGS section, SK-201-2, is a copper promoted iron/chromium catalyst. After the final plant shut down, the catalyst needs to be oxidized in a controlled manner to avoid that the catalyst will heat up during unloading (as the oxidation is an exothermic process). During oxidation, some amount of the Cr(III) present in the catalyst will be transferred into Cr(VI), which is recognized as a human carcinogen. This means that workers should wear proper protection gear in order to avoid getting in contact with the catalyst pellets and to inhale catalyst dust. The normal procedure prescribed by Haldor Topsøe is to purge the catalyst with steam until the temperature is 200-250°C, after which the airflow is gradually increased and controlled such that the catalyst temperature does not exceed 300°C. For operational reasons and the fact that catalyst sampling was planned, it was decided to perform the oxidation in nitrogen. Due to fact that the air flow could not be controlled carefully and the lower heat capacity of nitrogen, the catalyst at the centre of the bed has been exposed to temperatures (peaks) between 600 and 800°C.

Mass balances
Mass balances were calculated to check the quality of the raw measurement data from the plant and to see if these can be used for model validation. The overall mass balance as well as the mass balances for the individual plant sections close very well. For the overall mass balance the relative deviation between input and output is only 0.11%

at reference state (i.e. normal operating conditions close to original design point), which is significantly below the measurement accuracy of the individual measurement devices. Also for the sub-sections the mass balances close well (between 2 and 4%).

Pilot plant performance

The main performance parameters of the plant are the efficiencies for converting CO into CO_2 in the shift section and the CO_2 absorption efficiency in the absorption section as these determine the overall carbon capture efficiency of the plant.

Both Haldor Topsøe and CB&I Lummus calculations indicate a 92-93% overall CO conversion for the entire WGS section. Similar overall CO conversions are measured in the pilot plant. However, reactor 3 catalyst activity is insufficient i.e. not reaching equilibrium at the specified inlet temperature. In the pilot plant reactor 3 (and 2) indeed contribute less to the overall conversion efficiency in the pilot compared to the CB&I and Haldor Topsøe calculations. The poorer performance of reactor 3 is completely compensated by the much higher contribution of reactor 1 to the overall conversion due to a higher split flow of the syngas going towards reactor 1. In conclusion, the achieved CO conversion can be easily reached, especially if the unusual reactor 3 deactivation is avoided.

According to the heat and mass balances from CB&I Lummus, the absorption efficiency is 90.8%. The pilot plant average absorption efficiency is around 86% at the reference state. However, the results are incomparable as the design from CB&I Lummus was based on a Mellapak 350 Y structured packing at the bottom and a Mellapak 750 Y packing at the top whereas Raschig Super-Ring 0.6 and Raschig Super-Pak 250Y were tested in the pilot plant (which have a lower surface area).

The carbon capture efficiency (carbon in minus carbon out divided by carbon in) measured in the pilot plant is roughly 78%. As a check, the overall capture efficiency can be estimated by the product of the CO conversion efficiency and the CO_2 absorption efficiency. Using the CO conversion and CO_2 absorption efficiency mentioned above, the overall capture efficiency is approximately 80% (in reference state).

Pilot plant test programme

The test programme is subdivided into test campaigns covering a period in which a number of test runs are performed.

- TC-I: trial period to understand the operating window and limits of the pilot plan and to define reference state. No analyzers available (Jan 2011 – April 2011)
- TC-II: execution of main parametric tests of shift section and absorption section with random packing in absorber (September 2011 – April 2012, September 2012 - November 2012)

- TC-III: repetition of several parametric tests with structured packing in absorber (November 2012 – February 2013)

Parametric tests syngas conditioning and water-gas shift section

Several parametric tests were performed to evaluate the impact on the catalyst performance. The axial temperature profiles in the WGS reactors give a good indication whether and at which coordinate equilibrium is reached and how it moves in time and upon changes in process conditions. An optimal operation of the shift reactors could be achieved by adapting the reactor inlet temperatures such that equilibrium is just reached at the end of the catalyst bed. The first test run indicated that the inlet temperature of reactor 1 could be lowered to 315°C. For reactor 2 the reaction front at reference condition is well within the catalyst bed and hence the inlet temperature of reactor 2 can also be decreased. For reactor 3 the inlet temperature had to be increased to at least 355°C to boost the reaction rate and reach equilibrium.

In addition, a dynamic test has been performed with the purpose to study the dynamic behaviour of the 3rd reactor during a rapid variation in the inlet temperature. Starting at steady-state operation, a rapid temperature drop resulted in the expected inverse temperature response at the reactor outlet. The subsequent rapid temperature increase resulted in a dynamic response corresponding with a reactor start-up.

Changing the syngas composition to mimic gasifier part-load operation or biomass co-firing hardly influences the CO conversion and adiabatic temperature rise.

The variation of the syngas mass flow results in changes of the pressure losses along the process. For the reactors a clear almost linear relation between pressure loss and mass flow is observed whereby increasing mass flow leads to higher pressure loss. This was not apparent for other components in the syngas conditioning and water-gas shift section.

Catalyst stability and selectivity

Analysing the reference state operation throughout the entire operational period for the WGS reactors by means of modelling of the axial temperature profile yielded insights into the rate of decay of the catalyst activity. Initial rapid deactivation during the first 500 hr operation is observed for reactor 1 and reactor 2. Subsequently, the reactor 1 catalyst activity decreases at a much slower rate than expected. The reactor 2 catalyst first restores its activity after which a decrease in activity is observed at a slower rate compared to reactor 1. The reactor 3 catalyst has a much lower activity than anticipated. Repeated chemical analysis of reactor 3 catalyst samples hinted towards catalyst damage due to an over reduction as being the probable cause for the observed lower activity. This over reduction might result from steam condensation upstream of the reactor during start-up (large heat losses in between reactor 2 and 3 were observed in the commissioning phase), exposing the catalyst to hot dry syngas.

The high and stable activity directly following the rapid initial catalyst deactivation allows reduction of the reactor feed temperatures and lowering of the pilot steam consumption. For reactor 1 the lower overall temperature and lower steam content likely results in a more stable operation, prolonging catalyst lifetime. For reactor 2 the lower overall temperature is similarly beneficial and a prolonged catalyst lifetime is also expected for reactor 2. On the contrary, the increased pressure foreseen for the Magnum plant most likely leads to an increase in deactivation rate, which is not compensated by an increased pellet activity. Unfortunately, these effects cannot be quantified.

For FeCr-based catalysts, the catalyst CH_4 production is an indication of the catalyst selectivity. During the entire operating period, the CH_4 production by the catalyst is low (<50 ppm) and stable in time.

Catalyst coking (and the potential for reduced steam consumption)

This test run aimed to study the effect of reduced steam content on the catalyst resistance to iron carbide formation. Operation at a reduced steam/CO ratio would allow reducing the steam requirement for the WGS section and thus the CO_2 capture penalty, but can lead to reduction of the magnetite phase, Fe_3O_4, to FeC, which is active in hydrocarbon formation, noticeably CH_4. This so-called carbiding of the catalyst is reversible if the extent of carbide formation is not too severe. Severe carbiding can lead to permanent loss of catalyst activity and/or selectivity and even to physical damage of the catalyst pellets.

Compared to reference state operation at steam/CO=3.1 mol/mol (for reactor 2), operation at reduced ratios of 2.6 down to 1.5 leads to step-wise increases in the catalyst CH_4 formation while no continuous increase or light-off of the CH_4 content is observed. This indicates that at the conditions tested the catalyst does not display progressive carbiding. Other indications that excessive catalyst carbiding did not occur are i) the lower steam/CO testing does not appear to have influenced catalyst activity, ii) the absence of C_2+C_3 hydrocarbons in the reactor 2 effluent and iii) the uncompromised reactor 2 pellet strength measured after the entire campaign. It is concluded that the catalyst, which had more than 5000 h of operation, is stable at the reduced steam/CO ratios tested. Note that each set point representing a lower steam/CO ratio was performed for 10 up to 116 hours. The effect of prolonged operation at reduced steam content on the catalyst performance remains uncertain. Therefore, on-line monitoring of the CH_4 content is crucial: at the moment an exponential increase of the CH_4 content is observed, the steam content should be increased to stabilize the CH_4 content. As the CH_4 content of the entering syngas has the same order of magnitude as the CH_4 production by the catalyst at reduced steam/CO ratio operation, an accurate indirect measurement of catalyst carbiding is possible in entrained flow gasifier systems. Using this characteristic, the steam content

of the quench flow can be controlled by means of the measured CH_4 content in the reactor 2 effluent over the catalyst lifetime.

A trial and error procedure, in which the "carbiding turning point" for the first catalyst batch in the large-scale plant is used to anticipate carbiding in the next catalyst batch needs to be developed. Applying such procedure allows building up a strategy for the required steam content throughout the catalyst lifetime, such that the catalyst is always operated outside the carbiding regime. Note that increasing the operational pressure from 20 bar for the Buggenum pilot to 40 bar as the Magnum design will result in an increased tendency for catalyst carbiding. It is estimated that the steam/CO ratio for safe operation would increase by about 8% relative.

A reduction in reactor 2 steam content can lead to a significant energy saving at the expense of a slightly lower CO conversion. Lowering the reactor 2 steam/CO ratio from reference state conditions to 2.06 mol/mol results in a decrease of the overall conversion by 3.6%-points, while the overall steam/CO ratio decreases by 26%. This means that a small decrease in CO_2 capture ratio saves a significant amount of steam, thereby decreasing the efficiency penalty for CO_2 capture. For the most aggressive set point, the steam feed decreases by 35% resulting in a 9.2%-points drop in CO conversion. These results suggest that the increase in CO slip per amount of steam saved becomes larger at lower steam contents. Note that besides reactor 2, reactor 1 can also be operated at a reduced steam content of the feed. These aspects need to be investigated in an optimisation study for the full-scale plant.

Although the exact impact on the efficiency penalty has not yet been quantified, a breakdown of the efficiency penalty gives a first impression. The overall efficiency penalty when applying CO_2 capture at an IGCC using a Shell gasifier has been quantified at circa 9-10% absolute for a CO_2 capture rate of 85-90% (IEA GHG, 2003, NETL, 2007). The optimisation performed by CB&I Lummus decreased this number, although the numbers cannot be compared as the calculations from CB&I Lummus assumed a lower CO_2 capture efficiency (81%) and because co-firing of natural gas was assumed (thereby decreasing the amount of CO_2 avoided) to maximise the gas turbine output and minimise part-load effect due to the lower LHV of the syngas when applying CO_2 capture. The majority of the efficiency penalty is caused by the WGS. Considering the breakdown from the simulations performed by CB&I Lummus for Magnum, roughly 20% of the power loss is due to the steam consumption in the WGS.

Parametric tests CO_2 absorption section
Several parametric tests were performed to evaluate the impact on the CO_2 absorption efficiency, validate the mass transfer coefficients and the thermodynamic model developed for the solvent and the gas components. Most parametric tests were performed for both random packing Raschig Super-Ring 0.6 and structured pack-

ing Raschig Super-Pak 250Y, which enables a comparison between those packings.

All trends observed in the parametric tests are in line with expectations. The CO_2 absorption efficiency is slightly decreasing (0.6% absolute) with increasing water content from 1 to 4 wt%. The CO_2 absorption efficiency is increasing with decreasing solvent and shifted syngas temperature and with increasing absorber pressure, due to the higher partial pressure in the gas phase. Decreasing shifted syngas mass flow at constant solvent mass flow significantly increases the CO_2 absorption efficiency. Results also indicate that Raschig Super-Ring 0.6 has a better performance than Raschig Super-Pak 250Y. Decreasing solvent mass flow (while keeping shifted syngas mass flow constant) has the reverse effect. In addition, tests were done with extremely high solvent mass flows (240 $m^3/m^2/h$) as anticipated in the CB&I Lummus design for the full-scale capture plant. No experiments have been performed at such hydraulic conditions for structured packings. The main objective is to test the column hydraulics and the separation efficiency under these conditions. The test run showed a clear and expected relation between the solvent flow rate pressure drop and that flooding of the column can be identified based on the measured pressure drop for Raschig Super-Ring 0.6. For Raschig Super-Pak 250Y, the pressure drops show a much smoother behaviour and no sign of flooding of the packing or the distributor can be identified. Towards higher solvent flow rates, the CO_2 concentration at the absorber outlet levels out, indicating that the process becomes limited by mass transfer and no more CO_2 can be absorbed at these conditions.

Finally, the pressure of the 1st flash vessel was varied. The CO_2 concentration in the gas outlet is reduced significantly with increasing flash pressure, as less CO_2 is evaporated from the DEPEG solution. As a result, the H_2 concentration in the gas outlet increases. The pressure in the 1st flash vessel does not influence the overall CO_2 absorption efficiency of the plant as this is determined by the pressure in the 3rd flash vessel.

After the test programme was finished, a sample of fresh and spent solvent was taken for analysis by Clariant. The analysis indicates that the spent solvent is still in good conditions, which is confirmed by the fact that the solvent performance was not deteriorating in time and the solvent physical appearance did not change in time.

Process modelling

For a better understanding of the CO_2 capture process and explanation of observed performance a series of process models (described below) have been developed. By validating the pilot plant models against real operational data, more reliable and accurate models applicable to the large-scale capture plant can be obtained. For this purpose, the pilot plant models are to be extended and extrapolated to the full-scale operational range based on theoretical scale-up rules and physical insights. The developed process models serve multiple objectives:

- Verify overall pilot plant performance

- Evaluate the performance of a specific technology component (e.g. assess catalyst activity, mass transfer coefficients in the absorber, etc.)

- Identify measurement errors in the data obtained from the pilot plant

- Simulate different operation scenarios in order to perform energy optimisation with respect to input process variables.

- Evaluate the dynamic response of the system in order to improve the controllability and modifying/improving the control system.

- Develop methods for (automated) process and control optimisation

WGS reactor model
The WGS reactor model is a heterogeneous adiabatic plug-flow reactor using intrinsic reaction kinetics in the form of a power-law rate equation. Using 2 parameters, being the catalyst activity factor and the length of the dead zone, the axial temperature profiles for all variations are accurately predicted. The model has been validated successfully. Up-scaling the model for Magnum implies adjusting the geometrical parameters of the reactors, while no other parameters need adjustment.

Steady-state model of the WGS section
A simulation model for the syngas conditioning and WGS section has been developed in Aspen Plus V7.3 and validated against 20 experimental data sets obtained from the pilot test programme. The quantitative model validation has been carried out as simultaneous data reconciliation and parameter estimation using the contaminated Normal distribution in order to decrease the influence of gross errors affecting the measurements. The model predictions for mass flows, temperatures and compositions show good agreement with the measured values and 90% of the reconciled estimates are within $\pm 3.34\sigma$ (gross error cut point). It can be concluded that the steady-state model of the shifting section is capable of predicting the pilot plant performance throughout the entire operational range, and it can be used for the development of a large-scale model of the capture unit.

Steady-state model of the CO_2 absorption section
A simulation model for the absorption and regeneration section has been developed in Aspen Plus V7.3. The model was validated on seven sets of experimental data during which the shifted syngas and solvent flow rate were changed. The model parameters were multiplied constants (C_L and C_V) of the Billet and Schultes mass transfer coefficient correlation. The optimized values of the parameters for random packing Raschig Super-Ring 0.6 are $C_L = 0.1471$ and $C_V = 0.1085$. The absorber outlet molar fractions are on average fitted with an error of 0.72% absolute. The optimized values of the

parameters by using objective for structured packing Raschig Super-Pak 250 function f_2 are $C_L = 0.1179$ and $C_V = 0.06242$. The absorber outlet molar fractions are on average fitted with an error of 0.86% absolute. The CO_2 absorption efficiency is predicted with a standard deviation of 0.016 for both packings. The accuracy of the concentration measurements is sufficient in order to get reliable C_L value. The C_V value is much more sensitive to a change in the concentrations used for parameter estimation and is therefore not so reliable.

The optimization results show that the parameter C_L is about 25% higher for Raschig Super-Ring 0.6 than for Raschig Super-Pak 250. As the resistance against the mass transfer is concentrated in the liquid phase, Raschig Super-Ring 0.6 seems to be a more suitable packing for the physical absorption of CO_2 for the specific hydraulic conditions tested in the pilot plant.

However, the fitted values for C_L and C_V are approximately a factor 10 lower than the default values used in Aspen/Winsorp (Raschig's simulation tool). In other words, the pilot plant performance is below expectations. One explanation can be the occurrence of foaming in the absorber. A second possibility can be gas back-mixing as the gas velocity is very low and liquid can entrain the gas. As no clear evidence for either of these hypotheses is present, it may be recommended for the design of the large-scale plant to apply a higher gas velocity to avoid the risk of back-mixing and add some anti-foam to ensure that the mass transfer is optimal. Because the structured packing is more sensitive to foaming, the expected performance increase by adding anti-foam is higher for the structured packing. The mass transfer performance should improve similarly for both packings by increasing the gas velocity because the back-mixing is packing independent. Assuming approximately two times higher gas velocity for the large-scale plant design versus the pilot plant, the hydraulic limit (loading point) of the random packing Raschig Super-Ring 0.6 is reached. Hence it is recommended to use structured packing Raschig Super-Pak 250 for the large-scale plant.

The trends in CO_2 absorption efficiencies with the change of the process variables (mass flows, concentrations, temperatures, pressures) are predicted correctly by the model. The CO_2 absorption efficiency is slightly underestimated (in reference state) which results in a safe prediction for up-scaling. For the full-scale plant, the process conditions may be outside the validated range e.g. absorber pressure up to 40 bar and solvent temperatures down to 10°C. The CO_2 absorption efficiency at higher pressure is overestimated which can be resolved by refitting the VLE data for the right pressure range. The CO_2 absorption efficiency at lower temperature is slightly under predicted by the model. In conclusion, the full-scale capture plant performance can be predicted within similar accuracy as for the pilot plant (CO_2 absorption efficiency ± 1.6% absolute).

Dynamic model of the WGS section

A dynamic model has been developed following an object-oriented, lumped parameter modelling approach using the Modelica language to study transient behaviour. The subsystem models and the entire system model are validated by comparison with experimental data obtained from various open-loop and closed-loop transient tests performed on the pilot plant. The validated models provide a reliable basis for the development of large-scale system models of the pre-combustion capture process which can be used to design control strategies. This requires the assembly of the respective process and the adaptation of the available component models according to the commercial-scale equipment sizing. With the pilot plant system model it has been demonstrated that such a large-scale model can be used to investigate the load-following potential of the capture unit with respect to the power producing process. The models allow to easily determine the system time constants, responses of the integrated streams and any process limitations.

Dynamic model of the CO_2 absorption section

An equilibrium-based dynamic absorber model using the Modelica language is validated by comparison with experimental data obtained from two open-loop transient tests in which the shifted syngas and solvent mass flow are perturbed. Satisfactory agreement between the experimental data and model predictions considering absorber pressure and temperature and H_2-rich gas flow rate is achieved. The adopted holdup correlation can be used for predictions of the dynamic performance of the pilot plant absorber column. Hence, the validated model provides a reliable basis for the analysis of the transient performance of a large-scale absorber.

Value of the R&D and application of the results

With the exception of the combustion of H_2-rich gas in state-of-the-art gas turbines, the components of pre-combustion capture are in fact proven on an industrial-scale, which is also indicated by the ZEP technology matrix (http://www.zeroemissionsplatform.eu/). As is indicated in the ZEP studies, integration of already proven blocks is essentially the main challenge for IGCC and pre-combustion capture. The initial study performed by CB&I Lummus was a first attempt to develop an optimally integrated design for the Magnum IGCC using state-of-the-art capture technology. The specific objectives (and therefore conventions and assumptions in design and operation) of WGS and CO_2 absorption technologies in the chemical industry are slightly different in comparison to power generation. In most chemical plants, for instance, the objective is to maximise the H_2 production regardless of the steam production, as H_2 is a valuable commodity (e.g. in refinery or as feedstock for ammonia). This results in a design where the catalyst is operated at relatively high steam/CO ratios. These conventions and assumptions for use in the chemical industry have been challenged in discussion with the vendors and new ideas verified in the pilot plant test programme. The results of the test programme clearly show that there is still improvement potential in conventional WGS and absorption technologies, and

for some components even larger than anticipated by CB&I Lummus. Although several improvements have been suggested throughout this report, the implications are not yet quantified in detail for the large-scale capture plant. A study to calculate the impact of the improvements in the WGS section for the full-scale plant (in terms of overall plant efficiency and specific energy consumption per ton of capture CO_2) is ongoing together with Delft University of Technology. Next, more detailed economic evaluations are needed to assess the trade-off between CAPEX and OPEX. This is one of the tasks in the feasibility study for a future large-scale IGCC. It must be realised that by that time, the assumptions that determined the design of the Magnum IGCC (choice of gasifier etc.) may be outdated. The impact of some of the changes (e.g. higher gasifier pressure, different feedstock and hence syngas composition) could be predicted using the process models. More fundamental design changes would make part of the results obsolete though. For example, if CAPEX constraints/considerations drive towards a wet quench design, a sweet shift concept is not applicable. It may also happen that the 2nd generation technologies may have been tested in demonstration plants and are commercially available. The work in this project represents the current state-of-the-art to which the new developments can be benchmarked. In addition, there may be opportunities to apply some lessons learned and insights to a wider spectrum of technologies.

In summary, the project objectives to verify the technology performance and to generate knowledge in the form of validated models and operational experience are clearly achieved. However, the knowledge generated in the CO_2 Catch-up project will not be applied directly, as the investment decision for the gasification and CO_2 capture unit in the Magnum project has been postponed beyond 2020, after it was decided earlier to separate the development and realisation of the power plant in two phases. Phase 1 comprises the construction of three 400 MW_e M701F4 combined cycle units operated on natural gas. At the moment of writing the report, the three combined cycle units are in operation. Phase 2 comprises the coal gasification based system with integrated CO_2 capture, transport and storage (CCS) to provide a synthetic gas as fuel for one of the combined cycle units, including the replacement of the dry low NO_x burners for natural gas combustion installed in Phase 1 by diffusion burners to enable the combustion of (hydrogen-rich) syngas.

The commercial outlook for phase 2 and IGCC+CCS in general remains uncertain. According to the Global CCS Institute, a total of 34 large-scale integrated CCS projects using the pre-combustion technology are known at the time of writing this report. Of these 34 projects, 11 are power generation projects (IGCC), the rest being natural gas processing, fertiliser, SNG, hydrogen and Fischer-Tropsch liquids production. The only project under construction is the Kemper country IGCC. The other projects in the USA also aim to sell their CO_2 for EOR (which may increase the chance of realisation). The European projects are all in the UK and with the announced preferred bidders for the UK's £1bn Carbon Capture and Storage Commercialisation Pro-

gramme Competition (Peterhead Project in Aberdeenshire, Scotland, and the White Rose Project in Yorkshire), the future of the IGCC projects is rather uncertain. Apart from GreenGen, the Chinese projects are in the feasibility phase.

The main concern for IGCC plants remain the relatively high costs (both in terms of CAPEX and OPEX). The results of the CO_2 Catch-up project, basically promising an optimised design for the WGS and CO_2 absorption unit with reduced specific energy consumption (and hence OPEX) and possibly CAPEX, are not expected to change much to this problem. Although the CO_2 avoidance costs can be reduced, they are still far higher than the current ETS price.

Although direct application in the Magnum plant is not foreseen on the short term, the gasification projects under development in other parts of the world as well as new future projects may benefit from the achievements made in this project. Knowledge dissemination is aimed for by means of (scientific) publications of the researchers involved in the project. Papers in peer-reviewed journals are currently being prepared on the steady-state and dynamic pilot plant modelling work, as well as the results of the WGS reactor modelling and low steam/CO ratio test run. As the suppliers of catalyst, solvent and packing all have been heavily involved in the project to learn on the outcome of the test programme, hopefully the generated insights will be followed up and potentially discussed/offered in any new IGCC + CCS project. Finally, several seminars have been organised with Elcogas and J-Power, which operate(d) similar pre-combustion capture pilot plants, to exchange results.

9   Literature

Aspen Plus Help	Aspen Plus V7.1, 2010. Aspen Technology Inc., Burlington, MA, USA.
Billet and Schultes, 1993	Predicting Mass Transfer in Packed Columns. Chem. Eng. Technol. 1993, 16, 1.
Carbo et al., 2009	Staged water-gas shift configuration: Key to efficiency penalty reduction during pre-combustion decarbonisation in IGCC. Energy Procedia, 2009, 661-668.
Casella and Colonna, 2012	Dynamic modelling of IGCC power plants. Applied Thermal Engineering 2012, 35, 91–111.
Casella and Leva, 2006	Modelling of Thermo-Hydraulic Power Generation Processes Using Modelica. Math. Comput. Model. Dyn. Syst. 2006, 12(1), 19–33.
CB&I Lummus 2008a	Process description for the CO_2 Catch-up pilot plant
CB&I Lummus 2008b	Material selection report CO_2 Catch-up pilot plant
CB&I Lummus 2008c	HSE philosophy for the CO_2 Catch-up pilot plant
Colonna et al., 2004	FluidProp: a program for the estimation of thermophysical properties of fluids. Version 2.4. software, 2004-2012; http://www.FluidProp.com,
van Dijk and Boon, 2011	Dynamic WGS reactor modelling: Preliminary dynamic simulations of the Buggenum pilot WGS reactors, ECN report ECN-X--11-017, January 2011
van Dijk and Booneveld, 2011	WGS intrinsic kinetics for the Haldor Topsøe SK-201-2 catalyst, ECN-X--11-086, October 2011
van Dijk et al., 2011	WGS catalyst screening, ECN-X--11-024
van Dijk, 2012a	WGS reactor model validation. Doc. No. CO2 2012/0074
van Dijk, 2012b	Test run report TR-CII-017- Low steam/CO ratio operation (Doc. No. CO2 2012/0042)
van Dijk, 2012c	Test run report TR-CII-016- Catalyst stability and selectivity (Doc. No. CO2 2012/0043)
van Dijk, 2012d	Test run report TR-CII-007: 3rd Shift reactor inlet temperature (Doc. No. CO2 2012/0037)

Faber, 2012a	Dynamic modelling master plan (Doc. No. CO2 2012/0029)
Faber, 2012b	Re-evaluation of the mass balance of the CO2 Catch-up pilot plant (Doc. No. CO2 2012/0040)
Faber, 2012c	Test run report TR-CIII-031: High solvent flow rate (Doc. No. CO2 2013/0010)
Fritzson, 2003	Principles of Object-Oriented Modelling and Simulation with Modelica 2.1; Wiley 2003
Gross and Sadowski, 2001	Perturbed-Chain SAFT: An Equation of State Based on a Perturbation Theory for Chain Molecules. Ind. Eng. Chem. Res. 2001, 40, 1244–1260.
Hernandez, 2011	WGS Reactor Model of the NUON CO2 Catch-up Pilot Plant (Doc. No. CO2 2011/0060).
Huber, 1981	Robust Statistics, John Wiley & Sons, New York.
IEA GHG, 2003	Potential for improvement in gasification combined cycle power generation with CO_2 capture, PH4/19
Kaptein, 2010	Modelling Master plan (Doc. No. CO2 2010/0003)
Kaptein, 2011	Evaluation of the mass balance of the CO2 Catch-up pilot plant (Doc. No. CO2 2011/0042)
Kaptein, 2012	Test run report TR-CII-006: Verify axial and radial reactor temperatures with nitrogen (Doc. No. CO2 2012/0005)
Rejl et al., 2010	"Profile Method" for the measurement of kLa and kVa in distillation columns. Validation of rate-based distillation models using concentration profiles measured along the column. Ind. Eng. Chem. Res. 2010, 49, 4383.
De Servi, 2013a	On the modelling of the thermodynamic properties of the GENOSORB 1753 solvent with the PC-SAFT equation of state (Doc. No. CO2 2013/0018).
De Servi and Trapp, 2013b	Development and validation of a dynamic absorption column model (Doc. No. CO2 2013/0025)
Sundyne, 2010	04298-0600-C01-SD0009_PERFORMANCE_CURVES-DATA
Tjoa and Biegler, 1991	Simultaneous strategy for data reconciliation and gross error detection of nonlinear systems. Computers and Chemical Engineering 15, 679–690.

Trapp, 2011	Model development steps (project document)
Trapp, 2013a	Development and validation of steady-state CO2 Catch-up pilot plant model (Doc. No. CO2 2013/0004)
Trapp, 2013b	Development and validation of dynamic models of the shifting section of the CO2 Catch-up pilot plant model (Doc. No. CO2 2013/0024)
Valenz, 2012a	Test run report TR-CII-009: Water mass flow absorption section (Doc. No. CO2 2012/0055)
Valenz, 2012b	Test run report TR-CII-010: Solvent heater power input (Doc. No. CO2 2012/0056)
Valenz, 2012c	Test run report TR-CII-011: Solvent mass flow (Doc. No. CO2 2012/0052)
Valenz, 2012d	Test run report TR-CII-012: Shifted syngas mass flow (Doc. No. CO2 2012/0039)
Valenz, 2012e	Test run report TR-CII-014: Absorber pressure (Doc. No. CO2 2012/0053)
Valenz, 2012f	Test run report TR-CII-015: 1st flash vessel pressure (Doc. No. CO2 2012/0054)
Valenz, 2013a	Test run report TR-CIII-011: Solvent mass flow (Doc. No. CO2 2013/0005)
Valenz, 2013b	Test run report TR-CIII-011 repetition: Solvent mass flow (Doc. No. CO2 2013/00xx)
Valenz, 2013c	Test run report TR-CIII-012: Shifted syngas mass flow (Doc. No. CO2 2013/0006)
Valenz, 2013d	Test run report TR-CII-013: Solvent temperature (Doc. No. CO2 2013/0015)
Valenz, 2013e	Test run report TR-CIII-013: Solvent temperature (Doc. No. CO2 2013/0016)
Valenz, 2013f	Test run report TR-CIII-014: Absorber pressure (Doc. No. CO2 2013/007)
Valenz, 2013g	Aspen Plus model of the CO2 capture pilot plant absorption and regeneration section (Doc. No. CO2 2013/0011)

10 Abbreviations

ATE	approach to equilibrium
CAPEX	Capital expenditures
DAE	Differential and algebraic equations
DCS	Distributed control system
DEPEG	Dimethyl ethers of polyethylene glycol
DRPE	Data reconciliation and parameters estimation
ECN	Energy research Centre of the Netherlands
EOR	End of run
EPC	Engineering, procurement and construction
EoS	Equation of state
HP	High pressure
HRSG	Heat recovery steam generator
HTS	High temperature shift
IGCC	Integrated Gasification Combined Cycle
IP	Intermediate pressure
KKS	Kraftwerk-Kennzeichen System
L/G (ratio)	Liquid to gas ratio
LP	Low pressure
LHV	Lower heating value
LTS	Low temperature shift
MP	Medium pressure
O&M	Operation and maintenance
ODE	Ordinary differential equations
OPEX	Operating expenditures
PC-SAFT	Perturbed-Chain Statistical Associating Fluid Theory
PGIM	Power Generation Information Manager
ppm	Parts per million
RSD	Relative standard deviation
RSP	Raschig Super-Pak
RSR	Raschig Super-Rings
SOR	Start of run
SP	Set point
t.o.s.	time on stream
TR(-C-)	Test run - (campaign)
XRD	X-ray diffraction
VLE	vapour liquid equilibrium
WAC	Willem Alexander Centrale (Buggenum IGCC)
WGS	Water-gas shift
WLS	Weighted-Least-Squares

11 Appendices

A.1   Overview test runs

Test run	Date	Scope/purpose	Tested parameter / manipulated process variable	Range
Syngas conditioning and water-gas shift section – steady state				
TR-CII-001: Shift reactors inlet temperatures	07.12.2011 - 09.12.2011	Study the effect of inlet temperatures on the shift reactor performance	Inlet temperatures: Reactor 1 (ELF50 CT002) Reactor 2 (ELG20 CT003) Reactor 3 (ELG30 CT003)	325°C – 360°C 340°C – 360°C 340°C – 360°C
TR-CII-002: Syngas composition	13./14.12.2011 - 09.04.2012	Study the effect of inlet composition on the shift reactor performance	Syngas composition (ELF50 CQ201A)	CO [%]: 55.05 – 59.27 H_2 [%]: 27.05 – 31.88 CO_2 [%]: 1.71 – 6.24 N_2 [%]: 6.68 – 9.16
TR-CII-003: Syngas mass flow	15.12.2011 20./21.03.2012 01./02.10.2012	Investigation of part-load performance of the plant	Syngas mass flow (ELF20 CF001)	602 kg/h – 1241 kg/h

TR-CII-004: Steam to carbon ratio	20./21.12.2011 27./28.03.2012 02./03.04.2012 25.04.2012	Study the effect of the H_2O/CO ratio on the shift reactor performance	Temperature quench gas (ELF30 CT002) Resulting H_2O/syngas (ELG40 CX001)	151.2°C – 172°C 1.13 – 1.31 kg/kg
TR-CII-005: Part load operation (not successful – not enough steady-state data)	22.03.2012	Simulate gasifier part load operation	Syngas mass flow (ELF20 CF001)	800 kg/h
TR-CII-032: Minimal Energy Consumption	25.26.10.2012 29.10.2012	Operation at low water to syngas ratio corresponding to a state of minimal energy consumption including reduction of reactor 1 and 2 inlet T and increase reactor 3 inlet T.	H_2O/syngas (ELG40 CX001) ELF50 CT002 ELG20 CT003 ELG30 CT003	1.2 and 0.86 kg/kg 310.5°C (ref. 335.2°C) 309.8°C (ref. 334.3°C) 379.8°C (ref. 333.9°C)

Syngas conditioning and water-gas shift section – dynamic				
TR-CII-020: Dynamics ELF20 AC010	22./23.03.2012	Study the transients of the heater outlet temperature as a response to manual, instantaneous changes in the heater duty (open-loop) and as response to automatic controller actions (closed-loop).	Tout (ELF20 CT003) Duty (ELF20 AC010/OV)	T decrease with control: 174°C → 164°C Duty step up and down 54% → 72% → 54%
TR-CII-21: Dynamics ELF40 AC010	16./17.04.2012	Study the transients of the reboiler outlet temperature as a response to a manual, instantaneous change in the reboiler duty (open-loop).	Duty (ELF40 AC010/OV) Tout (ELF40 CT002)	Duty step down and up 58% → 42% → 58% Resulting temperature 199°C → 194°C → 199°C
TR-CII-022: Dynamics ELF50 AC010	12.09.2012	Study the transients of the superheater outlet temperature as a response to manual, instantaneous changes in the heater duty (open-loop) and as response to automatic controller actions (closed-loop).	Tout (ELF50 CT002) Duty (ELF50 AC010/OV)	T increase with control: 340°C → 350°C Duty step down and up: 76% → 71.7% → 76%

TR-CII-023: Dynamics ELG30 AC010	12.09.2012	Study the transients of the cooler outlet temperature as a response to manual, instantaneous changes in the cooler fan speed (open-loop) and as response to automatic controller actions (closed-loop).	Tout (ELG30 CT003) Fan speed (ELG30 AC010/OV)	T increase with control: 340°C → 350°C Fan speed step down and up: 13.8% → 10.7% → 13.8%
TR-CII-024: Dynamics ELG40 AC010	14.03.2012	Study the transients of the cooler outlet temperature as a response to manual, instantaneous changes in the cooler fan speed (open-loop) and as response to automatic controller actions (closed-loop).	Tout (ELG40 CT006) Fan speed (ELG40 AC010/OV)	T decrease with control: 134°C → 124°C Fan speed step down and up: 44.5% → 32.5% → 44.5%
TR-CII-025: Dynamics ELG50 AC010	19.03.2012	Study the transients of the condenser outlet temperature as a response to manual, instantaneous changes in the cooling water mass flow (open-loop) and as response to automatic controller actions (closed-loop).	Tout (ELG50 CT002) Valve opening (PGE10 AA351)	T decrease with control: 37°C → 27°C Valve opening step down and up: 16.5% → 6.1% → 16.5%

TR-CII-026: Dynamics conditioning section due to variation in syngas mass flow	17./18.04.2012	Study the transients of mass flows and drum levels within the conditioning section as a response to manual, instantaneous changes in ELF50 AA050 valve opening (partial open-loop).	Resulting syngas flow (ELF20 CF001) Valve position (ELF50 AA050)	Syngas flow decrease with control 1100kg/h → 1050kg/h Valve opening step down and up: 16% → 19% → 16%
TR-CII-027: Dynamics conditioning section due to variation in reaction water mass flow	13.09.2012	Study the transients of mass flows and drum levels within the conditioning section as a response to manual, instantaneous changes in reboiler duty (partial open-loop).	Resulting water flow (ELG40 CF001) Reboiler duty (ELF40 AC010/OV)	Water flow increase with control 1200kg/h → 1320kg/h Duty step down and up 46% → 37.5% → 46%

TR-CII-028: Dynamics conditioning and shifting section due to load variation	03.10.2012 15.10.2012	Study the transients of mass flows, drum levels, pressures and temperatures as a response to manual, instantaneous changes in ELF50 AA050 valve opening (partial open-loop) at part and full load of the pilot plant.	Resulting syngas flow (ELF20 CF001) Valve opening (ELF50 AA010)	Syngas flow decrease with control 1100kg/h → 1000kg/h→ 930kg/h Valve opening step up and down: 14.7 → 26.7 → 14.7 7.5 → 1.0 → 7.5 → 14.7
TR-CII-033: Dynamics shifting section due to syngas composition variation	03.12.2012	Study the transients of mass flows, drum levels, temperatures and compositions as a response to manual, instantaneous changes in H_2 recycle valve opening (partial open-loop).	Valve opening (ELH80 AA020) H2 recycle (ELH80 CF002)	Valve opening step up and down 0% → 100% → 0% Resulting H_2 recycle flow 0 kg/h →~35kg/h → 0kg/h
TR-CII-034: Dynamics ramping syngas mass flow	23./24.11.2012	Study the transients of mass flows and temperatures as a response to the ramping of the syngas mass flow with automatic controller actions (closed-loop).	Syngas flow (ELF20 CF001)	800 kg/h → 1100 kg/h

Water-gas shift reactors				
TR-CII-006: Verification reactor temperature measurements	14.09.2011 - 21.09.2011	Verify whether the thermocouples have been properly calibrated by exposing the reactor is exposed to an inert gas (nitrogen) at a constant temperature.	Inlet temperatures: Reactor 1 (ELF50 CT002) Reactor 2 (ELG20 CT003) Reactor 3 (ELG30 CT003)	250°C; 300°C; 350°C 210°C; 249°C; 287°C 141°C; 158°C; 130°C; 110°C
TR-CII-007: Dynamics 3rd shift reactor inlet temperature	12.12.2011	Study the dynamic behaviour of the 3rd WGS reactor during a variation in the inlet temperature.	Reactor inlet temperature (ELG30 CT003) due to a change in louvre position	Opening of the louvres: 350°C → 300°C (0.9K/min) Closing louvres: <300°C → 350°C
TR-CII-016: Catalyst stability & selectivity	23 periods from 03.02.2011 to 06.03.2013	Long-term testing to quantify catalyst deactivation and selectivity in time	NA	reference state

| TR-CII-017: Catalyst coking | 07.03.2012 26.03.2012 02.04.2012 22-23.04.2012 26.11.2012 04.12.2012 18-20.12.2012 | Investigation of the effect of the 2nd reactor inlet steam/CO ratio on the carbiding behaviour of the catalyst. | Temperature quench gas (ELF30 CT002) Resulting H_2O/syngas (ELG40 CX001) | 172.4°C → 126.5°C (8 set points) 1.23 → 0.74 kg/kg |

CO_2 Absorption section

TC-II (random packing) – steady state

| TR-CII-009: Water mass flow absorption section | 20-23.12.2011 04-19.01.2012 21.02.2012 - 09.03.2012 | validate the thermodynamic model with regard to the VLE of water – DEPEG | Water flow rate Resulting water content in DEPEG | 0.5 kg/h; 1.5 kg/h; 4 kg/h 1.09 wt%; 1.58 wt%; 4.74 wt% |

TR-CII-010: Solvent heater power input	09.03.2012 - 11.04.2012	Validate the temperature dependency of the thermodynamic model with regard to the VLE of water – DEPEG	Solvent temperature between 1st and 2nd flash vessel (ELH30 CT001) Resulting water content in DEPEG (at water flow rate 4kg/h)	48°C 2.14 wt%
TR-CII-011: Solvent mass flow	16.04.2012 18.04.2012 25.04.2012	Validate mass transfer coefficients	Solvent mass flow (ELH50 CF002)	13 kg/s; 11 kg/s; 10 kg/s
TR-CII-012: Shifted syngas mass flow	19.04.2012 - 22.04.2012	Validate mass transfer coefficients	Syngas mass flow (ELG60 CF006/IN)	1600kg/h (reference); 1754kg/h ; 1376kg/h; 786kg/h
TR-CII-013: Solvent temperature	11.12.2012 - 14.12.2012	Validate the model at different temperatures	Lean solvent temperature (ELH50 CT003) Solvent temperature between 1st and 2nd flash vessel (ELH30 CT001)	30°C; 25°C; 17.5°C 34°C; 38°C; 22.5°C
TR-CII-014: Absorber pressure	24.04.2012	Validate the influence of VLE on the absorption mass transfer rate	Absorber pressure (ELH80 CP001)	22 bara (reference) 23 bara; 21 bara

TR-CII-015: Pressure 1st flash vessel	23./24.04.2012	Investigate the influence of the pressure in the 1st flash vessel on gas composition	Pressure 1st flash (ELH20 CP001)	7.5 bara (reference) 8.5 bara; 6.5 bara
TC-III (structured packing) – steady state				
TR-CIII-011: Solvent mass flow	27.11.2012 – 29.11.2012	Validate mass transfer coefficients	Solvent mass flow (ELH50 CF002)	15kg/s (reference) 13kg/s; 11kg/s; 10kg/s
TR-CIII-012: Shifted syngas mass flow	24./25.11.2012	Validate mass transfer coefficients	Syngas mass flow (ELG60 CF006/IN)	1400kg/h (reference); 1573kg/h ; 1246kg/h; 819kg/h
TR-CIII-014: Absorber pressure	26./27.11.2012	Validate the influence of VLE on the absorption mass transfer rate	Absorber pressure (ELH80 CP001)	22 bara (reference) 23 bara; 21 bara
TR-CIII-31: High solvent flow rate	30.11.2012 – 04.12.2012	Investigate the influence of high solvent flow rate on pressure drop and absorption performance	Solvent mass flow (ELH50 CF002)	15kg/s (reference) 19kg/s; 22.5kg/s; 26.25kg/s; 30kg/s

TC-III (structured packing) – dynamic				
TR-CIII-029: Absorber dynamics - solvent flow rate	27./28.02.2013	Study the dynamic response of the absorption system to a perturbation in the solvent flow	Solvent mass flow (ELH50 CF002)	$15 \rightarrow 13 \rightarrow 15$kg/s $15 \rightarrow 11 \rightarrow 15$kg/s $15 \rightarrow 10 \rightarrow 15$kg/s
TR-CIII-030: Absorber dynamics – shifted syngas flow rate	01./02.03.2013	Study the dynamic response of the absorption system to a perturbation in the shifted syngas flow rate	Syngas mass flow (ELG60 CF006/IN)	$1400 \rightarrow 1600 \rightarrow 1400$kg/h $1400 \rightarrow 1100 \rightarrow 1400$kg/h $1400 \rightarrow 800 \rightarrow 1400$kg/h

A.2 Procedure for data handling and pre-processing used in the syngas conditioning and WGS section

For all composition measurements within the shifting section the measured dry gas composition is used (ELF50 CQ201) and it is determined by removing measured water content and by scaling of the remaining constituents such that their sum of moles is equal to one. Argon (not measured by ELF50 CQ201) is added to all composition measurements in the shifting section based on the measured N_2 content and N_2/Ar ratio recorded for the WAC syngas (EVB60 CQ007 and EVB60 CQ008 respectively).

Syngas composition:
Saturation of dry syngas composition (ELF50 CQ201A) with water based on measured P (ELF10 CP001) and T (ELF10 CT001).

Syngas mass flow (ELF20 CF001):
Correction of mass flow with actual density determined based on P (ELF10 CP001), T (ELF10 CT001) and wet syngas composition.

Reaction water mass flow (ELG40 CF001):
Correction of mass flow with actual density determined based on P (ELF10 CP001) and T (ELG40 CT005) and pure water (gaseous constituents neglected).

Quench mass flow (ELF31 CF001):
First, determination of wet quench composition by saturating dry syngas composition with water at P (ELF40 CP001/IN) and T (ELF30 CT002). Then correction of mass flow with actual density (same P, T and wet quench composition).

Reactor 1 inlet mass flow (ELF50 CF001):
First, determination of wet reactor 1 inlet composition by saturating dry syngas composition with water at P (ELF40 CP002/IN) and T (ELF40 CT002). Then correction of mass flow with actual density (same P, T and wet reactor 1 inlet com-position).

Shifted syngas mass flow:
First, determination of wet shifted syngas composition by saturating dry gas com-position at ELG50 BB010 outlet (ELF50 CQ201J) with water at P (ELG60 CP001) and T (ELG50 CT002). Then, calculation of syngas compressor drain mass flow based on volumetric

drain flow measurement (ELG60 CF003) and drain density determined at nominal conditions (P=1.013 bar, T=0 °C). Actual shifted syngas mass flow to the absorber is the result of subtracting drain mass flow from measured compressor outlet mass flow (ELG60 CF006/IN).

A.3   Formulation of EVM problem for DRPE

Generally, the EVM problem can be formulated as follows:

$$\min_{z_i, u_i, p} \sum_{i=1}^{J} f\left(\frac{z_i - z_i^M}{\sigma_i}\right) = \sum_{i=1}^{J} f\left(\epsilon_i\right)$$

s.t.

$$g_i(z_i, u_i, p) = 0$$

$$h_i(z_i, u_i, p) \leq 0$$

$$z^L \leq z_i \leq z^U$$

$$u^L \leq u_i \leq u^U$$

$$p^L \leq p \leq p^U$$

A-1

where the data reconciliation problem is described by f (generalized maximum likelihood objective function proposed by Huber (1981)), a function of the standard residual ϵ_i which expresses the deviation between the measured variables z_i^M and the reconciled variables z_i weighted by the standard deviation σ_i at the i-th data set. The set of parameter estimates is represented by p_i and the unmeasured variables by u_i. h_i corresponds to the equality and g_i to the inequality constraints which can represent either simple mass and material balance or non-linear process equations.

As objective function, the contaminated Normal has been used for the data reconciliation procedure in order to be more in-sensitive for large measurement errors and measurement outliers:

$$f = \ln\left\{(1 - p_{CN})\, exp\left(-\frac{\epsilon_i^2}{2}\right) + \frac{p_{CN}}{b_{CN}}exp\left(-\frac{\epsilon_i^2}{2b_{CN}^2}\right)\right\}$$

A-2

The contaminated Normal is constructed based on the maximum likelihood principle accounting both for contributions from random and gross errors in the measurements. The parameter p_{CN} is defined as the probability of a gross error in the measurements and b_{CN} as

the ratio of the standard deviation of the gross error to that of the random error. These values were chosen set to 0.05 and 10 respectively (Tjoa and Biegler 1991).

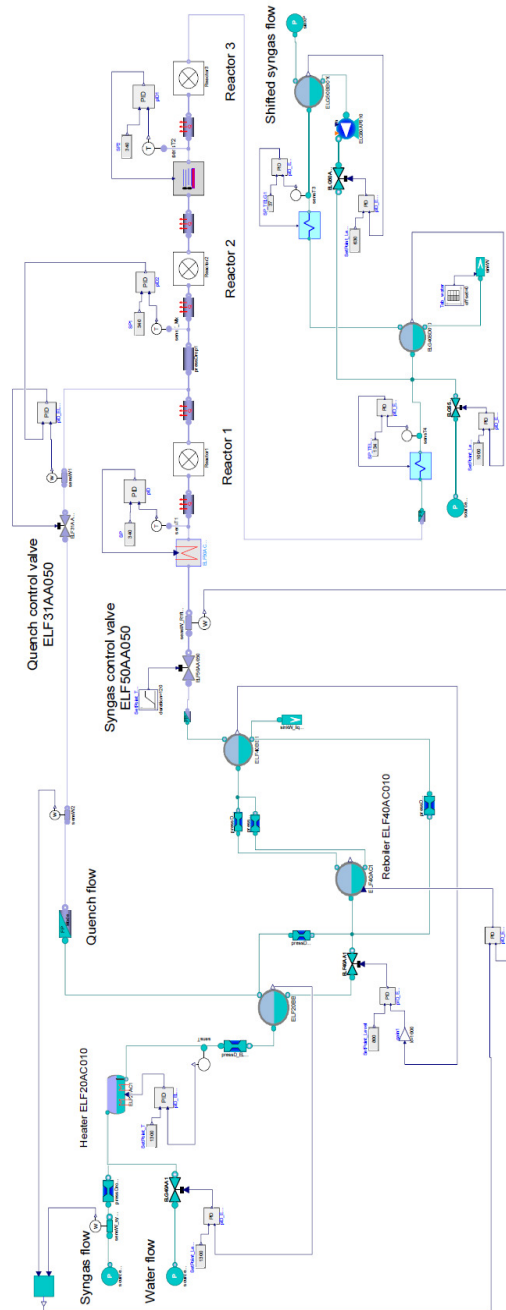## A.4   Flow sheet diagrams of dynamic process models

Figure A 1:   Flow sheet of the dynamic model of the syngas conditioning, WGS reactor and condensate recovery section
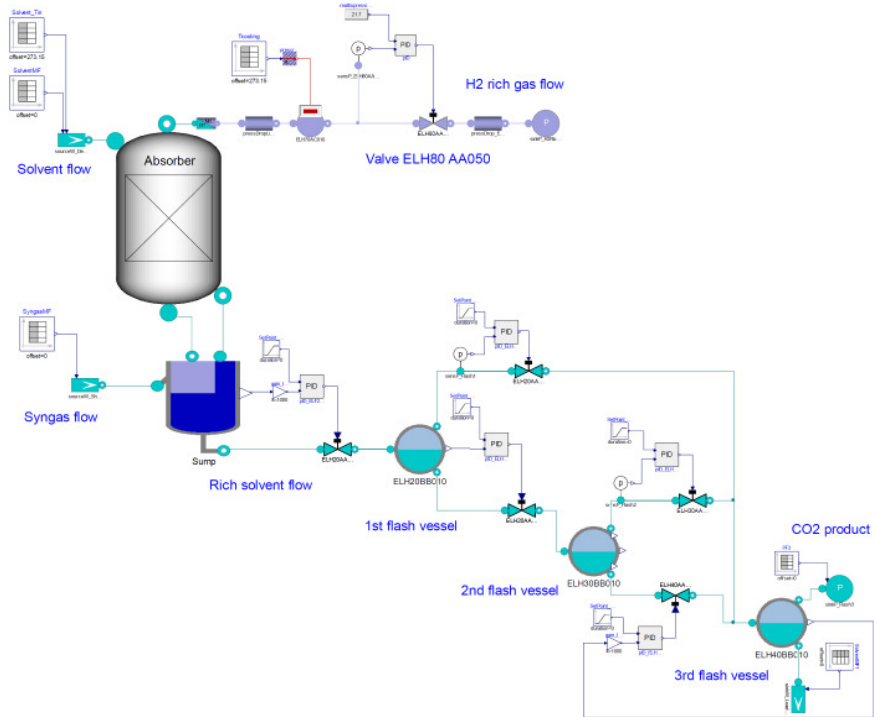
Figure A 2:   Flow sheet of the dynamic model of the absorption and regeneration section

A.5   Utilization of the dynamic model for the investigation of control strategies

Dynamic performance of fossil-fuelled power plants becomes increasingly important and hence an integrated capture process has to be able to follow load variations. However, it might also be required to temporarily only reduce the load of the energy-intensive CO_2 capture process while maintaining the gasifier load for an IGCC power plant, for example in case the market demands more energy or it is economically more favourable to produce energy instead of capturing CO_2. Therefore, the control system of the CO_2 capture unit should allow to perform frequent and prompt load variations.

In order to improve the dynamic performance of the pre-combustion CO_2 capture unit different control strategies have been investigated using the validated dynamic system model of the CO_2 capture pilot plant. On the basis that the pilot plant and large-scale process are very similar, with the main difference concerning the heat integration in the shifting section, a developed control strategy tested with the pilot plant model can be applied with modifications to the large-scale process.

Part-load and full-load operation of the CO_2 capture unit differs mainly in terms of the flow rates whereas the other process parameters are maintained. In order to allow for fast load variations it is particularly important to apply good set point management for the temperatures in the shifting section as the thermal inertia of the system is much higher than the mass inertia. Hence, a control strategy based on feed-forward, feed-back and cascade control has been implemented and tested with the CO_2 capture pilot plant model.

An example of cascade control as implemented in the dynamic model is shown in Figure A 3(a). Cascade control consists of two control loops. The master control compares the level measurement (process variable) with a given level set point and changes the set point of the slave control (control variable of the master control). The slave loop compares the flow measurement (process variable) with the set point provided by the master loop and changes the valve opening (control variable) accordingly. The advantage of cascade control is that it allows the system to be more responsive to disturbances and it is in particular useful for systems with long dead and lag times. However, this comes at a cost of higher system complexity and requires more process instrumentation. In case of the pilot plant model, cascade control has been implemented in the shifting section for the control of the liquid level in both vessels, the syngas mass flow rate and the reactor 2 inlet temperature.

Figure A 3(b) the application of feed-forward control is shown exemplary for the reaction water control loop. The aim of feed-forward control is to measure disturbances upstream

the system and compensate for them before the system variables deviate from the set point. In case of the capture unit, the main disturbance is the change in syngas load. Hence, the feed-forward control receives the syngas set point as input and determines based on an explicit equation the set point for the water flow control. The feed-back control ensures that the level set point is maintained.

The advantage of feed-forward control in comparison to feed-back control is that disturbances do not need to propagate through the process in order to take control actions and hence the set point management is much better. However, in order to accurately predict feed-forward control actions accurate measurements and adequate disturbance predictions are required, which in case of non-ideal processes require non-linear equations. In the pilot plant model feed-forward control has been implemented at all master control loops. The feed-forward action is determined based on the syngas set point, typically with a linear correlation, and sent together with the feed-back action to the slave control loop.

From the experimental tests at the pilot plant it was observed that the reactor performance varies from part-load to full-load, visible in the reactor outlet temperatures. In order to perform fast load variations changes in the reactor performance should, if possible, be avoided due to longer settling times related to the thermal inertia. The cause for the performance difference is related to changes in the thermodynamic state in terms of temperature and pressure in the second vessel (ELF40BB010) upstream the reactors, which subsequently leads to changes in the reactor 1 and 2 inlet composition. This applies in case the syngas inlet composition is constant, which is a justified assumption if the same type of fuel is used for gasification and the gasifier remains at the same load. In case of the pilot plant the inlet pressure of the capture unit is constant and hence the actual vessel pressure is a result of the difference between the inlet pressure and flow dependent frictional losses. Therefore, in order to maintain the vessel pressure at different loads a pressure controller is implemented in the pilot plant model.

Further, the vessel conditions at part-load and full-load differ because of changes in process heat losses. In the pilot plant large heat losses occur at the inlet and outlet of the reactors due to the fact that the reactor casing is over-dimensioned for the installed amount of catalyst. In a large-scale plant with well-sized reactors these particular heat losses will not be present. In addition, heat losses from piping upstream and downstream the reactors will be much smaller in a large-scale design because of better insulation and a smaller heat transfer area to volume ratio. Hence, the heat losses have been significantly reduced in the system model in order to perform the simulations at large-scale conditions. Both adaptations, the control of the vessel pressure and the heat loss reduction allow to

maintain the reactor performance and hence promote the ability of the CO_2 capture unit to perform fast load variations.

The simulation results obtained with the old and improved pilot plant control for a load variation from part-load to full-load are compared in Figure A 4 and Figure A 5. In the simulation with the improved control the syngas mass flow rate is ramped from 850 kg/h to 1100 kg/h in 10 minutes, whereby in the simulations with the old control the syngas set point is changed instantaneously and the control system takes care of the load change.

From the comparison of the old and improved control it can observed that it is possible to perform prompt load changes with the CO_2 capture process. The model predictions for the improved control indicate that for the mass flow rates in the shifting section more than 95 % of the final steady-state value can be reached within the ramping time. The vessel and reactor temperatures settle within approximately 60 minutes after the beginning of the perturbation. In addition, with the improved control (cascade and feed-forward) and the measures to maintain the reactor performance the maximum overshoot during the transient can be reduced significantly. Note that, due to the change in heat losses and vessel pressure for the improved control the steady-state values of most of the variables are different to the simulation results obtained with the old control.

In Figure A 6 the results of the absorption section are visualized. In the pilot plant no control was implemented to account for load variations such that the performance in terms of CO_2 absorption is maintained. In the dynamic model a ratio controller is implemented which maintains the mass-based liquid-to-gas ratio of the absorption column, which allows to maintain the CO_2 removal efficiency approximately constant for the operational range of the absorber. Consequently, if the mass flow rate of the shifted syngas changes the solvent mass flow rate is adapted accordingly. The results indicate, that the absorption section responds well to fast load variations.

To conclude, with the validated dynamic model of the CO_2 capture pilot plant it has been demonstrated that physical-based process models ease the design and testing of control strategies and that prompt load variations can be performed with a pre-combustion CO_2 capture unit. The qualitative results from this investigation with the pilot plant model can be applied for the design of the control strategies of the large-scale plant.
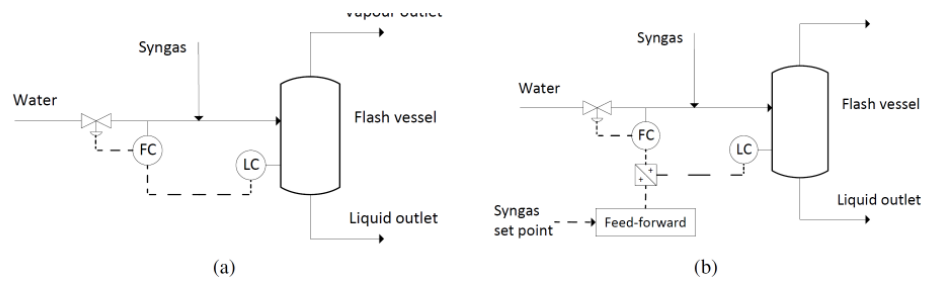
Figure A 3: Flash vessel level control via a) Cascade and feed-back control. b) Cascade, feed-back and feed-forward control.
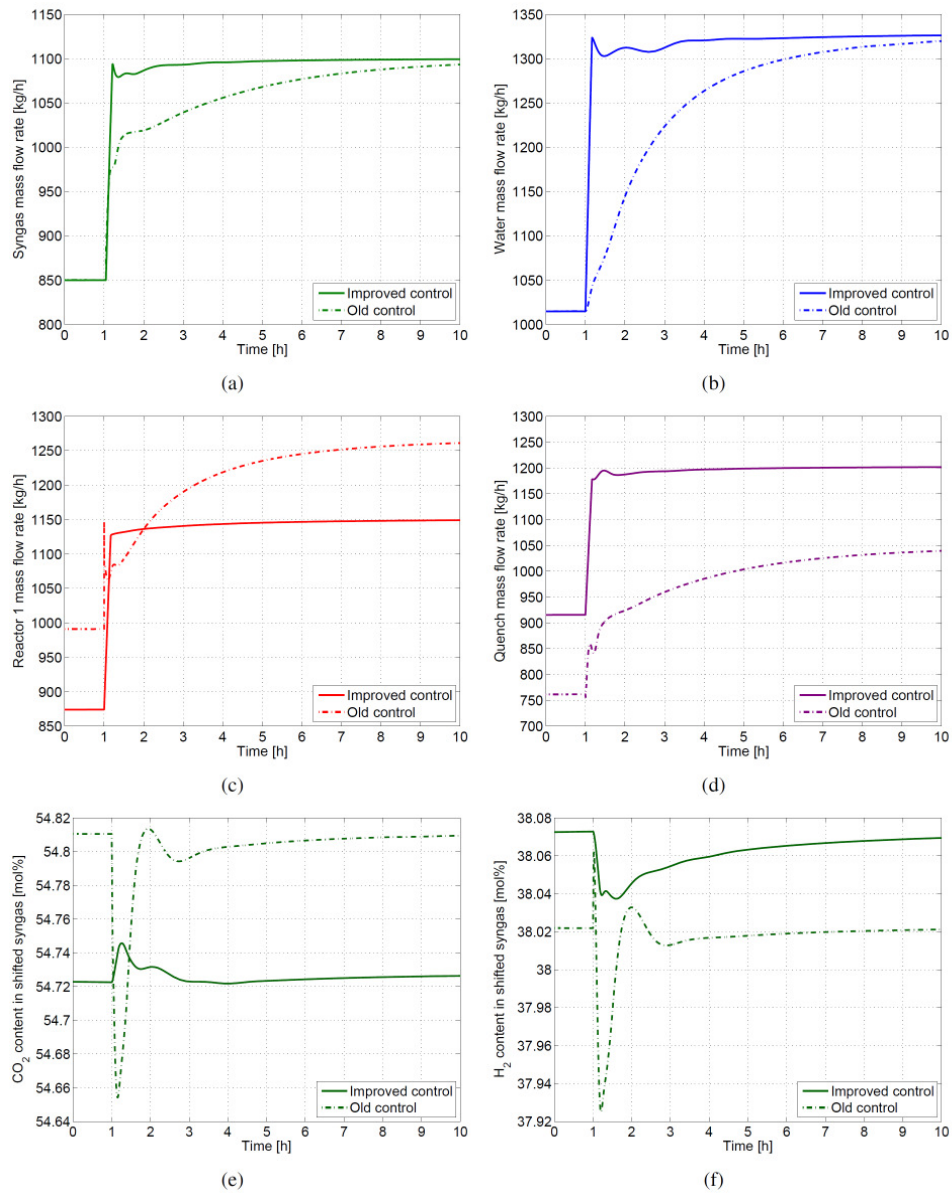
Figure A 4: Comparison of simulation results of old and improved control for change from part-load to full-load operation. a) Syngas mass flow rate. b) Water mass flow rate. c) Reactor 1 mass flow rate. d) Quench mass flow rate. e) CO_2 content in shifted syngas. f) H_2 content in shifted syngas.
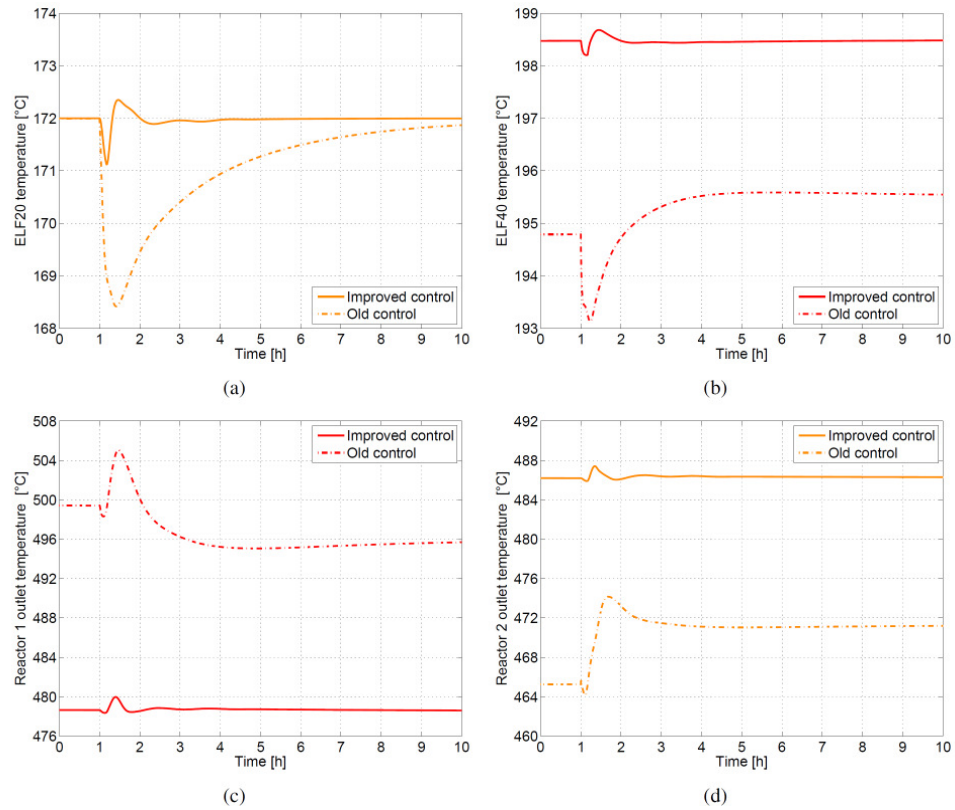
Figure A 5:   Comparison of simulation results of old and improved control for change from part-load to full-load operation. a) Quench temperature (ELF20BB010). b) Superheater inlet temperature (ELF40BB010). c) Reactor 1 outlet temperature. d) Reactor 2 outlet temperature.
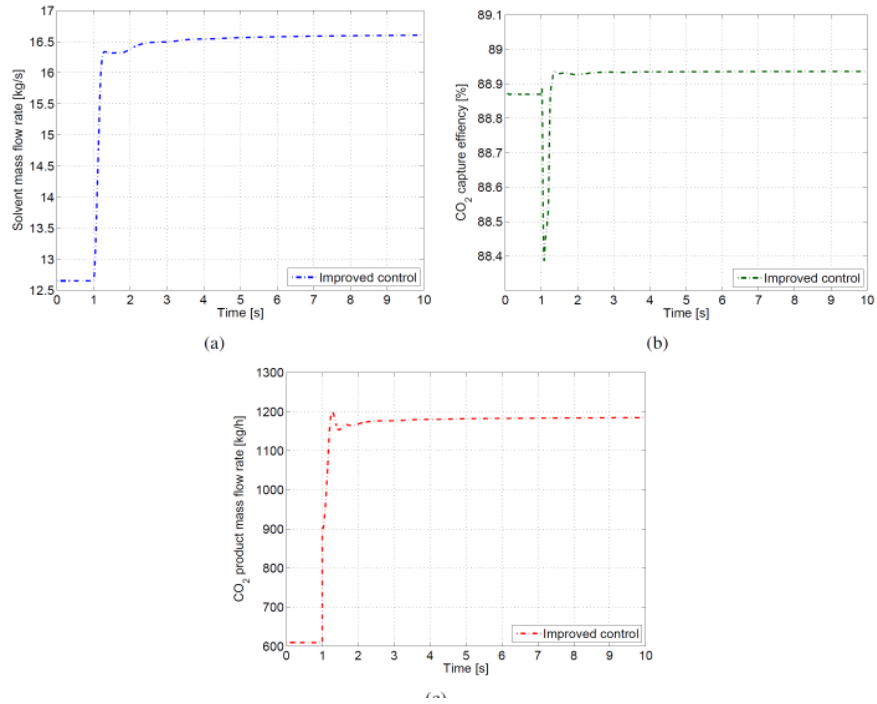
Figure A 6:   Simulation results of improved control for change from part-load to full-load operation. a) Solvent mass flow rate. b) CO_2 capture efficiency. c) CO_2 product mass flow rate.

A.6   Initialisation routine for dynamic absorber model

1. Provided (i) the boundary conditions of the column, (ii) the assumed temperature in each equilibrium stage and (iii) the values of first attempt for pressure and liquid holdup, the mass balance of the column is solved by applying the Sum-Rates Method.
2. On the basis of the liquid (Lj) and vapour (Vj) mass flow rate obtained by solving the mass balance of the column, pressure and holdup in each stage are updated according to the empirical pressure drop and holdup correlation assumed.
3. The mass balance of the column is again solved, on the basis of the new values of pressure and holdup. Then the sequence of phases 1-2 is repeated till convergence.

Solve Mass Balance of the column with the *Sum Rates Method*

Eternal loop - tear variables: P_j, LL_j

Inner loop - tear variables: overall composition in the stage ($Xtot_j$)

Estimate $K_{i,j} = y_{i,j}/x_{i,j}$ by Fluidprop

Compute $(x)_j$ by Thomas algorithm

Compute the liquid and vapor mass flow between each column stage $(L, V)_j$ from "sum rates relation"

Normalize $(x)_j$ and calculate $(y)_j$ according to the definition of $K_{i,j}$

Update $Xtot_j$ given LL_j

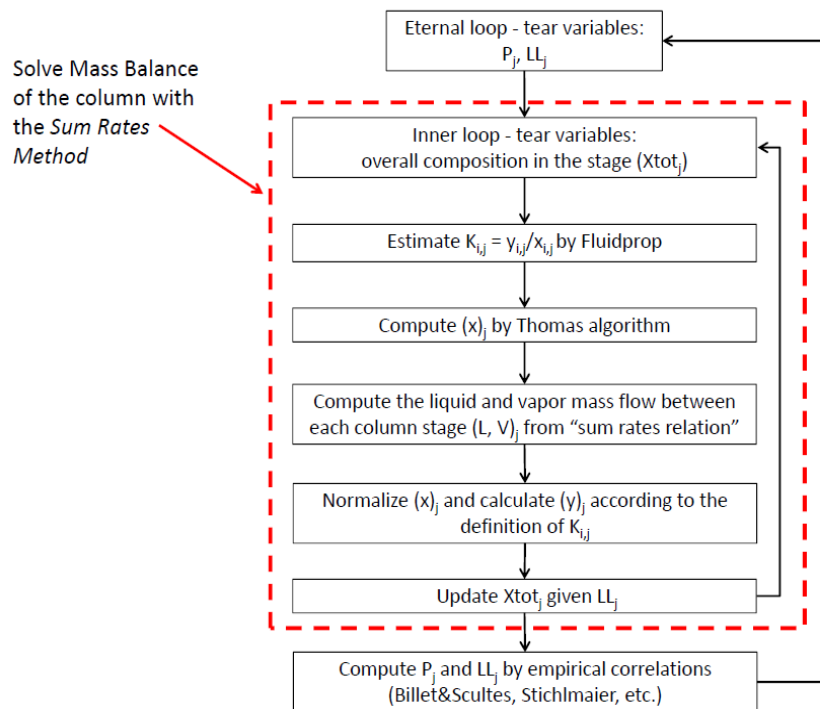Compute P_j and LL_j by empirical correlations (Billet&Scultes, Stichlmaier, etc.)

Figure A 7: Main steps of the initialization algorithm used to evaluate accurate initial guesses of pressure, liquid holdup and composition of the liquid and vapour phase in each equilibrium stage that discretize the column.

Note that the initialization algorithm does not solve the energy balance of the column, because the convergence of the dynamic model is not particularly affected by the assumed initial value of temperature in the equilibrium stages of the column. Thus, a rough estimation of the likely temperature distribution inside the column is enough to ensure the convergence of the dynamic simulation.